

Univerza v Ljubljani  
Fakulteta za Elektrotehniko

mag. Nataša Pavšelj, univ. dipl. inž. el.

# **Vnos genov v kožo z elektroporacijo**

DOKTORSKA DISERTACIJA

Mentor: prof. dr. Damijan Miklavčič

Somentorica: prof. dr. Véronique Préat

Ljubljana, 2006



University of Ljubljana  
Faculty of Electrical Engineering

Nataša Pavšelj, M.Sc.

**Gene transfection in skin by means of  
electroporation**

DOCTORAL DISSERTATION

Mentor: prof. Damijan Miklavčič, Ph.D.

Co-mentor: prof. Véronique Préat, Ph.D.

Ljubljana, 2006



# Table of contents

<b>ABSTRACT .....</b>	<b>i</b>
<b>RAZŠIRJENI POVZETEK .....</b>	<b>v</b>

## **CHAPTER 1**

<b>INTRODUCTION .....</b>	<b>1</b>
1.1. ELECTROPERMEABILIZATION OF CELLS .....	1
1.2. APPLICATIONS OF CELL ELECTROPERMEABILIZATION .....	3
1.2.1. <i>Electrochemotherapy (ECT)</i> .....	3
1.2.2. <i>Electrogene transfer (EGT)</i> .....	4
1.2.3. <i>Transdermal drug delivery</i> .....	4
1.3. SKIN.....	5
1.3.1. <i>Skin structure</i> .....	5
1.3.2. <i>The electric properties of the skin</i> .....	7
1.3.3. <i>Electrogene transfection of the skin</i> .....	8
1.3.4. <i>Electrodes for skin electropermeabilization</i> .....	9
1.4. OBJECTIVES OF THE THESIS .....	10
1.4.1. <i>The use of the combination of a high and a low-voltage pulse</i> .....	10
1.4.2. <i>Skin gene expression kinetic study, gene immunization by means of electroporation and safety aspects of skin electroporation</i> .....	10
1.4.3. <i>Numerical model of skin electroporation</i> .....	11
1.4.4. <i>Study of electrode geometries</i> .....	11

## **CHAPTER 2**

<b>CURRENT FIELD AND FINITE ELEMENTS METHOD THEORY .....</b>	<b>13</b>
2.1. VOLUME CONDUCTOR THEORY .....	14
2.2. FINITE ELEMENTS METHOD .....	17
2.3. ELECTRIC PROPERTIES OF TISSUES .....	23

## **CHAPTER 3**

<b>MATERIALS AND METHODS .....</b>	<b>25</b>
3.1. <i>IN VIVO</i> EXPERIMENTS .....	25
3.1.1. <i>Reporter genes and plasmid injection</i> .....	25
3.1.2. <i>Animals</i> .....	25
3.1.3. <i>DNA electrotransfer</i> .....	26
3.1.4. <i>Current-voltage dependences of rat skin</i> .....	26
3.1.5. <i>GFP localization</i> .....	26
3.1.6. <i>Luciferase assay</i> .....	27
3.1.7. <i>Immunization study</i> .....	27
3.1.8. <i>Tolerance study</i> .....	27
3.1.9. <i>Statistical analysis</i> .....	28
3.2. NUMERICAL MODELING .....	28
3.2.1. <i>COMSOL numerical modeling package</i> .....	28
3.2.2. <i>Numerical model of skin fold electropermeabilization</i> .....	29
3.2.3. <i>Numerical model of skin electropermeabilization with local transport regions (LTRs)</i> 31	
3.2.4. <i>Numerical models of microelectrode arrays</i> .....	33

## CHAPTER 4

<b>IN VIVO RESULTS .....</b>	<b>37</b>
4.1. CURRENT VS. VOLTAGE CURVES.....	37
4.2. GFP EXPRESSION IN SKIN .....	39
4.2.1. <i>The protocols used in GFP expression study</i> .....	39
4.2.2. <i>Confocal images of GFP expression in skin</i> .....	40
4.3. LUCIFERASE EXPRESSION IN SKIN.....	45
4.3.1. <i>The protocols used in luciferase expression study</i> .....	46
4.3.2. <i>Luciferase activity after different EP protocols</i> .....	46
4.4. KINETIC STUDY (PCMV <sub>LUC</sub> REPORTER GENE) .....	51
4.4.1. <i>The protocols used in the kinetic study</i> .....	52
4.4.2. <i>The duration of the luciferase expression in skin</i> .....	52
4.5. IMMUNIZATION STUDY .....	53
4.5.1. <i>The protocols used in the immunization study</i> .....	53
4.5.2. <i>The immune responses</i> .....	53
4.6. TOLERANCE STUDY .....	54
4.6.1. <i>The protocols used in the tolerance study</i> .....	55
4.6.2. <i>The effects of electroporation protocols on skin</i> .....	55

## CHAPTER 5

<b>NUMERICAL MODELS .....</b>	<b>57</b>
5.1. THE NUMERICAL MODEL OF A SKIN FOLD .....	58
5.2. THE NUMERICAL MODEL OF SKIN ELECTRO-PERMEABILIZATION WITH MODELED LOCAL TRANSPORT REGIONS (LTRS) IN THE <i>STRATUM CORNEUM</i> .....	64
5.3. THE NUMERICAL MODELS OF MICRONEEDLE ARRAYS.....	69

## CHAPTER 6

<b>DISCUSSION .....</b>	<b>75</b>
6.1. <i>IN VIVO</i> EXPERIMENTS.....	75
6.1.1. <i>The effect of the use of the HV+LV protocols on the GFP and luciferase expression in         skin</i> .....	77
6.1.2. <i>Other in vivo studies</i> .....	78
6.2. NUMERICAL MODELS.....	79
6.2.1. <i>The numerical model of a skin fold</i> .....	79
6.2.2. <i>The numerical model of skin with local transport regions</i> .....	80
6.2.3. <i>The numerical models of microneedle arrays</i> .....	82

## CHAPTER 7

<b>CONCLUSIONS .....</b>	<b>83</b>
7.1. <i>IN VIVO</i> EXPERIMENTS.....	83
7.2. NUMERICAL MODELS.....	84

<b>ORIGINAL SCIENTIFIC CONTRIBUTIONS.....</b>	<b>85</b>
---	-----------

<b>REFERENCES.....</b>	<b>87</b>
------------------------	-----------

<b>APPENDIX.....</b>	<b>97</b>
----------------------	-----------

## Abstract

Cell electropermeabilization is the phenomenon of transient permeabilizing of the cell membrane by exposing it to electric field. Even a short electric pulse causes an increased transmembrane potential in the cell membrane. The cell membrane is permeabilized when the threshold transmembrane voltage is exceeded. If the electric pulses are of adequate amplitude, the electric field strength and consequently the transmembrane potential are high enough (above the reversible threshold) for cell electropermeabilization. After pulsing, cell membrane reseals provided the applied voltage was not too high (exceeding the irreversible threshold) which would cause permanent cell membrane damage. An increase in permeability of the cell membrane makes it possible for larger molecules which otherwise can not cross the membrane, such as drugs or DNA, to enter the cell. Electropermeabilization of cells and the exogenous molecule cell uptake depends on different factors. The cell and tissue parameters (tissue specific conductivity, cell size, shape, density, distribution and interactions between them, pulse parameters (pulse duration, amplitude and number of pulses) and, consequently the most important parameter, the electric field strength and its distribution in tissue.

Electroporation is used in different applications, such as electrochemotherapy, transdermal drug delivery and gene transfection. Electrochemotherapy is a treatment of solid tumors which combines a cytotoxic non-permeant drug with locally delivered permeabilizing electric pulses. It is very successful in eliminating tumors locally, e.g. subcutaneous tumors and is more efficient than chemotherapy alone. Electroporation is also widely used to introduce small molecules and macromolecules, including DNA, into prokaryotic and eukaryotic cells *in vitro*. Electroporation is currently one of the most promising and simple non-viral methods of *in vivo* gene transfer. Transdermal drug delivery has many advantages over conventional routes of drug administration. However, the barrier properties of the skin limit transdermal drug transport. One of the methods to enhance it is electroporation which causes reversible permeabilization of the outer layer of the skin — the *stratum corneum*.

Skin is an attractive target tissue for gene therapy because of its size and accessibility, its large number of potent antigen presenting cells, critical to an effective immune response, and its role in secreting a variety of important systemic proteins. Therefore, it can be used for treatments of skin disorders, DNA immunization, and for

treatments of diseases of other organs through systemic response. Beside controversial viral methods, chemical and physical methods have been developed to enhance gene expression in skin. Electroporation seems particularly effective to improve DNA transfection after intradermal or topical delivery without any significant alteration of skin structure. However, from the electrical point of view, skin is a very intricate tissue due to its highly inhomogeneous electric properties. It consists of three different layers: the epidermis, dermis, and the subcutaneous tissue. The outermost layer of the epidermis, the highly resistive *stratum corneum*, although very thin (typically around 20  $\mu\text{m}$ ), makes skin one of the most resistive tissues in human body. Deeper skin layers: the rest of the epidermis (important in the immune response), the dermis (gives firmness and elasticity) and the subcutaneous tissue (fat, connective tissue, larger blood vessels and nerves), all have much lower resistivities.

High voltage pulses applied on the skin cause a significant decrease in skin resistance of up to three orders of magnitude, due to the newly created pathways for ionic current. At the onset of electric pulses, most of the potential drop rests across the highly resistive *stratum corneum*. Consequently, the electric field in that layer is likely to rise above the critical strength, the reversible electropermeabilization threshold, which causes the breakdown of the skin's protective function and a decrease in its resistance. Due to this decrease, the skin layers underneath *stratum corneum* are subjected to an electric field of high enough strength to permeabilize the cells and achieve an efficient gene transfection.

The effect of electrical parameters and electrode design on the efficacy of transfection in skin and the process of skin electropermeabilization have not been studied systematically so far. It has been shown for the skeletal muscle tissue that a combination of one short high voltage (HV) pulse, followed by a long, low voltage (LV) pulse, can achieve a high gene transfection. The experiments showed that the high voltage pulse alone results in a high level of tissue permeabilization but unfortunately still a very low DNA transfection in the target tissue. However, if the high voltage pulse is followed by a longer, low voltage electrophoretic pulse, the uptake of the DNA into the cells is substantially increased. We used a similar protocol for *in vivo* gene transfection in skin. Gene expression by means of two reporter genes after different electroporation protocols was assessed, the kinetics of this expression, and intradermal DNA immunization. In addition, possible side effects on skin using the combination of a short high voltage and a long low voltage pulse were tested.

Two reporter genes were used in the study: pCMVluc and pCMVGFP. They were injected intradermally into male Wistar rats that were anaesthetized before experiments. For pulse delivery, we used the square-wave electropulsator Cliniporator. The electric pulses were delivered using two parallel, stainless-steel plate electrodes of 0.5 mm thickness, 4 mm distance and 1 x 1  $\text{cm}^2$  surface, with a conductive gel applied between the electrodes and the skin. During the electric pulse delivery, the actual current delivered and the applied voltage were acquired and stored by the Cliniporator. Two days after the electroporation, the rats were sacrificed and the electroporated areas of the skin were excised. To assess the pCMVGFP expression, the epidermal and the dermal side of the skin samples were observed with a confocal microscope without fixation or freezing. For the pCMVluc expression, the luciferase activity was assessed on the lysate supernatant, using a luminometer.

The GFP results show that when a single high voltage or a single low voltage pulse was applied, the expression of GFP remained very low both in the epidermis and dermis, comparable to the expression in the samples where no electroporation was used

after the intradermal injection of plasmid. Using a combination of a high voltage pulse, followed by a low voltage pulse, the expression of GFP in the skin was enhanced. The expression at the anodal side was slightly higher than the expression at the cathodal side. The analysis of the influence of electroporation on luciferase expression in the skin after intradermal injection of DNA demonstrates that the combination of HV+LV is more efficient than HV or LV pulse(s) alone and that the splitting of the LV pulse and the delay between the HV and the LV pulse has no positive nor adverse effect on luciferase expression in skin. Of the different HV+LV electroporation protocols tested, no statistical difference was found. The luciferase expression was the highest at 24 h to 48 h after the electroporation, and decreased rapidly to control values after two days.

The immune response after intradermal delivery of a plasmid coding for the immunogenic model protein ovalbumin (pcDNA 3.1-OVA), followed by the electroporation, was assessed. Balb/c mice were used in the study. Two and four weeks after the priming, two boosts were applied. The humoral immune response to ovalbumin in the serum was measured by ELISA. The immunization experiment demonstrated that electroporation enhances the immune response induced after intradermal injection of a DNA plasmid coding for the antigen ovalbumin, and that the proposed HV + LV protocols are more efficient than protocols (6 to 8 HV pulses) previously described. However, the immune responses in groups where DNA electrotransfer with HV + LV was used, were somewhat lower than in mice immunized with OVA and the standard adjuvant alum.

Also, noninvasive bioengineering methods were used to evaluate *in vivo* if electroporation induced any trauma in the skin. Transepidermal water loss – TEWL – measurements were used to assess the barrier function of the skin after electroporation, and possible skin erythema was measured by means of chromametry. Histology was used to investigate possible effects on the skin structure. The tolerance study showed only small and transient increase in the transepidermal water loss, and no erythema due to electroporation. There was a consistent difference between the anode and the cathode side of the electroporation sites. Also, no damage in the histologic structure of the skin was found.

The explanation of the intricate processes taking place in the tissue during electropermeabilization, and even monitoring the process in real time, has been of interest of many researchers, as it would give us valuable feedback that could be used in planning of the pulse parameters and electrode geometries. Various electrical parameters can be evaluated by means of numerical modeling and the real process can be modeled with its simplified, numerical version with help from the experimental data. We modeled the process of skin electropermeabilization with a numerical model, taking into account tissue and electrode setups and pulse parameters used in experiments, and the changes in the specific conductivities of tissues during electroporation. Current and voltage measurements during the delivery of pulses were used to build the model as the output of the model should be as close to the measured data as possible. Because of the many skin layers with very different electric properties and layer thicknesses, the skin fold model is numerically quite a complicated one. When the electric field is applied to the skin fold, almost the entire voltage drop rests on the highly resistive *stratum corneum*. However, because of the rise in the specific conductivities of tissues, the electric field “penetrates” to deeper layers. Therefore, the process of skin permeabilization was modeled as a nonlinear problem.

Electric field and current computations were made by means of commercially available computer program COMSOL Multiphysics, based on the finite elements

method, solving partial differential equations by dividing the model into smaller elements where the quantity to be determined is approximated with a function. Finite elements can be of different shapes and sizes, which allows modeling of intricate geometries. Nonhomogeneities and anisotropies can also be modeled and different excitations and boundary conditions applied easily. Due to the symmetry, only one fourth of the geometry was modeled. The process of tissue permeabilization was modeled as a nonlinear problem, taking into account the increase in tissue conductivity due to cell membrane permeabilization. Namely, when the electric field exceeds the reversible threshold, the tissue conductivity increases and in the next iteration, changed electric field distribution is computed. Using voltage and current measurements recorded during pulse delivery, we aimed at making the response of the model as close as possible to the experimental data. Parameters such as specific conductivities of the tissues before and after electropermeabilization and the reversible and irreversible electric field thresholds were taken from the literature or determined by experiments.

The results, such as electric currents and the voltage needed for a successful electropermeabilization of the tissue are in correspondence with the experimental results. Comparing the voltages needed for a successful electropermeabilization of the skin fold as suggested by the model, with voltages achieving high *in vivo* gene transfection, a good agreement can be observed. Further, the voltage amplitudes suggested by the model are also well in the range of the voltage amplitudes found to cause skin permeabilization, reported in literature. Even though some approximations were made in the model, we can conclude that with the model presented, the mechanism of tissue electropermeabilization, taking into account changes in tissue conductivities is well described.

The experiments of other researchers showed highly localized molecular transport in skin after electroporation. The highly conductive areas were termed local transport regions (LTRs). We constructed a model of skin with local transport regions embedded in the *stratum corneum* based on the data on size, density and electrical properties of LTRs found in the literature. Comparing the results of the LTR model with the results of the skin fold model and the *in vivo* experiments, the voltages suggested for successful electropermeabilization by the LTR model are somewhat higher and the electric currents at the end of the electropermeabilization process are shifted towards lower values. As the electroporation protocols and circumstances of our *in vivo* experiments are not directly comparable to the experiments the geometry of our model was based on, we can accept this as a good agreement of the results. We can conclude that the numerical model of skin with local transport regions in the *stratum corneum* is a good representation of the electropermeabilization process in skin.

Recently, a great deal of research is devoted to development of painless microneedle electrodes to be used in transdermal drug delivery and gene transfection in skin, where the electrical high resistance and non-permeability of skin is breached by piercing the outermost layer of the skin, the *stratum corneum*. A preliminary comparison between different settings of microneedle arrays was made and only small differences were found between different microelectrode geometries. Although the models of the microneedle arrays could not be validated, due to the lack of experimental data, we suggest that a more uniform tissue permeabilization can be reached than when using plate electrodes on a skinfold. Also, lower voltages can be used for a successful tissue permeabilization, as the electrical barrier of the *stratum corneum* is breached by piercing it.

## Razširjeni povzetek

### 1. Uvod

Raziskovanju bioloških učinkov elektromagnetnih polj v zadnjem času posvečamo vedno več pozornosti, predvsem zaradi čedalje večje izpostavljenosti sodobnega človeka različnim virom elektromagnetnega sevanja (daljnovodi, antene, mobilni telefoni). Učinki elektromagnetnih polj na biološke sisteme pa se v zadnjih desetletjih s pridom uporabljajo tudi v mnoge diagnostične (rentgen, CT (računalniška tomografija ali angleško *computerized tomography*), MRI (magnetna resonanca ali angleško *magnetic resonance imaging*...)) in terapevtske namene (elektronevrostimulacija, zdravljenje ran z električnim tokom, hipertermija, elektrokemoterapija...).

#### 1.1. Elektropermeabilizacija celic in tkiv

Membrana biološke celice v splošnem ni prepustna za večje molekule. Ob prisotnosti že kratkotrajnega visokonapetostnega električnega pulza pa v celični membrani nastanejo strukturne spremembe - največkrat jih imenujemo kar "pore". Ob zadostnem številu le-teh in njihovi ustrezni gostoti se poveča prepustnost celične membrane. To povečanje prepustnosti membrane – permeabilizacija – omogoči velikim molekulam, kot so nekatere zdravilne učinkovine in molekule DNK, za katere je sicer celična membrana neprepustna ali slabo prepustna, neposreden vstop v celično notranjost. Sprememba celične membrane je reverzibilna, ob dovolj visokem električnem polju in njegovem dovolj dolgem trajanju pa je lahko ireverzibilna, kar povzroči celično smrt.

Prepustnost celične membrane nastopi pri pragovni vrednosti vsiljene transmembranske napetosti, ki je med 200 mV in 1 V. Vsiljena transmembranska napetost, ki nastane na celični membrani kot posledica zunanega električnega polja, se prišteje takoimenovani mirovni vrednosti transmembranske napetosti (med 30 mV in 100 mV), ki nastane zaradi izmenjave predvsem  $\text{Na}^+$  in  $\text{K}^+$  ionov skozi celično membrano.

Z elektroporacijo lahko v celično membrano vstavljamo beljakovine, preučujemo aktivnosti encimov *in vivo*, olajšamo vstop v celice specifičnim inhibitorjem znotrajcelične encimske aktivnosti, zlivamo celice ali pa preučujemo celično signalizacijo preko nadzora koncentracije ionov v citosolu. Najpomembnejše in

najpogosteje uporabljane elektroporacijske aplikacije pa so elektrokemoterapija, vnos genov in vnos zdravilnih učinkovin v kožo.

Elektropermeabilizacija je odvisna od različnih dejavnikov: prevodnosti medija, parametrov pulzov ter od velikosti, oblike, orientacije in gostote celic. Najpomembnejši parameter je lokalna električna poljska jakost, ki na celičnih membranah vsili transmembransko napetost. Z višanjem električne poljske jakosti se povečuje prepustnost membrane, s tem pa se povečuje tudi vnos molekul, ki hitro doseže najvišjo vrednost. Toda hkrati se povečuje tudi delež celic, ki jih visoko električno polje uniči. Kadar je električna poljska jakost zelo velika, je verjetnost za preživetje celic majhna. Ker so parametri električnih pulzov ter oblika in postavitev elektrod edini dejavniki elektroporacije celic, na katere imamo vpliv, lahko zasledimo v literaturi veliko število raziskav katerih cilj je bil razviti najbolj uspešne elektroporacijske protokole za različne vrste celic in aplikacij. Poskusi so pokazali, da tako število pulzov, kot tudi njihova amplituda in trajanje vplivajo na uspešnost elektroporacije. Nekateri predlagani protokoli zato združujejo električne pulze različnih amplitud in trajanj.

Spremljanje prepustnosti tkiva v realnem času je želja mnogih raziskovalcev na tem področju, saj bi povratno informacijo o poteku elektropermeabilizacije tkiva lahko uporabili za prilagajanje električnih parametrov med samo terapijo. Med in po elektroporaciji se električne lastnosti tkiva spremenijo, morda najbolj pomembna merljiva posledica je povečanje specifične prevodnosti tkiva, podvrženega elektroporaciji, ob dosegu reverzibilnega praga električne poljske jakosti. Posledično skozi tkivo steče višji tok, porazdelitev električnega polja v tkivu pa je drugačna kot na začetku. Poznavanje porazdelitve električne poljske jakosti je torej pomembno, če želimo raziskovati potek elektroporacije v tkivu.

Potek elektropermeabilizacije tkiva in vpliv spremembe nekaterih parametrov na porazdelitev električnega polja v tkivu in tokove skozenj, med elektroporacijo in po njej, lahko preučujemo z numeričnimi modeli. Teoretična razlaga dogajanja nam namreč nudi pomemben vpogled v proces elektropermeabilizacije celic, tkiv in organov, pri čemer si lahko pomagamo z analitičnimi izračuni in numeričnim modeliranjem. Predvsem slednje se je izkazalo za nepogrešljivo pri izračunih porazdelitve električne poljske jakosti v tkivih in organih, kjer so obravnavane geometrije preveč zapletene za analitične metode. Z numeričnim modeliranjem lahko ovrednotimo spremembe vrednosti specifičnih prevodnosti posameznih tkiv, poteka elektroporacije med reverzibilnim in ireverzibilnim pragom permeabilizacije tkiva, ter spremembe v geometriji modela, saj vemo, da je pri meritvah na realnih objektih, torej pri poskusih na živalih, natančna ponovljivost geometrije skoraj nemogoča.

## **1.2. Uporaba elektropermeabilizacije celic**

### **1.2.1. Elektrokemoterapija**

Problem uničevanja tumorskih celic s kemoterapevtiki je njihova nespecifična citotoksičnost, ki škoduje tudi zdravim celicam, ter rezistenca tumorskih celic zaradi genetskih sprememb. Prav tako pa problem predstavlja tudi visoka koncentracija kemoterapevtika, ki mora biti prisotna v ciljnim tkivu, kar povzroča neželene stranske učinke. Zaradi slabe prepustnosti celične membrane namreč molekule nekaterih kemoterapevtikov težko vstopajo v notranjost tumorskih celic. Ob hkratni uporabi kemoterapevtikov in elektroporacije ciljnega tkiva se učinkovitost kemoterapije močno poveča, zmanjšajo pa se stranski učinki. Prvi poskusi na področju elektrokemoterapije

segajo v leta 1987 in 1988. Številne raziskave kažejo na več sto-kratno povečanje učinkovitosti citostatika bleomicina ter do 70-kratno povečanje kemoterapevtika cisplatina *in vitro*, kadar ju uporabimo v kombinaciji z dovajanjem električnih pulzov. Elektrokemoterapijo vedno bolj uspešno uporabljajo tudi v klinični praksi za zdravljenje tumorjev vratu in glave, malignih melanomov, bazalnih celičnih karcinomov in adenokarcinomov.

### **1.2.2. Vnos genov z elektroporacijo**

Z gensko terapijo dodajamo in "popravljamo" gene, ki so odgovorni za nastanek mnogih dednih bolezni, z vnašanjem genov, ki kodirajo širok spekter proteinov, pa lahko zdravimo tudi nekatere pridobljene in celo nalezljive bolezni. Napredek na področju razkrivanja zapletenega človeškega genoma je povzročil pravo evforijo v farmacevtskih in medicinskih znanstvenih krogih. Pretirani optimizem se je kmalu izkazal za preuranjenega, saj je uspešen vnos genov v ciljne celice in tkiva še vedno problematičen. Virusni vektorji, čeprav uspešni pri vključitvi svojega genskega zapisa s terapevtskimi geni v ciljne celice, prinašajo mnogo vprašanj glede z virusi povezanega tveganja. Veliko raziskav je zato v zadnjem času posvečeno razvoju nevirusnih metod vnosa terapevtskih genov v ciljna tkiva in organe. Ena od metod je tudi uporaba električnih pulzov za povečanje prepustnosti membrane, imenovana vnos genov z elektroporacijo. Poskusi kažejo na dvojnost delovanja električnih pulzov za vnos genskega materiala v celice; ti namreč povečajo prepustnost celične membrane, s pomočjo električnega toka pa električno negativne molekule DNK elektroforetično potisnejo v notranjost celice. Pri vnosu genov z elektroporacijo moramo biti še posebej pazljivi, da s prevelikim električnim poljem ne ogrozimo celičnega preživetja, kar pri elektrokemoterapiji ne predstavlja posebne nevarnosti, saj je uničenje tumorskih celic pravzaprav naš cilj.

### **1.2.3. Vnos zdravilnih učinkovin v kožo**

Zdravilne učinkovine lahko vnašamo v telo skozi kožo. Zaradi nizke permeabilnosti kože si lahko pri tem pomagamo z različnimi metodami, kot so ultrazvok, iontoforeza in elektroporacija. Takšen vnos zdravilnih učinkovin ima določene prednosti, saj je manj invaziven kot intravenski vnos, izognemo pa se tudi škodljivemu vplivu prebavnih encimov in nizkih pH vrednosti. Nadalje lahko s transdermalnimi terapevtskimi sistemi dosežemo postopen, konstanten vnos zdravilne učinkovine v telo, namesto hitrega intravenoznega dajanja. Vendar pa je zaradi zaščitne funkcije kože in njene zelo nizke prepustnosti vnos molekul v kožo težaven. Elektroporacija je ena od metod, s katero začasno povečamo prepustnost kože brez škodljivih posledic, električni tok pa lahko dodatno pospeši prenos ionov in električno nabitih molekul v kožo.

## **1.3. Elektropermeabilizacija in vnos genov v kožo**

Koža je zanimiv ciljni organ za gensko terapijo. Je lahko dostopen organ, ki zaradi njene velikosti ponuja široko področje delovanja in omogoča nadziranje morebitnih neželenih sprememb. Z vnosom genov v kožo pa lahko poleg kožnih bolezni zdravimo tudi določene bolezni drugih organov. Koža je tudi zelo primeren ciljni organ za gensko imunizacijo, saj so v njej Langerhansove celice, ki so odgovorne za imunski odziv po vstopu tujih spojin v kožo. Elektroporacijo lahko uporabljamo za vnos genov (angleško *electrogene transfer* – EGT), kar predstavlja varnejšo alternativo vnosu genov z

virusnimi vektorji. Uporaba električnih pulzov poveča vnos genov v celice po predhodnem intradermalnem vnosu ali površinskem nanosu genskega materiala.

### **1.3.1. Struktura kože**

Koža je največji organ v človeškem telesu, saj predstavlja približno 15% telesne mase, njena površina pa je med 1,5 in 2 m<sup>2</sup>. Koža ločuje telo od okolja, preko nje poteka interakcija z zunanjim svetom, hkrati pa koža predstavlja prvi obrambni mehanizem pred škodljivimi zunanjimi vplivi, pomaga pri uravnavanju vlage ter telesne temperature in izloča odpadne snovi. Sestavljajo jo tri glavne plasti: *epidermis*, *dermis* in podkožno tkivo.

**Epidermis** (ali vrhnjica) je zunanja plast kože, sestavljena iz ploščatih, odmrlih celic, ki vsebujejo beljakovino keratin. Njena debelina je od 0,5-2 mm in je debelejša na mestih, ki so najbolj izpostavljena obrabi (dlani, podplati), ter najtanjša na nežnejših predelih, kot so recimo veke. Razdelimo jo lahko na več podplasti, ki si od spodaj navzgor sledijo: *stratum basale* (bazalna plast), *stratum spinosum* (trnasta plast), *stratum granulosum* (zrnata plast), in *stratum corneum* (rožena plast). Celice *stratum corneum*-a nenehno odpadajo, sproti pa jih nadomeščajo nove iz nižjih plasti vrhnjice. Tako se epidermis popolnoma obnovi vsakih 3-5 tednov. Debelino *stratum corneum*-a sestavlja od 15 do 100 plasti oroženelih celic, ki predstavljajo primarno zaščitno pregrado pred okoljem. V zarodni plasti *epidermis*-a najdemo melanocite, celice v katerih nastaja barvilo melanin, ki daje koži barvo. Pri obsevanju z ultravijoličnimi žarki te celice proizvajajo več melanina, zato koža porjavi, kar je obrambna reakcija kože na škodljive vplive ultravijoličnih žarkov. V *epidermis*-u najdemo tudi Langerhansove celice, ki igrajo pomembno vlogo pri imunskem odzivu, ter čutne Merkelove celice, ki so občutljive na dotik. V *epidermis*-u ni žil, zato je ta plast za prehranjevanje odvisna od pod njo ležečega *dermis*-a.

**Dermis** (ali usnjica) je najdebelejša plast kože (približno trikratna debelina *epidermis*-a) in je zgrajena iz čvrstega, prožnega vezivnega tkiva. Primarna naloga te plasti je oskrbovanje *epidermis*-a, celotni koži pa daje čvrstost, prožnost in odpornost, za kar skrbita proteina kolagen in elastin. V *dermis*-u se prepletajo krvne žilice, številni živčni končiči ter receptorji za bolečino in dotik, žleze lojnice in znojnice ter lasne korenine.

**Podkožno tkivo** tvorijo prepletajoča kolagenska vlakna in maščobne celice. Vezivno tkivo je rahlejšje kot v *dermis*-u, žile in živci so debelejši. Prevladujejo maščobne celice, tako imenovani adipociti, velike celice, ki shranjujejo maščobe. Podkožno maščevje varuje pod kožo ležeče organe pred mehanskimi vplivi iz okolice, zaradi njegove slabe toplotne prevodnosti pa preprečuje tudi čezmerno oddajanje toplote.

### **1.3.2. Električne lastnosti kože**

Koža je precej kompleksno tkivo, saj je tako po zgradbi kot po prisotnih lipofilnih in hidrofilnih spojinah nehomogena. Sestavlja jo več plasti z različno vsebnostjo vode in elektrolitov, kar se odraža v električnih lastnostih. Plast, ki kožo z električnega vidika najbolj definira, je zunanja plast *epidermis*-a, *stratum corneum*. Kljub temu, da je debelina te plasti tipično nekje okoli 20 μm (glede na lokacijo na telesu lahko tudi več ali manj), je zaradi visoke specifične električne upornosti te plasti koža eno najmanj električno prevodnih tkiv v človeškem telesu (poleg kosti).

Električni pulzi dovolj visoke amplitude povzročijo strukturne spremembe kože in s tem padec električne upornosti tudi do 1000-krat. Če pulzi niso previsoki, se specifična upornost kože vrne na prvotno vrednost v nekaj mikrosekundah, okrevanje pa lahko traja tudi vse tja do nekaj ur, odvisno od parametrov, predvsem števila in trajanja električnih pulzov. Ob aplikaciji električnih pulzov se praktično celoten padec napetosti nahaja na *stratum corneum*-u, plasti z najvišjo specifično upornostjo, kar ob uporabi zadosti visoke napetosti pulzov posledično povzroči permeabilizacijo te plasti, saj je električna poljska jakost v njej zagotovo nad kritičnim pragom permeabilizacije. Električna upornost *stratum corneum*-a se med permeabilizacijo zato močno zmanjša, kar spremeni porazdelitev električne poljske jakosti tudi v preostalih plasteh kože. Tako zadosti močno električno polje "doseže" tudi nižje plasti kože, s čimer lahko dosežemo uspešno elektropermeabilizacijo ciljnih celic v katere želimo vnesti gene. Preboj zaščitne funkcije kože pa omogoči tudi vnos zdravilnih učinkovin skozi kožo, še posebej v kombinaciji s šibkimi elektroforetičnimi tokovi. Naj na tem mestu poudarimo osnovno razliko med elektroporacijo in elektroforezo. Čeprav oba procesa vključujeta uporabo električnih pulzov, elektroporacija deluje neposredno na kožo, v kateri ustvarja nove pore za prehod večjih molekul, elektroforeza pa deluje na ionizirano zdravilno učinkovino in jo vodi skozi permeabilizirano kožo.

Poskusi so pokazali, da visokonapetostni pulzi v koži ustvarijo nove poti za transport molekul skozi kožo, ki se lahko poveča do 10000-krat. Transport naj bi bil skoncentriran v takoimenovanih lokalnih transportnih območjih (ang. *local transport regions* – LTRs), katerih gostota in velikost sta odvisni od električnih parametrov pulzov. V grobem bi lahko električno vzbujanje in odziv kože nanj razdelili v tri razrede: nizko, srednje in visokonapetostno vzbujanje. Pri nizkonapetostnem vzbujanju ( $U_{kože} < 5$  V) je transport molekul omejen na okolico lasnih mešičkov in znojnic, dominantni mehanizem transporta pa je elektroforeza. Srednjenapetostno vzbujanje ( $5$  V  $< U_{kože} < 50$  V) vključuje oba mehanizma, elektroforezo in elektroporacijo, molekularni transport pa poteka tako skozi že obstoječe poti (lasni mešički, znojnice), kot tudi čez novo nastale poti skozi strukturo plasti lipidnih dvoslojev *stratum corneum*-a, pri čemer specifična električna upornost kože pade za do približno 100-krat. Uporaba visoke napetosti ( $U_{kože} > 50$  V) povzroči hiter padec upornosti kože (do 1000-kraten padec) in s tem povezan hiter molekularni transport, že nekaj mikrosekund po aplikaciji električnih pulzov. Značilnost visokonapetostnega vzbujanja kože je molekularni transport v takoimenovanih lokalnih transportnih področjih (LTR). Velikost teh področij narašča s trajanjem pulza, tipično pa v premeru merijo nekje med 100 in 300  $\mu$ m. Povečanje amplitude električnega vzbujanja nima velikega vpliva na velikost LTR, poveča pa se njihova gostota.

## **1.4. Cilji naloge**

### **1.4.1 Vpliv visoko in nizko napetostnih pulzov na vnos genov v kožo**

Vpliv električnih parametrov in geometrije elektrod na uspešnost vnosa genov v kožo do danes še ni bil sistematično raziskan. Za mišično tkivo so pokazali, da s kombinacijo kratkega pulza visoke amplitude in dolgega pulza nizke amplitude dosežejo uspešen vnos genov. V mišico so injicirali plazmid, ki kodira protein luciferazo. Opazovali so izražanje proteina po elektroporaciji z različnimi kombinacijami visoko- in nizkonapetostnih pulzov. Pokazali so, da sam kratek visokonapetostni pulz močno poveča prepustnost celičnih membran v tkivu, vendar je bil vnos DNK še vedno zelo nizek. Če je temu sledil še drugi, nizkonapetostni pulz, pa je elektroforetično delovanje povzročilo vnos genskega materiala v celice. Mi smo s

poskusi preverili, ali podobno velja tudi za kožo. Uporabili smo različne elektroporacijske protokole, kjer uporabljamo samo visokonapetostne pulze, samo nizkonapetostne pulze, in pa kombinacijo obojih, ter poizkušali najti parametre pulzov, ki dajejo najvišjo stopnjo izražanja genskega materiala.

#### **1.4.2. Preučevanje kinetike izražanja genov v koži, uporaba za gensko imunizacijo in varnostni vidiki elektroporacije kože**

Moč in trajanje izražanja genskega materiala v tkivu nam kažeta na uporabnost metode za različne aplikacije. Zato smo opazovali odziv na elektroporacijske protokole, ki kombinirajo visoko- in nizkonapetostni pulz, v odvisnosti od časa (1-25 dni po vnosu genov z elektroporacijo). Zanimala nas je tudi uporabnost takšnega protokola za gensko imunizacijo. V literaturi zasledimo protokole, ki so bili v ta namen uporabljeni do sedaj. Učinkovitost le-teh smo primerjali z na novo predlaganimi protokoli (kombinacija visoko- in nizkonapetostnega pulza). Poleg tega se moramo zavedati, da je vsaka klinična metoda uporabna le, če je varna in nima nesprejemljivih stranskih učinkov. Zato smo za detekcijo morebitnih poškodb na koži, ki jih povzroči elektroporacija, uporabili standardne metode za ocenjevanje učinkov kliničnih in ostalih postopkov na koži.

#### **1.4.3. Numerični model elektroporacije kože**

Rezultati eksperimentov kažejo na spremembe specifične prevodnosti tkiva med elektroporacijo. Elektropermeabilizacijo tkiva smo opisali z numeričnim modelom, pri čemer smo uporabili geometrijo tkiva in elektrod ter parametre pulzov iz prej omenjenih poskusov *in vivo*. Meritve toka in napetosti med dovajanjem pulzov so nam služile pri izgradnji modela, saj morata biti odziv modela ter vrednosti toka in napetosti, izmerjene med poskusi, čim bolj enaka. Model kože je numerično dokaj zapleten, saj je koža sestavljena iz več plasti, ki pa se med seboj močno razlikujejo po debelini in električnih lastnostih. Ob aplikaciji pulzov je na začetku praktično celoten padec napetosti na najbolj zunanji plasti povrhnjice, *stratum corneum*-u, zaradi njene izredno visoke upornosti. Šele kasneje se zaradi sprememb upornosti tkiva električno polje seli proti nižje ležečim plastem.

#### **1.4.4. Preučevanje vpliva različnih geometrij elektrod na učinkovitost elektroporacije**

Danes je za vnos genov v kožo najbolj razširjena uporaba zunanjih ploščatih elektrod različnih geometrij (ploskovne, paralelne...). Uporabljajo se tudi za vnos zdravilnih učinkovin skozi kožo in zdravljenje podkožnih tumorjev. Vendar mora biti pri uporabi zunanjih elektrod amplituda električnih pulzov zadosti visoka, da električno "predremo" zaščitno funkcijo kože, kar lahko povzroči blažje opekline in bolečine za bolnika. Zato je v zadnjem času vedno več dela posvečenega razvoju nebolečih mikroelektrod. Če namreč želimo premostiti visoko upornost in neprepustnost kože, zadošča, da predremo le tanko zunanjo plast, *stratum corneum*, debeline okoli 20  $\mu\text{m}$ . Ob tem ne čutimo bolečine, saj v zgornji plasti kože ni živčnih končičev. Z numeričnimi modeli smo zato naredili uvodno primerjavo med različnimi postavitvami polja votlih mikro-igel, ki služijo kot mikroelektrode in bi hkrati omogočile vnos DNK v kožo.

## 2. Metodologija

### 2.1. Vnos in izražanje genov v koži po elektroporaciji *in vivo*

Učinkovitost vnosa genov v kožo z elektroporacijo smo vrednotili z dvema reporterskima genoma, pCMVluc in pCMVGFP. Plazmide smo vnesli intradermalno, 30 sekund pred dovajanjem električnih pulzov. Pri poskusih smo uporabljali laboratorijske podgane Wistar (poskusi so bili opravljeni na Université Catholique de Louvain, Belgija, z dovoljenjem etične komisije za poskuse na živalih), stare od 8-10 tednov. Dlake na hrbtu živali smo odstranili dva dni pred poskusi, zaradi lažjega injiciranja plazmida in dovajanja pulzov. Pred eksperimenti smo živali anestezirali. Kvalitativne podatke o uspešnosti vnosa genov smo dobili z lokalizacijo GFP gena v koži s konfokalno mikroskopijo, kvantitativne podatke pa z merjenjem fluorescence, ki je posledica izražanja gena luciferaze.

Za dovajanje pulzov smo uporabili klinični elektroporator CLINIPORATOR. Med dovajanjem pulzov smo merili napetost in tok; tako dobljen profil spreminjanja specifične prevodnosti tkiva pa smo kasneje uporabili pri gradnji modela. Parametre pulzov smo spreminjali in tako poizkušali najti kombinacijo, ki nam da najboljše rezultate. Uporabljali smo kombinacijo kratkega pulza visoke napetosti in dolgega pulza nizke napetosti, ki se je pri vnosu genov v mišico izkazala za uspešno, in primerjali predlagane protokole z elektroporacijskimi protokoli, ki jih zasledimo v literaturi (vlak kratkih visokonapetostnih ali dolgih nizkonapetostnih pulzov). Za dovajanje pulzov smo uporabljali ploščate elektrode z razmikom med ploščama 4 mm in površino plošč v kontaktu s kožo približno 1 cm<sup>2</sup>. Za doseg dobrega stika med kožo in elektrodama smo uporabili prevodni gel.

Naredili smo tudi kinetično študijo, kjer smo opazovali trajanje izražanja plazmida luciferaze v koži. Odziv na elektroporacijski protokol, ki kombinira visoko- in nizkonapetostni pulz, smo opazovali 1-25 dni po vnosu genov.

### 2.2. Ostale študije *in vivo*

Opazovali smo imunski odziv po vnosu plazmida, ki kodira imunogeni protein, antigen ovalbumin (pcDNA3.1-OVA). Plazmid, ki kodira ovalbumin, in pa tudi sam ovalbumin smo intradermalno vbrizgali 6 tednov starim laboratorijskim mišim Balb/c (poskusi so bili opravljeni na Université Catholique de Louvain, Belgija, z dovoljenjem etične komisije za poskuse na živalih). Dlake na hrbtu živali smo odstranili 1-2 dni pred poskusi, zaradi lažjega injiciranja plazmida in dovajanja pulzov. Pred eksperimenti smo živali anestezirali. Za dovajanje pulzov smo uporabljali CLINIPORATOR in ploščate elektrode z razmikom med ploščama 2,5 mm in površino plošč v kontaktu s kožo približno 1 cm<sup>2</sup>. Za doseg dobrega stika med kožo in elektrodama smo uporabili prevodni gel. Primerjali smo imunске odzive ob uporabi predlaganih elektroporacijskih protokolov kombinacije visoko- in nizkonapetostnega pulza, in tistih, ki jih najdemo v literaturi. Po prvi imunizaciji smo izvedli še dve sekundarni in sicer dva in štiri tedne kasneje. Imunski odziv smo izmerili z metodo ELISA.

Morebitne stranske učinke elektroporacije kože smo ocenili s standardnimi metodami za merjenje učinkov kliničnih in ostalih postopkov na koži. Za ocenitev poškodb kože smo uporabili neinvazivni metodi, ki merita rdečico kože (angleško *chromametry*) ter izgubo vlage skozi kožo zaradi morebitne zmanjšane zaščitne funkcije kože (angleško *transepidermal water loss*). Meritve smo izvedli pred, takoj po aplikaciji pulzov, 30, 60, 120 minut ter 24 ur kasneje. Poleg tega smo histološko ocenili morebitno spremenjeno strukturo kože. V ta namen smo tkivo en teden fiksirali v 4% raztopini formalina, ga obdali s parafinskim voskom in narezali na 3  $\mu\text{m}$  debele rezine pravokotno na površino kože. V histoloških preparatih smo iskali morebitna vnetja ali nekrozo tkiva.

### 2.3. Numerični izračuni

Na področju bioelektromagnetike predstavljajo numerični izračuni porazdelitev električnih tokov in elektromagnetnih polj znotraj bioloških sistemov pomembno orodje za analizo in razlago kompleksnih dogajanj v bioloških sistemih. Z numeričnimi izračuni porazdelitve električnih tokov in elektromagnetnih polj lahko ovrednotimo različne električne pogoje (velikosti tokov oziroma napetosti, velikosti in smeri polj, geometrijo elektrod,...). Eksperimentiranje na modelih je namreč lažje kot na realnih bioloških sistemih, kjer v nekaterih primerih sploh ni mogoče oziroma je nedopustno. Spreminjanje vzbujanja je poenostavljeno, saj gre le za spremembe robnih oziroma začetnih pogojev na istem modelu; le začetna faza – izgradnja modela – zahteva precej časa, natančnosti in izkušenj. Dober model, verificiran z rezultati meritev, zato nudi zelo široke možnosti uporabe. Kljub temu se moramo zavedati dejstva, da imamo opravka z zelo poenostavljeno sliko realnih razmer. Numerični izračuni ne morejo nadomestiti eksperimentalnega dela, ampak služijo kot vir dodatnih informacij za osvetlitev dogajanj in načrtovanje eksperimentov. Do enostavnih analitičnih izračunov porazdelitve elektromagnetnih polj pridemo samo v primerih, ko lahko geometrijo, nehomogenosti in anizotropnosti materialov ter robne pogoje opišemo v izbranem koordinatnem sistemu (npr. kartezičnem, cilindričnem ali sferičnem). V nasprotju s tem numerične metode reševanja večinoma omogočajo približevanje dejanskim oblikam in robnim pogojem. Pri večini numeričnih metod je mogoče definirati nehomogenosti materiala in pri nekaterih tudi anizotropnosti. Za večino bioloških sistemov so značilne zapletene in nepravilne geometrije ter nehomogenosti in anizotropnosti materialov, kar kaže na nujnost uporabe numeričnih metod v tovrstnih raziskavah.

Metoda končnih elementov se je v naših predhodnih raziskavah izkazala za zelo učinkovito pri številnih izračunih porazdelitve električnega polja znotraj bioloških struktur. Bistvo metode je v razdelitvi geometrije, ki jo modeliramo, v manjše sestavne dele - končne elemente. Iskane veličine se znotraj elementov spreminjajo kot funkcije polinomov nižjega reda, odvisno od vrste elementa. Materialne lastnosti pa so znotraj elementov homogene. V področjih, kjer pričakujemo dinamično spreminjanje računanih veličin, je ponavadi potrebno postaviti gostejšo mrežo, prav tako tudi v področjih, kjer nas porazdelitve električnega polja še posebej zanimajo. Mreža mora biti gostejša tudi v področjih okoli meje med dvema materialoma, katerih snovne lastnosti se močno razlikujejo. Slabo zgrajena mreža končnih elementov je najpogostejši vzrok za slab izračun, zato je treba gradnji mreže posvetiti še posebno pozornost. Eden od

najosnovnejših postopkov preverjanja modela, ki ga običajno opravimo na samem začetku raziskave, je gostitev mreže v opazovanih področjih (na primer znotraj tumorja ali v okolici elektrod). Če se pri gostejši mreži rezultati bistveno ne spremenijo, je gostota mreže ustrezna. Gradnja mreže je močno poenostavljena pri modelih, katerih geometrija je pravilne ali simetrične oblike. Z definiranjem osi oziroma ravnin simetrije se zmanjša tudi potrebno število končnih elementov in s tem močno poenostavi in skrajša izračun.

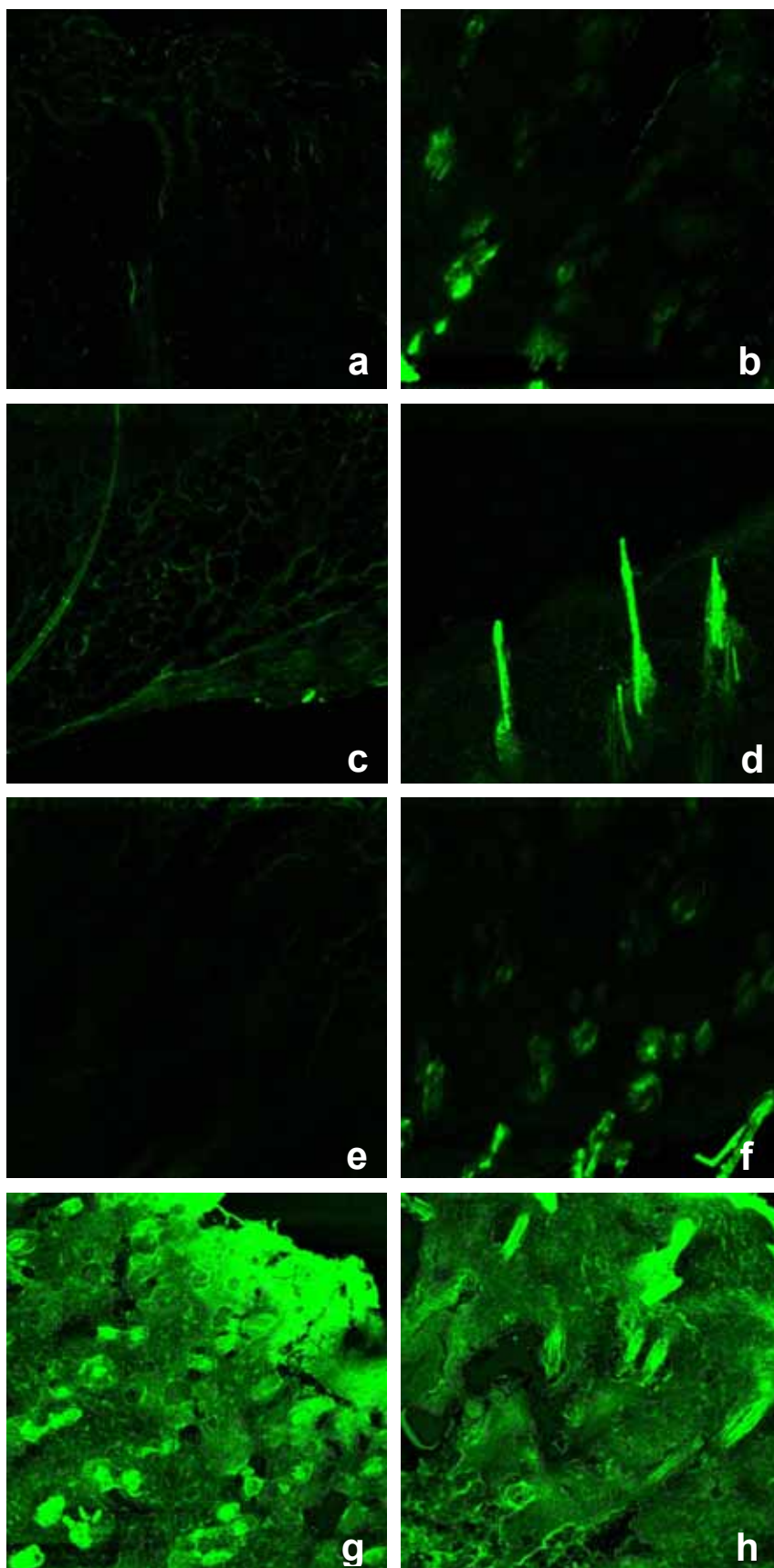
Proces elektropermeabilizacije tkiva smo modelirali z nelinearnim numeričnim modelom upoštevajoč spremembo specifičnih prevodnosti plasti kože zaradi permeabiliziranosti tkiva. Na začetku procesa elektropermeabilizacije kože je praktično celoten padec napetosti na najmanj prevodni plasti, *stratum corneum*-u, šele kasneje se električno polje "seli" v nižje ležeče plasti, zaradi spreminjanja električnih prevodnosti v modelu. Ob prekoračitvi praga permeabilizacije se električne prevodnosti plasti kože spreminjajo, to pa vpliva na porazdelitev električnega polja. Izračun je iterativen in se zaključí, ko električna poljska jakost doseže stacionarno stanje. Numerične izračune smo izvedli s programskim orodjem COMSOL Multiphysics.

### 3. Rezultati raziskav *in vivo*

Z opravljenimi raziskavami *in vivo* smo pokazali učinkovitost kombinacije elektroporacijskega kratkega visokonapetostnega (HV – *high voltage*) in elektroforetičnega dolgega nizkonapetostnega pulza (LV – *low voltage*) za vnos genov v kožo. Rezultati raziskav so bili objavljeni v članku, ki ga podajamo na koncu doktorske disertacije (*Appendix, Paper 3*).

V prvem delu smo preučevali lokalizacijo genskega izražanja z genom, ki kodira protein GFP (angleško *green fluorescent protein*). Uporabili smo tri različne HV+LV protokole (HV: 400 V, 100  $\mu$ s + LV: 32, 56 ali 80 V, 400 ms), ter jih primerjali s kontrolnimi skupinami, kjer smo uporabili le en HV pulz (400 V, 100  $\mu$ s), le en LV pulz (80 V, 400 ms), samo intradermalni vnos plazmida brez elektroporacije, vse to pa smo primerjali tudi z naravno fluorescenco kože. Izražanje v *dermis*-u in *epidermis*-u smo opazovali s konfokalnim mikroskopom in sicer anodno in katodno stran posebej. Slika i prikazuje izbrane slike izražanja GFP za različne elektroporacijske protokole.

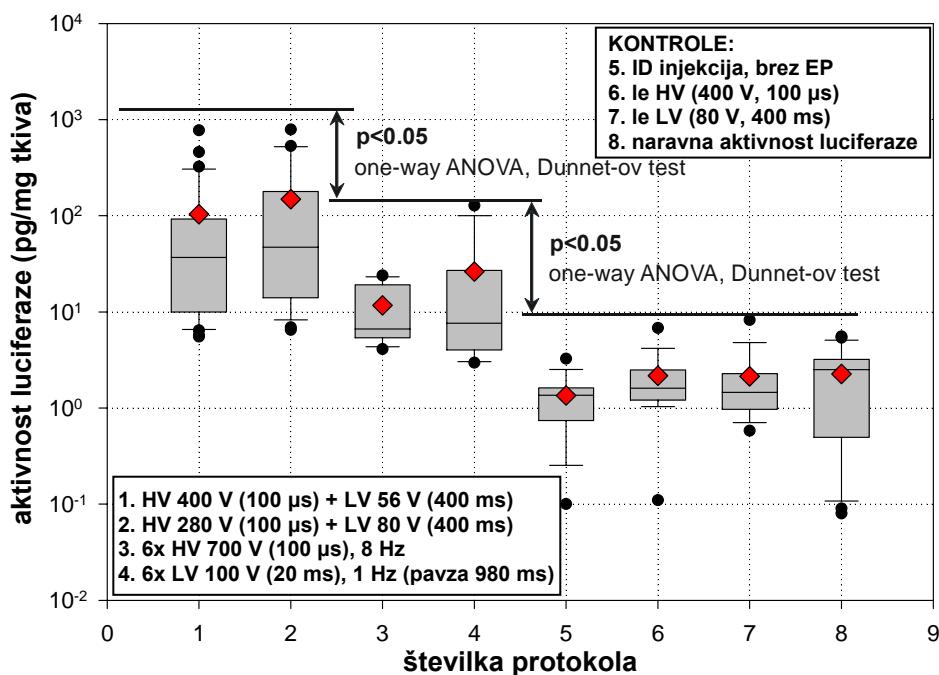
Rezultati kažejo, da pri uporabi le enega HV (Slika i c,d)) ali le enega LV pulza (Slika i e,f)) izražanje v *dermis*-u in *epidermis*-u ostane nizko, opazimo le avtofluorescenco lasnih mešičkov. Fluorescenca po uporabi le HV ali le LV pulza je primerljiva s fluorescenco po intradermalnem vnosu plazmida brez elektroporacije (Slika i a,b)) in naravno fluorescenco kože (slike so prikazane v glavnem delu besedila, v podpoglavju 4.2.2.). Uporaba kombinacije HV in LV pulza pa izražanje močno poveča (Slika i g,h)). Če primerjamo anodno in katodno stran elektroporacijskega vzorca, opazimo konsistentno nekoliko višje izražanje na anodni strani (slike so prikazane v glavnem delu besedila, v podpoglavju 4.2.2.). Razlog za to je najbrž negativen naboj DNK verige, zaradi česar molekule DNK od negativne elektrode (katode) migrirajo proti pozitivni elektrodi (anodi), kjer opazimo višje izražanje.



**Slika i: Fluorescenca kože zaradi izražave gena, ki kodira protein GFP, po različnih elektroporacijskih protokolih: slike a,c,e,g) prikazujejo izražanje v dermisu; b,d,f,h) epidermis. a,b) samo intradermalni vnos plazmida, brez elektroporacije; c,d) samo HV pulz (400 V, 100  $\mu$ s); e,f) samo LV pulz (80 V, 400 ms); g,h) HV: 400 V, 100  $\mu$ s + LV: 56 V, 400 ms**

Kvantitativne podatke o uspešnosti vnosa genov smo dobili s pomočjo reporterskega gena luciferaza. Preizkušali smo različne amplitude visokonapetostnega (HV) in nizkonapetostnega pulza (LV), preučevali vpliv razbitja daljšega LV pulza na osem krajših, ter vpliv zakasnitve LV pulza za HV pulzom. Na koncu smo predlagane HV+LV protokole primerjali s protokoli, ki jih zasledimo v literaturi (6xHV pulz ali 6xLV pulz).

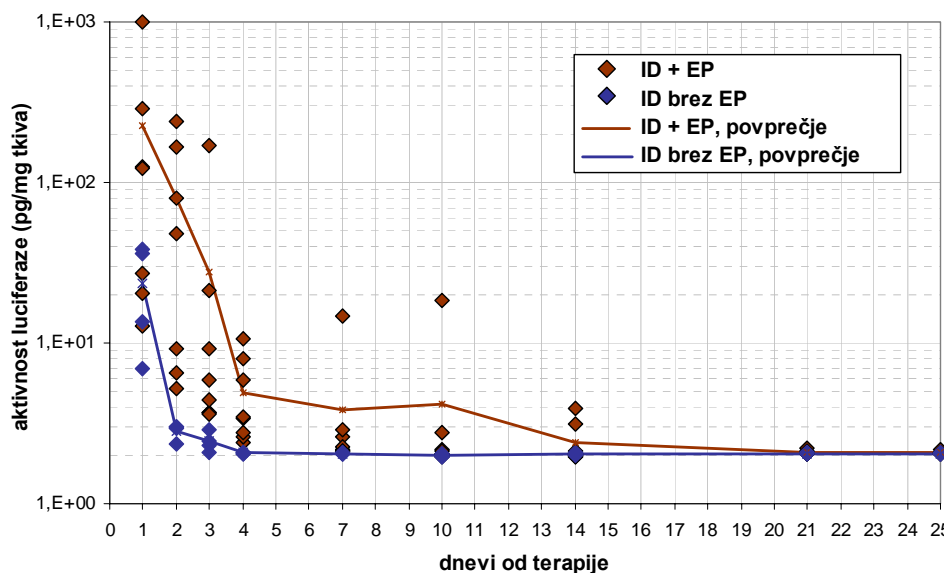
Slika ii prikazuje primerjavo izražanja luciferaze v koži po uporabi obojih, skupaj s kontrolnimi skupinami (intradermalna injekcija brez elektroporacije, le en HV, le en LV, naravna aktivnost luciferaze). Statistična obdelava podatkov pokaže značilno razliko med predlaganimi protokoli, protokoli iz literature in kontrolnimi skupinami. Rezultati kažejo, da je vnos genov bolj uspešen pri uporabi kombinacije visoko in nizkonapetostnega pulza, kot če uporabimo le en HV, en LV, ali pa vlak HV oziroma LV pulzov. Razbitje LV pulza na več krajših in zakasnitev med HV in LV pulzom nista imela značilnega vpliva na izražanje (podatki so prikazani v glavnem delu). Visoka razpršenost rezultatov izražanja luciferaze je najbrž eden od razlogov za to, da med uporabljenimi HV+LV protokoli ni opaziti statistično značilnih razlik. Razpršenost pa je lahko posledica različne debeline kože, različnih bioloških odzivov in nenazadnje neponovljivosti podkožnega vnosa plazmida in geometrije kožne gube.



Slika ii: Primerjava izbranih HV+LV protokolov s protokoli, ki jih zasledimo v literaturi (6xHV ali 6xLV) ter kontrolnimi skupinami (ID injekcija brez elektroporacije, le en HV, le en LV, naravna aktivnost). Podatki so prikazani s 25-im in 75-im percentilom (siv okvir), mediano (horizontalna črta znotraj sivga okvirja) črtice v podaljšku označujejo 10-i in 90-i percentil. Črne pike so podatki, ki ležijo zunaj tega. Z rdečo so označene povprečne vrednosti vsake skupine.

Kinetična študija, v kateri smo opazovali trajanje izražanja luciferaze v koži in sicer 1-25 dni po vnosu genov z elektroporacijo, je pokazala kratkotrajno prisotnost proteina (Slika iii). Izražanje je bilo najvišje 24-48 ur po vnosu genov, potem pa je

naglo upadlo proti kontrolnim vrednostim (samo intradermalni vnos plazmida, brez elektroporacije). Vnos genov v kožo z elektroporacijo je tako bolj primeren za aplikacije, kjer ne potrebujemo dolgotrajne prisotnosti proteina ali je kratkotrajna prisotnost celo zaželena (imunizacija, lokalno zdravljenje tumorjev).



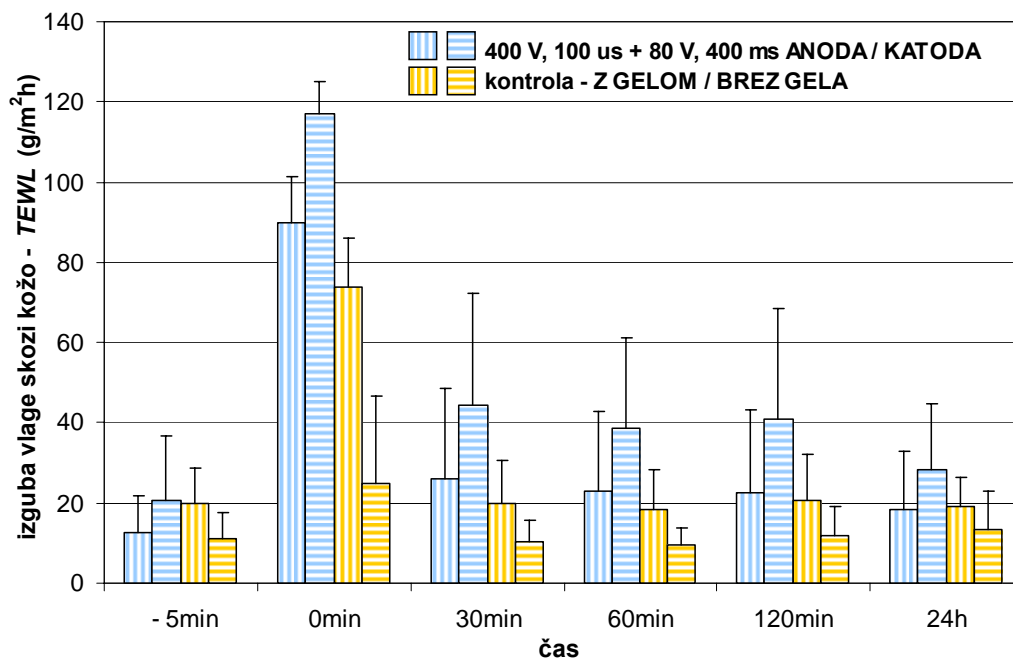
**Slika iii:** Kinetika izražanja gena luciferaze v koži po intradermalnem vnosu 50 µg plazmida pCMVluc. Z rdečo je označeno izražanje v vzorcih pri katerih je vnosu plazmida sledila elektroporacija (280 V, 100 µs + 80 V, 400 ms); modra pa označuje vzorce, ki niso bili podvrženi elektroporaciji. Črti označujeta povprečne vrednosti.

Kombinacijo HV+LV pulza smo uporabili tudi za gensko imunizacijo kože, pri kateri smo uporabljali plazmid, ki kodira antigen ovalbumin (pcDNA 3.1-OVA), ter naše protokole primerjali s protokoli iz literature. Temu smo dodali 4 kontrolne skupine: v prvi intradermalnemu vnosu plazmida ni sledila elektroporacija; v drugi smo namesto plazmida vnašali sam antigen ovalbumin; v tretji smo antigenu dodali pomagalo alum; v četrti pa smo intradermalno vbrizgali fosfatni pufer (angleško *phosphate buffered saline* – PBS). Imunizacijo smo ponovili 2 in 4 tedne po primarni imunizaciji; vzorce krvi pa smo odvzeli 2, 4 in 6 tednov po primarni imunizaciji.

Imunski odziv smo dosegli v vseh skupinah razen tiste, v kateri smo uporabili PBS. Elektroporacija je pozitivno vplivala na imunski odziv po vnosu plazmida, ki kodira antigen ovalbumin. HV+LV protokoli so bili pri tem uspešnejši kot vlak šestih kratkih visokonapetostnih pulzov. Imunski odziv skupin, kjer je vnosu plazmida sledila elektroporacija s HV+LV protokoli, je bil primerljiv z imunskim odzivom skupine, ki je bila imunizirana z antigenom ovalbumin, a nekoliko nižji od imunskega odziva skupine, ki smo jo imunizirali s kombinacijo ovalbumin+alum.

Stranske učinke elektroporacije kože smo ocenili z dvema neinvazivnima metodama, kjer smo opazovali spremembe barve kože (angleško *chromametry*) in izgubo vlage skozi kožo (angleško *transepidermal water loss* – TEWL). S histološkimi preparati pa smo ocenili morebitno spremenjeno strukturo kože. Skupino, ki je bila podvržena elektroporaciji (po intradermalnem vnosu PBS-a), smo primerjali s kontrolnima skupinama. V prvi smo na kožno gubo postavili elektrode, brez nanosa prevodnega gela, za tako dolgo, kot traja elektroporacijski protokol, vendar pulzov

nismo dovedli. V drugi kontrolni skupini pa smo poleg tega nanesli še prevodni gel. Anodno in katodno stran smo opazovali posebej, saj smo opazili razliko tudi pri izražavi gena GFP. Opazili smo dvig v vrednostih TEWL takoj po elektroporaciji, a je bila sprememba kratkotrajna (30 min), velik del te spremembe pa lahko pripišemo izparevanju vlage zaradi prevodnega gela, saj so bile tudi kontrolne vrednosti precej visoke (Slika iv).



Slika iv: Izguba vlage skozi kožo (*transepidermal water loss* – TEWL) izpostavljeno elektroporaciji s kombinacijo HV+LV pulza v odvisnosti od časa preteklega po dovajanju pulzov.

Konsistentno smo opazili tudi nekoliko nižje vrednosti TEWL na anodni strani kožne gube. Razloga za to ne poznamo, lahko pa so te razlike povezane z razlikami v koncentraciji ionov v koži med anodno in katodno stranjo. Kromameter ni pokazal rdečice na koži po dovajanju električnih pulzov, čeprav je bila le-ta nekaj minut po elektroporaciji vidna. Razlog za to je po vsej verjetnosti zmanjšanje prekrvavitve tkiva tik po elektroporaciji. Vseeno pa je bila rdečica blaga in kratkotrajna. Prav tako histološki preparati niso pokazali nobenih strukturnih poškodb na koži.

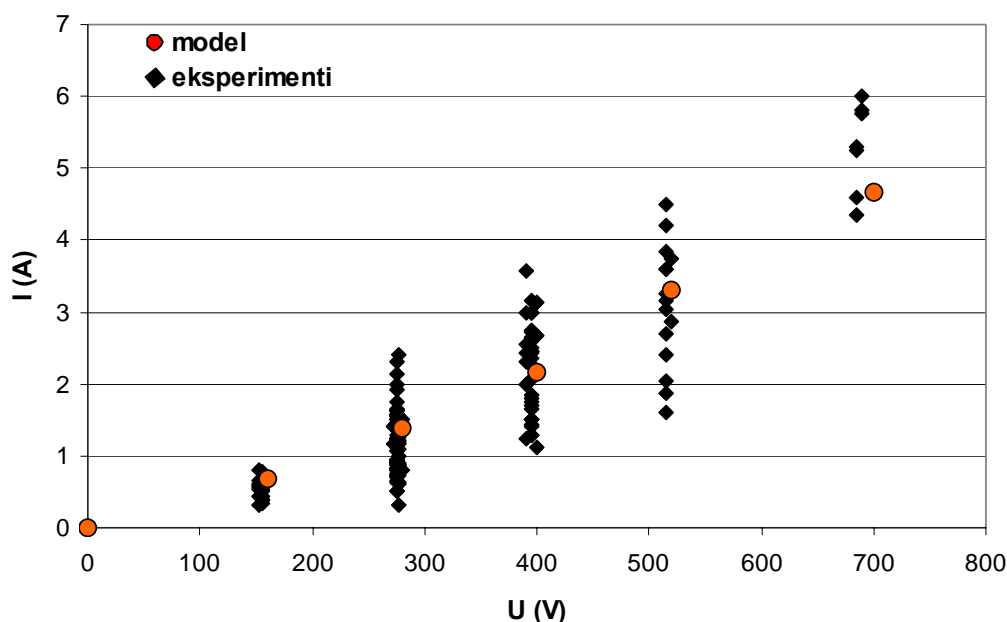
## 4. Numerični modeli

### 4.1. Model elektropermeabilizacije kožne gube

Geometrijo modela kožne gube smo zgradili kar se da podobno eksperimentalnim razmeram, pri čemer smo modelirali različne plasti kože ter upoštevali prisotnost prevodnega gela med dovajanjem pulzov, kar nekoliko poveča površino stika kože in elektrod. V numeričnem modelu smo zgradili le četrtino geometrije kožne gube, saj zaradi simetrije modela s pravilno postavitvijo robnih pogojev dobimo enak rezultat, kot bi ga dobili z modeliranjem celotne geometrije, hkrati pa močno skrajšamo čas računanja.

Vnos reporterskega gena, ki kodira protein GFP, je pokazal izražanje gena v *epidermis*-u in *dermis*-u, kljub visoki električni upornosti zunanje plasti kože, *stratum corneum*-a. Razlog za to leži v spreminjanju električnih upornosti bioloških tkiv, podvrženih elektropermeabilizaciji. Zato smo z metodo končnih elementov proces elektropermeabilizacije modelirali kot nelinearen proces, pri katerem je specifična prevodnost tkiva odvisna od izhoda iz modela – električne poljske jakosti. Pri tem smo potrebovali podatke o začetnih vrednostih specifičnih prevodnosti plasti kože in njihovih spremembah zaradi elektropermeabilizacije, ter pragovnih vrednostih električnega polja, pri katerih je tkivo reverzibilno oziroma ireverzibilno permeabilizirano. Pomagali smo si z literaturo in rezultati meritev na kožni gubi.

Za vzbujanje modela smo uporabili amplitude napetosti, ki smo jih uporabili za permeabilizirni visokonapetostni pulz v naših *in vivo* raziskavah. Namreč, modelirali smo proces elektropermeabilizacije, ki nastopi znotraj 100  $\mu$ s, kolikor traja visokonapetostni pulz, pri čemer smo zanemarili proces celjenja por v membrani celic, ki nastopi že med dovajanjem pulzov. Prav tako nismo modelirali procesa elektroforeze med dovajanjem dolgega nizkonapetostnega pulza. Podatke o napetosti in toku, ki smo jih merili med dovajanjem pulzov, smo uporabili za primerjavo odziva modela z odzivom realnega sistema. Ugotovili smo dobro ujemanje električnih tokov med modelom in eksperimenti (Slika v). Prav tako porazdelitve električne poljske jakosti v modelu kažejo na ujemanje z eksperimenti, saj teoretična permeabilizacija v modelu nastopi pri istih amplitudah pulzov kot uspešen vnos genov *in vivo* (podatki prikazani v glavnem delu besedila). Opazili smo tudi dobro ujemanje s podatki iz literature.



Slika v: Tokovi, izmerjeni med dovajanjem visokonapetostnih pulzov, ter električni tokovi modela v odvisnosti od amplitude pulzov.

## 4.2. Model elektropermeabilizacije kože z vključenimi lokalnimi transportnimi področji

S poskusi drugih avtorjev je bilo pokazano, da sprememba prevodnosti *stratum corneum*-a ni homogena po celi površini podvrženi elektroporaciji. Namesto tega se v koži pojavijo tako imenovana lokalna transportna področja (angleško *local transport regions – LTRs*), mesta kjer je opaziti močno povečanje električne prevodnosti in transport molekul ter ionov v kožo. Velikost teh področij je odvisna od trajanja pulzov, amplituda pulzov pa vpliva na njihovo gostoto.

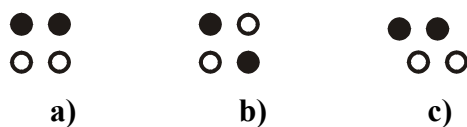
Zgradili smo numerični model kože, pri katerem smo v *stratum corneum* vključili lokalna transportna področja. Za osnovo smo vzeli geometrijo modela kožne gube iz prejšnjega podpoglavja, vendar pa smo za model z lokalnimi transportnimi področji vzeli le rezino kožne gube, in s postavitvijo periodičnih robnih pogojev modelirali celotno področje med elektrodama. Tako smo zmanjšali zapletenost numeričnega modela, ki jo prinese vključitev lokalnih transportnih področij v strukturo *stratum corneum*-a. Podatke o velikosti, gostoti in električni prevodnosti lokalnih transportnih področij, ki nastanejo kot posledica kratkih visokonapetostnih pulzov, smo vzeli iz literature.

Proces elektropermeabilizacije smo v ostalih plasteh kože, razen v *stratum corneum*-u tudi tu modelirali kot nelinearen proces, pri katerem je specifična prevodnost tkiva odvisna od izhoda iz modela – električne poljske jakosti. Uporabili smo enake začetne vrednosti specifičnih prevodnosti plasti kože, njihove spremembe med elektropermeabilizacijo tkiva in pragovne vrednosti električnega polja kot pri modelu opisanem v prejšnjem podpoglavju.

Za vzbujanje modela smo tudi tu uporabili amplitude napetosti visokonapetostnega pulza iz naših *in vivo* raziskav. V modelu z vključenimi lokalnimi transportnimi področji uspešna permeabilizacija tkiva nastopi pri nekoliko višjih amplitudah napetosti kot pri modelu kožne gube in eksperimentih *in vivo*, tok skozi model pa je približno 1,7x nižji. Ker smo si podatke o velikosti, gostoti in prevodnosti lokalnih transportnih področij sposodili od drugih avtorjev, ki so uporabljali tako drugačne elektroporacijske protokole kot tudi drugačno postavitev elektrod na tkivo, lahko to označimo kot dobro ujemanje obeh modelov in eksperimentov *in vivo*.

## 4.3. Modeli polja mikroelektrod

Modelirali smo tri različne postavitve polja mikroelektrod, pri čemer je bila dimenzija polja pri vseh treh 10x10 elektrod; razdalja med posameznimi elektrodami je bila 1 mm. Osnovno geometrijsko celico linijske, prekrižane in šestkotne postavitve kaže Slika vi kjer črne in bele točke pomenijo mikroelektrode različnih polaritet. Prav tako kot pri kožni gubi, smo tudi v modelih polja mikroelektrod upoštevali spremembe specifičnih prevodnosti med procesom elektropermeabilizacije, vendar pa tu nismo modelirali različnih plasti kože – koža je bila modelirana kot homogeno tkivo. S pravilno postavitvijo robnih pogojev smo model močno poenostavili, saj nam zaradi simetrije in periodičnih robnih pogojev ni potrebno modelirati vseh 100 elektrod.



Slika vi: Osnovna geometrijska celica a) linijske, b) prekrižane in c) šestkotne postavitve polja mikroelektrod.

Po primerjanju porazdelitev električnih poljskih jakosti in tokov različnih postavitvev polja mikroelektrod opazimo, da je delež tkiva, v katerem je vrednost električne poljske jakosti med pragoma reverzibilne in ireverzibilne permeabilizacije, najmanjši pri linijski in večji pri prekrižani in šestkotni postavitvi, vendar pa so te razlike majhne. Vseeno pa se zdita prekrižana in šestkotna postavitvev bolj primerni, saj so področja permeabiliziranega tkiva bolj simetrično porazdeljena okoli elektrod kot pri linijski postavitvi.

Čeprav zaradi odsotnosti eksperimentalnih podatkov modelov nismo uspeli ovrednotiti, prva primerjava z modelom kožne gube kaže na bolj enakomerno porazdelitev permeabiliziranih področij. Za uspešno permeabilizacijo nižjih plasti kože - in s tem vnos genov v kožo - so potrebne manjše napetosti, saj nam *stratum corneum*-a ni potrebno predreti električno, temveč fizično.

## 5. Izvirni prispevki k znanosti

- **Uporaba kombinacije visoko- in nizkonapetostnega pulza za učinkovit elektroporacijski vnos genov v kožo**

Za mišično tkivo so s poskusi pokazali, da s kombinacijo kratkega, visokonapetostnega elektroporacijskega pulza, ki mu sledi dolg, nizkonapetostni elektroforetični pulz, dosežemo uspešen vnos genov. S pomočjo dveh reporterskih genov smo izmerili izražanje genskega materiala v koži po uporabi različnih elektroporacijskih protokolov, kjer smo uporabljali samo visokonapetostne pulze, samo nizkonapetostne pulze ali pa kombinacijo obojih. Pokazali smo, da slednji bistveno povečajo izražanje genov v koži.

- **Metode vrednotenja kinetike izražanja genskega materiala v koži in varnostni vidiki elektroporacije kože**

Moč in trajanje izražanja genskega materiala v tkivu nam kaže na uporabnost metode za različne aplikacije. Kinetična študija izražanja genov v koži je pokazala, da je vnos genov v kožo z elektroporacijo primeren za aplikacije kot je imunizacija kože, kjer potrebujemo kratkotrajno prisotnost genov. Kombinacijo visoko- in nizkonapetostnega pulza smo v naših raziskavah tudi uspešno uporabili za gensko imunizacijo kože. Nadalje smo s poskusi pokazali, da uporaba predlaganih elektroporacijskih protokolov na koži podgan ne pusti poškodb.

- **Matematični model elektroporacije kože**

Proces elektropermeabilizacije kožnega tkiva smo opisali z numeričnim modelom, ki upošteva spremembe prevodnosti tkiva med elektroporacijo, pri čemer smo uporabljali metodo končnih elementov. V modelu smo uporabili geometrijo tkiva in elektrod ter parametre pulzov iz prej omenjenih poskusov *in vivo*. Po primerjavi rezultatov modela z eksperimenti *in vivo* in podatki iz literature smo ugotovili dobro ujemanje. Tudi drugi model, kjer smo v *stratum corneum* vključili lokalna transportna področja, je pokazal dobre rezultate.

- **Študij vpliva različnih geometrij elektrod na gensko transfekcijo kože z elektroporacijo.**

Danes je za gensko transfekcijo kože z elektroporacijo najbolj razširjena uporaba zunanjih ploščatih elektrod s katerimi visoko upornost *stratum corneum*-a premostimo z zadosti visoko amplitudo pulzov. V zadnjem času pa so v razvoju neboleče igelne mikroelektrode, s katerimi mehansko predremo *stratum corneum*. S pomočjo numeričnih modelov smo naredili uvodno primerjavo med ploščatimi elektrodami in različnimi postavitvami polja votlih mikroelektrod. Rezultati kažejo, da z mikroelektrodami dosežemo bolj enakomerno porazdelitev permeabiliziranih področij ob uporabi nižjih amplitud.



## CHAPTER 1

# Introduction

The biological effects of electromagnetic fields (EMF) have been investigated for many years for possible damaging, diagnostic and therapeutic effects. Concerns have especially been raised over the rise in human exposure to different sources of electromagnetic radiation, such as high voltage lines, antennas used for mobile communications, antennas used for the radio/TV broadcasting and mobile radio systems (e.g., mobile phones).

A large number of diagnostic methods based on electromagnetic fields are successfully used in medicine (x-rays and CT (computerized tomography) scanners, MRI (magnetic resonance imaging), electrocardiograms, electroencephalograms, measurement of electrical properties of tissues for tumor diagnosis...), as well as electromagnetic field based therapies. Historically, electromagnetic fields have been used on patients, successfully or not, to try to relieve pain or cure an illness. An increase in successful EMF-based treatments and therapies was seen in the twentieth century, especially in the last couple of decades (microwave-induced hyperthermia, electro neurostimulation, electric current wound healing, electromagnetic field bone healing, electrochemotherapy, electrogene transfer...) [Rosch and Markov, 2004].

### 1.1. Electroporabilization of cells

A biological cell is the structural and functional unit of all living organisms. Some organisms, such as bacteria, are unicellular, consisting of a single cell. Other organisms, such as humans, are multicellular. The cytoplasm of a eukaryotic cell is surrounded by a cell membrane. This membrane serves to separate and protect a cell from its surrounding environment and is made mostly from a double layer of lipids and proteins. A variety of other molecules are embedded within the membrane which act as channels and pumps, moving different molecules in and out of the cell. The cell membrane serves as the interface between the interior of the cell and the extracellular fluid that bathes all cells.

A cell membrane is, in general, impermeable for larger molecules; however, the application of electric pulses to cells, either in suspension or in tissue, causes structural

changes in the cell membrane [Tsong, 1991; Barnett and Weaver, 1991; Chizmadzhev *et al.*, 1995; Prausnitz *et al.*, 1995; Weaver and Chizmadzhev, 1996; Teissié *et al.*, 1999]. Cell electropermeabilization is a phenomenon of transiently permeabilizing the cell membrane due to an increased electric field. Even a short electric pulse of a high enough voltage causes an increased transmembrane potential in the cell membrane. If the pulse is of adequate amplitude, the electric field strength and consequently the transmembrane potential are high enough for cell membrane permeabilization. The increase in permeability of the cell membrane makes it possible for larger molecules that otherwise can not cross the membrane, such as drug molecules or DNA, to enter the cell. After pulsing, the cell membrane reseals provided the applied voltage was not too high to cause permanent cell membrane damage.

Different models exist for explaining of the changes occurring during cell membrane permeabilization [Kotnik, 2000; Tieleman, 2003]; however, none of them has been definitely confirmed by experiments. Even so, enough is known about electropermeabilization at the cell level for it to be successfully used for different applications, most important of which are electrochemotherapy, gene transfection and transdermal drug delivery [Maček-Lebar *et al.*, 1998; Neumann *et al.*, 1999].

The cell membrane is permeabilized when a threshold transmembrane voltage is reached. The critical value for the reversible cell electropermeabilization is believed to be between 200 mV and 1 V [Kinoshita and Tsong, 1977; Teissié and Rols, 1993]. This voltage is superimposed on the resting transmembrane voltage the origin of which arises from the exchange of (mostly) Na<sup>+</sup> and K<sup>+</sup> ions across the cell membrane. It can be understood in terms of an equilibrium potential, which is the membrane voltage at which the voltage force precisely balances the concentration gradient force of an ion. When a cell is placed in an electric field, the differences in the conductivities of the cell membrane, the intracellular and the extracellular medium cause a large gradient of the electric field in the membrane inducing a transmembrane voltage that is superimposed on the resting potential of the membrane [Tekle *et al.*, 1990]. However, if the electric field is further increased, the transmembrane potential might cause irreversible membrane permeabilization, which leads to cell death.

Electropermeabilization of cells and the exogenous molecule cell uptake depends on different factors, some of which have not been fully understood so far: the cell and tissue parameters (tissue conductivity, cell size, shape, density, distribution and interactions between them (some results have been published in Paper 1, Appendix)) [Susil *et al.*, 1998; Kotnik and Miklavčič, 2000; Pavlin *et al.*, 2002; Valič *et al.*, 2003, Valič *et al.*, 2004], pulse parameters (pulse duration, amplitude and number of pulses) [Wolf *et al.*, 1994, Maček-Lebar and Miklavčič, 2001], and the most important parameter, the electric field strength [Prausnitz *et al.*, 1993; Miklavčič *et al.*, 1994]. Since the electric pulse parameters are the only factors affecting cell permeabilization which can be influenced, a wide range of studies have been made in order to find the most successful pulsing protocols for different cell types and applications. Roughly speaking, experiments have shown that the number of pulses and their duration determine the molecular transport across the permeabilized membrane, while the pulse amplitude determines the surface of the membrane that is permeabilized [Rols and Teissié, 1990; Rols and Teissié, 1998; Teissié and Rols, 1993; Canatella *et al.*, 2001]. Since both the electric field strength and its duration are important determining factors in cell electropermeabilization, protocols combining pulses of different amplitudes and durations have been investigated [Mir *et al.*, 1998; Mir *et al.*, 1999; Bureau *et al.*, 2000].

Monitoring cell or tissue permeabilization in real time has been addressed by a number of researchers. The most notable measurable change in the tissue undergoing electric pulsing is an increase in tissue conductivity due to cell membrane electropermeabilization, as well as Joule heating of the tissue [Pliquett *et al.*, 1995; Pliquett and Weaver, 1996; Loste *et al.*, 1998; Davalos *et al.*, 2002; Davalos *et al.*, 2004; Davalos and Rubinsky, 2004; Pliquett *et al.*, 2004]. Namely, when the electric field exceeds the reversible threshold, tissue conductivity increases. This change subsequently causes a change in the electric field distribution and of the corresponding current. To effectively use electroporation in clinical applications, we need to detect whether the target tissue area has been permeabilized. This feedback can then be used to adjust the electroporation parameters during the treatment to make it more efficient. A feasibility study for electrical impedance tomography as a means of monitoring tissue electroporation was conducted [Davalos *et al.*, 2002]. In this preliminary demonstration, the electroporated regions in liver were clearly distinguishable. However, more work needs to be done to bring this technique to clinical practice.

## 1.2. Applications of cell electropermeabilization

Electropermeabilization of the cell membrane, when used properly, can be used on different types of cells, does not affect cell survival and does not disrupt cell functions. Therefore, it can be used for wide range of applications, the most advanced being electrochemotherapy, electrogene transfer and transdermal drug delivery.

### 1.2.1. Electrochemotherapy (ECT)

Chemotherapeutic drugs are aimed at stopping the cell from replicating by inhibiting the synthesis of new DNA strands or by damaging the DNA of the affected cancer cells. The problem in chemotherapy is not as much the efficiency of the drug, as their non-specificity towards healthy cells, acquired tumor resistance to the drug due to genetic mutations of tumor cells, and the high concentrations needed around the target cells due to the low permeability of the cell membrane, which causes unwanted side effects. Chemotherapy, when combined with cell electropermeabilization (the combined treatment is called electrochemotherapy), requires much lower drug doses and provides localized treatment. Permeabilization of cells by electric pulses allows the otherwise non-permeant drug to penetrate into the cells. Lower doses than those required in classical protocols of chemotherapy are needed for a good cytotoxic effect. The first experiments with electrochemotherapy were reported by Okino and Mohri and by Mir in 1987 and 1988, respectively [Okino and Mohri, 1987; Mir *et al.*, 1988; Mir *et al.*, 1991]. Two non-permeant anticancer drugs, bleomycin (most often used in clinical trials) and, to a lesser degree cisplatin, were found to be the most suitable candidates for combined use with electric pulses [Mir and Orłowski, 1999]. *In vitro* experiments showed that the cytotoxicity of bleomycin is potentiated by several hundred times [Poddevin *et al.*, 1991] and the cytotoxicity of cisplatin up to 70 times [Serša *et al.*, 1995]. *In vivo*, anti tumor effectiveness of bleomycin and cisplatin after electropermeabilization of cells is increased several-fold [Mir *et al.*, 1991; Heller *et al.*, 1995; Serša *et al.*, 1995]. Electrochemotherapy has already been successfully applied to mice and rats for a large variety of tumors. Clinical trials have been performed in humans and have demonstrated excellent results in antitumor therapy, especially for treatment of head and neck squamous cell carcinoma, melanoma, basal cell carcinoma and adenocarcinoma [Serša *et al.*, 1995; Heller *et al.*, 1998; Heller *et al.*, 1999; Gehl, 2003; Serša *et al.*, 2003].

### 1.2.2. Electrogene transfer (EGT)

Gene therapy is a technique for correcting defective genes responsible for disease development [Rubanyi, 2001]. In most gene therapy studies, a "normal" gene is inserted into the genome to replace an "abnormal," disease-causing gene. A carrier called a vector must be used to deliver the therapeutic gene to the patient's target cells. With the decoding of the human genome, many believed gene therapy was going to be a revolutionary new technology which will eradicate inherited diseases and treat cancer, heart disease and even infectious diseases. Unfortunately, it was soon discovered that the delivery of therapeutic genes to the target tissue was a serious bottleneck in gene therapy based treatments. Viral vectors, although successful in unloading their genetic material containing the therapeutic human gene into the target cells, pose a safety issue [Ferber, 2001]. Namely, vector interactions with the human immune system could have fatal consequences. In addition, some retroviruses could cause the inactivation of tumor suppressor genes or activation of a proto-oncogene, causing oncogenesis. Therefore, a large portion of the research in this area is aimed at finding an efficient and safe gene delivery method. Different chemical (phospholipids in form of liposomes, calcium phosphate, diethylaminoethyl-dextran...) and physical (direct single injection of DNA, microinjection, ultrasound, iontophoresis, electroporation...) methods have been developed and are being improved [Yang and Sun, 1995; Parker *et al.*, 2003; Mehier-Humbert and Guy, 2005]. Electrogenettransfer is a method using electric pulses to temporarily and reversibly permeabilize the cell membrane and to drive the DNA into the cell electrophoretically [Somari *et al.*, 2000]. This method can be used both *in vivo* and *in vitro* and when a transient (e.g. skin) or long-term (e.g. muscle) transfection is needed. The first study showing an efficient *in vitro* gene transfection by means of electric pulses was published in 1982 [Neumann *et al.*, 1982; Wong and Neumann, 1982]. Promising results led to *in vivo* experiments on tumors, muscle, liver, skin and other organs [Heller *et al.*, 1996; Nishi *et al.*, 1996; Kong and Crystal, 1998; Rols *et al.*, 1998; Gehl and Mir, 1999; Jaroszeski *et al.*, 1999; Mir *et al.*, 1999; Bettan *et al.*, 2000; Payen *et al.*, 2001; Zhang *et al.*, 2002; Kesmodel and Spitz, 2003; Khan *et al.*, 2005; Zampaglione *et al.*, 2005]. Studies showed electrogene transfer works in two stages; permeabilizing the target cells and electrophoretically driving the DNA through the permeabilized cell membrane. Therefore, longer pulses are needed for electrogenettransfer, compared to electrochemotherapy [Mir *et al.*, 1999]. The most recent experiments on muscle tissue proposed the use of a pulsing protocol, consisting of a high-voltage, permeabilizing pulse, followed by a low-voltage, electrophoretic pulse [Mir *et al.*, 1998; Mir *et al.*, 1999; Bureau *et al.*, 2000; Šatkauskas *et al.*, 2002; Šatkauskas *et al.*, 2005]. In electrogene transfer, caution must be taken not to exceed the irreversible electric field value in the target tissue which causes cell death, as gene therapy will be successful only if there are enough viable transfected cells. In contrast, in the case of electrochemotherapy, exceeding the irreversible threshold in a tumor is less problematic, as killing tumor cells is the aim of the treatment.

### 1.2.3. Transdermal drug delivery

Transdermal drug delivery is an approach used to deliver drugs through the skin and into systemic circulation for therapeutic use by means of chemical enhancers, iontophoresis, electroporation, ultrasound [Prausnitz, 1997; Barry, 2001; Prausnitz *et al.*, 2004], as an alternative to oral, intravascular, subcutaneous and transmucosal routes. It is distinct from topical drug penetration, which targets local areas. Only a small number of drug products can be used for transdermal delivery, the most determining factors being a drug's physical properties, including molecular size and polarity, and

biological properties of drug molecules, including dermal irritation and insufficient bioavailability. Transdermal drug delivery offers several important advantages over more traditional dosage forms. First, it is less invasive for the patient than, for example, intravenous injection. Second, the steady permeation of drug across the skin allows for more consistent serum drug levels, which is often a goal of therapy. Transdermal drug delivery can be used as an alternative administration route for patients who cannot tolerate oral dosage forms. Good candidates for transdermal delivery are drugs that may cause gastrointestinal upset and drugs which are degraded by the enzymes and acids in the gastrointestinal system. First pass metabolism, an additional limitation to oral drug delivery, can be avoided with transdermal administration. Also, the accessibility and facilitated monitoring of possible unwanted side effects makes skin an attractive organ for drug delivery. One of the problems to be addressed in transdermal drug delivery is the possibility of local irritation at the application site. However, the biggest disadvantage is the low permeability of the skin which limits the number of drugs that can be delivered in this manner. The protective function of the skin presents a formidable obstacle to transdermal drug delivery. One of the possibilities to temporarily breach the barrier function of skin is using electroporation thereby creating aqueous pathways across lipid-based structures [Vanbever and Pr at, 1995; Prausnitz, 1996; Prausnitz, 1999; Denet and Pr at, 2003; Denet *et al.*, 2004]. Another method using electric current to deliver substances through the skin is iontophoresis. Sweat gland ducts and hair follicles provide preexisting aqueous pathways that potentially allow the passage of water-soluble molecules upon the application of low voltages across the skin. However, the permeation flux provided by iontophoresis is often much lower than desirable. Single lipid bilayers in biological systems have been extensively electroporated, and recently more complex biological barriers, such as frog skin [Powell *et al.*, 1989], containing a monolayer barrier consisting of two bilayer membranes, have been electroporated. For transdermal delivery, the interest lies primarily in electroporating human skin, and this has been done using high voltage pulses resulting in transdermal voltages greater than 50 volts [Pliquett *et al.*, 1995; Pliquett *et al.*, 1998; Pliquett, 1999; Vanbever *et al.*, 1999; Weaver *et al.*, 1999]. This voltage is enough to cause electroporation within the *stratum corneum*, which results in new aqueous pathways. Also, electric current provides a driving force for ionic and molecular transport across the skin.

### 1.3. Skin

Skin covers the entire external surface of the human body and is the principle site of interaction with the surrounding world [Menon, 2002]. It serves as a protective barrier preventing internal tissues from exposure to trauma, ultraviolet radiation, temperature extremes, toxins, and bacteria. Other important functions include sensory perception, immunologic surveillance, thermoregulation, and control of insensible fluid loss.

#### 1.3.1. Skin structure

The skin is the largest organ in the body, comprising about 15% of body weight. The total skin surface of an adult ranges from 1.5 to 2 square meters. In terms of chemical composition, the skin is about 70% water, 25% protein and 2% lipids. The remainder includes trace minerals, nucleic acids, glycosoaminoglycans, proteoglycans and numerous other chemicals. The skin completely renews itself every 3-5 weeks. It consists of three main layers: epidermis, dermis and subcutaneous tissue (Figure 1. 1).

**The epidermis** contains no blood vessels and is entirely dependent on the underlying dermis for nutrient delivery and waste disposal via diffusion through the dermoepidermal junction. The total thickness of the epidermis is usually about 0.5-1 mm. The epidermis consists primarily of keratinocytes in progressive stages of differentiation from deeper to more superficial layers. The named layers of the epidermis include the *stratum germinativum*, *stratum spinosum*, *stratum granulosum*, and *stratum corneum*. The *stratum germinativum* or basal layer is immediately superficial to the dermoepidermal junction. This single cell layer of keratinocytes is attached to the basement membrane. As keratinocytes divide and differentiate, they move from this deeper layer to the more superficial layers. Once they reach the *stratum corneum*, they are fully differentiated keratinocytes devoid of nuclei and are subsequently shed in the process of epidermal turnover. Cells of the *stratum corneum* are the largest and most abundant of the epidermis. This layer ranges in thickness from 15-100 or more cells depending on anatomic location and is the primary protective barrier from the external environment. Melanocytes primarily function to produce a pigment, melanin, which absorbs radiant energy from the sun and protects the skin from the harmful effects of ultraviolet radiation. Melanin accumulates in organelles termed melanosomes that are incorporated into dendrites anchoring the melanosome to the surrounding keratinocytes. Langerhans cells originate from the bone marrow and are found in the basal, spinous, and granular layers of the epidermis. They serve as antigen-presenting cells. They are capable of ingesting foreign antigens, processing them into small peptide fragments, binding them with major histocompatibility complexes, and subsequently presenting them to lymphocytes for activation of the immune system. An example of activation of this component of the immune system is contact hypersensitivity. Merkel cells, derived from neural crest cells, are specialized in the perception of light touch.

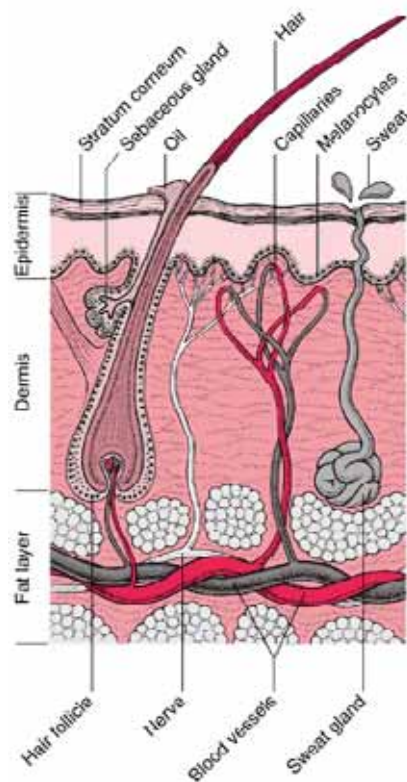


Figure 1. 1: Skin structure

**The dermis** is the middle layer of the skin located between the epidermis and the subcutaneous tissue. It is the thickest of the skin layers and is made mainly of collagen and elastin fibers. The primary function of the dermis is to sustain and support the epidermis. Both collagen and elastin are critically important skin proteins: collagen is responsible for the structural support and elastin for the resilience of the skin. The key type of cells in the dermis is fibroblasts, which synthesize collagen, elastin and other structural molecules. The proper function of fibroblasts is highly important for overall skin health. The dermis also contains capillaries (tiny blood vessels) and lymph nodes (depots of immune cells). The former are important for oxygenating and nourishing the skin, and the latter for protecting it from invading microorganisms. Finally, the dermis contains sebaceous glands, sweat glands and hair follicles as well as a relatively small number of nerve and muscle cells. Sebaceous glands, located around hair follicles, are of particular importance for skin health as they produce sebum, an oily protective substance that lubricates and waterproofs the skin and hair. The dermis is the layer responsible for the skin's structural integrity, elasticity and resilience.

**Subcutaneous tissue** is the innermost layer of the skin located under the dermis and consisting mainly of fat. The predominant type of cells in the subcutaneous tissue is adipocytes or fat cells. Subcutaneous fat acts as a shock absorber and heat insulator, protecting underlying tissues from cold and mechanical trauma. Interestingly, most mammals lack subcutaneous tissue because their fur serves as a shock absorber and heat insulator. Sweat glands and minute muscles attached to hair follicles originate in subcutaneous tissue.

### 1.3.2. The electric properties of the skin

When referring to its electric properties, skin is a very intricate tissue due to its highly inhomogeneous structure, which thus leads to inhomogeneous electric properties. As already mentioned, skin has three different layers: the epidermis, dermis, and the subcutaneous tissue. The epidermis contains different layers, but the one that defines its electric properties the most is the outermost layer, the *stratum corneum*, composed of dead, flat skin cells that shed about every two weeks. Although very thin (typically around 20  $\mu\text{m}$ ), it contributes a great deal to the electric properties of the skin. Its high resistivity makes skin one of the most resistive tissues in the human body. Deeper layers, including the rest of the epidermis (important in the immune response), the dermis (which gives firmness and elasticity) and the subcutaneous tissue (fat, connective tissue, larger blood vessels and nerves), all have much lower resistivities [Suchi, 1955; Lawler *et al.*, 1960; Lane, 1974; Yamamoto and Yamamoto, 1976; Yamamoto and Yamamoto, 1976a; Chizmadzhev *et al.*, 1998].

High voltage pulses applied on the skin cause a significant drop in skin resistance of up to three orders of magnitude due to the created pathways for ionic current [Prausnitz *et al.*, 1993; Gallo *et al.*, 1997; Pawlowski *et al.*, 1998; Jadoul *et al.*, 1999; Pliquett and Prausnitz, 1999]. If the applied voltage is not too high, partial or full recovery of the skin resistance can be observed within a period of microseconds up to several hours [Pliquett *et al.*, 1995; Pliquett and Weaver, 1996; Gallo *et al.*, 1997; Vanbever *et al.*, 1999]. At the onset of electric pulses, most of the potential drop rests across the highly resistive *stratum corneum*. Consequently, the electric field in that layer is likely to rise above its critical strength, the reversible electroporation threshold, which causes a breakdown of the skin protective function and a drop in its resistance. As a result, the barrier to molecular transport is greatly reduced which facilitates transdermal drug delivery, especially when used in combination with

electrophoretic pulses. Although both electroporation and iontophoresis involve electric pulses, the two are fundamentally different. Namely, while electroporation acts directly on the skin, making transient changes in its permeability, iontophoresis acts on the drug as a driving force transporting it through the skin [Hui, 1998; Banga *et al.*, 1999]. Also, due to the drop in the resistance of the *stratum corneum*, the skin layers lying below *stratum corneum* are subjected to an electric field high enough to permeabilize cells in those layers.

It has been shown that pulses of high voltage create aqueous pathways penetrating the multi-lamellar lipid bilayer membranes of the *stratum corneum*. In this process, adjacent corneocytes become connected, and pathways spanning the *stratum corneum* result. Pulses lasting as short a time as 1 ms cause an increase of up to four orders of magnitude in the transdermal transport of charged molecules up to 1,000 grams/mol (most pharmaceutical compounds fall within this range of sizes). Even larger molecules (e.g. heparin), as well as highly charged ones (antisense oligonucleotides) can be transported across the skin efficiently using electroporation techniques. Transport is believed to be generally localized to small local transport regions (LTRs) [Pliquett *et al.*, 1998; Pliquett, 1999; Vanbever *et al.*, 1999; Weaver *et al.*, 1999; Pliquett and Gusbeth, 2004]. When describing the response of the skin to voltage stimulation, it is useful to categorize the stimulation as low-, medium- or high-voltage [Weaver *et al.*, 1999]. In low-voltage stimulation ( $U_{\text{skin}} < 5 \text{ V}$ ), the mechanism responsible for ionic and molecular transport through the skin is iontophoresis and takes place mainly through preexisting pathways (skin appendages). In moderate-voltage stimulation ( $5 \text{ V} < U_{\text{skin}} < 50 \text{ V}$ ), two parallel pathways are involved: one involving the appendages and the other one crossing the multilamellar lipid bilayers and corneocytes within the *stratum corneum*. High-voltage stimulation ( $U_{\text{skin}} > 50 \text{ V}$ ): The decrease in  $R_{\text{skin}}$  by up to three orders of magnitude is very rapid, typically occurring within a few microseconds. Also the onset of molecular transport is much faster than for iontophoresis. A distinct difference of the skin's response to high-voltage stimulation is highly localized molecular transport. Transport is generally localized to local transport regions (LTRs). For short pulses, typical minimum LTR size is about 100 micrometers in diameter; for longer pulses, the sizes increase up to 300 micrometers. An increase in pulse voltage increases the density of the LTRs but not their size, while longer lasting pulses produce larger LTRs with almost no changes in their density [Vanbever *et al.*, 1999; Pliquett and Gusbeth, 2004]. Also, skin resistance after applying short, high-voltage pulses, drops by up to three orders of magnitude, while for longer, medium-voltage pulses, the drop is up to two orders of magnitude.

### **1.3.3. Electrogene transfection of the skin**

Skin is an attractive target tissue for gene therapy for a variety of reasons. Its size and accessibility facilitates *in vivo* gene delivery. It can be used for the treatment of disorders of the skin or, being a known secretor of a variety of important systemic (blood borne, body-wide) proteins, it can be used for systemic effect to treat diseases of other organs (reference). Skin is also a very good target organ for DNA immunization because of the large number of potent antigen presenting cells, critical to an effective immune response [Drabick *et al.*, 2001; Zhang *et al.*, 2004]. If necessary, large areas of skin can be treated and can easily be monitored for potential complications, such as infection and neoplasia, by observation or biopsy. Beside viral methods that are controversial because of their safety issues, chemical and physical methods have been developed to enhance gene expression in the skin [Glasspool-Malone *et al.*, 2000; Lee

Lucas *et al.*, 2002; Zhang *et al.*, 2002; Mehier-Humbert and Guy, 2005]. Electroporation seems particularly effective to improve DNA transfection after intradermal and topical delivery without any significant alteration of skin structure. Transdermal gene delivery by electroporation consists of topically applying DNA on the skin before electroporation [Dujardin *et al.*, 2000]. Unfortunately, due to the barrier function of the skin, the transfection is rather low and restricted to the epidermis. However, by using intradermal injection in combination with electric pulses, we avoid having to break the protective function of the skin, thus concentrating only on successful permeabilization of target cells for gene transfection.

### 1.3.4. Electrodes for skin electropermeabilization

The efficacy and the sensation during skin electroporation can to some extent be controlled not only by using appropriate electric protocols but also by using electrodes designed for the purpose of either electrogene transfection of the skin, or transdermal drug delivery.

Widely used for transdermal drug delivery by means of iontophoresis are surface electrodes [Zhang and Rabussay, 2002; Denet and Pr at, 2003]. A drug reservoir is placed on the skin under the active electrode with the same charge as the penetrant. An indifferent counter electrode is positioned elsewhere on the body (ref). The active electrode effectively repels the active substance and forces it into the skin. This simple electrorepulsion is known as the main mechanism responsible for penetration enhancement by iontophoresis. The number of charged molecules that are moved across the barrier correlates directly to the applied current and thus can be controlled by the current density. Other factors include the possibility to increase the permeability of the skin barrier in the presence of a flow of electric current and electroosmosis. Contrary to electrorepulsion, electroosmosis can be used to transport uncharged and larger molecules. Electroosmosis results when an electric field is applied to a charged membrane such as the skin and causes a solvent flow across this membrane. This stream of solvent carries dissolved molecules along with it. It enhances the penetration of neutral and especially polar substances.

Plate electrodes are one of the simplest electrode designs for the delivery of pulses to the skin or through the skin to the tissues below [Belehradek *et al.*, 1991; Bureau *et al.*, 2000; Šatkauskas *et al.*, 2002; Pliquett *et al.*, 2004; Šatkauskas *et al.*, 2005] and generate a more uniform electric field between the plates than the surface or the needle versions [Gehl *et al.*, 1999; Gehl and Mir, 2000]. They are suitable for electrochemotherapy of subcutaneous tumors close to the surface [Čemažar *et al.*, 2001], and can be used in applications where skin electropermeabilization is needed. They can be mounted on a caliper and the distance between the plates can easily be adjusted, depending on the size of the tumor or the skin fold. However, high enough voltages to cause the breakdown of the *stratum corneum* have to be applied and concerns regarding possible skin burning have been raised.

Recently, several attempts have been made to enhance the transport of substances across the skin barrier using minimally invasive techniques, focusing on the concept of microneedles [Henry *et al.*, 1998; Davis *et al.*, 2004; Mukerjee *et al.*, 2004; Prausnitz, 2004; Davis *et al.*, 2005]. Namely, for disruption of the skin barrier function only the thickness of the *stratum corneum* (around 20  $\mu\text{m}$ ) has to be breached. Microneedle arrays are applied to the skin surface so that they pierce the upper epidermis far enough to increase skin permeability and allow drug delivery, but too short to cause any pain to

the receptors in the dermis. When hollow microneedles containing DNA are used in combination with electric pulsing, the cells in the deeper skin layers can be permeabilized and transfected.

## **1.4. Objectives of the thesis**

### **1.4.1. The use of the combination of a high and a low-voltage pulse**

The effect different electric parameters and electrode geometries have on the efficacy of the skin gene transfection, has to date not been studied systematically. It has been shown for skeletal muscle tissue that a combination of one short high voltage followed by a long, low voltage pulse, a very successful gene transfection can be achieved [Mir *et al.*, 1998; Mir *et al.*, 1999; Bureau *et al.*, 2000; Šatkauskas *et al.*, 2002; Šatkauskas *et al.*, 2002]. A plasmid, coding for luciferase protein was injected into the muscle and the protein expression was studied, using different treatments using the combination of a high and a low voltage pulse. It has been shown that a high voltage pulse alone results in a high level of tissue permeabilization but unfortunately still a very low DNA transfection in the target tissue. However, if the high voltage pulse is followed by a longer, low voltage electrophoretic pulse, this substantially increases the uptake of the DNA into the cells.

We used a similar protocol for *in vivo* gene transfection in skin. Gene expression by means of two reporter genes after different electroporation protocols was assessed. We compared protocols consisting solely of high voltage pulses, solely of low voltage pulses protocols, and the proposed combination of a high voltage pulse, followed by a low voltage one, and tried to find the most efficient pulse parameters for the latter.

### **1.4.2. Skin gene expression kinetic study, gene immunization by means of electroporation and safety aspects of skin electroporation**

Usefulness of a gene transfection method for different applications depends on the level and duration of the gene expression in the tissue. Therefore the gene expression after using the combination of the high voltage pulse + low voltage pulse was measured from one to twenty-five days after transfection.

Genetic (DNA) immunization is a novel technique used to efficiently stimulate humoral and cellular immune responses to protein antigens. Over the past decade of research and clinical trials, several possible routes of plasmid delivery have been found. Successful immunization of mice has been demonstrated after delivery of plasmids through intramuscular, intradermal and intravenous injection [Drabick *et al.*, 2001; Cui *et al.*, 2003; Lombry *et al.*, 2004; Zhang *et al.*, 2004]. Skin is considered one of the best sites for immunization due to its high concentrations of immuno-competent cells. In our study, the proposed combination of HV+LV pulses was also used for gene immunization. We compared our protocols with the protocols that have been used for gene immunization to date [Glasspool-Malone *et al.*, 2000].

Any treatment can only be used in clinics if it is safe for the patient and has no unacceptable side effects. Electroporation of skin causes electric breakdown of lipid bilayers and consequently skin electric resistance drop by several orders of magnitude. Partial or full recovery can be observed provided that the amplitude of the electric

pulses is not too high. We used standard methods to assess effects of skin treatments to evaluate possible skin damage caused by electroporation [Vanbever *et al.*, 1998; Vanbever and Pr at, 1999; Dujardin *et al.*, 2002; Mathy *et al.*, 2003].

### 1.4.3. Numerical model of skin electroporation

Experiments show that the conductivity of a tissue changes during electroporation [Prausnitz *et al.*, 1993; Pliquett *et al.*, 1995; Pliquett and Weaver, 1996; Gallo *et al.*, 1997; Pawlowski *et al.*, 1998; Jadoul *et al.*, 1999]. We simulated that process with a numerical model of tissue electropermeabilization, modeling tissue and electrode setups and pulse parameters used in the abovementioned experiments. Current and voltage measurements during the delivery of pulses were used to build the model as the output of the model should be as close to the measured data as possible.

Because of the many skin layers with very different electric properties and layer thicknesses, the skin fold model is numerically quite complicated. When the electric field is applied to the skin fold, almost the entire voltage drop is on the outermost layer of the skin called *stratum corneum*, which has the lowest conductivity. However, because of the changes of bulk electric properties of the tissues, electric field “penetrates” to the layers underneath *stratum corneum*. With our model we aimed to describe the electropermeabilization process in the skin, taking into account the changes of bulk electric properties, due to the electropermeabilization of the skin layers.

### 1.4.4. Study of electrode geometries

The most widely used electrodes in gene transfection in the skin are external plate electrodes of different geometries. They are also used for the treatment of the subcutaneous tumors and for transdermal drug delivery. However, using external electrodes, the pulse amplitude has to be sufficiently high in order to cause the electrical breakdown of the skin, which could pose a safety issue and cause discomfort for the patient. Therefore, new electrode geometry for transdermal drug delivery and electrogene transfection in skin was proposed – painless microneedle electrodes [Henry *et al.*, 1998; Davis *et al.*, 2004; Mukerjee *et al.*, 2004; Prausnitz, 2004; Davis *et al.*, 2005]. Namely, in order to breach the high electrical resistance and non-permeability of skin, only its outermost layer, the *stratum corneum* needs to be pierced. The depth of penetration does not exceed 50  $\mu\text{m}$ , which causes no pain for the patient, since epidermis contains no nerves or nerve endings.

A preliminary comparison, by means of numerical models, between different settings of microelectrode arrays was made. The microelectrodes were modeled hollow to be used as microneedles, allowing the DNA to be injected into the skin.



## CHAPTER 2

# Current field and Finite elements method Theory

Numerical modeling of the electric field and the electric current distributions inside the biological systems represent an important field in the study of the effects of the electromagnetic fields on cells, tissues and organs [Šemrov and Miklavčič, 1995; Fear and Stuchly, 1998; Debruin and Krassowska, 1999; Debruin and Krassowska, 1999a; Tungjikusolmun *et al.*, 2000]. It is a relatively simple but powerful tool for the analysis and the explanation of the intricate processes taking place inside the biological systems. Various electrical parameters (current and voltage amplitude, field strength and orientation, electrode geometries...) can be evaluated by means of numerical modeling [Šemrov and Miklavčič, 1998; Brandisky and Daskalov, 1999; Miklavčič *et al.*, 2000; Dev *et al.*, 2003]. Namely, experimenting with such models is easier and sometimes the only possible or ethically acceptable alternative other than experimenting on real biological systems.

In such models, the excitations can be changed easily, being that it only involves changing the boundary conditions on the same model. The model geometry, however, takes time and precision to be built and generalizations and simplifications need to be used where possible. Once built, a good model verified with experimental results can be a powerful tool and can offer useful insight into the understanding of biological processes modeled. However, one has to be aware of the fact that the processes involved are much more complex and the model is merely a simplified representation that can not replace experimental work. Still, it helps us as a source of extra information and helps us to plan future *in vivo* experiments.

Analytical methods used to be the only option for theoretic studying of the effects of electromagnetic fields on biological systems. They are rather complicated and are only feasible for use on problems where the geometry, material properties and boundary conditions can be described in a defined coordinate system (like Cartesian, cylindrical or polar). In the last decades, however, numerical modeling is mostly carried out on computers due to the miniaturization and accessibility of both computer hardware and software. Increased computer capabilities and speed led to the development of powerful commercial numerical methods software packages based on finite elements method that

can easily be used to model intricate biological systems. The principle of the finite elements method is the discretization of the geometry into smaller elements where the quantity to be determined is approximated with a function or is assumed to be constant throughout the element. Discrete elements can be of different shapes and sizes, which allows modeling of intricate geometries. Nonhomogeneities and anisotropies can also be modeled and different excitations and boundary conditions can be applied easily. When constructed, our model consists of a system of equations that can be solved by an appropriate numerical method.

## 2.1. Volume conductor theory

Electrical response of biological tissues when stimulated with direct electric current can be seen as quasi-stationary. Namely, for any material whose electric properties are in the range of those of biological tissues or organs and its dimensions do not exceed 1 m and the frequency of the electric field stays below 1 kHz, the electrical behavior in any given moment as a response to electric current can be described with a set of equations describing stationary fields. Electric field can be simplified as time independent thus the capacitive and the inductive effects and the finite propagation of the electric current in the biological tissue are disregarded.

When biological tissues and organs are excited with constant direct electric field (DC field), their response can be described with equations for DC conductive media. The electric current field thus induced is not a source field (has no sources nor drains), which can be described with the following equation [Sinigoj, 1996]:

$$\oint_S \vec{J} \cdot d\vec{S} = 0, \quad (2.1)$$

where  $S$  is a closed surface enclosing the volume  $V$  and  $\vec{J}$  represents the current density vector (in units: A/m<sup>2</sup>). Ohm's law applies, and can be written in differential equation as:

$$\vec{J} = \sigma \cdot \vec{E}, \quad (2.2)$$

where  $\vec{E}$  is the vector of the electric field (in units: V/m), inducing the electric current in the material (free charge displacement).

Electric field is defined as a negative gradient of the potential  $u$  (in units: V):

$$\vec{E} = -\nabla u, \quad (2.3)$$

The conductivity of the material (in units: S/m) can in general (in the case of an anisotropic conductor) be represented with a tensor:

$$\sigma = \begin{bmatrix} \sigma_{xx} & \sigma_{xy} & \sigma_{xz} \\ \sigma_{yx} & \sigma_{yy} & \sigma_{yz} \\ \sigma_{zx} & \sigma_{zy} & \sigma_{zz} \end{bmatrix} \quad (2.4)$$

Whenever the material's conductivity can be described in the orthogonal cartesian system and its spatial dependence can be aligned with the axes, the electric field and the current density can also be further described in the same way; the non-diagonal elements of the matrix (2.4) equal zero, hence the matrix (2.4) becomes diagonal:

$$\sigma = \begin{bmatrix} \sigma_{xx} & 0 & 0 \\ 0 & \sigma_{yy} & 0 \\ 0 & 0 & \sigma_{zz} \end{bmatrix} \quad (2.5)$$

In the case of anisotropic biological tissues (skeletal muscle, heart muscle), we have two different values for the conductivity, in two different directions: one for the direction along the length of the muscle fibers and one that is perpendicular to it. If the muscle tissue is aligned with one of the axes of the coordinate system, two diagonal elements in the matrix (2.5) have the same value. The anisotropies can be further simplified if we are using the cylindrical coordinates.

Some authors, instead of using the electrical conductivity  $\sigma$ , use its inverse value, the electrical resistivity  $\rho = 1/\sigma$  (in units:  $\Omega\text{m}$ ).

The current field on the border of two different conductors ( $\sigma_1$  and  $\sigma_2$ ), follows the equation:

$$J_{n1} = J_{n2}, \quad (2.6)$$

where  $J_{n1}$  and  $J_{n2}$  are the normal components of the current densities in materials 1 and 2, respectively, and:

$$E_{t1} = E_{t2}, \quad (2.7)$$

where  $E_{t1}$  and  $E_{t2}$  are the tangential components of the electric field in materials 1 and 2.

Things change when we look at the border between a conductor and an insulator. Let's name the insulator material number 1 and the conductor material number 2. In the case when there is no current inside the conductor, the situation can be described with the equations for the electrostatic fields. We know that the electric field inside the conductor equals zero and that a surface charge density  $Q_{\text{surface}}$  (in units:  $\text{As/m}^2$ ) is distributed on the surface of the conductor. On the border between the conductor and the insulator, we only get the normal component of the electric field:

$$E_{n1} = \frac{Q_{\text{surface}}}{\varepsilon_1} \quad (2.8)$$

where  $\varepsilon_1$  (in units:  $\text{As/Vm}$ ) is the dielectric constant of the material number 1 (the insulator); And the normal component of the electric flux density  $\vec{D}$  (in units:  $\text{As/m}^2$ ) is:

$$D_{n1} = Q_{\text{surface}}. \quad (2.9)$$

The situation changes where a current field with current density  $\vec{J}_2$  exists inside the conductor. Following from the equation (2.7) and Ohm's law (equation (2.2)), we get:

$$\frac{J_{t1}}{\sigma_1} = \frac{J_{t2}}{\sigma_2}. \quad (2.10)$$

Material 1 being an ideal insulator (its conductivity  $\sigma_1$  equals zero), current density  $\vec{J}_1$  inside it also equals zero. On the contrary, both, conductivity  $\sigma_2$  and current

density  $\vec{J}_2$  in material 2, the conductor, have a value greater than zero. So equation 2.10 makes more sense in the following form:

$$E_{t1} = \frac{J_{t2}}{\sigma_2}. \quad (2.11)$$

The electric field is no longer orthogonal to the conductor's surface; instead the vector of the electric field changes its direction on the border between the two materials. The angle between the two vectors can be expressed by:

$$\text{tg}\alpha = \frac{E_{t1}}{E_{n1}}. \quad (2.12)$$

The power representing losses due to the collisions between the free charges is defined by Joule's law:

$$p = \frac{dP}{dv} = \vec{J} \cdot \vec{E}. \quad (2.13)$$

Where  $p$  is the loss per volume or power density (in units: W/m<sup>3</sup>).

Further, the equation 2.1 can be written as:

$$\nabla \cdot \vec{J} = 0. \quad (2.14)$$

Using Ohm's law, it transcribes into:

$$\nabla \cdot (\sigma \cdot \vec{E}) = 0. \quad (2.15)$$

Combining equation 2.15 with the definition of the electric field (equation 2.3), we get:

$$\nabla \cdot (\sigma \cdot (-\nabla u)) = 0. \quad (2.16)$$

In the case of a homogeneous isotropic material (constant  $\sigma$ ) we get a Laplace differential equation:

$$\nabla^2 u = 0, \quad (2.17)$$

or:

$$\nabla^2 u = \frac{\partial^2 u}{\partial x^2} + \frac{\partial^2 u}{\partial y^2} + \frac{\partial^2 u}{\partial z^2} \quad \text{in the volume } V, \quad (2.18)$$

The equation 2.18 is an elliptic partial differential equation that in combination with the boundary conditions:

$$u = \bar{u}, \quad \text{on the surface } S_1 \quad (2.19)$$

and the derivation  $u$  in the direction of the normal vector:

$$q = \frac{\partial u}{\partial n} = \bar{q}, \quad \text{on the surface } S_2, \quad (2.20)$$

defines the mixed or Robin's problem, where:

$$S = S_1 + S_2 \quad (2.21)$$

is the surface enclosing the volume  $V$ . In the instance when only the first boundary condition is given (the equation (2.19)), we are dealing with the Dirichlet boundary condition, while, when we know the derivation from the equation 2.20, we have the Neumann boundary condition. The Laplace equation can be solved analytically or numerically, using one of the numerical methods. The analytical solution is only possible for the problems where the geometry, the nonhomogeneities and the anisotropies can be described in one of the coordinate systems (like Cartesian, cylindrical or polar). In the case of any other geometries and boundary conditions, numerical methods can give us an approximation. Most methods enable us to include nonhomogeneities and anisotropies. Most biological systems have very intricate geometries, along with material nonhomogeneities and anisotropies, which means numerical methods are a more suitable option for studying the effects of electromagnetic fields on cells, tissues and organs.

## 2.2. Finite elements method

The finite elements method (FEM) turned out to be a very useful method for solving partial differential equations when studying electric field distributions inside biological systems. The essence of the method is the discretization of the geometry into smaller elements – finite elements – where the quantity of interest is approximated with a simple function or is assumed to be constant throughout the element. Material properties inside a finite element are homogeneous. Mathematically, the finite element method is used for finding an approximate solution of partial differential equations (PDE) as well as of integral equations such as the heat transport equation. The solution approach is based either on eliminating the differential equation completely (steady state problems), or rendering the PDE into an equivalent ordinary differential equation, which is then solved using standard techniques such as finite differences, etc.

In solving partial differential equations, the primary challenge is to create an equation which approximates the equation to be studied, but which is numerically stable, meaning that errors in the input data and intermediate computations do not accumulate and cause the resulting output to be meaningless.

In order to design a numerical model of a physical structure, the modeler must decide the appropriate resolution for modeling each component part, a task requiring considerable expertise and experience. Too fine a mesh will cause unnecessary computational overheads when running the model, whereas too coarse a mesh will produce intolerable approximation errors. A simple rule is to choose a better resolution in the regions where we expect large gradients of the computed quantities or in the regions of our interest. Borders between regions with very different material properties represent an additional problem, which again calls for higher mesh resolution. Badly chosen resolution values can lead to unsatisfactory results and numerical error due to too coarse a mesh. On the other hand, we are limited by computer capabilities and reducing the error by increasing the mesh resolution means taking up more computer time and the model can even end up being too complex to be solved. A simple way to optimize mesh density is increasing its resolution and if the results stay the same, the mesh was adequate. Furthermore, using appropriate symmetries of the model can simplify our model a great deal.

An equation solving for the unknown quantity has to be defined in each element. Several approaches are used for this. The Galerkin method relies on the weak

formulation of an equation and works in principle by restricting the possible solutions as well as the test functions to a smaller space than the original one. In this way, an infinite dimensional differential equation may be converted to a problem of linear algebra or a high dimensional linear system of equations may be projected to a low dimensional one. These small systems are easier to solve than the original problem, but their solution is only an approximation to the original solution. Weak formulations have been an important means in the analysis of mathematical equations since they allow transfer of the concepts of linear algebra to fields like partial differential equations. The main feature of weak formulations is that an equation is not required to hold absolutely anymore (and this is not even well defined), but only with respect to certain test vectors or test functions. Another approach is using a calculus of variations. In general, calculus of variations deals with functions of functions, as opposed to ordinary calculus which deals with functions of numbers. Such functionals can for example be formed as integrals involving an unknown function and its derivatives and can have a physical meaning. The interest is in functions making the functional attain a maximum or minimum value. Whatever the method, we get a system of linear equations in matrix form that can be solved by numerical methods.

Maxwell equations along with boundary conditions describe electromagnetic quantities in a material and can be written as:

$$\oint_L \vec{H} \cdot d\vec{l} = \int_S (\sigma \cdot \vec{J} + \rho \cdot \vec{v} + \frac{\partial \vec{D}}{\partial t}) \cdot d\vec{S} + \oint_L (\vec{v} \times \vec{D}) \cdot d\vec{l}, \quad (2.22)$$

$$\oint_L \vec{E} \cdot d\vec{l} = - \int_S \frac{\partial \vec{B}}{\partial t} \cdot d\vec{S} + \oint_L (\vec{v} \times \vec{B}) \cdot d\vec{l}, \quad (2.23)$$

$$\oint_S \vec{D} \cdot d\vec{S} = \int_V \rho \, dv, \quad (2.24)$$

$$\oint_S \vec{B} \cdot d\vec{S} = 0. \quad (2.25)$$

or as:

$$\nabla \times \vec{H} = \vec{J} + \dot{\vec{D}}, \quad (2.26)$$

$$\nabla \times \vec{E} = -\dot{\vec{B}}, \quad (2.27)$$

$$\nabla \cdot \vec{D} = \rho, \quad (2.28)$$

$$\nabla \cdot \vec{B} = 0. \quad (2.29)$$

Solving that system directly by calculating vectors  $\vec{E}$  and  $\vec{B}$  has certain disadvantages [EMAS User's Manual, 1997]. First, the number of the unknowns in the system is larger than necessary. Namely, every vector has to be solved for its three spatial coordinates. Consequently, we get 6 unknowns and only 4 equations. Secondly, the following boundary conditions:

$$D_{n1} = D_{n2}, \quad (2.30)$$

$$H_{t1} = H_{t2}, \quad (2.31)$$

hold true on the border between two materials as well as on every border between two finite elements which represents a burden for the calculation.

Also, choosing  $\vec{E}$  and  $\vec{B}$  as the unknowns of the system can lead to singularities on the sharp edges of regions with different material properties which poses another serious problem when solving such a system with numerical methods on digital computers.

To avoid the abovementioned problems, we define a potential function. In vector calculus, any vector field of a certain type has an associated scalar field called the potential. Equation 2.29 reads as: "divergence of  $\vec{B}$  equals zero". In vector calculus, the divergence is an operator that measures a vector field's tendency to originate from or converge upon a given point. A vector field which has zero divergence everywhere is called solenoidal and can be expressed as a curl of another vector field. Therefore, we introduce a vector potential  $\vec{A}$ :

$$\vec{B} = \nabla \times \vec{A}. \quad (2.32)$$

Electric field can be expressed with a vector potential  $\vec{A}$ , representing the vector potential of magnetic field, and a scalar potential  $u$ :

$$\vec{E} = -\nabla u - \dot{\vec{A}}. \quad (2.33)$$

Finally, to simplify the equations when working with finite elements, we introduce a new form of the scalar potential, defined as the time integral of the potential  $u$ :

$$\psi = \int_t u dt. \quad (2.34)$$

Equation (2.33) transcribes into:

$$\vec{E} = -\nabla \psi - \dot{\vec{A}}. \quad (2.35)$$

Thus defined scalar potential  $\psi$  leads to a simplified, symmetrical system of equations when solving electromagnetic quantities with finite elements method. The three spatial components of the vector potential  $\vec{A}$  and the scalar potential  $\psi$  represent all the unknowns of the system in the case of a generalized electromagnetic problem, described by Maxwell equations. In the case of the DC current field, the problem is simplified. All three components of  $\vec{A}$  equal zero and only the scalar potential  $\psi$  or its time derivative  $\dot{\psi} = u$  needs to be calculated.

As already mentioned, the system of equations to be solved with finite elements can be derived from the Maxwell equations by using the Galerkin method or a calculus of variations. With the latter, we minimize the functional that can, in the case of the DC current field, be defined as the ohmic losses in the system. The energy loss per volume can be written as:

$$w = \int_t p dt. \quad (2.36)$$

Taking into account equations (2.13), (2.3) and (2.34), we get:

$$w = \int_t \vec{E} \cdot \vec{J} dt = - \int_t \nabla u \cdot \vec{J} dt = - \nabla \left( \int_t u dt \right) \cdot \vec{J}, \quad (2.37)$$

or:

$$w = - \nabla \psi \cdot \vec{J}. \quad (2.38)$$

The differential of the virtual work in the system  $\delta W$  as a result of the forces originating from changes of the scalar potential  $\delta \psi$ , is defined as:

$$\delta W = \int_V \delta (\nabla \psi) \cdot \vec{J} dV. \quad (2.39)$$

Integrating *per partes* the expression on the right in the equation 2.39, we get the following:

$$\int_S \delta \psi \cdot \vec{n} \cdot \vec{J} dS, \quad (2.40)$$

where  $S$  is the surface enclosing the volume of our calculations,  $\vec{n}$  is the unit vector normal to that surface, and  $\vec{n} \cdot \vec{J}$  is the normal component of the current density vector on the surface.

We add the energy arising from the constant value of the current density  $\vec{J}^*$  and we get:

$$\int_S \delta \psi \cdot \vec{n} \cdot (\vec{J} - \vec{J}^*) dS. \quad (2.41)$$

The so defined expression equals zero in two cases:

- when there are no changes in the potential  $\delta \psi$  on the surface  $S$  – the Dirichlet boundary condition, or
- when the normal component of the current density on the surface  $S$  equals  $J_n^*$ , hence  $\vec{n} \cdot (\vec{J} - \vec{J}^*) = 0$  – Neumann boundary condition.

Combined with the equation 2.39, we get:

$$\delta W = \int_V \delta (\nabla \psi) \cdot \vec{J} dV - \int_S \delta \psi \cdot \vec{n} \cdot \vec{J}^* dS. \quad (2.42)$$

Taking into account the equations 2.2, 2.3 and 2.34, the current density can be expressed with the scalar potential  $\psi$ :

$$\delta W = - \int_V \delta (\nabla \psi) \cdot \gamma \cdot \nabla \psi dV - \int_S \delta \psi \cdot \vec{n} \cdot \vec{J}^* dS. \quad (2.43)$$

Expression 2.43 is the basis for our finite elements calculation. The first part represents the energy due to ohmic losses, while the second part is the energy due to our boundary conditions and the energy of the sources.

The next step of our finite elements analysis is the discretization of the geometry into smaller elements – finite elements – of relatively simple shapes. Every finite element has its homogeneous material properties attributed to it and the expressions for the potential inside the finite elements are described with low-order polynomials. In this way, intricate geometries can be modeled.

Suppose the potential  $\psi$  in a given element can be described as a sum:

$$\psi(\vec{r}) = N_1(\vec{r}) \cdot \psi_1(t) + N_2(\vec{r}) \cdot \psi_2(t) + N_3(\vec{r}) \cdot \psi_3(t) + \dots, \quad (2.44)$$

where  $N_1, N_2, N_3, \dots$  are the so-called shape functions, depending only on the position of  $\vec{r}$ ; and  $\psi(t)$  is the value of the scalar potential at a given point (node) inside the element. The number of the points where scalar potential is evaluated depends on geometry and element shape. They are usually in the elements' corners but can also be put on the edges or inside the elements (higher-order elements). Shape functions are altered, the calculation is more precise and consequently more complex.

Equation 2.44 can in the matrix form be written as:

$$\psi = \{N\}^T \cdot \{\psi^e\}, \quad (2.45)$$

where  $\{N\} = \{N_1, N_2, N_3, \dots\}^T$  is the shape functions vector of a given element and  $\{\psi^e\} = \{\psi_1, \psi_2, \psi_3, \dots\}^T$  is the scalar potential vector in the nodes of an element. The dimension of both vectors equals the number of nodes  $n$  of a given element.

We want to use the so defined vectors in equation 2.43, for every finite element in the geometry. First, the time derivation  $\dot{\psi}$  can be written as:

$$\dot{\psi} = \{N\}^T \cdot \{\dot{\psi}^e\}. \quad (2.46)$$

Shape functions are constant, hence:

$$\delta \psi = \{N\}^T \cdot \delta \{\psi^e\}. \quad (2.47)$$

The gradient of the potential  $\nabla \psi$  can be described with shape functions as:

$$\nabla \psi = [\nabla N] \cdot \{\psi^e\}, \quad (2.48)$$

where the dimension of the matrix  $[\nabla N]$  is  $3 \times n$ :

$$[\nabla N] = \begin{bmatrix} \frac{\partial N_1}{\partial x} & \frac{\partial N_2}{\partial x} & \dots \\ \frac{\partial N_1}{\partial y} & \frac{\partial N_2}{\partial y} & \dots \\ \frac{\partial N_1}{\partial z} & \frac{\partial N_2}{\partial z} & \dots \end{bmatrix}. \quad (2.49)$$

Hence equation 2.43 becomes:

$$\delta W^e = - \int_{V^e} ([\nabla N] \cdot \delta \{\psi^e\})^T \cdot \gamma \cdot ([\nabla N] \cdot \{\dot{\psi}^e\}) dV - \int_{S^e} (\{N\} \cdot \delta \{\psi^e\})^T \cdot (\vec{n} \cdot \vec{J}^*) dS. \quad (2.50)$$

Because of the spatial independence of the scalar potential vectors  $\{\psi^e\}$ , we can put them in front of the integrals:

$$\delta W^e = -\delta\{\psi^e\}^T \cdot \left( \int_{V^e} [\nabla N]^T \cdot \gamma \cdot [\nabla N] dV \right) \cdot \{\dot{\psi}^e\} - \delta\{\psi^e\}^T \cdot \int_{S^e} \{N\}^T \cdot (\vec{n} \cdot \vec{J}^*) dS. \quad (2.51)$$

The conductivity matrix of an element is:

$$[C^e] = \int_{V^e} [\nabla N]^T \cdot \gamma \cdot [\nabla N] dV, \quad (2.52)$$

and contains the information about the geometry of the element in combination with its material properties. The surface excitations vector of the system is:

$$\{J^e\} = - \int_{S_e} \{N^T\} \cdot (\vec{n} \cdot \vec{J}^*) dS, \quad (2.53)$$

where (\*) denotes a Neumann boundary condition. The integration is only carried out on the surfaces of the elements that form a part of the model's surface.

Equation 2.50 can now be written as:

$$\delta W^e = -\delta\{\psi^e\}^T \cdot [C^e] \cdot \{\dot{\psi}^e\} + \delta\{\psi^e\}^T \cdot \{J^e\}. \quad (2.54)$$

The next step is the summing up of the contributions from all elements. The result gives us the work of the whole model:

$$\delta W = -\delta\{\psi\}^T \cdot [C] \cdot \{\dot{\psi}\} + \delta\{\psi\}^T \cdot \{J\}, \quad (2.55)$$

where the vector  $\{\psi\}$  is composed of vectors  $\{\psi^e\}$  of all the elements in the model. The structures of the matrix  $[C]$  and the vector  $\{J\}$  are similar to that.

The last step defines the dynamic equilibrium:

$$0 = -[C] \cdot \{\dot{\psi}\} + \{J\}_S. \quad (2.56)$$

Matrix equation in its final form reads as follows:

$$[C] \cdot \{\dot{\psi}\} = \{J\}_S, \quad (2.57)$$

or

$$[C] \cdot \{u\} = \{J\}_S. \quad (2.58)$$

Adding boundary conditions – potential values in the grid points – we get the equation 2.59:

$$\mathbf{A} \cdot \mathbf{x} = \mathbf{C} \cdot \mathbf{f}, \quad (2.59)$$

where  $\mathbf{A}$  is the system matrix,  $\mathbf{x}$  is the vector of the unknowns (potentials),  $\mathbf{C}$  is the complementary matrix and  $\mathbf{f}$  is the boundary conditions vector. This matrix equation can be solved directly or using one of the iterative (indirect) numerical methods. They solve the system of linear equations by choosing an initial value, find a solution and use that solution in the next iteration. This process is repeated until a certain criterion is met. Iterative methods are especially useful when solving sparse systems where a large number of elements in the matrix equal zero which is true for the finite elements method.

With a similar procedure, solving the whole system of Maxwell equations, in the case of the generalized electromagnetic problem would give the following two matrix equations:

$$\begin{bmatrix} M^{AA} & M^{A\psi} \\ M^{\psi A} & M^{\psi\psi} \end{bmatrix} \cdot \begin{Bmatrix} \ddot{\vec{A}} \\ \ddot{\psi} \end{Bmatrix} + \begin{bmatrix} C^{AA} & C^{A\psi} \\ C^{\psi A} & C^{\psi\psi} \end{bmatrix} \cdot \begin{Bmatrix} \dot{\vec{A}} \\ \dot{\psi} \end{Bmatrix} + \begin{bmatrix} K^{AA} & 0 \\ 0 & 0 \end{bmatrix} \cdot \begin{Bmatrix} \vec{A} \\ \psi \end{Bmatrix} = \begin{Bmatrix} \vec{M}_0 \\ 0 \end{Bmatrix}_V + \begin{Bmatrix} \vec{H}_t \\ \vec{J}_n \end{Bmatrix}_S + \begin{Bmatrix} I \\ 0 \end{Bmatrix}_{point} \quad (2.60)$$

$$\begin{bmatrix} 0 & 0 \\ M^{\psi A} & M^{\psi\psi} \end{bmatrix} \cdot \begin{Bmatrix} \dot{\vec{A}} \\ \dot{\psi} \end{Bmatrix} = \begin{Bmatrix} 0 \\ \rho_0 \end{Bmatrix}_V + \begin{Bmatrix} 0 \\ \vec{D}_n \end{Bmatrix}_S + \begin{Bmatrix} 0 \\ Q \end{Bmatrix}_{point}, \quad (2.61)$$

where  $[M]$  is the permittivity matrix,  $[K]$  the permeability matrix, and  $[C]$  the conductivity matrix.  $\vec{M}_0$  represents the magnetization vector,  $\rho_0$  charge density and  $Q$  quantity of the electric charge. In the case of DC current field, that system simplifies into the equation 2.57.

### 2.3. Electric properties of tissues

The bulk properties of biological materials are important in many applied problems of electrical stimulation. They dictate the current densities and pathways that result from an applied stimulus and are thus very important in the analysis of a wide range of biomedical applications such as functional electrical stimulation and the diagnosis and treatment of various physiological conditions with weak electric currents, radio-frequency hyperthermia, electrocardiography, and body composition. To analyze the response of a tissue to electric excitation, we need data on the conductivities and relative permittivities of the tissues or organs. The measurement of tissue electric properties can be complicated because of several factors, such as tissue inhomogeneity, anisotropy, the physiological state of the tissue, and electrode polarization. Also, the lack of standardization of the measurement technique leads to large discrepancies in the reported data on tissue electric properties. The topic of electric properties of biological tissues is discussed in detail in Paper 2 in Appendix (chapter "Electric properties of tissues" in the Encyclopedia of Biomedical Engineering, John Wiley & Sons, Inc.)

In our numerical model of the skin fold during the process of the electropermeabilization, the conductivities of the skin layers before and after electropermeabilization were taken from the literature and experiments [Yamamoto and Yamamoto, 1976; Yamamoto and Yamamoto, 1976a; Prausnitz *et al.*, 1993; Pliquett *et al.*, 1995; Gabriel C. *et al.*, 1996; Gabriel S. *et al.*, 1996; Pliquett and Weaver, 1996; Gallo *et al.*, 1997; Jadoul *et al.*, 1999; Pliquett, 1999; Pavšelj *et al.*, 2005]. In the model only the conductivity data were used. Namely, direct current analysis was performed, so different permittivity values of the tissues do not play any role in the electric field distribution. However, data on virtually everything, except the conductivities before the electropermeabilization, is very scarce, sometimes nonexistent. Namely, the subject of tissue conductivity changes due to electroporation is still an unexplored area. Also, due to different measuring conditions, measuring techniques and species used by different researchers, large discrepancies are found in the reported data. However, with the model presented we used the available data to try to explain the mechanism of the tissue electropermeabilization propagation beyond the initial conditions dictated by the tissue initial conductivities.



## CHAPTER 3

# Materials and Methods

### 3.1. *In vivo* experiments

#### 3.1.1. Reporter genes and plasmid injection

Gene electrotransfer in the skin was evaluated and optimized with two reporter plasmids – pCMVluc and pCMVGFP – coding for luciferase and green fluorescent protein, respectively.

Luciferase is a generic name for enzymes commonly used in nature for bioluminescence (light-emitting enzymes). A diverse group of organisms use luciferase-mediated bioluminescence to startle predators or to attract prey or mates. The luciferase from the North American firefly releases green light during the oxidation of its chemical substrate, luciferin (a pigment). The rates of this reaction between luciferin and oxygen are extremely slow unless stimulated by luciferase. The glow is widely used as an assay for LUC expression, which acts as a "reporter" for the activity of any regulatory elements controlling its expression. Luciferase is particularly useful as a reporter in living cells and organisms.

The green fluorescent protein (GFP) is a protein from the jellyfish *Aequorea victoria* that fluoresces green when exposed to blue light. In cell and molecular biology, the GFP gene is frequently used as a reporter of expression.

We prepared the plasmids using a Qiagen kit for plasmid purification. The plasmids were injected intradermally (50 µg/25 µl PBS (phosphate buffered saline)) using a Hamilton syringe with a 27 gauge needle 30 seconds before the application of the electric pulses.

#### 3.1.2. Animals

The animals used in all studies except the immunization study, were male Wistar rats from Laboratoires Janvier, France, 8-10 weeks old. The animals were kept in ambient temperature (20°C) with a natural day/night cycle and access to water and food *ad libitum*. Prior to the experiments they were anaesthetized by intraperitoneal administration of 700 µl of the anesthetic consisting of a mixture of ketamine (100

mg/kg, Ketalar, Panpharma) and xylazine (40 mg/kg, Rompun, Bayer). The skin on the back was removed 1-2 days prior to the experiments, first with an electric razor, then with a depilatory cream (Veet for sensitive skin, Veet) to thoroughly remove all the hair. Removal of hair allowed a better visualization of DNA injection and the electroporated areas. We used 5 to 8 electroporation sites on the back of each rat.

For the immunization study we used 6 week old female Balb/c mice (Janvier, France). They were anaesthetized with 15  $\mu$ l of a mixture of ketamine and xylazine. The skin on the back was removed with depilatory cream (Veet for sensitive skin) one day prior to immunization.

### **3.1.3. DNA electrotransfer**

For delivery of high voltage (HV) and/or low voltage (LV) pulses, we used a square-wave electropulsator Cliniporator (IGEA, Carpi, Italy). In the GFP and the luciferase expression studies, different protocols, all consisting of a single HV pulse (160, 280, 400 or 520 V, 100  $\mu$ s), followed by a single LV pulse (32, 56 or 80 V, 400 ms) or 8 LV pulses (56 or 80 V, 8x50 ms) were tested. In most protocols tried, there was no delay between the HV and the LV pulse. However, delays of 1 second and 4.2 seconds were tested as well. We compared these protocols with protocols reported in literature [Mir *et al.*, 1998; Mir *et al.*, 1999; Glasspool-Malone *et al.*, 2000]. For the protocols used in the immunization study, see subchapter 3.1.7.

The electric pulses were delivered about 30 seconds after the intradermal injection of plasmid ((50  $\mu$ g/25  $\mu$ l PBS) using two parallel, stainless-steel plate electrodes of 0.5 mm thickness and 4 mm distance (IGEA, Carpi, Italy). Skin fold was formed and placed between the electrodes. The area of the electrodes in contact with skin was about 1 cm x 1 cm. To assure good contact between the skin fold and the electrodes, a conductive gel (EKO-GEL, ultrasound transmission gel, Egna, Italy) was applied on the skin. The electrodes used for the immunization study were 2.5 mm apart due to the lower thickness of mouse skin.

The voltage and the electric current were measured during experiments by the Cliniporator and stored on the computer.

### **3.1.4. Current-voltage dependences of rat skin**

We observed the current-voltage curves to approximately set the permeabilization threshold and tested the current-voltage curve shape for possible dependence on the quantity of the intradermally injected substance: 0 (no injection), 25  $\mu$ l and 50  $\mu$ l of injected PBS before the electroporation. Different pulsing protocols were used, all consisting of a high voltage – HV pulse (80, 120, 160, 200, 240, 280, 320, 360, 400, 440, 480 V (100  $\mu$ s)) followed by a low voltage – LV pulse (32 V (20 ms)). There was no lag between the HV and the LV pulse. The current and the voltage of both pulses were recorded during pulsing, however, only the HV pulse data were used, as, at this point, we were only interested in the electropermeabilization threshold.

### **3.1.5. GFP localization**

Two days after the electroporation, the rats (n=3 per group) were sacrificed and skin samples were taken. Both the epidermal and dermal sides of the skin were observed without fixation or freezing by means of a confocal microscope. Two "blinded" observers evaluated the fluorescence intensity (2 skin samples per rat).

### 3.1.6. Luciferase assay

Two days after electroporation (1, 2, 3, 4, 7, 10, 14, 21, 25 days for the kinetic study), the rats were sacrificed and the electroporated areas of the skin were removed. The skin samples were weighed to 200 mg, cut into pieces and homogenized in 1 ml cell culture lysis reagent solution (10 ml cell culture lysis reagent (Promega) diluted with 40 ml distilled water and supplemented with one tablet of protease inhibitor cocktail (Boehringer Mannheim)). After centrifugation at 12000 rpm for 10 minutes at 4°C, we assessed the luciferase activity on 10 µl of the supernatant, using a luminometer, with delay time 3 s and integration time 15 s, starting after the addition of 50 µl of Luciferase Assay Substrate (Promega) to the skin lysate. The results from the luminometer were collected in relative light units (RLU). Final results were expressed as pg of luciferase per mg of tissue by calibration with purified firefly luciferase protein (Sigma).

### 3.1.7. Immunization study

The immune response after delivery of a plasmid coding for an immunogenic model protein ovalbumin (pcDNA 3.1-OVA) was assessed. Mice were injected intradermally with 2x15 µl of a plasmid coding for ovalbumin at 2 mg/ml (groups 1 to 4), ovalbumin at 1 mg/ml (group 5), ovalbumin 1 mg/ml+ adjuvant Alum (group 6) and PBS (negative control, group 7). Electric pulses (1 HV + 1 LV pulses in the first two groups and 6 HV pulses [Drabick *et al.*, 2001] in the third group) were applied 30 seconds after DNA injection. Two and four weeks after the priming, 2 boosts were applied. Blood samples were collected by retroorbital bleeding 2, 4 and 6 weeks after priming.

The humoral immune response i.e. titers of antibodies (IgG) to ovalbumin in the serum was measured by ELISA. Isotypes (IgG1, IgG2a or IgG2b) were determined using appropriate secondary antibodies as described previously [Lombry *et al.*, 2004]. The antibodies were first measured in the pools coming from individual mice in equivalent part. Individual mice responses were measured when a positive response was detected in the pooled sera.

### 3.1.8. Tolerance study

The side effects on the skin of a combination of a HV, followed by a LV pulse (400 V, 100 µs + 80 V, 400 ms, as this was the combination with the highest HV, LV amplitudes used in our studies) generated by the Cliniporator were investigated by standard methods [Vanbever *et al.*, 1998; Vanbever and Pr at, 1999; Dujardin *et al.*, 2002]. Skin fold with and without gel with the electrodes applied for as long as needed to deliver pulses (30 seconds) were used as controls.

Noninvasive bioengineering methods were used to evaluate *in vivo* if electroporation induced a trauma in the skin (transepidermal water loss – TEWL, chromametry). TEWL measurement is a noninvasive method for assessing the skin barrier function. The probe of the Tewameter TW 210 (Germany) was placed on the electroporation site and the measurements were taken when TEWL values stabilized. The TEWL values are expressed in g/m<sup>2</sup>h. Skin color and erythema were measured by Minolta Chromameter CR-200 (Minolta, Japan) calibrated using a white calibration tile. During measurements, the apparatus was kept perpendicularly to the skin surface. The measurements were taken before pulse delivery, immediately after pulse delivery, 30, 60, 120 minutes and 24 hours after pulsing. We separately measured the anode and the cathode side of each electroporation site.

In addition, histology was used to investigate the effect on the skin structure. For the histology study, the tissue was fixed in a 4% formalin solution for at least a week and embedded in paraffin wax. Sections 3  $\mu\text{m}$  thick were cut perpendicular to the surface of the skin and stained with hematoxylin-eosin.

### 3.1.9. Statistical analysis

For the statistical analysis of the results, we used Sigma Stat for Windows, version 2.0, Jandel Corporation. In the case of a normal distribution, the data were represented with mean and standard deviation. When normality test over the experimental groups failed, the data were represented with a median (horizontal line), 25<sup>th</sup> and 75<sup>th</sup> percentile (grey box) and 10<sup>th</sup> and 90<sup>th</sup> percentile (error bars). Black dots represent all the outliers. The ANOVA on ranks and Dunnet's test were used to compare different protocols.

## 3.2. Numerical modeling

### 3.2.1. COMSOL numerical modeling package

Electric field and current calculations were made by means of commercially available computer program COMSOL Multiphysics, version 3.2 (COMSOL, Los Angeles, CA, USA) based on finite elements method [COMSOL User's guide, 2005]. This method solves partial differential equations by dividing the model into smaller elements where the quantity to be determined is approximated with a function or is assumed to be constant throughout the element. Finite elements can be of different shapes and sizes, which allows modeling of intricate geometries. Nonhomogeneities and anisotropies can also be modeled and different excitations and boundary conditions can be applied easily.

COMSOL Multiphysics is a powerful interactive environment for modeling and solving all kinds of scientific and engineering problems based on partial differential equations (PDEs). With this package, it is possible to build models by defining the relevant physical quantities – such as material properties, loads, constraints, sources, and fluxes – rather than by defining the underlying equations. COMSOL Multiphysics then internally compiles a set of PDEs representing the entire model. Models can be built through a flexible graphical user interface, or by script programming in the COMSOL Script language or in the MATLAB language. Also, conventional models of one type of physics can easily be extended into multiphysics models that solve coupled physics phenomena simultaneously. Three ways of describing PDEs through the following mathematical application modes are possible:

- Coefficient form, suitable for linear or nearly linear models;
- General form, suitable for nonlinear models;
- Weak form, for models with PDEs on boundaries, edges, or points, or for models using terms with mixed space and time derivatives.

Using these application modes, one can perform various types of analysis including:

- Stationary and time-dependent analysis;
- Linear and nonlinear analysis;
- Eigenfrequency and modal analysis.

When solving the PDEs, COMSOL Multiphysics uses the finite element method (FEM). The software runs the finite element analysis together with adaptive meshing and error control using a variety of numerical solvers.

### 3.2.2. Numerical model of skin fold electropermeabilization

In the numerical model, the process of tissue permeabilization is modeled as a nonlinear problem, taking into account the increase in tissue conductivity due to cell membrane electroporation [Pavšelj *et al.*, 2005; Šel *et al.*, 2005]. Namely, when the electric field exceeds the reversible threshold, tissue conductivity increases. This change subsequently causes the change of the electric field distribution and of the corresponding current. Therefore, the final solution has to be reached iteratively. At the beginning, the electric field distribution is that of the nonpermeabilized tissue, where all the tissues involved have their initial conductivity values. In the regions where electric field exceeds reversible electropermeabilization threshold  $E_{rev}$ , the conductivity ( $\sigma$ ) changes from its lower value  $\sigma_1$  to its higher value  $\sigma_2$ , according to the predefined functional dependence  $\sigma(E)$  between the reversible and the irreversible thresholds. The electric field distribution is computed again with new conductivity values. The process is repeated until the electric field distribution reaches its steady state.

The ratios of the conductivities of the skin layers suggest that the highest voltage drop rests across the *stratum corneum*. That would cause a very high electric field in that layer while its strength would stay below the permeabilization threshold in the layers beneath *stratum corneum*. However, the electric conductivities of tissues subjected to electric pulses increase. As a result, the electric field “penetrates” deeper into the skin and permeabilizes the target cells. Using voltage and current measurements recorded during pulse delivery by the Cliniporator, we aimed at making the response of the model as close as possible to the experimental data (the current and the voltage measured during experiments). However, we focused on the process of electropermeabilization, which takes place inside the first, high-voltage pulse, so the electrophoretic low voltage pulse was not modeled. Other processes, such as the tissue-electrode polarization or the resealing of the cell membranes, were not modeled at this instance [Abidor *et al.*, 1993; Hibino *et al.*, 1993]. We obtained the electric conductivity values and their changes during electroporation from the literature and experiments, as well as the reversible and irreversible electric field electropermeabilization thresholds [Yamamoto and Yamamoto, 1976; Yamamoto and Yamamoto, 1976a; Prausnitz *et al.*, 1993; Pliquett *et al.*, 1995; Gabriel C. *et al.*, 1996; Gabriel S. *et al.*, 1996; Pliquett and Weaver, 1996; Gallo *et al.*, 1997; Jadoul *et al.*, 1999; Pliquett, 1999; Pavšelj *et al.*, 2005].

The geometry of the numerical model of a skin fold was made as close to the *in vivo* experimental tissue-electrode setup as possible. Four layers of skin were modeled: *stratum corneum*, epidermis, dermis and the underlying layer of fat and connective tissue. The electric pulses were applied on the skin with plate electrodes pressed against the skin and were modeled as a boundary condition. The distance between the electrodes was 4 mm and the area in contact with the skin was 1 cm<sup>2</sup>. However, to account for the presence of the conductive gel used in experiments in order to assure good contact between the skin and the electrodes, the voltage boundary condition was set somewhat beyond the size of the electrodes. A drawing of the whole skin fold geometry of our numerical model is shown in Figure 3. 1.

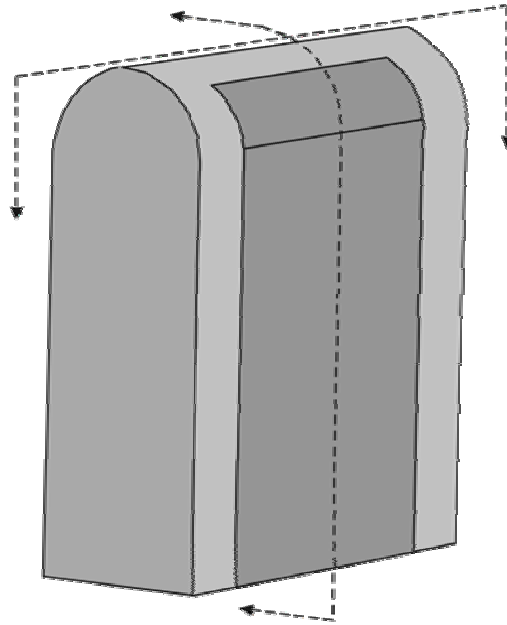


**Figure 3. 1:** A drawing of the whole skin fold, showing the directions in which the model was cut in order to get only one fourth of the geometry modeled to save computer time.

The mesh of the model was set more densely around the electrodes and in the thinner skin layers. Only one fourth of the geometry can be modeled as to avoid numerical problems due to the complexity of the model and computer memory limitations. The simplification was possible due to the symmetry of the geometry by applying appropriate boundary conditions. Therefore the boundary conditions on the section planes cut through the middle of the geometry had to be set as shown in Figure 3. 2. The thickness of the *stratum corneum* in the model is set larger than in real skin (around 6 times thicker). Namely, due to the large differences in layer thicknesses, numerical problems can occur and can make the calculation impossible. To make up for the *stratum corneum* being modeled thicker than it is, the conductivity of this very resistive layer was also set higher (6 times). As the experiments showed, the epidermis and the dermis were transfected, which means the electric field strength was high enough in those layers, due to the rise in electric conductivity of the *stratum corneum*. Therefore, we constructed a nonlinear numerical model where the electric field distribution depends on the changes in the electrical conductivity of the tissues involved. It is difficult to get the exact values of the reversible and the irreversible thresholds and the conductivities due to the lack of measurements of electrical properties of tissues during electroporation. However, we used the data found in literature, as well as our own experiments to set those parameters for all the tissues involved except the layer of fat with connective tissue. Therefore the permeabilization parameters were set similar to those of fat.

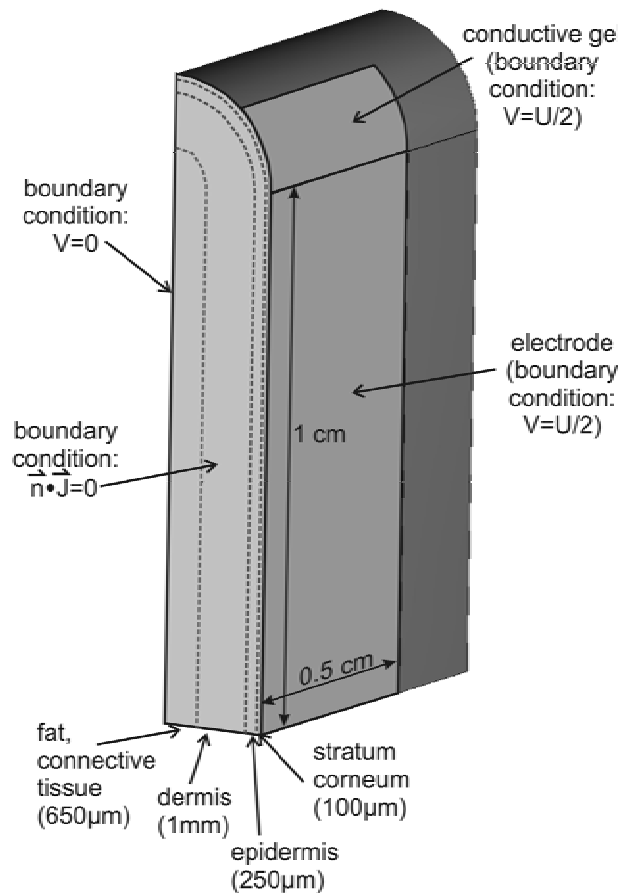


**Figure 3. 2: Geometry of the skin fold finite elements model made in COMSOL Multiphysics. Only one fourth of the skin fold was modeled to avoid numerical problems and save computer time. Boundary conditions were therefore set as shown.**

### 3.2.3. Numerical model of skin electroporation with local transport regions (LTRs)

The electroporation and consequently the increase in the conductivity of the *stratum corneum* is not homogeneous throughout the electroporated area. It has been shown that molecular and ionic transport across skin subjected to high voltage pulses is highly localized. The localized sites of molecular transport are called local transport regions (LTRs) [Pliquett *et al.*, 1998; Pliquett, 1999; Vanbever *et al.*, 1999; Weaver *et al.*, 1999; Pliquett and Gusbeth, 2004]. The authors have shown that the size of the LTRs depends on pulse duration, while pulse amplitude dictates their density. Local transport regions are formed in the sites of the so called *stratum corneum* "defects" [Pliquett, 1999] that are expanded by Joule heating caused by high local current density at the sites of the defects. Therefore, we made another numerical model of skin electroporation, where local transport regions were modeled as highly

conductive structures in the *stratum corneum*. The results obtained from this model were compared to the results from the skin fold model and with the *in vivo* data.

In the model where local transport regions were introduced, the same geometry as described in the subchapter 3.2.2 was used, consisting of four layers of skin: *stratum corneum*, epidermis, dermis and fat with connective tissue. The thicknesses of the skin layers were the same as in the skin fold model without LTRs, however, only a slice of the skin fold was modeled, as shown in Figure 3. 3. The thickness of the slice was 1 mm and periodic boundary conditions were set as to model the whole skin fold while simplifying the otherwise intricate geometry including local transport regions. The same nonlinear  $\sigma(E)$  dependences as well as the conductivity values before and after permeabilization as in skin fold model were used for all the skin layers except *stratum corneum*. In our model, the process of the LTR formation was not described. Instead only the steady state of the electropermeabilization process of the *stratum corneum* was modeled, with local transport regions exhibiting highly increased conductivity, while the conductivity of the rest of the *stratum corneum* remained low.

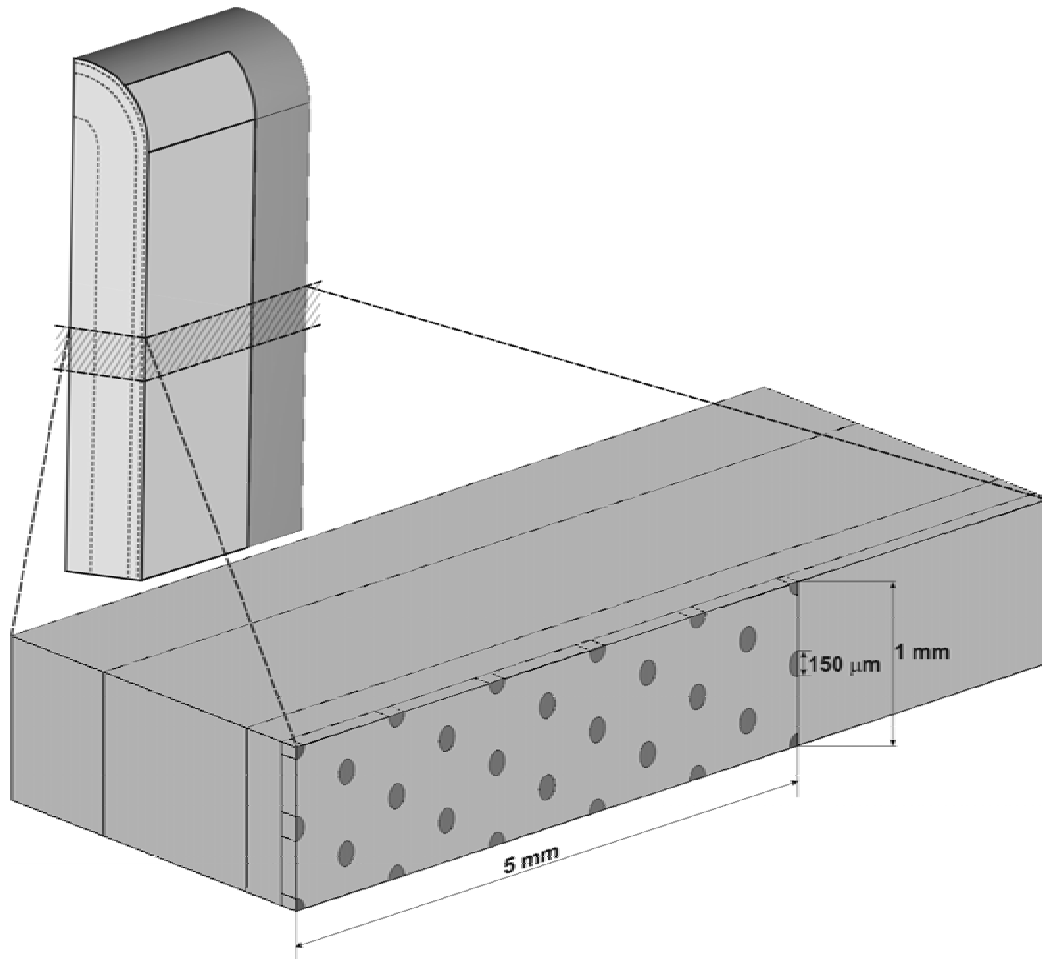


**Figure 3. 3: Geometry of the finite elements model representing a slice of a skin fold with local transport regions. Using periodic boundary conditions, only one tenth of the skin fold model described in subchapter 3.2.2 was modeled to avoid numerical problems and save computer time.**

As we made no attempt on visualizing local transport regions during our *in vivo* experiments, we took the data on LTR size and density and their conductivity from the literature [Pliquett *et al.*, 1998; Vanbever *et al.*, 1999; Pliquett and Gusbeth, 2004]. Reported sizes of local transport regions range from 50  $\mu\text{m}$  to 600  $\mu\text{m}$  in diameter and their density from 5 to 90 LTRs per 0.1  $\text{cm}^2$ . Specifically for high voltage pulses, the size of the resulting LTRs is typically around 100  $\mu\text{m}$  in diameter and their density 25 to 90 LTRs per 0.1  $\text{cm}^2$ . However, skin-electrode setups and electroporation protocols used in the literature were not directly comparable with our experiments. Therefore, we expected the results from this model to somewhat differ from both the results of the skin fold model and our *in vivo* experiments.

### 3.2.4. Numerical models of microelectrode arrays

Three different settings of the microneedle arrays were modeled with all consisting of arrays of 10x10 needles 1 mm apart. All three geometries are shown in Figure 3. 4 where black and white dots denote electrodes of different polarities.

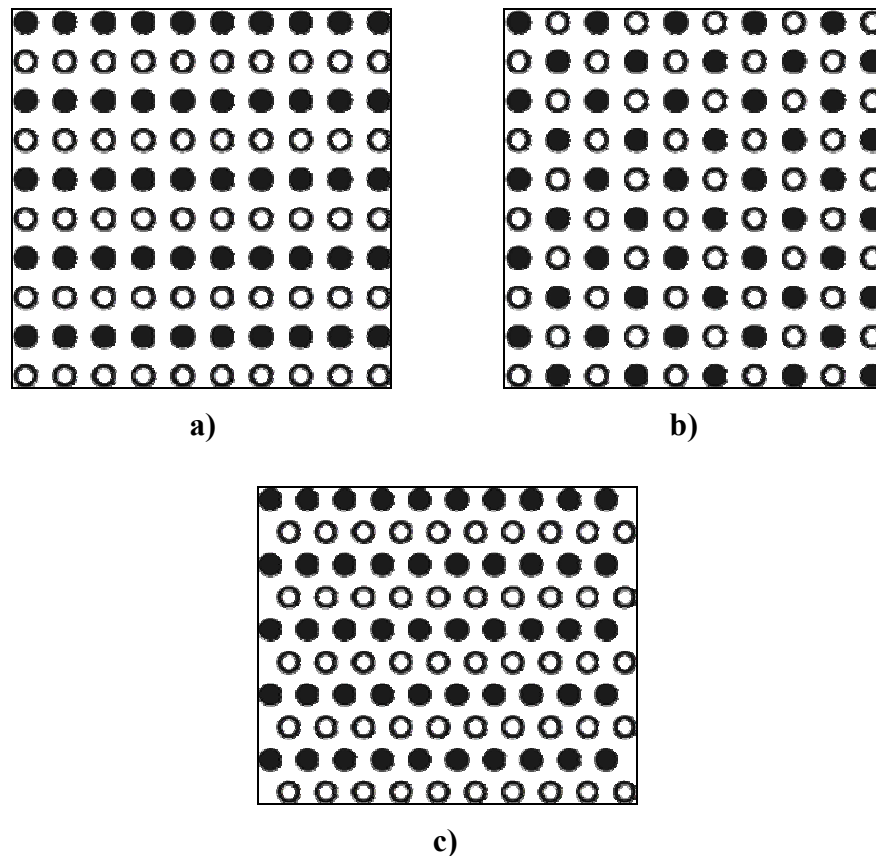


**Figure 3. 4: Different settings of microneedle arrays: a) lined; b) crossed; c) hexagonal. Black and white dots denote electrodes of different polarities.**

The microelectrodes were modeled hollow, namely, they can be used as microneedles, delivering the DNA into the skin. Electrode length is 500  $\mu\text{m}$ , however,

their modeled penetration depth is 400  $\mu\text{m}$ . The outer and the inner diameter of the hollow microneedle are 150  $\mu\text{m}$  and 60  $\mu\text{m}$ , respectively. In our models, the electrodes are modeled as a boundary condition; the content of the hollow needle array (DNA with its properties) was not modeled at this stage. Figure 3. 5 shows the geometry of a microneedle.

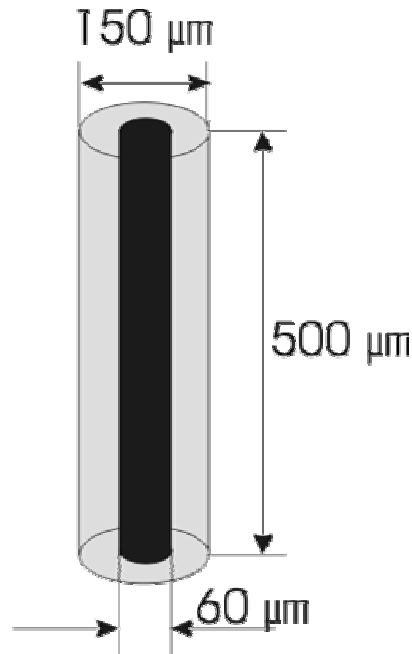


**Figure 3. 5: The geometry of a microneedle**

Modeling the whole array would be a wasteful task from both the modeler's and computer time point of view. Therefore, using the symmetry, only a small portion of the whole array, a unit cell, need be modeled by applying appropriate periodic boundary conditions [Susil *et al.*, 1998]. However, the calculation thus made will only hold true for the microneedles inside the array which are surrounded by neighboring microneedles, and not on the edges of the array. Figure 3. 6 shows unit cells of each microelectrode array, along with the dimensions and the boundary conditions that model an infinite array of microelectrodes. The unit cells are shown in black, while the surrounding needles are grayed out. Although the unit cell of the "crossed" geometry (Figure 3. 6b) can be chosen differently (smaller, with each corner of the unit cell containing a quarter of a microelectrode and the electric insulation boundary condition on all edges), we modeled the one on Figure 3. 6b for an easier comparison of the results later on.

No skin layers were modeled in the microneedle array models. Instead, skin was modeled as a homogeneous structure with the initial conductivity of 0.002 S/m and an 80-fold increase in the conductivity when in a permeabilized state. Again, tissue permeabilization was modeled as a nonlinear problem, as described in the previous subchapter (3.2.2.).

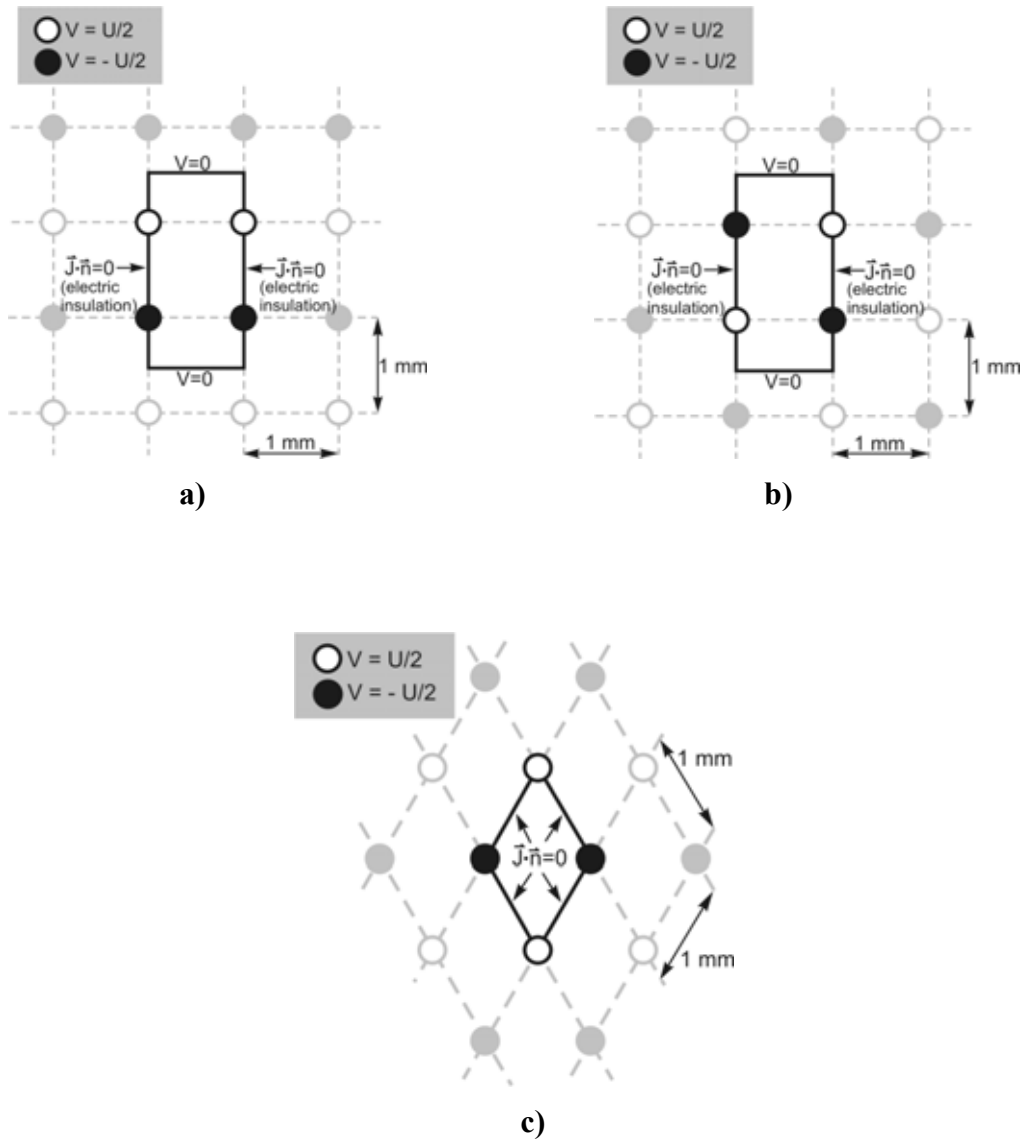


Figure 3. 6: Dimensions, unit cells and boundary conditions of the microelectrode array geometries: a) lined geometry; b) crossed geometry; c) hexagonal geometry



---

## CHAPTER 4

### ***In vivo* results**

The aim of our *in vivo* experiments was to demonstrate the efficacy of a combination of one short high voltage pulse, followed by a long, low voltage pulse for gene transfection in skin. Namely, a short, high-voltage pulse causes tissue permeabilization, while a longer, low voltage pulse works electrophoretically, promoting DNA delivery by electromigration. The proposed protocols were tried against protocols, reported in literature, consisting of a train of high-voltage or low-voltage pulses, and against control protocols of only one high- or one low-voltage pulse. To localize the expression of a gene in the skin after intradermal injection of a plasmid, followed by electroporation, a plasmid coding for GFP was used as a reporter gene. For a quantitative measure of the expression, however, a plasmid coding for luciferase was used.

In additional experiments, we followed the kinetics of gene expression in the skin, 1, 2, 3, 4, 7, 10, 14, 21 and 25 days after electroporation with the HV+LV pulse protocol. We also tried the proposed pulsing protocols for gene immunization as well as assessed damage on skin which may have been caused by electroporation.

Some of the *in vivo* results described in this chapter have been published in Paper 3, Appendix.

#### **4.1. Current vs. voltage curves**

To set the electropermeabilization thresholds on the rat skin and check the reproducibility of previous measurements, we first measured the I/U curves on the rat skin and their dependence on the quantity of the intradermally injected PBS. Three quantities were tested:

- no intradermal injection
- 25  $\mu$ l of PBS
- 50  $\mu$ l of PBS

##### Pulsing protocols:

- HV (80, 120, 160, 200, 240, 280, 320, 360, 400, 440, 480 V (100  $\mu$ s)) + LV (32 V (20 ms))

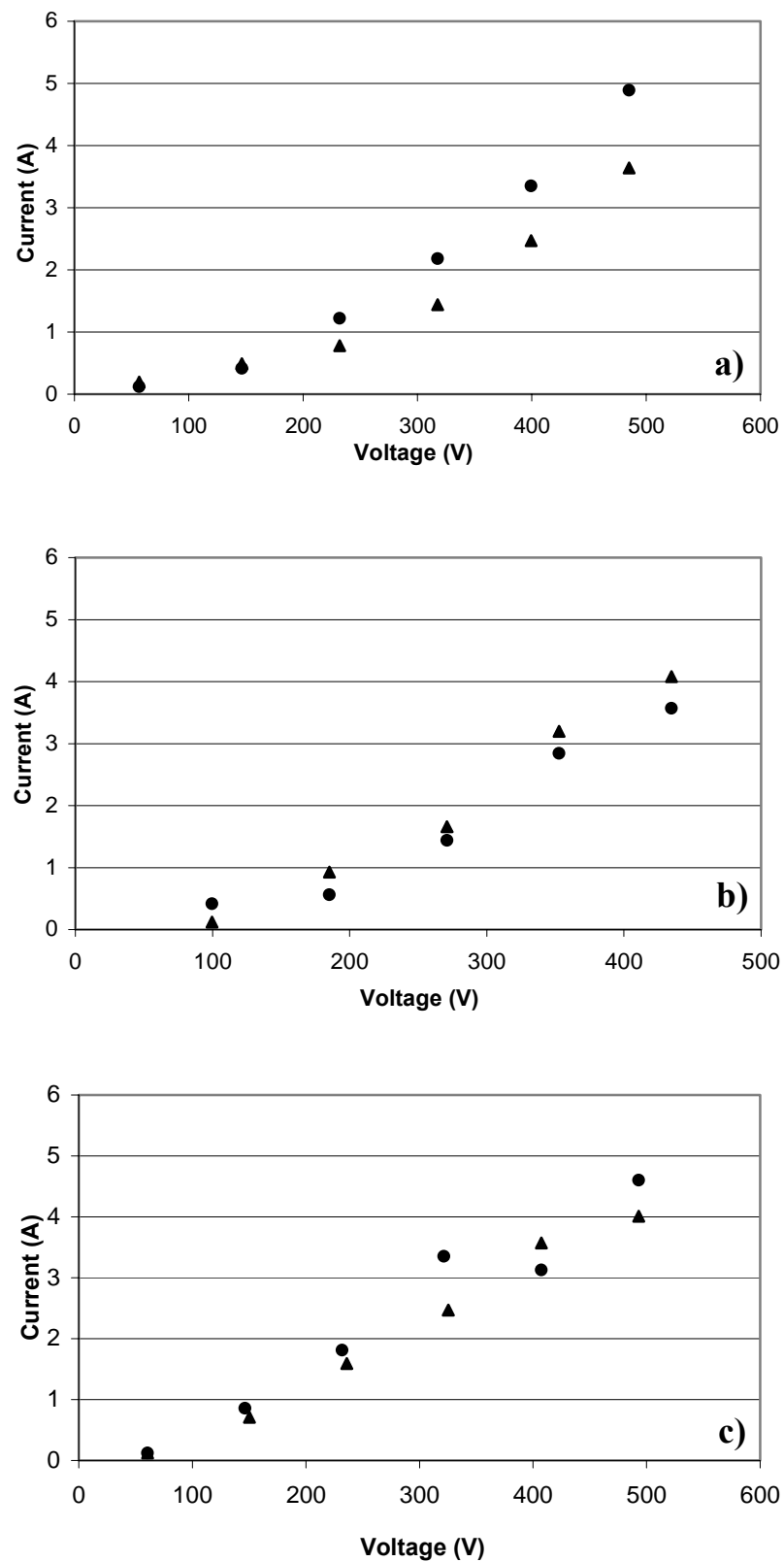


**Figure 4. 1:** The comparison of U/I dependences between a) no intradermal injection; b) 25  $\mu$ l; and c) 50  $\mu$ l of intradermally injected PBS, measured on the backs of two rats (triangles: rat one, circles: rat two)

The results showed that the quantity of the injected PBS has an effect on the I/U curves, namely the I/U dependence became more linear when we increased the quantity of the injected PBS (Figure 4. 1). Hence, we decided to use an intradermal injection of 25  $\mu$ l for future experiments dealing with gene transfer to the skin cells.

The electric field threshold values of the reversible and the irreversible electropermeabilization of the skin were estimated based on current vs. voltage curves measured during experiments. Linear regressions of current to voltage measurements corresponding to slope changes in the I/U dependences on Figure 4. 1a, give us an estimation of the points where the slope changes from the non-permeabilized to the permeabilized state and later on, to above the irreversible threshold. Threshold values of reversible and irreversible electroporation were determined as intersections of consecutive linear regressions. From our measurements we determined the reversible threshold for skin to be approximately 180 V, which agrees well with the measurements done on rat skin so far [Pavšelj *et al.*, 2005].

## 4.2. GFP expression in skin

To localize gene expression in rat skin, in order to see if the target skin tissue below *stratum corneum* has been successfully transfected after electroporation, and to perform a semi-quantitative analysis of the expression after different electroporation protocols, a plasmid coding for GFP (Green Fluorescent Protein) was injected intradermally (pCMVGFP) before application of the electric pulses. Three different electroporation protocols were used, each one consisting of one high voltage pulse, followed by one low voltage pulse.

### 4.2.1. The protocols used in GFP expression study

The plasmid was injected intradermally 30 seconds before the pulses were delivered. Plate electrodes of 4 mm spacing were used. Six rats were used in the study. Three pulsing protocols were used for the localization of a fluorescent labeled plasmid in skin (GFP) after an intradermal injection of plasmid, coding for GFP (25  $\mu$ l) with 3 repetitions for each pulsing protocol, changing the locations on the back of the rats. Three controls were included in the study, each with three repetitions. Also, the basal fluorescence of the skin was assessed.

#### Pulsing protocols:

- HV 400 V (100  $\mu$ s) + LV 32 V (400 ms)
  - HV 400 V (100  $\mu$ s) + LV 56 V (400 ms)
  - HV 400 V (100  $\mu$ s) + LV 80 V (400 ms)
- (no lag between HV and LV)

#### Controls:

- one HV pulse alone (400 V (100  $\mu$ s))
- one LV pulse alone (80 V (400 ms))
- ID injection with no electroporation
- basal skin fluorescence

Two days after the electroporation, the rats were sacrificed and skin samples were taken. Skin samples were observed without fixation or freezing with a confocal microscope. The anode and the cathode side of each electroporation site were assessed separately.

#### 4.2.2. Confocal images of GFP expression in skin

In continuation, selected confocal images for all protocols used as well as the controls are presented. Both, dermal and epidermal sides were observed for fluorescence separately, as well as the anode and the cathode sides of the electroporation site. Figure 4. 2 and Figure 4. 3 show fluorescence when only one high-voltage pulse was used (400 V, 100  $\mu$ s); Figure 4. 4 and Figure 4. 5 the expression after one low-voltage pulse (80 V, 400 ms); Figure 4. 6, Figure 4. 7 and Figure 4. 8 show GFP expression after three different HV+LV protocols: i) 400 V (100  $\mu$ s) + 32 V (400 ms), ii) 400 V (100  $\mu$ s) + 56 V (400 ms) and iii) 400 V (100  $\mu$ s) + 80 V (400 ms), respectively; and Figure 4. 9 shows fluorescence after intradermal plasmid injection without electroporation and basal skin fluorescence.

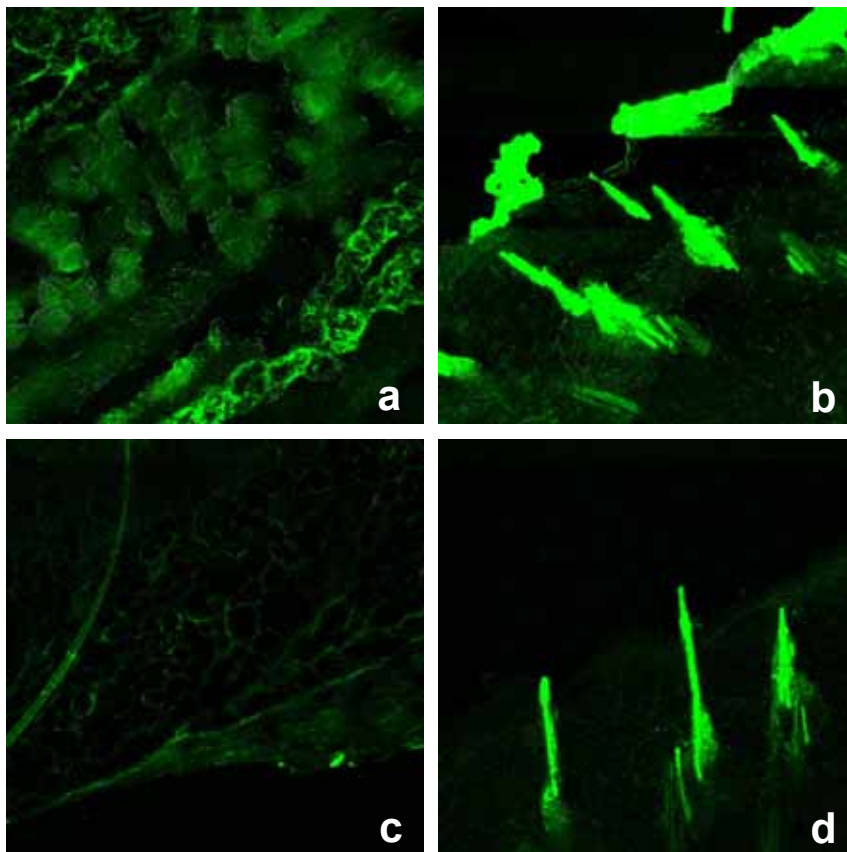
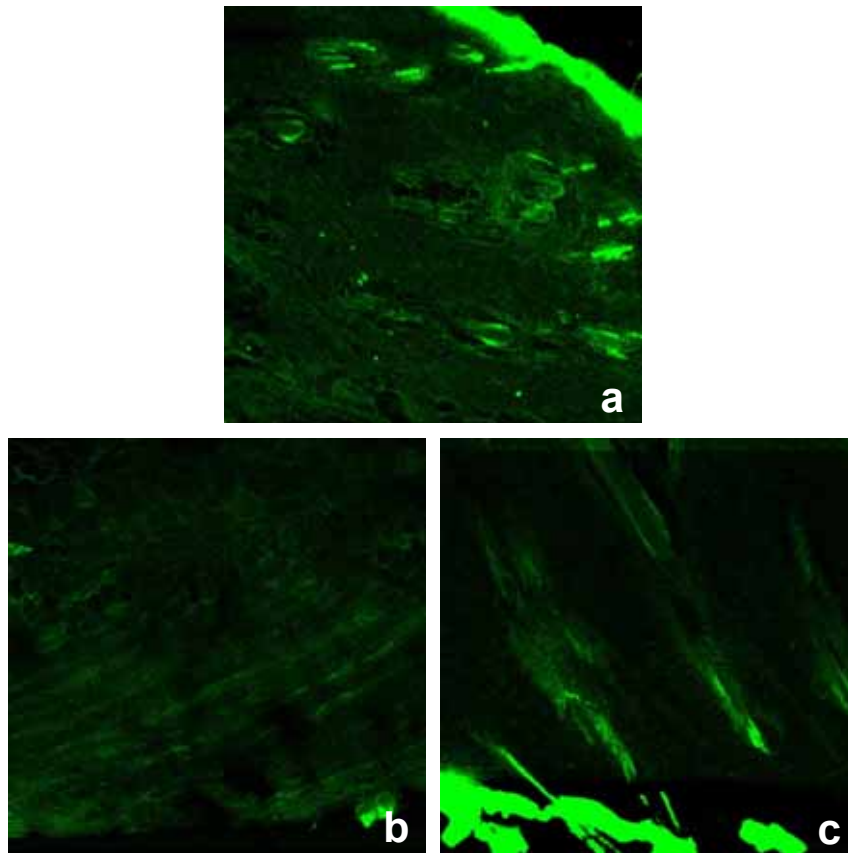


Figure 4. 2: GFP expression after high voltage pulse only (400 V, 100  $\mu$ s), rat 5; a) dermal side, anode; b) epidermal side, anode; c) dermal side, cathode; d) epidermal side, cathode



**Figure 4. 3: GFP expression after high voltage pulse only (400 V, 100  $\mu$ s), rat 6; a) dermis+epidermis, anode; b) dermal side, cathode; c) epidermis+dermis, cathode**

Looking at Figure 4. 2 and Figure 4. 3, we can establish that when only one high voltage pulse (400 V, 100  $\mu$ s) was applied, the expression of GFP remained very low both in the epidermis and to a lesser extent in the dermis. Autofluorescence of the hair follicles can be observed on the epidermal side.

Similarly, we could say that expression stays low in both the dermal and epidermal side when using only one low voltage pulse (80 V, 400 ms); (Figure 4. 4, Figure 4. 5). Again, autofluorescence of the hair follicles can be seen.

Comparing the anodal and the cathodal side of each sample, it seems like the expression is consistently slightly higher on the anodal side. Also, comparing protocols of solely one HV pulse and solely one LV pulse (Figure 4. 2 to Figure 4. 5), we can conclude that the expression is somewhat higher after the latter.

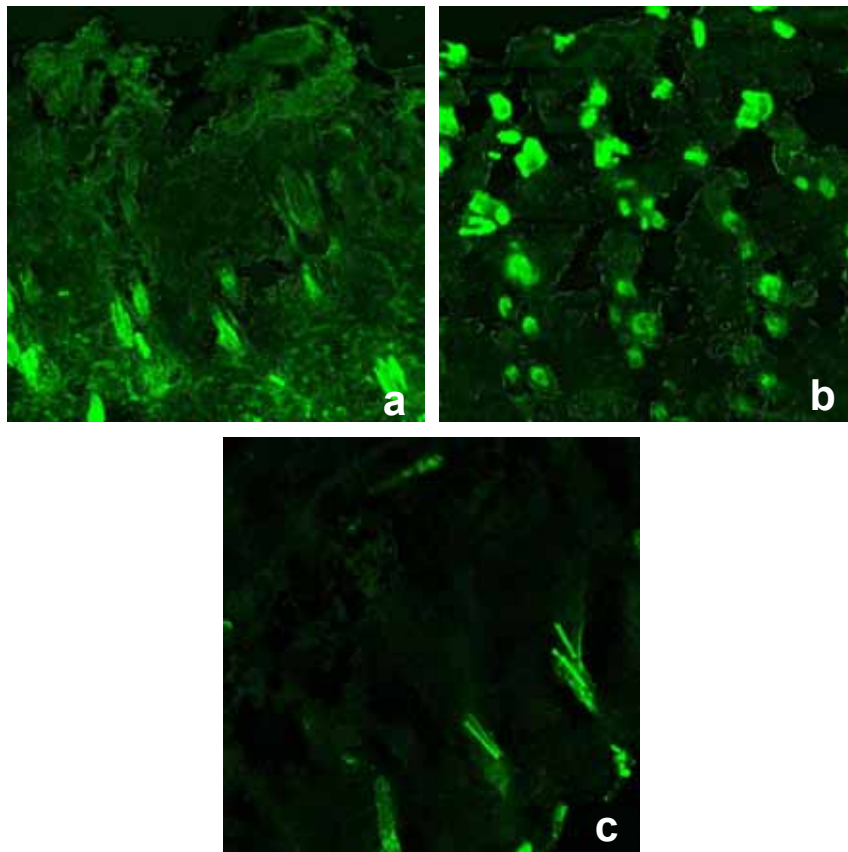


Figure 4. 4: GFP expression after low voltage pulse only (80 V, 400 ms), rat 5; a) epidermis+dermis, anode; b) epidermal side, anode; c) epidermal side, cathode

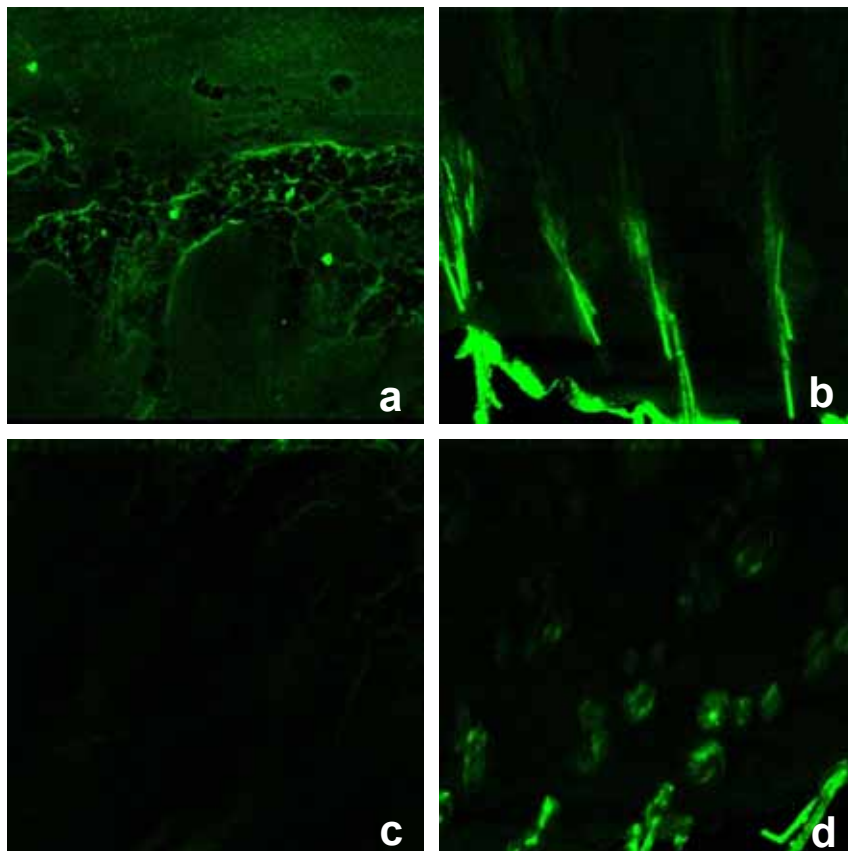
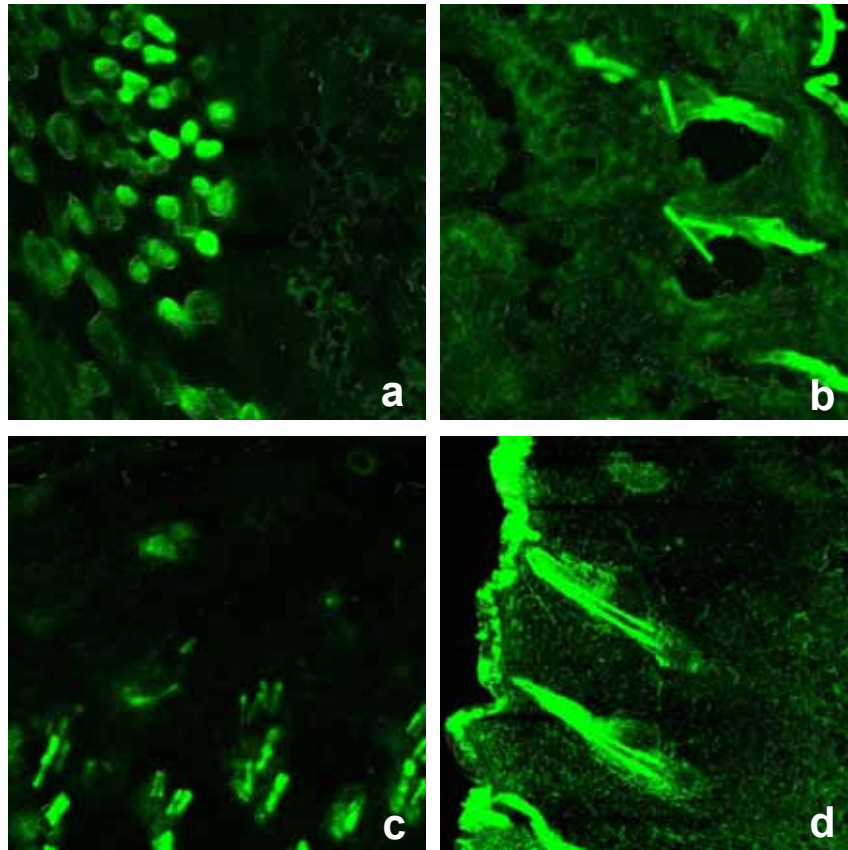
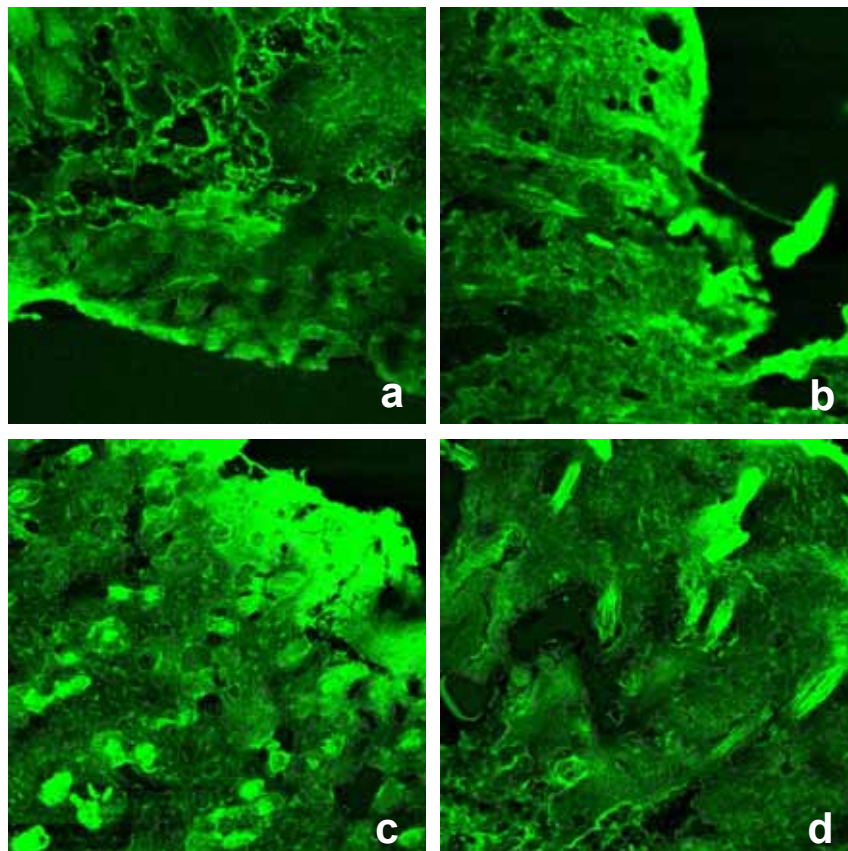


Figure 4. 5: GFP expression after low voltage pulse only (80 V, 400 ms), rat 6; a) dermal side, anode; b) dermis+epidermis, anode; c) dermal side, cathode; d) epidermis+dermis, cathode



**Figure 4. 6:** GFP expression after electroporation with HV (400 V (100  $\mu$ s)) + LV (32 V (400 ms)); a) dermal side, anode; b) epidermal side, anode; c) dermal side, cathode; d) epidermal side, cathode



**Figure 4. 7:** GFP expression after electroporation with HV (400 V (100  $\mu$ s)) + LV (56 V (400 ms)); a) dermal side, anode; b) epidermal side, anode; c) dermal side, cathode; d) epidermal side, cathode

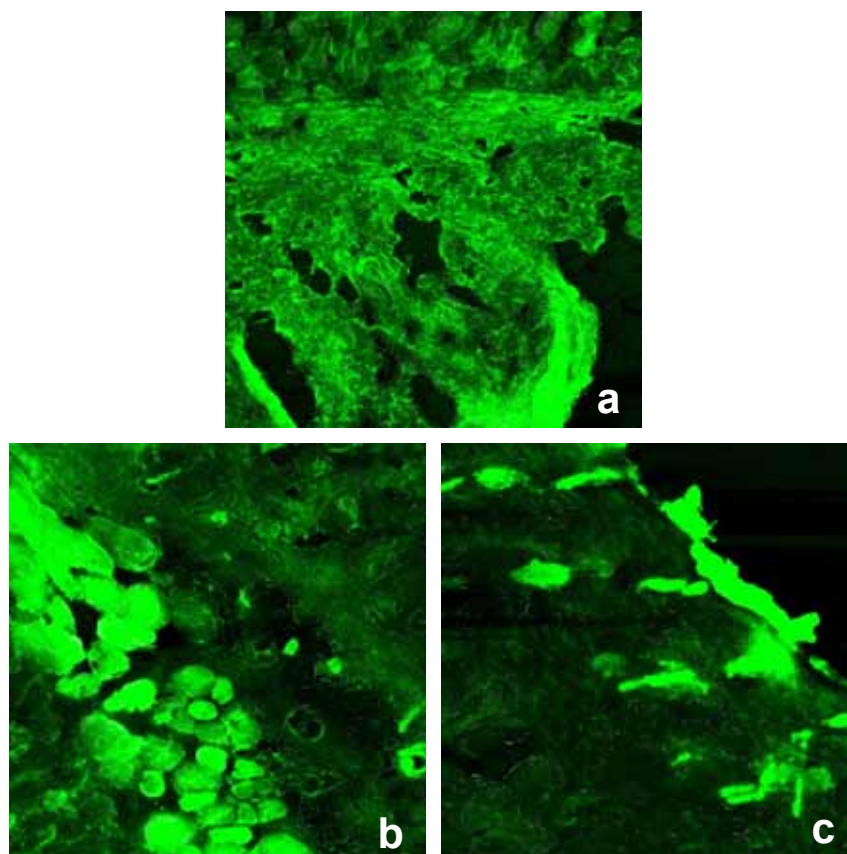


**Figure 4. 8: GFP expression after electroporation with a combination of high voltage pulse (400 V (100  $\mu$ s)) + low voltage pulse (80 V (400 ms)); a) dermis+epidermis, anode; b) dermal side, cathode; c) epidermal side, cathode**

Using a combination of a high voltage pulse (400 V, 100  $\mu$ s), followed by a low voltage pulse (32, 56 or 80 V, 400 ms), the expression of GFP in the skin was enhanced (Figure 4. 6 to Figure 4. 8). Elevated fluorescence in the dermis and the epidermis was observed. Semi-quantitative analysis indicates that protocols of HV + 56 or 80 V LV pulses were more efficient than 32 V LV. Again, the expression at the anodal side was slightly higher than expression at the cathodal side.

If we compare GFP expression after electroporation with the expression after intradermal injection of the plasmid without pulse application (Figure 4. 9), a large difference can be observed. Figure 4. 9a-d) shows a very slight and diffuse fluorescence in some area of the dermis and some autofluorescence of hair follicles. The control epidermis showed some autofluorescence of the hair follicles but no fluorescence in the dermis (Figure 4. 9e,f))

In conclusion, pulse application enhances GFP expression in the dermis and epidermis after intradermal injection of a DNA plasmid coding for GFP. The combination of a HV pulse and a LV pulse was more efficient than HV or LV pulses alone. A slightly higher expression on the anodal side can be observed.

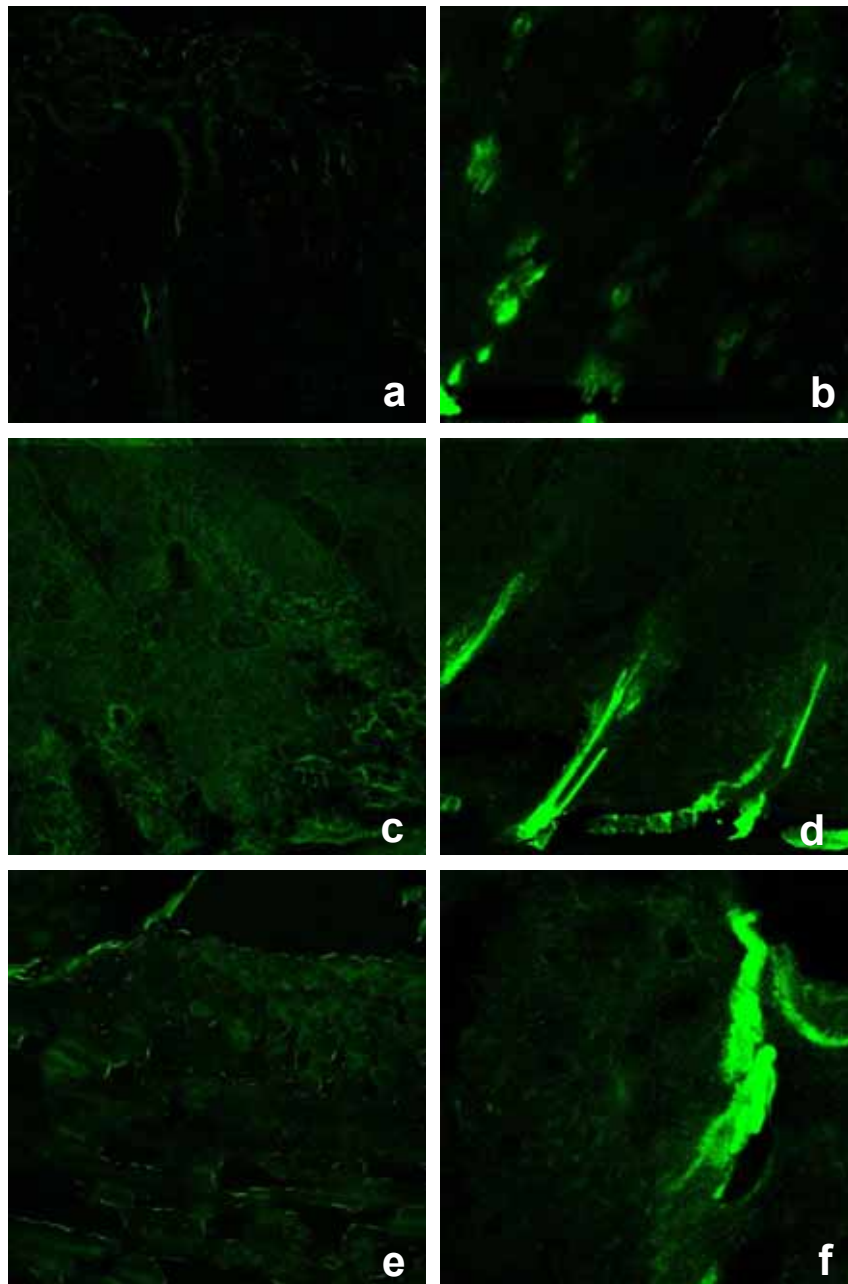


**Figure 4. 9:** GFP expression in control groups: a, c) Only intradermal injection, no electroporation, dermis; b, d) Only intradermal injection, no electroporation, epidermis; e) Basal skin fluorescence, dermis; f) Basal skin fluorescence, epidermis

### 4.3. Luciferase expression in skin

The efficacy of electroporation for gene transfer in the skin was evaluated using luciferase as a reporter gene. The efficacy of the high voltage and low voltage pulses to enhance gene transfer in rat skin was investigated in order to find the most efficient combination of the high and low voltage pulses delivered by the Cliniporator. The protocols used always consisted of one high voltage (HV) pulse followed by one low voltage (LV) pulse. We tried different amplitudes of both, HV and LV; we studied the efficacy of one long LV pulse vs. eight shorter LV pulses and the effect of delay

between the HV and the LV pulse. We also compared our proposed best protocols with those reported in literature so far [Mir *et al.*, 1998; Mir *et al.*, 1999; Glasspool-Malone *et al.*, 2000; Drabick *et al.*, 2001].

### 4.3.1. The protocols used in luciferase expression study

The pCMVluc protein was injected intradermally (50 µg/25 µl PBS) 30 seconds before pulsing. Plate electrodes of 4 mm spacing were used.

#### Pulsing protocols:

1. HV 400 V (100 µs) / LV 32 V (400 ms)
2. HV 400 V (100 µs) / LV 44 V (400 ms)
3. HV 400 V (100 µs) / LV 56 V (400 ms)
4. HV 400 V (100 µs) / LV 80 V (400 ms)
5. HV 400 V (100 µs) / LV 56 V (8x50 ms)
6. HV 400 V (100 µs) / LV 80 V (8x50 ms)
7. HV 400 V (100 µs) / LV 56 V (400 ms) -1s delay
8. HV 400 V (100 µs) / LV 80 V (400 ms) -1s delay
9. HV 400 V (100 µs) / LV 56 V (400 ms) -4.2s delay
10. HV 400 V (100 µs) / LV 80 V (400 ms) -4.2s delay
11. HV 160 V (100 µs) / LV 56 V (400 ms)
12. HV 280 V (100 µs) / LV 56 V (400 ms)
13. HV 280 V (100 µs) / LV 80 V (400 ms)
14. HV 280 V (100 µs) / LV 56 V (400 ms) -4.2s delay
15. HV 280 V (100 µs) / LV 80 V (400 ms) -4.2s delay
16. HV 280 V (100 µs) / LV 56 V (8x50 ms)
17. HV 280 V (100 µs) / LV 80 V (8x50 ms)
18. HV 520 V (100 µs) / LV 56 V (400 ms)
19. 6x HV 700 V (100 µs), 8 Hz
20. 6x LV 100 V (20 ms), 1 Hz (pause 980 ms)

#### Controls:

21. only intradermal injection, no EP
22. only HV (400 V, 100 µs)
23. only LV (80 V, 400 ms)
24. basal luciferase activity

### 4.3.2. Luciferase activity after different EP protocols

Results are represented on a log scale with pg of luciferase per mg of tissue of all the samples in each group. Normality test over the experimental groups failed, so the data is represented with a median (horizontal line), 25th and 75th percentile (grey box) and 10th and 90th percentile (error bars). Black dots represent all the outliers. Red diamonds represent the mean of each group. We can see the comparison of different protocols in Figure 4. 10 - Figure 4. 17.

All electroporation protocols used in the luciferase expression study are gathered in Figure 4. 10. Effects of different HV and LV amplitudes, the splitting of the LV pulse and the delay between the HV and the LV pulse are shown in Figure 4. 11 to Figure 4. 17.

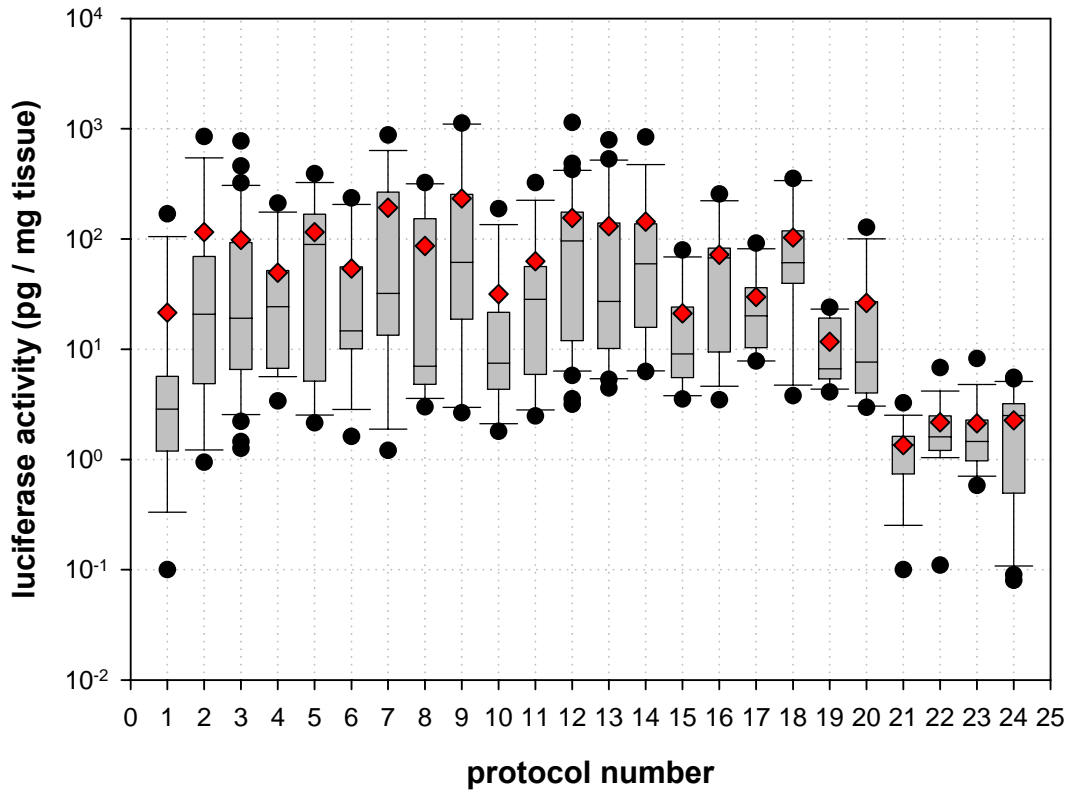


**Figure 4. 10: Luciferase expression after different electroporation protocols. All protocols used in the study are shown in the figure. For protocol descriptions see previous page. Red diamonds represent the means of each group.**

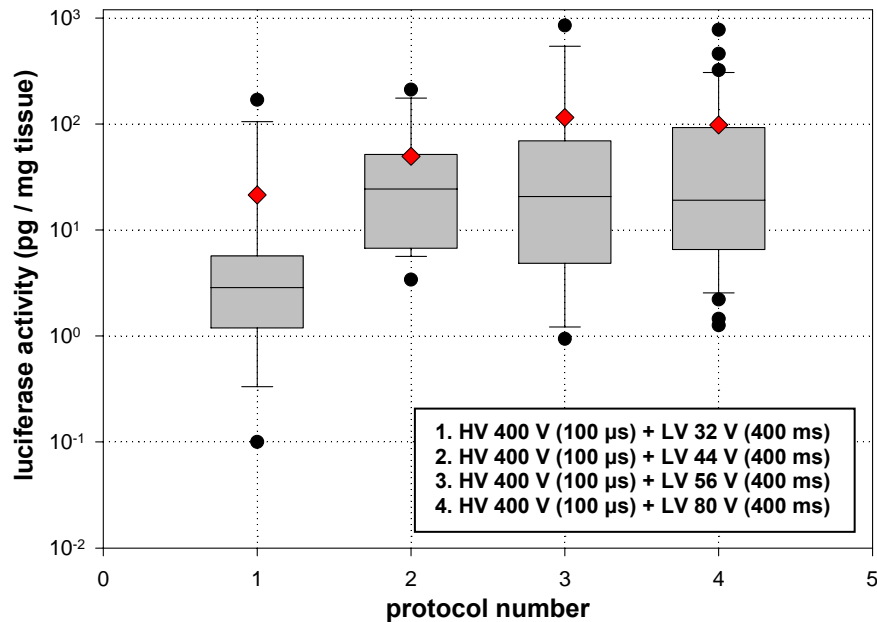


**Figure 4. 11: Effect of different amplitudes of LV pulse (400 ms) applied after 1 HV (400 V, 100µs) on luciferase activity in the skin. Red diamonds represent the means of each group.**

The first step consisted in investigating the influence, on DNA expression in the skin, of the amplitude of the low voltage pulse (32, 44, 56 and 80 V (400 ms)) applied after 1 high voltage pulse of 400 V (100 $\mu$ s). Although no statistical difference was found between the four groups in Figure 4. 11, it seems like the expression after the LV pulse of 32 V is somewhat lower than in the rest of the groups.

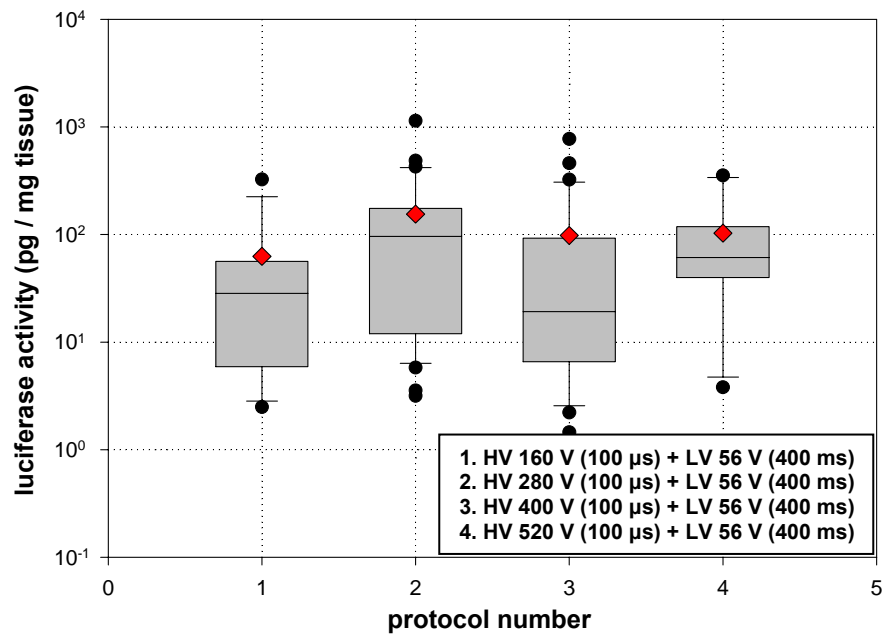


**Figure 4. 12:** Effect of different amplitudes of the HV pulse (100  $\mu$ s) applied before 1 LV (56 V, 400 ms) on luciferase activity in the skin. Red diamonds represent the means of each group.

The second step consisted of analyzing the influence of the amplitude of the 100  $\mu$ s long HV pulse (160, 280, 400 or 520 V) applied before a LV pulse of 56 V and 400 ms duration (Figure 4. 12). Again, no statistical difference was found between the four groups.

To optimize the combination of a permeabilizing HV pulse and an electrophoretic LV pulse, the influence of the delay between HV and LV pulses (1 or 4.2 s) as well as the splitting of the LV pulse (1 x 400 ms vs. 8 x 50 ms) was analyzed. The rationale for those experiments was that a lag time between HV and LV or a splitting of the LV would allow a better diffusion of the DNA.

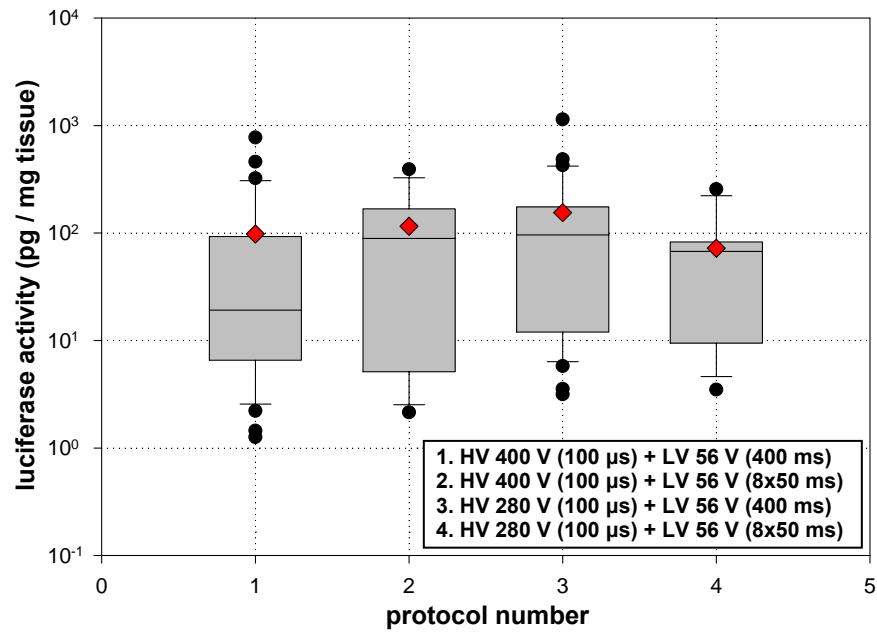


Figure 4. 13: Effect of one long LV pulse (400 ms) vs. eight shorter (50 ms) LV pulses of 56 V applied after 1 HV pulse (280 or 400 V, 100 μs) on luciferase activity in the skin. Red diamonds represent the means of each group.

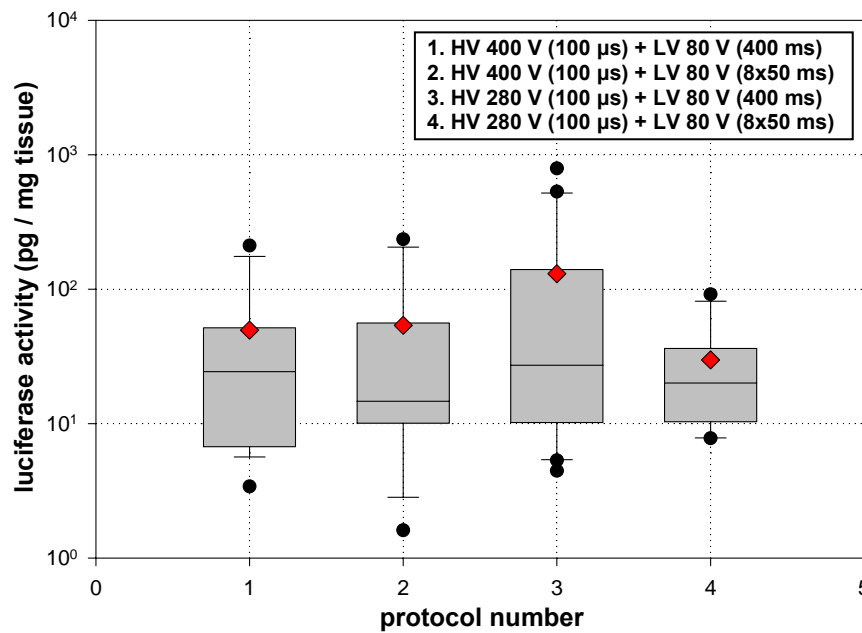


Figure 4. 14: Effect of one long LV pulse (400 ms) vs. eight shorter (50 ms) LV pulses of 80 V applied after 1 HV pulse (280 or 400 V, 100 μs) on luciferase activity in the skin. Red diamonds represent the means of each group.

As shown in Figure 4. 13 and Figure 4. 14, the splitting of the LV pulses did not result in a higher efficacy of electrotransfer. Similarly, no difference was observed between a delay of 1 second and a delay of 4.2 seconds (Figure 4. 15 and Figure 4. 16). Once again, the statistical difference was too low to ascertain that the splitting of the LV pulse or the delay works either in favor of or against the luciferase expression in skin.

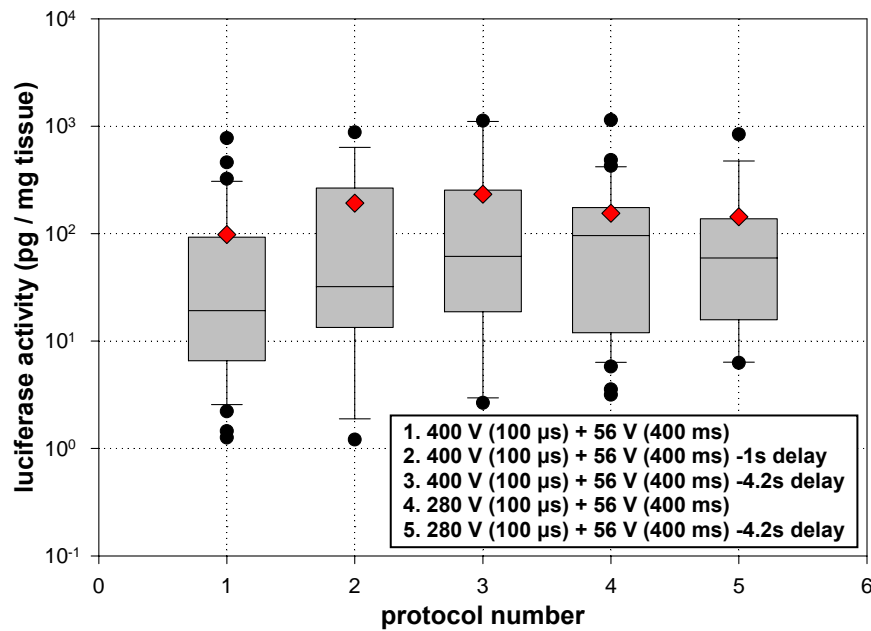


Figure 4. 15: Effect of delay between HV (280 or 400 V, 100  $\mu$ s) and LV (56 V, 400 ms) vs. no delay on luciferase activity in the skin. Red diamonds represent the means of each group.

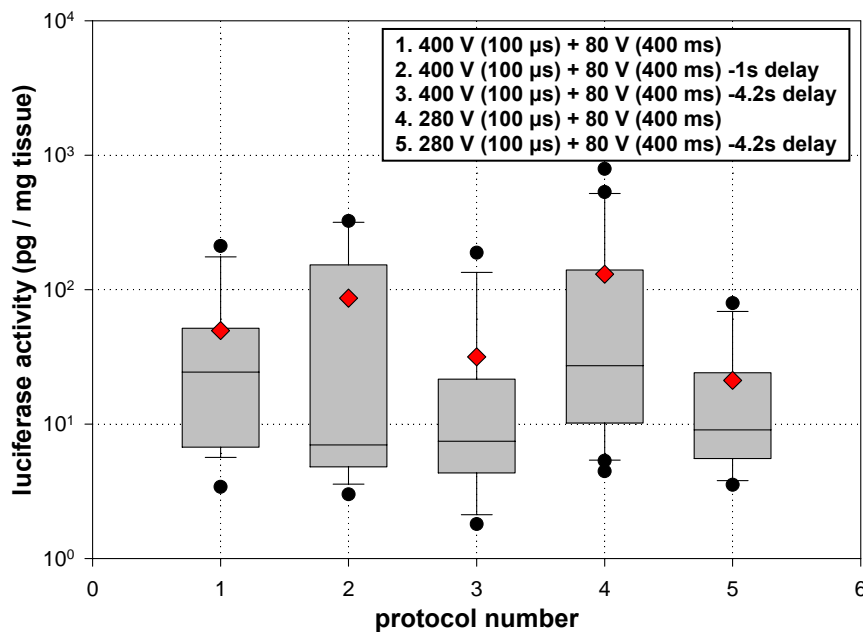


Figure 4. 16: Effect of delay between HV (280 or 400 V, 100  $\mu$ s) and LV (80 V, 400 ms) vs. no delay on luciferase activity in the skin. Red diamonds represent the means of each group.

Finally, to prove that the combination of 1 HV, to permeabilize the skin cells, and a LV pulse, to enhance DNA transfer by electrophoresis, is an efficient approach, selected protocols of HV+LV combinations were compared to protocols described in the literature: 1) 6 to 8 HV pulses (1500 to 1750 V/cm 100  $\mu$ s) previously shown to enhance local and systemic expression or induce immune response of different plasmids

[Drabick *et al.*, 2001]; 2) 6 LV pulses of 5 to 20 ms which were shown to be more effective than 6 HV pulses in muscle [Mir *et al.*, 1998; Mir *et al.*, 1999; Glasspool-Malone *et al.*, 2000].

Due to the scattering of the data which were not normally distributed, a non parametric statistical analysis was performed. The data in Figure 4. 17 clearly demonstrate that the luciferase activity was higher when the combination of HV + LV was used. A statistically significant difference was found between the HV+LV and 6xHV or 6xLV pulse protocols.

The analysis of the influence of electroporation on luciferase expression in the skin after intradermal injection of DNA demonstrates: i) The combination of HV+LV is more efficient than HV or LV pulse(s) alone; ii) Of the HV+LV electroporation protocols tried, almost no statistical difference was found, iii) The splitting of the LV pulse and the delay between the HV and the LV pulse has no positive nor adverse effect on luciferase expression in skin.

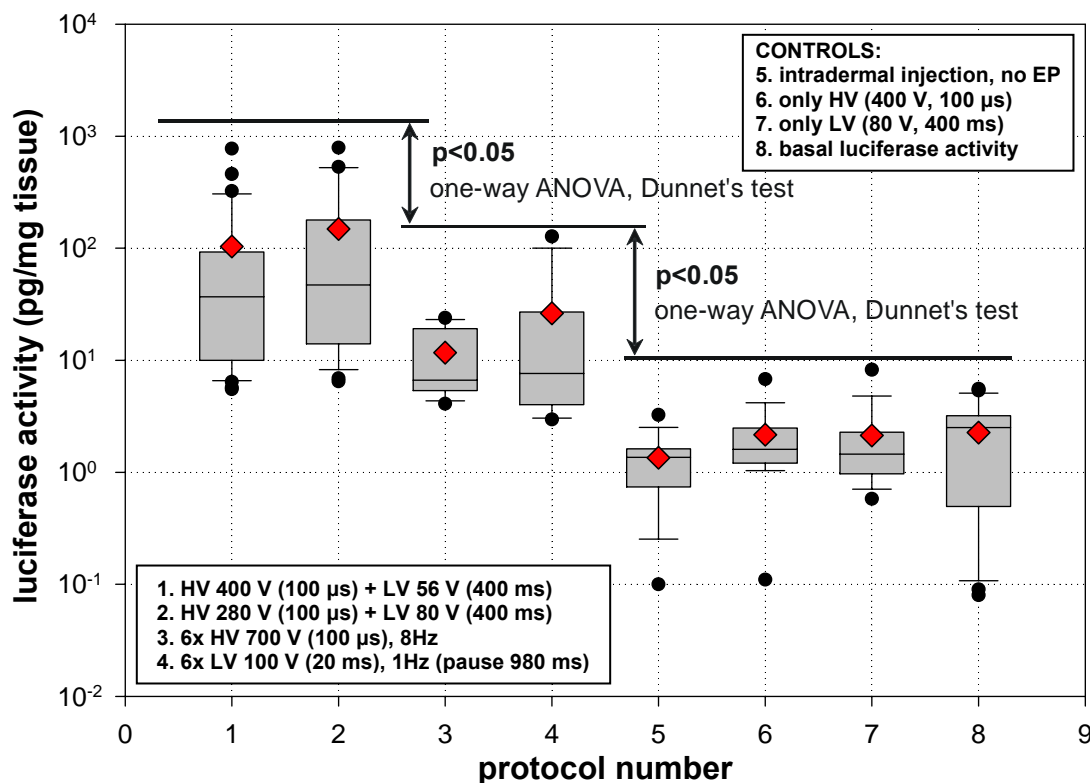


**Figure 4. 17: Comparison of selected HV +LV protocols vs. "old" protocols (6 HV or 6 LV) and controls (1 HV, 1 LV, only intradermal injection, basal luciferase activity). Red diamonds represent the means of each group.**

#### 4.4. Kinetic study (pCMVluc reporter gene)

To assess the duration of gene expression coding for luciferase in the skin, a kinetic study was performed. The expression of the luciferase gene was measured at different days after electroporation.

#### 4.4.1. The protocols used in the kinetic study

The pCMVluc plasmid was injected intradermally 30 seconds before pulsing. Plate electrodes of 4 mm spacing were used. Eighteen rats were used in the study. Only one pulsing protocol was used to assess the duration of the luciferase expression. Since we found no statistical difference between the HV+LV protocols tested, one of the successful protocols with the lowest HV amplitude was used. One control was included in the study.

##### Pulsing protocol:

- HV 280 V (100  $\mu$ s) + LV 80 V (400 ms).

##### Control:

- Only intradermal injection, no electroporation

The animals were sacrificed 1, 2, 3, 4, 7, 10, 14, 21, 25 days after the experiment and the electroporated areas of the skin were taken. We assessed the luciferase activity on 10  $\mu$ l of the lysate supernatant. The final results in Figure 4. 18 are expressed as pg of luciferase per mg of tissue by calibration with purified firefly luciferase protein.

#### 4.4.2. The duration of the luciferase expression in skin

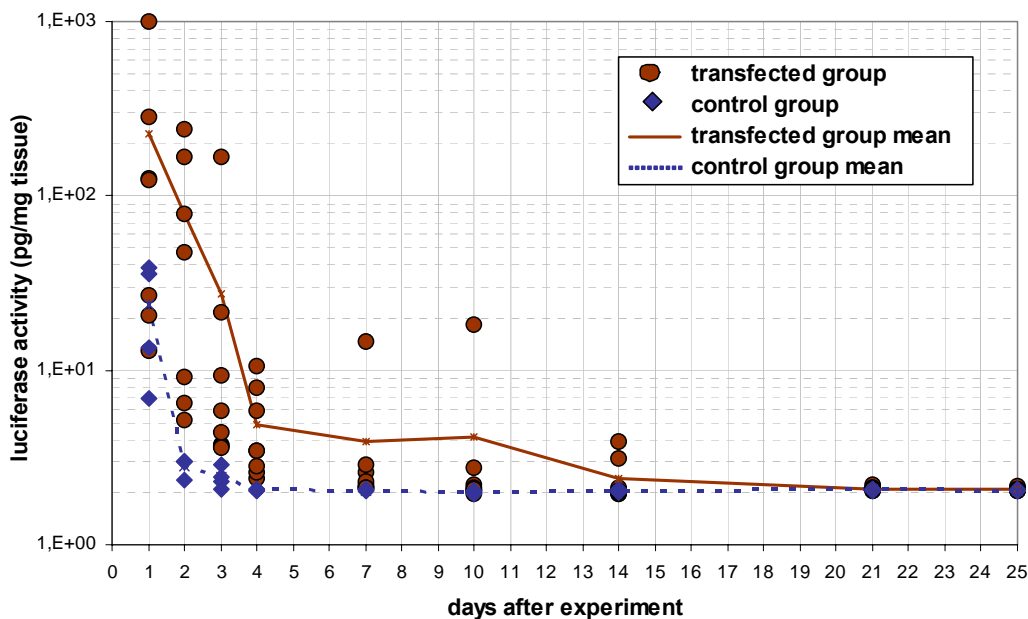


**Figure 4. 18: Kinetics of luciferase expression in the skin after intradermal injection of 50  $\mu$ g pCMVluc. Red diamonds denote expression when ID injection was followed by electroporation: 280 V, 100  $\mu$ s + 80 V, 400 ms (n=8); Blue diamonds: no electroporation (n=4). The data are also represented with mean values (red and blue lines). The data are in general not normally distributed.**

The data shown in Figure 4. 18 indicate that that pulsing increases both the amount and the duration of gene expression in the skin. This expression was maximum at 24 h to 48 h and decreased rapidly to control values in 2 days. In the control group of intradermal injection alone, without electroporation, a rather high expression was observed the first day after the injection, then the expression dropped close to zero already on the second day. Statistical analysis showed statistically significant differences between the electroporated group and the control group on days: 2, 3, 4, 7 ( $p < 0.05$ ).

The apparent inability to produce prolonged, high level gene expression in skin *in vivo* can be seen as a deficiency in skin gene therapy as longer expression durations are needed for the treatment of many of the genetic skin disorders.

## 4.5. Immunization study

An immunization study using a plasmid coding for a model antigen ovalbumin was performed. Optimized protocols from previous studies were compared to electroporation protocols described in the literature [Drabick *et al.*, 2001].

### 4.5.1. The protocols used in the immunization study

Female Balb/c mice were injected intradermally with PBS (negative control), ovalbumin (OVA – with or without alum as adjuvant) or a plasmid coding for ovalbumin (see Table 4. 1). Electrical pulses were applied 30 seconds after DNA injection. Two and four weeks after the priming, two boosts were applied. Blood samples were collected by retroorbital bleeding before, two weeks, four weeks and six weeks after priming.

**Table 4. 1: Protocols of the immunization study**

Group	ID injection	Electroporation protocol
1	DNA	HV 280 V (100 $\mu$ s), LV 80 V (400 ms)
2	DNA	HV 280 V (100 $\mu$ s), LV 80 V (400 ms), delay 4.2 s
3	DNA	6x 700 V (100 $\mu$ s), 8 Hz (125 ms lag between pulses)
4	DNA	-
5	OVA	-
6	OVA + alum	-
7	PBS	-

### 4.5.2. The immune responses

Titers of antibodies (IgG) to OVA were determined by ELISA. Isotypes (IgG1, IgG2a or IgG2b) were determined using appropriate secondary antibodies.

**Table 4. 2: Total IgG in individual mice and number of responding mice.**

Group	Week 4		Week 6	
	IgG <sup>a</sup>	responder <sup>b</sup>	IgG <sup>a</sup>	responder <sup>b</sup>
1	3.41 ± 0.44	8/8	3.49 ± 0.40	5/5
2	3.24 ± 0.35	5/5	4.14 ± 0.13	5/5
3	2.61 ± 0.16	3/7	3.03 ± 0.29	7/7
4	2.80 ± 0.42	2/7	2.86 ± 0.45	8/8
5	3.39 ± 0.64	8/8	3.49 ± 0.38	8/8
6	4.0 ± 0.14	6/6	4.45 ± 0.2	5/5
7	/	/	/	/

<sup>a</sup> Mean IgG titer (+/- SD) in responding mice determined by ELISA in individual mice

<sup>b</sup> number of mice showing IgG titers > background values

IgG responses were detected in the mice immunized with OVA or the plasmid coding for OVA whereas no response was observed in the control group 7 (Table 4. 2). Application of electrical pulses increased the immune response (group 1, 2, 3 vs. group 4). The groups receiving HV + LV protocols had a higher immune response (groups 1, 2) than the group treated with several HV pulses alone (group 3). The IgG levels after DNA electrotransfer with HV + LV were equivalent to the IgG level in mice immunized with OVA (group 5) but somewhat lower than in mice immunized with OVA and the standard adjuvant alum (group 6). No significant difference was found between week 4 and week 6.

No IgG2a and IgG2b responses were detected (except for 2 mice in group 1), suggesting that only a Th2 response was induced.

In conclusion, this immunization experiment demonstrates that i) electroporation enhances the immune response induced after intradermal injection of a DNA plasmid coding for an antigen, and ii) the proposed HV + LV protocols are more efficient than protocols (6 to 8 HV pulses) previously described.

## 4.6. Tolerance study

We studied the effect of the proposed protocols on the skin. The side effects were investigated by standard methods used to assess the effect of skin treatments [Vanbever *et al.*, 1998; Vanbever and Pr at, 1999; Dujardin *et al.*, 2002]. Non invasive bioengineering methods were used to evaluate *in vivo* if Cliniporator induces an erythema (chromametry) or impairment of barrier function (transepidermal water loss). Histology was used to investigate possible effects on the skin structure. One pulsing protocol and two controls were tested.

### 4.6.1. The protocols used in the tolerance study

The PBS was injected intradermally 30 seconds before the pulses were delivered, using plate electrodes of 4 mm spacing. Eighteen rats were used in the study. Only one pulsing protocol was used, along with two controls. For the pulsing protocol we chose the one with the highest HV, LV amplitudes used in our studies.

#### Pulsing protocol:

- HV 400 V (100  $\mu$ s) + LV 80 V (400 ms).

#### Controls:

- Skin fold with gel. The electrodes were applied for as long as we usually need to deliver pulses but no actual pulses delivered.
- Skin fold without gel. The electrodes were applied for as long as we usually need to deliver pulses but no actual pulses delivered.

The anode and the cathode side of each electroporation site were measured before electroporation, shortly after, and 30, 60, 120 minutes and 24 hours after the pulse application. Transepidermal water loss was used to assess the barrier function of the skin. Chromametry was used to measure the color (erythema) of the skin. Histology was used to investigate the effect on the skin structure.

### 4.6.2. The effects of electroporation protocols on skin

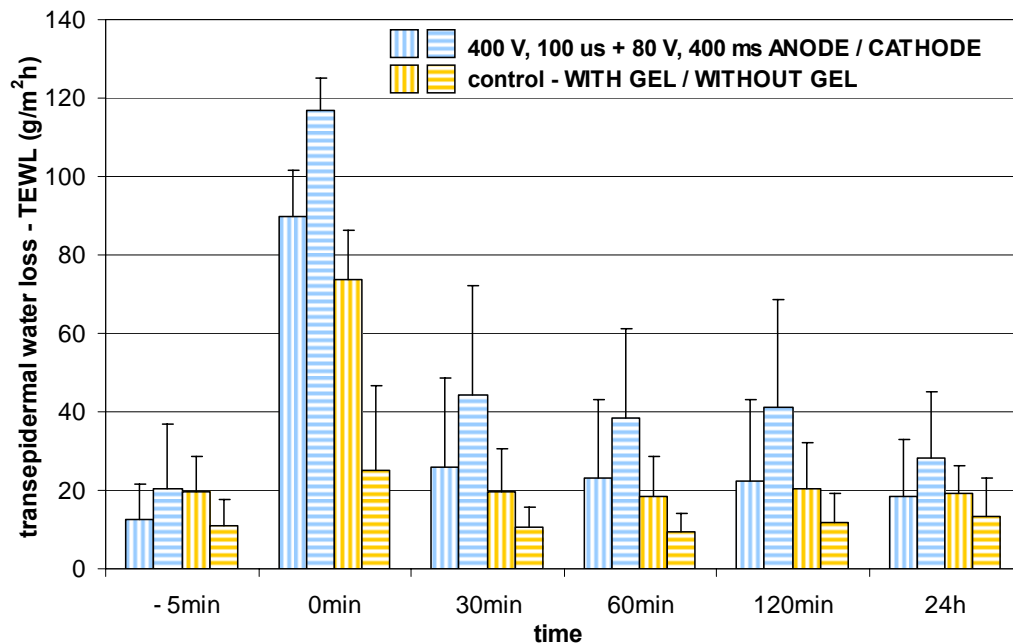


**Figure 4. 19: Transepidermal water loss (TEWL) of rat skin exposed to electroporation with one HV and one LV pulse as a function of time after electroporation. The data are represented with means and standard deviations.**

Figure 4. 19 shows an increase in the transepidermal water loss (TEWL) values right after the delivery of the pulses. However, the controls where we applied conductive gel also had high TEWL values, suggesting that the high TEWL values resulted from evaporation of gel water from the skin surface. Although the barrier function of the skin was slightly impaired just after electroporation, as evidenced by the drop in the resistance of the skin, the change in TEWL was small and transient. TEWL values were down to normal within 30 min. TEWL values on the anode side of the electroporation side were consistently lower than those on the cathode side.

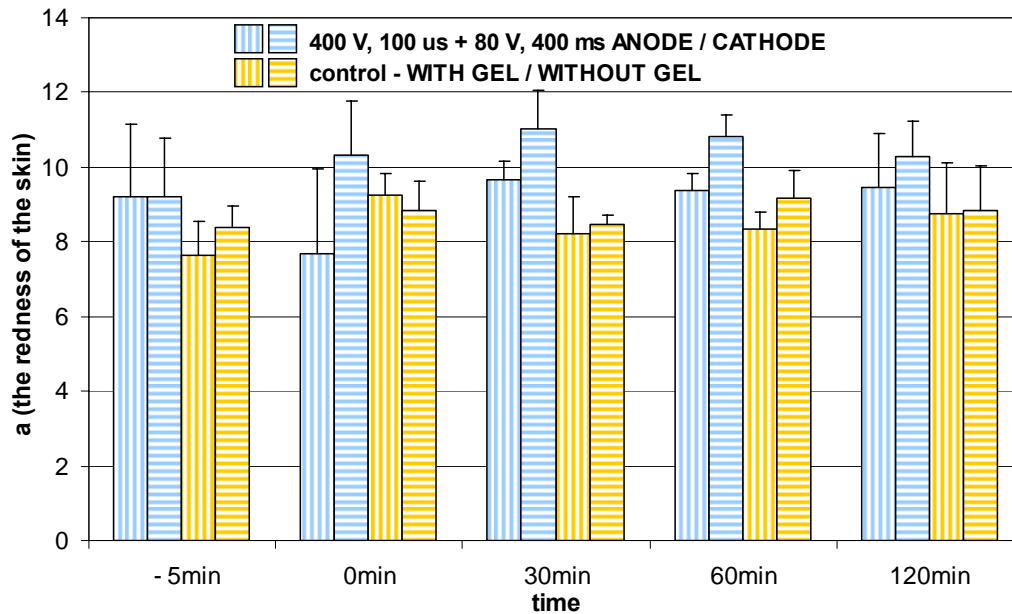


**Figure 4. 20: The redness of rat skin exposed to electroporation with one HV and one LV pulse as a function of time after electroporation. The data are represented with means and standard deviations.**

Values of parameter a (redness of skin) indicate that no erythema was induced by HV+LV pulses (Figure 4. 20). During the experiments we noticed some redness with the naked eye. The electroporation site turned red a few minutes after pulsing but it was a short-term change. There was a consistent difference between the anode and the cathode side of the electroporation sites.

No damage in the histological structure of the skin was observed. Neither inflammation nor necrosis was detected 24 h after application of HV+LV pulses.

## CHAPTER 5

# Numerical models

Skin consists of different layers. Its outermost layer, the *stratum corneum*, although very thin, presents a formidable barrier for the entry of ions and molecules into the body, protects the underlying tissues and is therefore a primary immune organ in human body. Its conductivity is very low and three to four orders of magnitude lower than the conductivities of deeper skin layers and tissues [Yamamoto and Yamamoto, 1976; Yamamoto and Yamamoto, 1976a; Pliquett *et al.*, 1995]. From the electrical aspect, applying electric pulses on skin means that almost the entire voltage drop rests across the *stratum corneum*. That causes a very high electric field in that layer, while the electric field in deeper layers of the skin remains too low for a successful electroporation. However, experiments show a successful DNA electrotransfer into the skin can be achieved and is probably due to the rise in conductivity of the *stratum corneum* during electroporation (see GFP localization results in the previous chapter). The electric field “penetrates” deeper into the skin and permeabilizes the target cells. A similar problem can be encountered during electrochemotherapy of subcutaneous tumors, where the electrical barrier of skin needs to be breached in order to permeabilize the tumor lying underneath. We undertook a study where we described this process with a numerical model where the electric field distribution and the electric current were computed in discrete steps according to the conductivity changes of tissues involved (published in Paper 4, Appendix).

We constructed a numerical model of the skin fold as was used in the *in vivo* experiments to try to describe the process of skin electroporation. Using voltage and current measurements recorded during pulse delivery, we aimed at making the response of the model as close as possible to the real system. However, we only focused on the first, permeabilizing, high voltage pulse. The length of the high voltage pulse was 100  $\mu\text{s}$  which is long enough for tissue permeabilization to take place if other pulse parameters are adequate. The nonlinear nature of the process was taken into account. Namely, the increase of conductivity of the tissue being permeabilized causes electric field distribution to change during the process which can again change the conductivity [Pavlin *et al.*, 2005; Pavšelj *et al.*, 2005, Šel *et al.*, 2005]. So the model needs to be solved in as many iterations as needed to reach a steady state.

## 5.1. The numerical model of a skin fold

The geometry of our numerical model was as described in subchapter 3.2.2. (Figure 3. 1 and Figure 3. 2). During the finite model analysis, tissue conductivities were changed according to the electric field strength throughout the model. The iterative nonlinear computation was repeated until the electric field distribution reached its steady state. We modeled the process of tissue permeabilization inside the high-voltage (HV) pulse. The resealing process after the pulse was not modeled, nor was the low-voltage electrophoretic pulse. The conductivities and the electric field electropermeabilization thresholds used are given in Table 5. 1. We used the same values for the dermis and the epidermis, as we could not find any separate data for the two layers. However, in the model, the dermis and the epidermis were modeled separately (Figure 3. 2), so different parameters can be used in each layer.

**Table 5. 1: Parameters used in the numerical model of the electropermeabilization process in skin**

Tissue	$\sigma_0$ (S/m)	$\sigma_1$ (S/m)	$\sigma$ increase	$E_{rev}$ (V/cm)	$E_{irrev}$ (V/cm)
stratum corneum	0.000075	0.0375	500x	400	900
epidermis, dermis	0.2	0.6	3x	400	900
fat, connective tissue	0.03	0.09	3x	200	400

The  $\sigma(E)$  dependences of biological tissues are another unknown of tissue electropermeabilization. The simplest of the dependences is the step function, where, once the reversible electric field threshold is reached, the conductivity changes from its low to its high value. However, to improve convergence of the numerical calculation, the smoothed step functions were used to describe the  $\sigma(E)$  dependences of the skin layers (matlab function *flchs*). Also, a kind of a smoothed model of the electropermeabilization seems the most logical. Namely, due to the non-uniformity of the cell size and shape in the tissue, not all the cells are permeabilized at the same time once the threshold electric field is reached. Furthermore, when the electric field is reaching the irreversible threshold, cell non-uniformity would also lead to a gradual saturation of the curve [Pavšelj *et al.*, 2005]. The  $\sigma(E)$  curves are shown in Figure 5. 1. The curves were set with help from literature and experiments, however, due to the very scarce data on virtually everything but the initial conductivities, the curves were chosen semi-arbitrarily. Namely, very little data exists on the conductivities of permeabilized tissues and electroporation thresholds. We obtained the latter from the measurements during experiments done on skin folds so far [Pavšelj *et al.*, 2005]. Skin thresholds stated in Table 5. 1 also correspond well to the I/U curves described in subchapter 4.1. The initial conductivities and the ranges of the conductivity changes were taken from the literature [Yamamoto and Yamamoto, 1976; Yamamoto and Yamamoto, 1976a; Prausnitz *et al.*, 1993; Pliquett *et al.*, 1995; Gabriel C. *et al.*, 1996; Gabriel S. *et al.*, 1996; Pliquett and Weaver, 1996; Gallo *et al.*, 1997; Jadoul *et al.*, 1999; Pliquett, 1999; Pavšelj *et al.*, 2005].

The *stratum corneum* shows the most drastic conductivity increase, while the tissues below experience a much lower rise in conductivity when permeabilized. We found no measurements on subcutaneous connective tissue and fat, so the permeabilization parameters were set similar to those of fat.

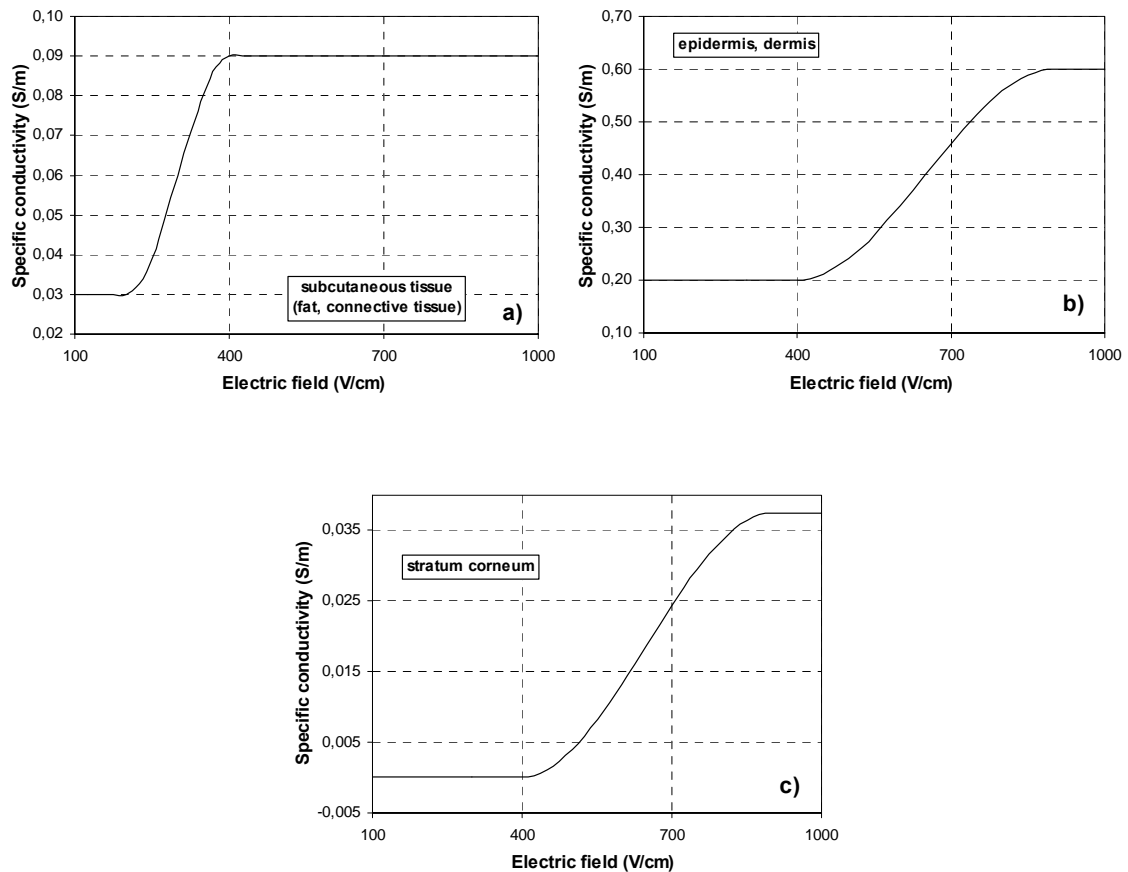


**Figure 5. 1:** The  $\sigma(E)$  electropermeabilization curves of the skin layers: a) subcutaneous tissue; b) epidermis, dermis; c) *stratum corneum*

Figure 5. 2 shows the electric field distribution in the skin fold for the applied voltage of 400 V, not taking into account the conductivity changes during electropermeabilization. The electric field in the *stratum corneum* is well above the critical value, as most of the voltage applied occurs across this highly resistive layer, while the rest of the modeled skinfold is not permeabilized.

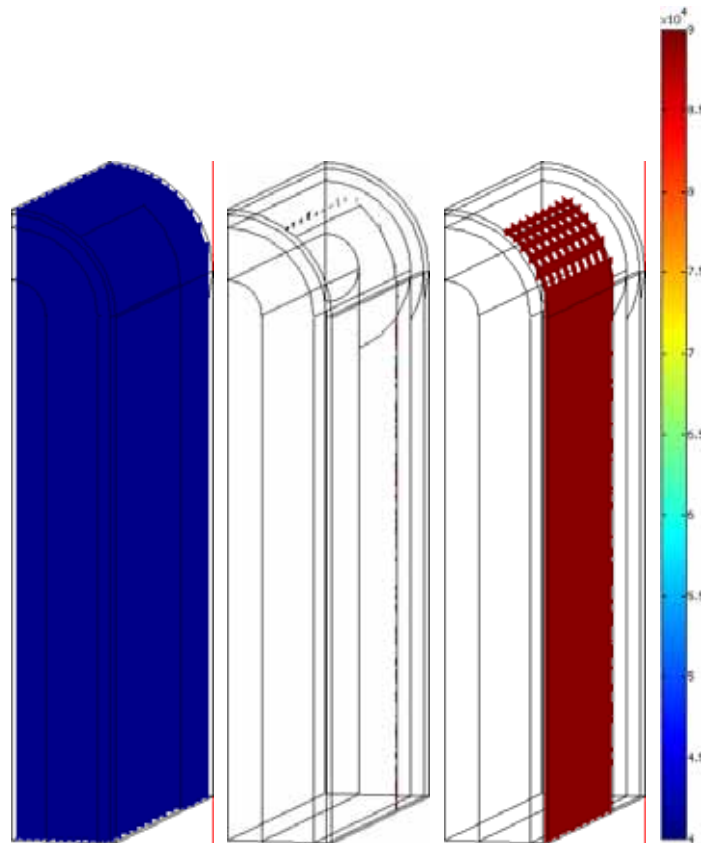


**Figure 5. 2:** 3D slice plots of the electric field distribution of the linear model of the skin fold, not changing tissue conductivities. The applied voltage was 400 V. The electric field is shown in volts per meter.

In our *in vivo* experiments we tested different amplitudes of the HV and the LV pulse. Five different voltages were used for the permeabilizing, high-voltage pulse (160, 280, 400, 520 and 700 V). During the pulse, the voltage between the electrodes and the current through the skin fold were measured by the Cliniporator and stored on the computer for future use. The finite elements model of skin electropermeabilization was run at all five voltages used and the electric currents obtained from the model were compared to our experimental data. Figure 5. 3 shows the currents of the model compared to the currents measured *in vivo* during the pulse. A good agreement can be observed in the current-voltage dependence between the *in vivo* data and the output of the model.

Electric field distributions of the skin fold, represented with slice plots in 3D at the end of the electropermeabilization process for the applied voltages of 160, 280, 400, 520 and 700 V, respectively, are presented in Figure 5. 4 to Figure 5. 8. The figures show only one fourth of the distribution, as only one fourth of the skin fold was modeled, due to the symmetry of the model. The first distribution on each figure shows the area below the reversible electric field threshold of 400 V/cm (blue color); The second distribution shows the area between the reversible and the irreversible thresholds – 400 V/cm <math>E</math> <math>900</math> V/cm – (blue to red colors); And the third one shows the area above the irreversible threshold of 900 V/cm (red color).

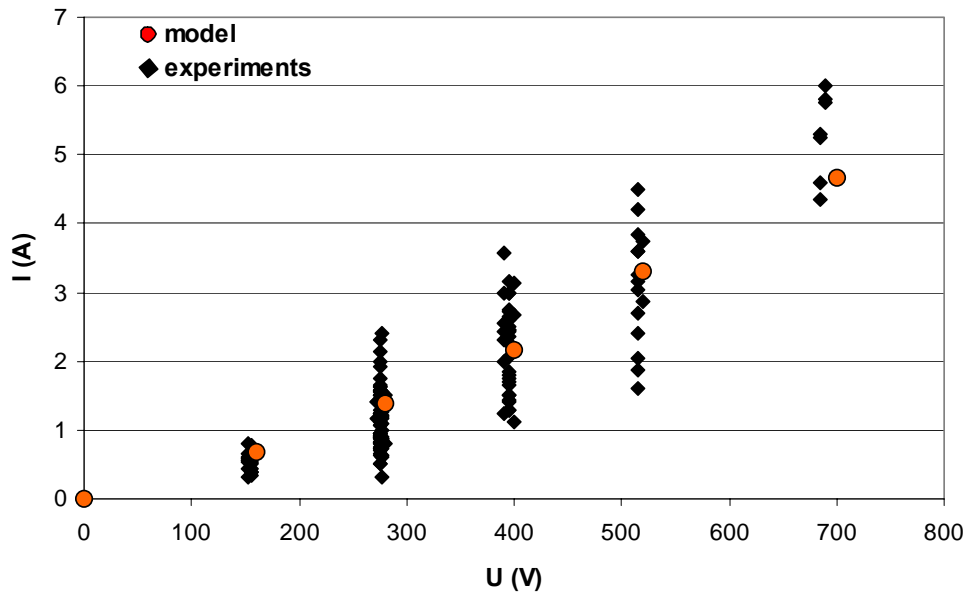


**Figure 5. 3: Currents measured during the pulse (black diamonds), compared to the currents given by the model (red circles), with respect to the applied voltages.**

Looking at Figure 5. 4, we can say that 160 V is too low for a successful permeabilization of the skin fold, as the electric field in the dermis and the epidermis is still below the reversible threshold value. Dividing the applied voltage with the distance between the electrodes, we get the approximate electric field between the plates, which, in the case of 160 V, results in 400 V/cm. According to the experiments, 400 V/cm is the approximate reversible electric field threshold, thus a successful electropermeabilization should occur for applied voltages above 160 V. Figure 5. 5 denotes the electric field distribution for the applied voltage of 280 V, corresponding to an approximate electric field of 700 V/cm, which should be enough for a successful electropermeabilization of the skin fold. Indeed, the electric field distribution in Figure 5. 5 suggests that most of the dermis and the epidermis is between the reversible and the irreversible thresholds. Increasing the voltage (Figure 5. 6 to Figure 5. 8) shifts the average electric field magnitude in skin towards the irreversible threshold value, while enlarging the areas above the irreversible threshold (red areas). All of the above is in good agreement with the experiments; hence changing the electric conductivities in the model according to the level of the tissue permeabilization gives good results.

It needs to be emphasized that the numerical model of the skin fold presented here is merely an approximation of the real biological processes involved in the tissue permeabilization. Not all processes were modeled and some simplifications of the geometry were necessary due to its complexity. However, with the model presented we were able to explain the mechanism of the tissue electropermeabilization propagation beyond the initial conditions dictated by the tissue initial conductivities.

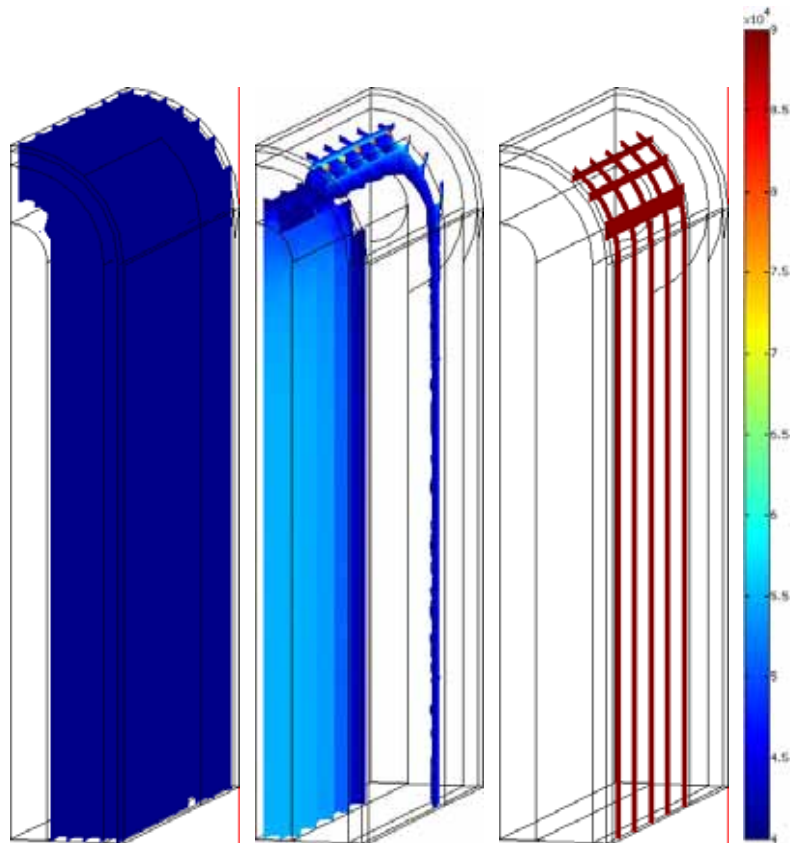


Figure 5. 4: 3D slice plots of the electric field distribution in the skin fold for the applied voltage of 160 V. The electric field is shown in volts per meter.

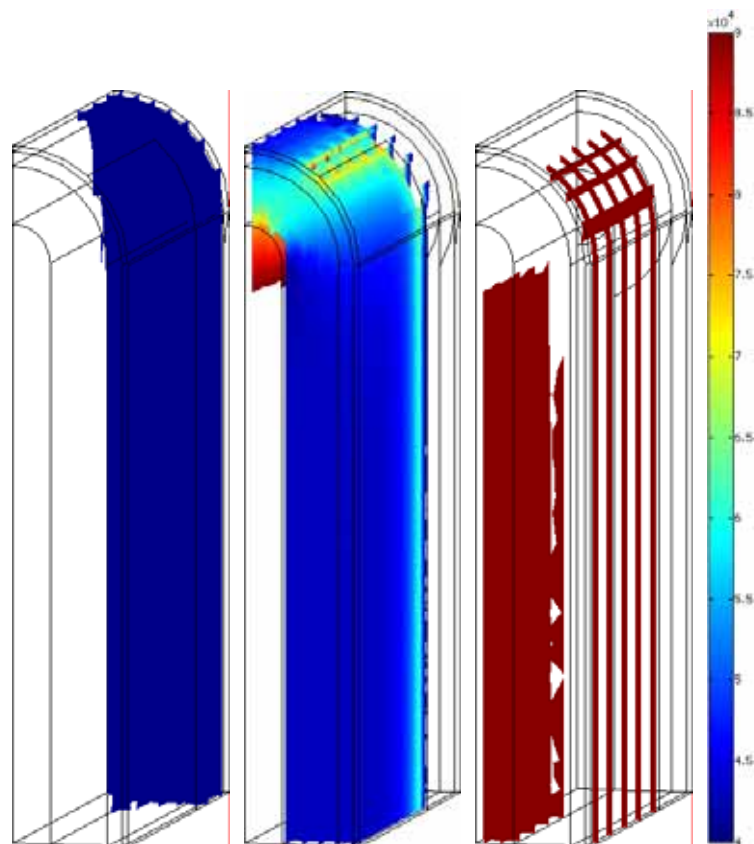


Figure 5. 5: 3D slice plots of the electric field distribution in the skin fold for the applied voltage of 280 V. The electric field is shown in volts per meter.

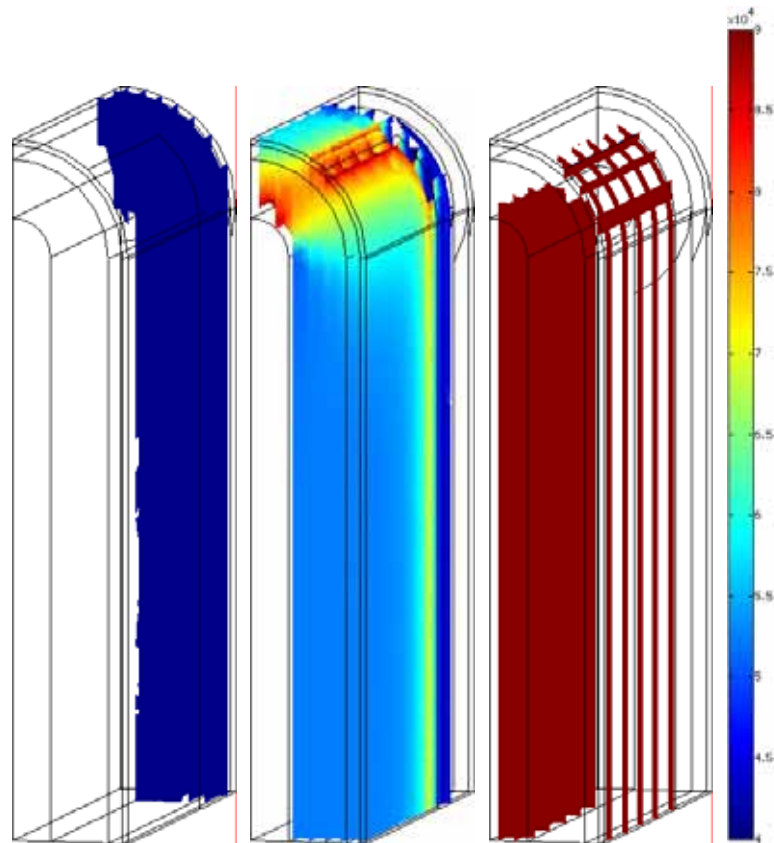


Figure 5. 6: 3D slice plots of the electric field distribution in the skin fold for the applied voltage of 400 V. The electric field is shown in volts per meter.

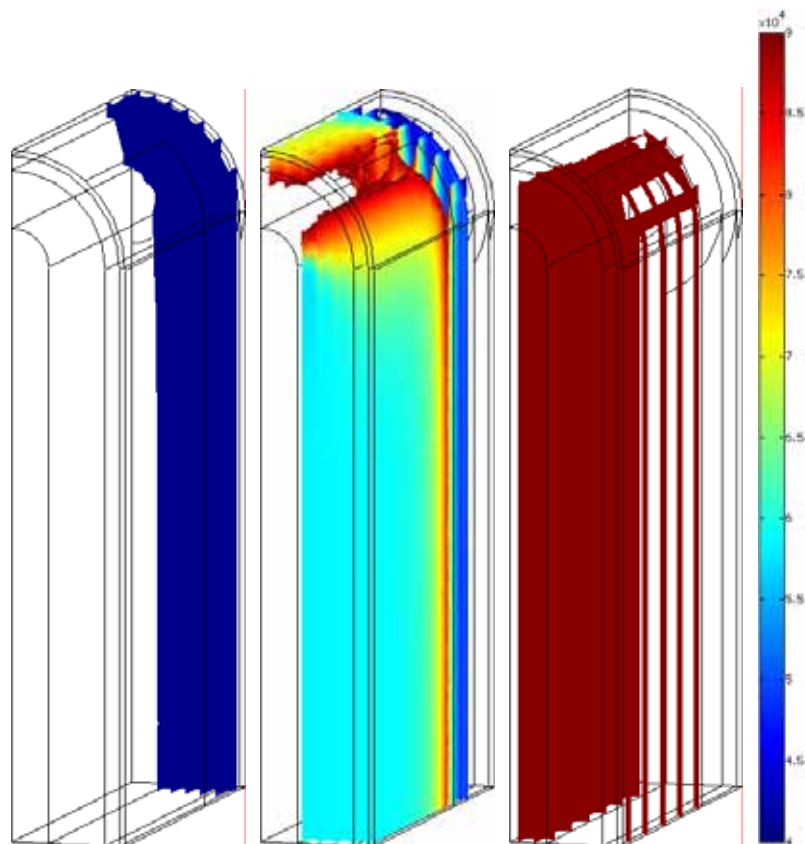


Figure 5. 7: 3D slice plots of the electric field distribution in the skin fold for the applied voltage of 520 V. The electric field is shown in volts per meter.

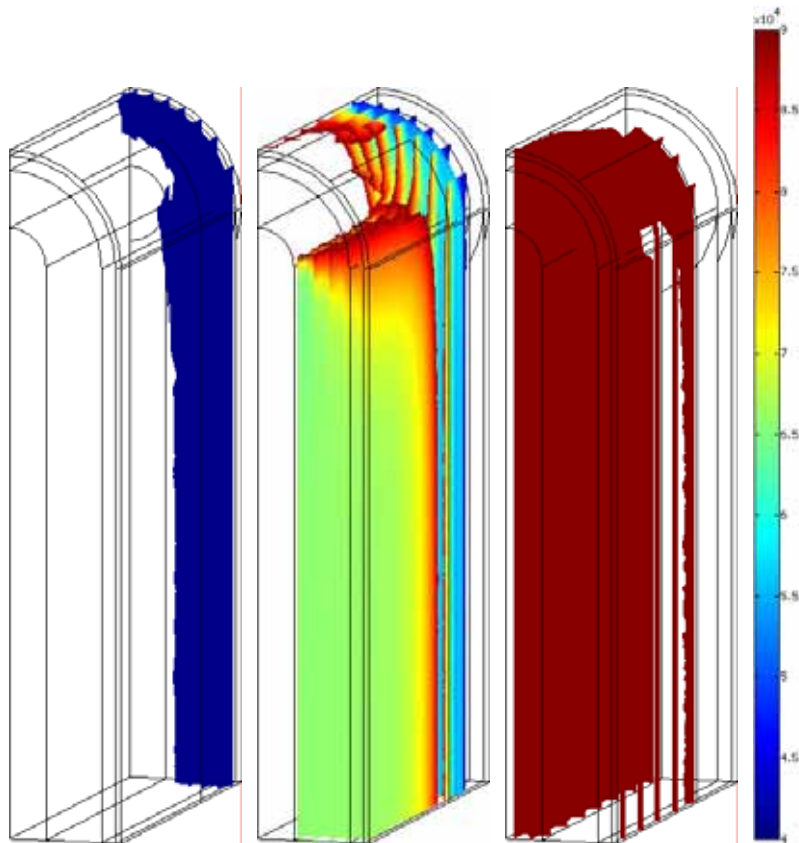


Figure 5. 8: 3D slice plots of the electric field distribution in the skin fold for the applied voltage of 700 V. The electric field is shown in volts per meter.

## 5.2. The numerical model of skin electro-permeabilization with modeled local transport regions (LTRs) in the *stratum corneum*

The geometry of the LTR model is described in subchapter 3.2.3 (Figure 3. 3). As in the case of the whole skin fold model, the iterative nonlinear computation of the conductivities of the epidermis, dermis and subcutaneous tissue was repeated until the electric field distribution reached its steady state. The same nonlinear  $\sigma(E)$  dependences as well as the conductivity values before and after permeabilization as in skin fold model were used (see Table 5. 1 and Figure 5. 1 for dermis, epidermis and subcutaneous fatty and connective tissue). Again, we only modeled the process of skin electropermeabilization occurring during the high voltage (HV) pulse. The resealing process and the electrophoretic pulse were not modeled.

In this model, the conductivity of the *stratum corneum* was not changed nonlinearly according to the electric field strength as in other layers. Instead, local transport regions – areas of highly increased electric conductivity in the *stratum corneum* – were modeled in the geometry. The LTRs are the result of the permeabilization of the *stratum corneum*; hence the *stratum corneum* was already permeabilized at the beginning of the simulation, while the permeabilization of other skin layers was computed in the same way as in the skin fold model.

We found the data on LTR size and density and their conductivity in the literature [Pliquett *et al.*, 1998; Vanbever *et al.*, 1999; Pliquett and Gusbeth, 2004]. For high voltage pulses, the size of the resulting LTRs is typically around 100  $\mu\text{m}$  in diameter, while their density can be anywhere between 25 and 90 LTRs per  $0.1\text{ cm}^2$  [Vanbever *et al.*, 1999] The size of the LTRs increases with longer pulse duration, while their density is increased with increasing pulse voltage. The geometry of our model of the skin electropermeabilization taking into account local transport regions gives the following values describing LTRs and *stratum corneum*:

- LTR size: 150  $\mu\text{m}$  in diameter (The size of the LTRs was modeled somewhat larger than typical LTR size when applying high voltage pulses (100  $\mu\text{m}$ ), which was compensated by choosing lower LTR density. By this choice, the model was numerically less demanding.)
- LTR density: 40 per  $0.1\text{ cm}^2$
- LTR covered surface: 7 % of the *stratum corneum* surface beneath the electrode (According to the literature, the application of high voltage pulses produces LTRs that cover up to 10% of the *stratum corneum* surface [Pliquett *et al.*, 1998; Pliquett and Gusbeth, 2004])
- LTR conductivity: 2500 times higher than that of the *stratum corneum* [Pliquett and Gusbeth, 2004]
- the calculated average conductivity of the modeled *stratum corneum* with LTRs (the region covered by electrode): 0.013 S/m (For comparison, the conductivity of the permeabilized *stratum corneum* in the skin fold model, where LTRs were not modeled, was 0.0375 S/m)

The model was again run at all five voltages used in the *in vivo* experiments (160, 280, 400, 520 and 700 V). The LTR size, density and electrical conductivity was modeled the same for all five voltages applied. Electric field distributions of the LTR model, represented with slice plots in 3D at the end of the electropermeabilization process for the applied voltages of 160, 280, 400, 520 and 700 V, respectively, are presented in Figure 5. 9 to Figure 5. 13. The first distribution on each figure shows the area below the reversible electric field threshold of 400 V/cm (blue color); The second distribution shows the area between the reversible and the irreversible thresholds – 400 V/cm < E < 900 V/cm – (blue to red colors); And the third one shows the area above the irreversible threshold of 900 V/cm (red color).

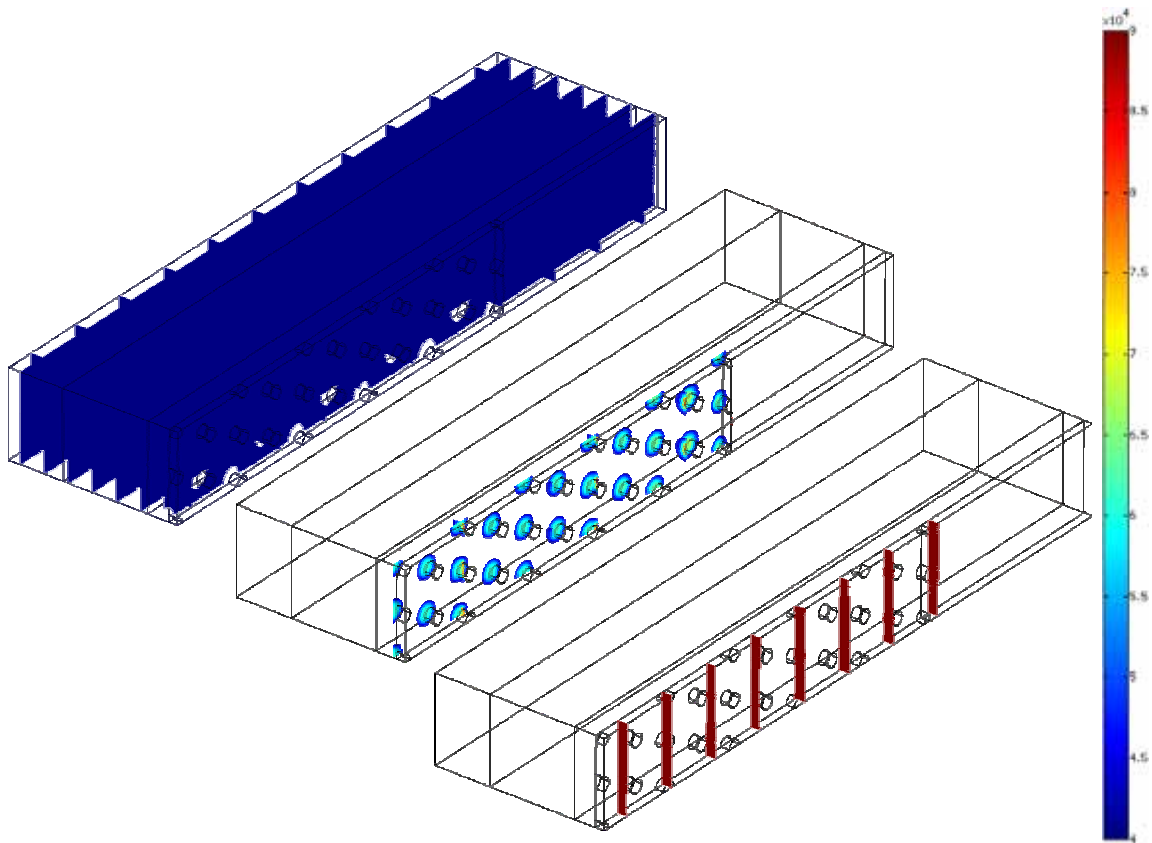


Figure 5. 9: 3D slice plots of the electric field distribution in the LTR model for the applied voltage of 160 V. The electric field is shown in volts per meter.

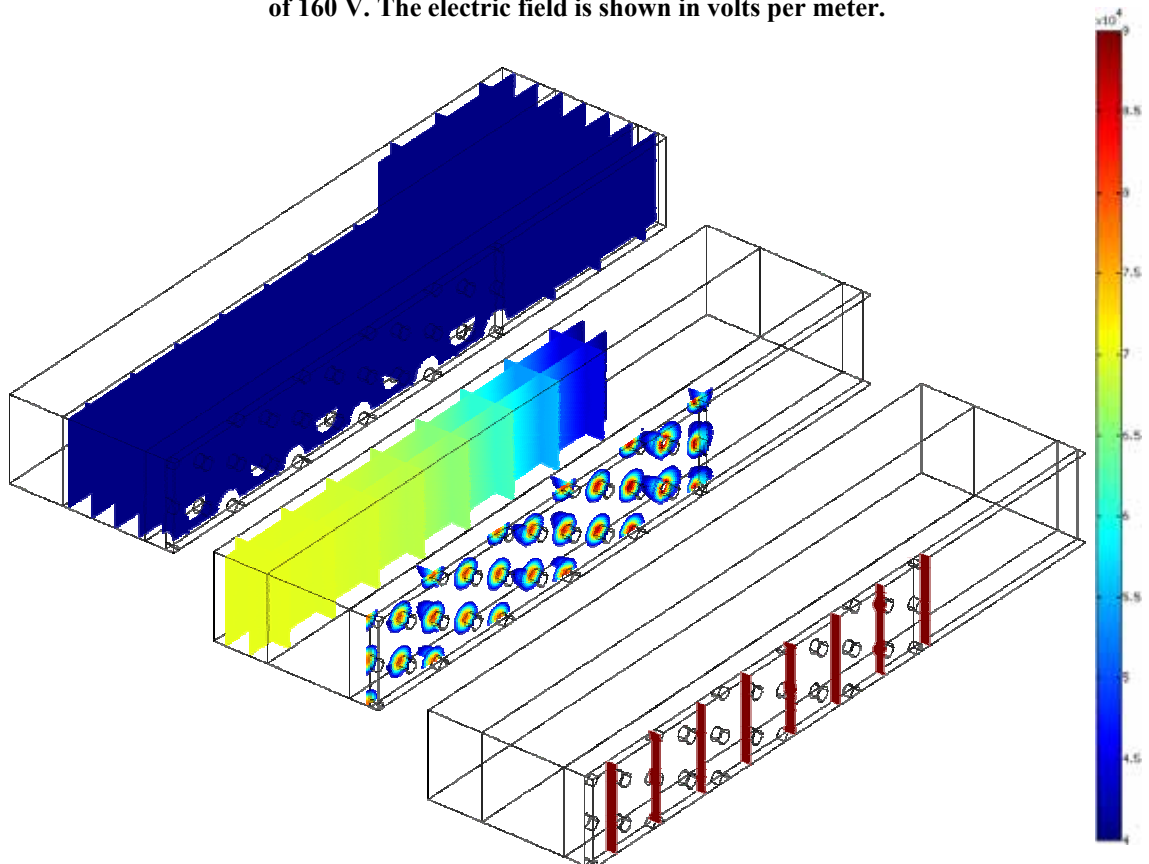


Figure 5. 10: 3D slice plots of the electric field distribution in the LTR model for the applied voltage of 280 V. The electric field is shown in volts per meter.

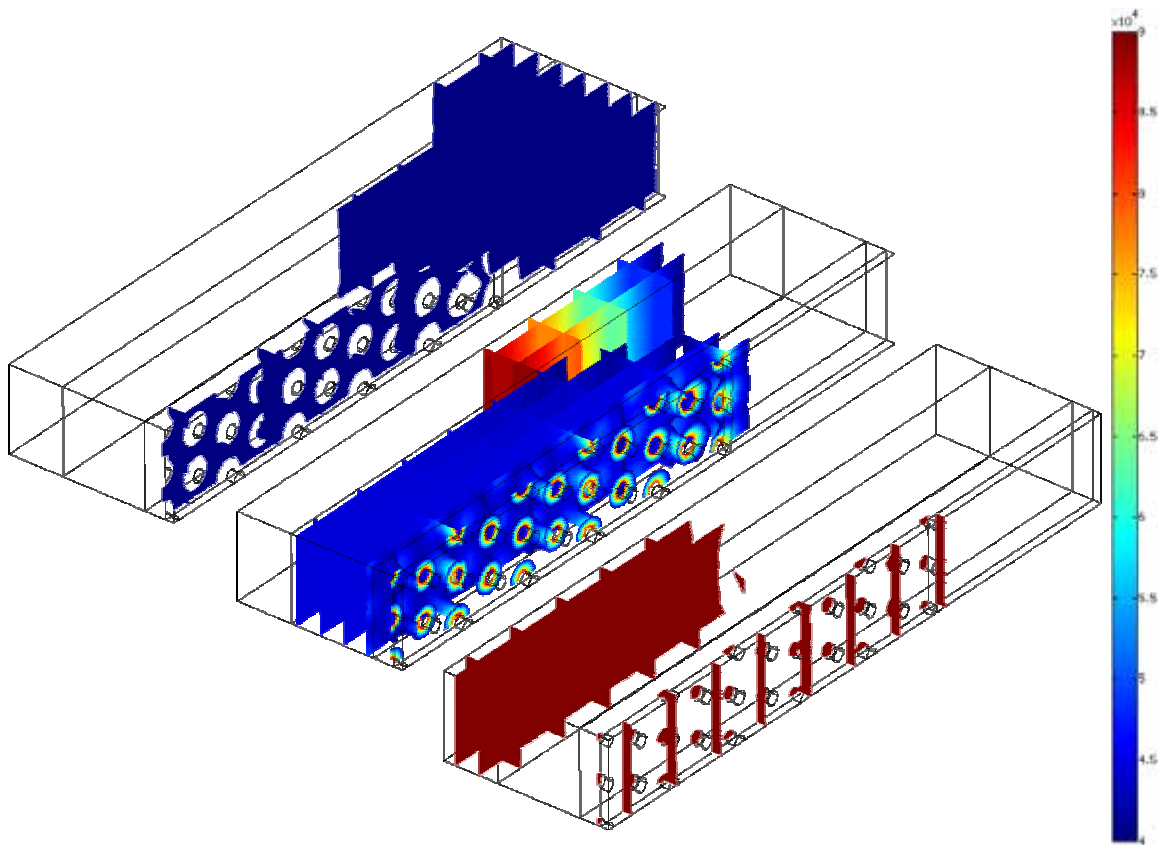


Figure 5. 11: 3D slice plots of the electric field distribution in the LTR model for the applied voltage of 400 V. The electric field is shown in volts per meter.

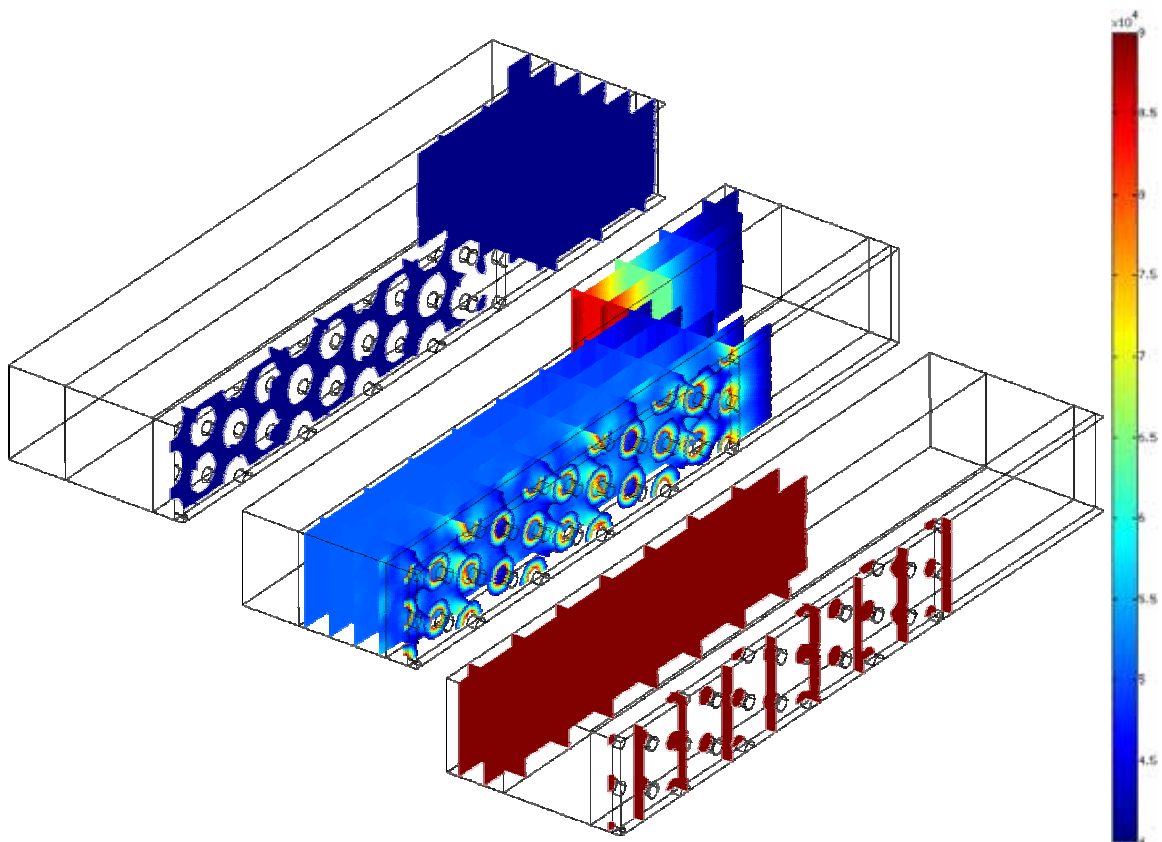
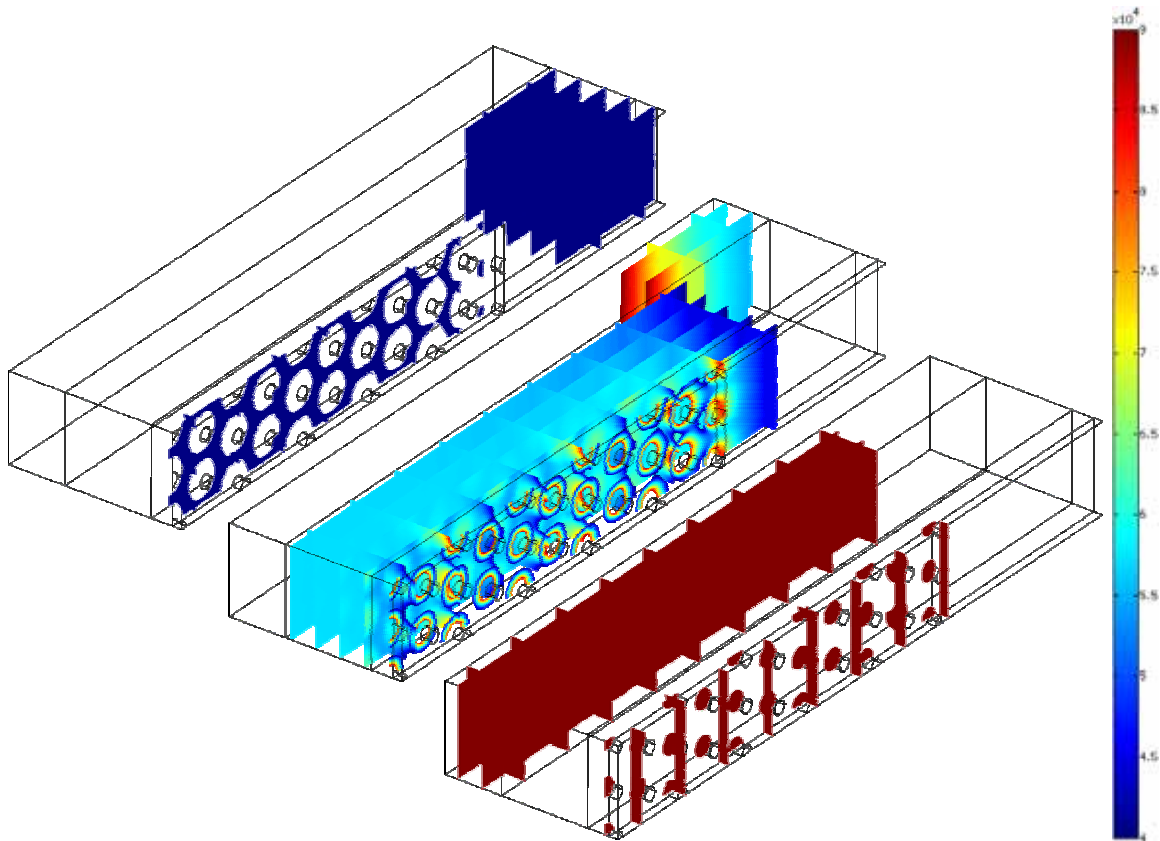


Figure 5. 12: 3D slice plots of the electric field distribution in the LTR model for the applied voltage of 520 V. The electric field is shown in volts per meter.



**Figure 5. 13: 3D slice plots of the electric field distribution in the LTR model for the applied voltage of 700 V. The electric field is shown in volts per meter.**

Just like in the case of the skin fold model, the criterion for successful theoretical permeabilization given by the model was the electric field between the reversible and the irreversible electric field thresholds ( $400 \text{ V/cm} < E < 900 \text{ V/cm}$ ). These values were taken from literature and given by experiments. If we look at the electric field distributions on Figure 5. 9 to Figure 5. 13, it seems like 160 V and 280 V is too low for successful permeabilization of the epidermis and the dermis. Further, the LTR model shows electric field in the epidermis and the dermis to be just above the reversible threshold for the applied voltage of 400 V, and most of the epidermis and the epidermis in the area between the electrodes being permeabilized for the pulse amplitudes of 520 and 700 V. Comparing these results (Figure 5. 9 to Figure 5. 13) with the ones given by the whole skin fold model (Figure 5. 4 to Figure 5. 8), it seems like the theoretical successful permeabilization in the LTR model is shifted towards higher pulse amplitudes.

Since only a slice of the skinfold was modeled in the LTR model, the current through the skin fold slice with local transport regions was multiplied by 24; The factor of 2 to account for the vertical cut through the skin fold so that only one half of the skin fold volume between the electrodes was modeled. And the factor of 12 to account for the horizontal cut, modeling a slice of only one tenth the volume between the electrodes and adding the area of the skin fold where conductive gel was applied. As well as the electric field values, the currents given by the LTR model were shifted towards lower values by factor 1.5 – 2 (see Table 5. 2 and Figure 5. 14) when compared to the whole skin fold model. Still, the results of the LTR model are well in the range of the whole skin fold model and the *in vivo* experiments.

**Table 5. 2: Comparison of the currents given by the LTR model with currents given by the whole skin fold model.**

Voltage	$I_2$ (LTR model)	$I_1$ (skin fold model)	$I_1 / I_2$
160 V	0.46 A	0.69 A	1.5
280 V	0.84 A	1.4 A	1.7
400 V	1.23 A	2.17 A	1.76
520 V	1.67 A	3.3 A	1.97
700 V	2.37 A	4.7 A	1.98

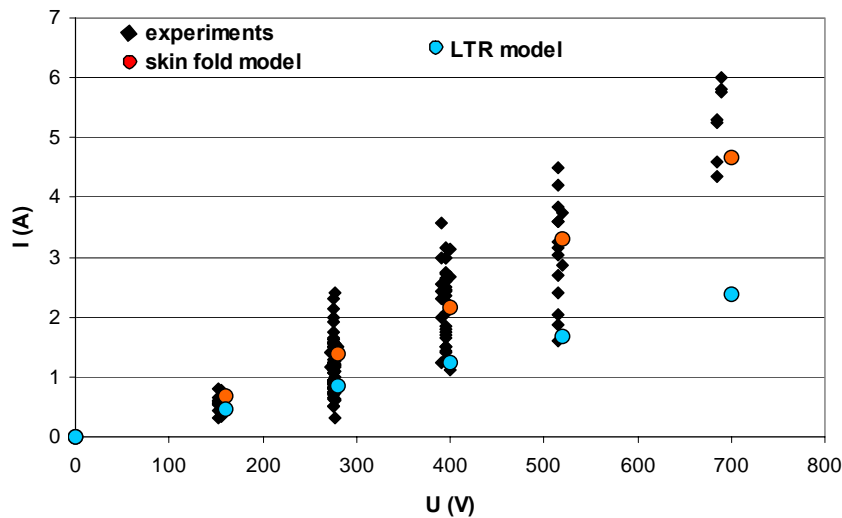


**Figure 5. 14: Currents measured during the pulse (black diamonds), compared to the currents given by the whole skin fold model (red circles) and those given by the LTR model (blue circles) with respect to the applied voltages.**

### 5.3. The numerical models of microneedle arrays

The geometries of the numerical models of microneedle arrays are described in subchapter 3.2.3. (Figure 3. 4 to Figure 3. 6). The skin was modeled as a homogeneous tissue with the initial conductivity of 0.002 S/m and an 80-fold increase in the conductivity when permeabilized [Pavšelj *et al.*, 2005]. During the finite model analysis, the conductivity was changed according to the electric field strength throughout the model. The process of tissue electropermeabilization was again modeled as a nonlinear problem, as described in subchapter 3.2.2.

The electric field distributions in skin where pulses of 60 V between the negative and the positive electrodes are delivered through different set-ups of microneedle electrode arrays are shown in Figure 5. 15 to Figure 5. 17. Colored areas denote reversibly permeabilized tissue, thus regions in the model where the electric field is between the reversible and the irreversible thresholds ( $400 \text{ V/cm} < E < 900 \text{ V/cm}$ ). The 3-dimensional view of the models is shown in a); b) shows the electric field distributions in the horizontal section plane on the skin surface; c) in the horizontal section plane at the electrode tip; and d) the vertical section plane cut through the middle of the electrodes.

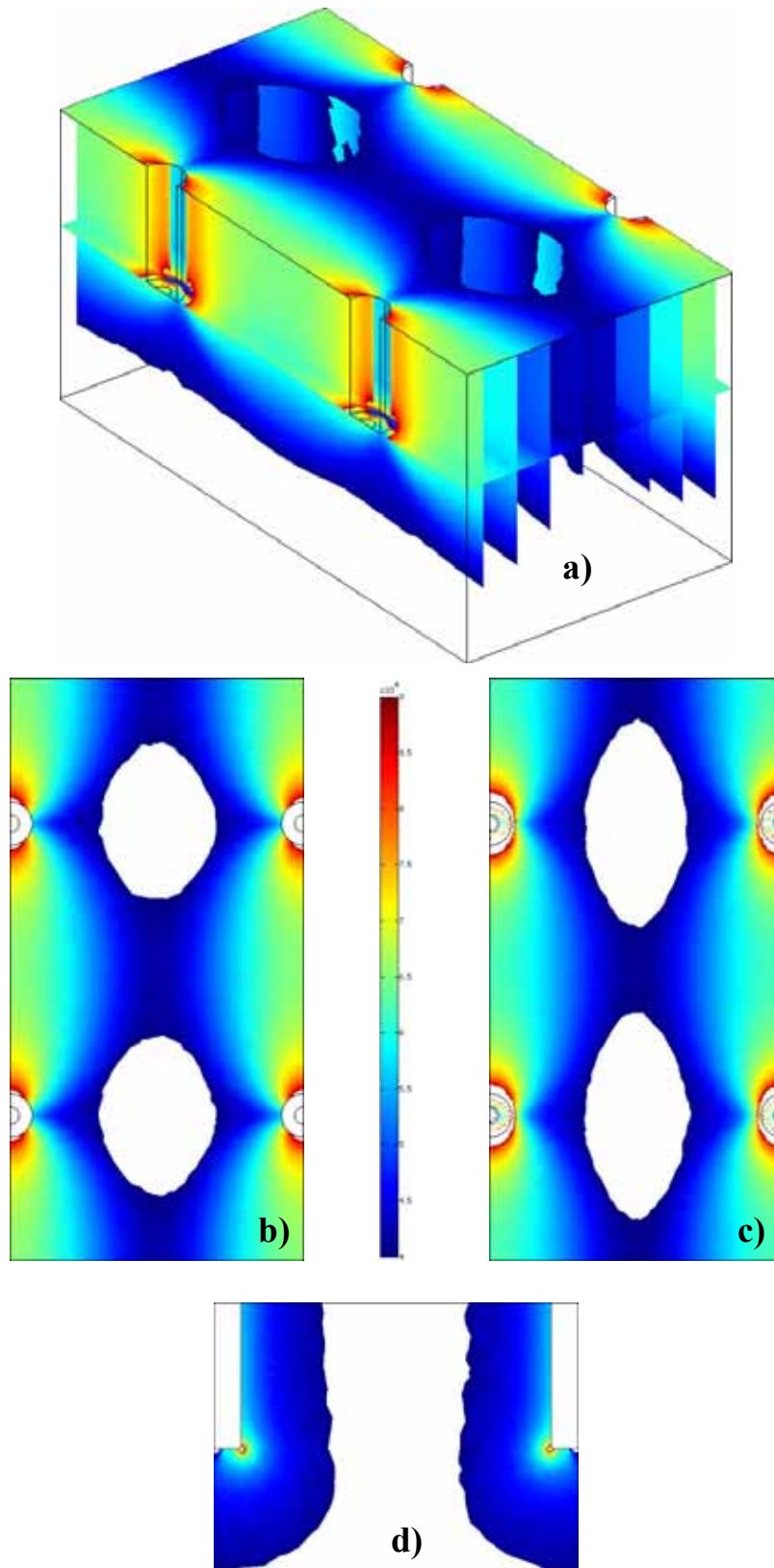


**Figure 5. 15:** The electric field distributions in the "lined" microelectrode array. The colored areas denote regions where the electric field is between  $400 \text{ V/cm} < E < 900 \text{ V/cm}$ .

a) The 3-dimensional view; b) the horizontal section plane on the skin surface; c) the horizontal section plane at the electrode tip; d) the vertical section plane cut through the middle of the electrodes.

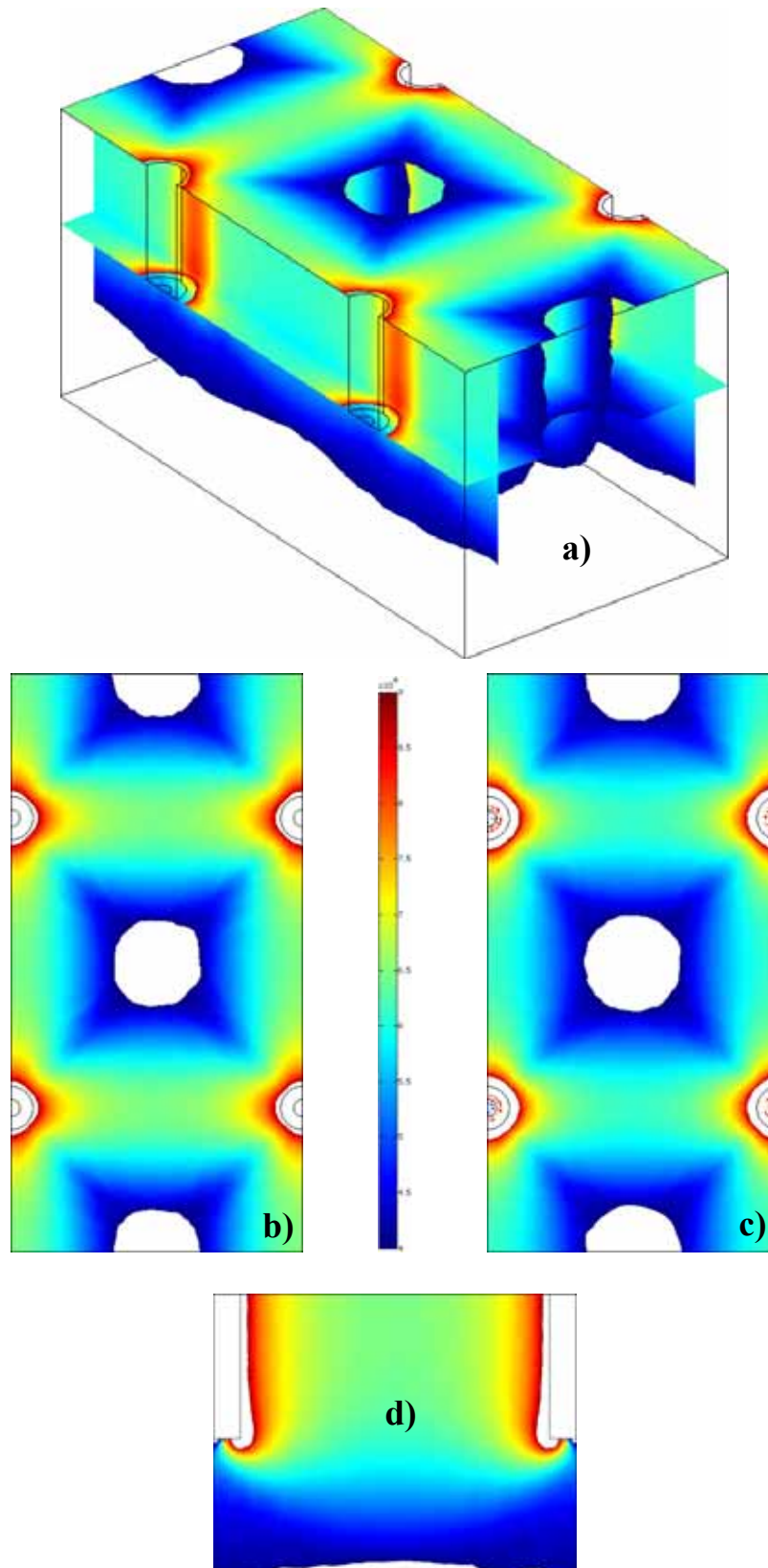


**Figure 5.16:** The electric field distributions in the "crossed" microelectrode array. The colored areas denote regions where the electric field is between  $400 \text{ V/cm} < E < 900 \text{ V/cm}$ .

a) The 3-dimensional view; b) the horizontal section plane on the skin surface; c) the horizontal section plane at the electrode tip; d) the vertical section plane cut through the middle of the electrodes.

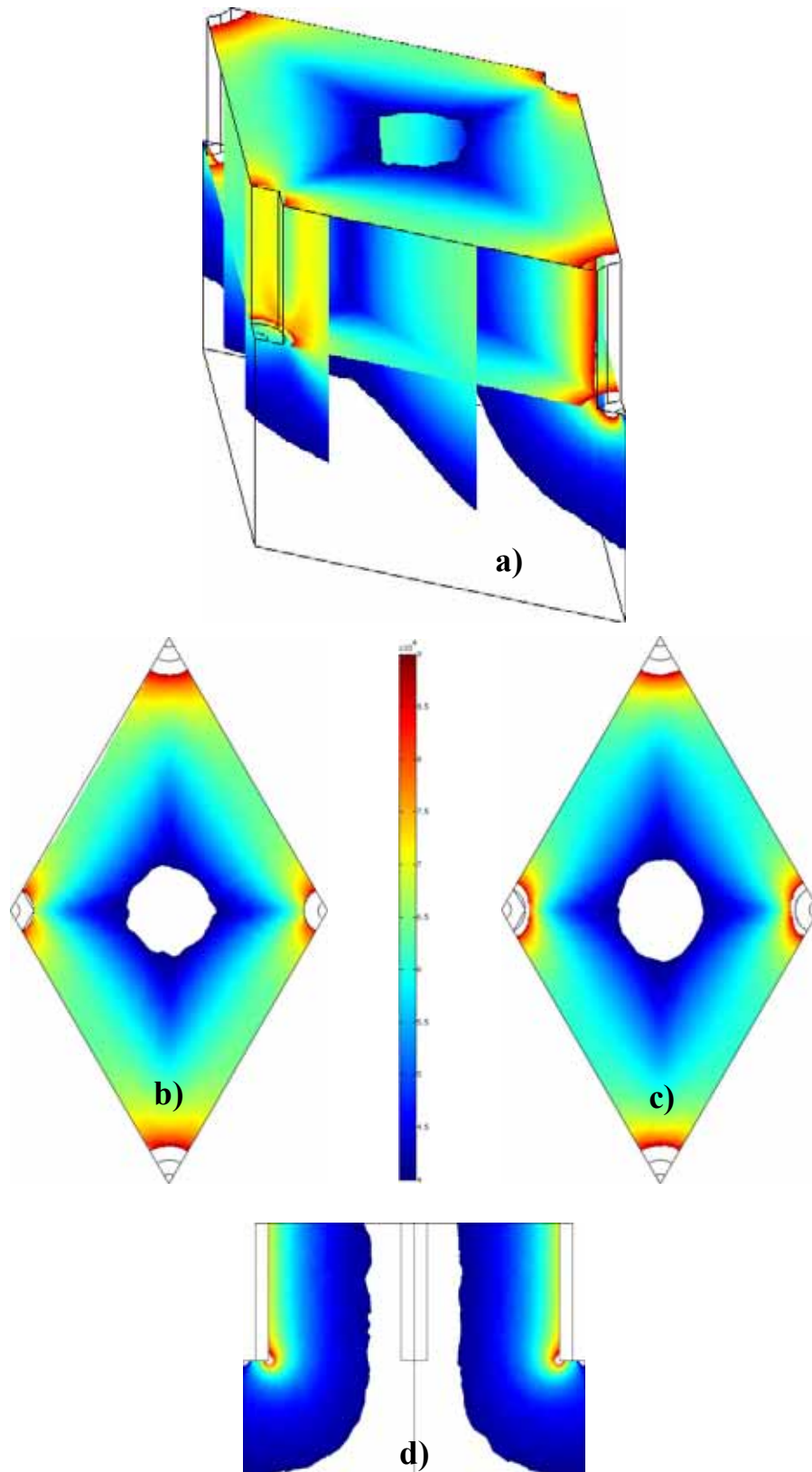


**Figure 5.17:** The electric field distributions in the "hexagonal" microelectrode array. The colored areas denote regions where the electric field is between  $400 \text{ V/cm} < E < 900 \text{ V/cm}$ .

a) The 3-dimensional view; b) the horizontal section plane on the skin surface; c) the horizontal section plane at the electrode tip; d) the vertical section plane cut through the middle of the electrodes.

From the electric field distributions on Figure 5. 15 to Figure 5. 17 we can see that when using an array of needle electrodes, a more uniform tissue permeabilization can be reached than when using plate electrodes.

Comparing the portions of skin tissue above the reversible and the irreversible thresholds, respectively, and the electric currents through different microelectrode arrays, very small differences can be observed (Table 5. 3). Although the tissue volumes where the reversible electric field threshold is exceeded might seem somewhat low, one has to take into account the tissue volume below the electrode tips that was included in the calculation. Namely, enough tissue volume was modeled below the electrode tips in order not to restrain the natural current flow, which would lead to an incorrect representation of the process.

**Table 5. 3: Electric currents, percentages of the reversibly and the irreversibly permeabilized tissue, and the difference between the two for the applied voltage of 60 V.**

<b>U=60 V</b>			
electric current	0.117 A	0.118 A	0.122 A
volume above $E_{rev}$	54.7 %	64.4 %	64.8 %
volume above $E_{irrev}$	0.125 %	0.45 %	0.5 %



---

## CHAPTER 6

# Discussion

Reversible increase of the cell membrane permeability caused by the electric field is called electroporation and facilitates the entry of larger molecules, deprived of transport mechanism, such as some drugs or DNA, into the cell. Cell electroporation and uptake of exogenous molecules depends on different cell and tissue parameters and pulse parameters, like their duration, number and amplitude. In this study, the efficiency of various combinations of a short high voltage, followed by a long low voltage pulse on DNA electrotransfer in skin was investigated.

### 6.1. *In vivo* experiments

It has been shown for skeletal muscle that efficient cell electrotransfection can be achieved using a combination of short high-voltage (HV) and long low-voltage (LV) pulses. HV pulses alone resulted in a high level of tissue permeabilization (permeabilizing pulse), but very low DNA transfer. However, in combination with one or more LV pulses (electrophoretic pulse), large increase in DNA transfer occurred [Bureau *et al.*, 2000; Šatkauskas *et al.*, 2002; Šatkauskas *et al.*, 2005]. We hypothesized that DNA electrotransfer into the skin is also a two-step process consisting of membrane permeabilization and DNA electrophoresis and that a combination of a high-voltage pulse to permeabilize target cells, followed by a low-voltage pulse to electrophoretically transport DNA molecules would improve gene transfection in skin too. Hence, the efficacy of the delivery of two reporter genes into the skin was investigated using a combination of a high voltage and a low voltage pulse in comparison to protocols reported in literature, consisting of 6 to 8 high voltage pulses or of 6 to 16 low voltage pulses [Glasspool-Malone *et al.*, 2000; Mir *et al.*, 1998; Mir *et al.*, 1999]. To test if a combination of a short high voltage pulse followed by a long low voltage pulse yields efficient electrogene transfer in skin, a qualitative and a quantitative analysis by means of two reporter genes was performed.

Skin accessibility and its role in the immune response make skin an attractive target tissue for gene therapy. Unfortunately, a successful and safe delivery of genes into the target cells of any tissue is still a serious hindrance to gene treatments. Electroporation is one of the options to enhance the delivery of genes into the skin, and seems particularly effective for DNA transfection after intradermal or topical administration.

However, from an electrical point of view, skin is a very challenging tissue due to the high resistivity and non-permeability of its outermost layer, the *stratum corneum*. From the electromagnetic field theory, we know that in the case of serially connected conductors, the highest voltage drop occurs on the conductor with the highest resistance; hence the electric field in that conductor is the highest. Therefore, when applying electric pulses to a skin fold through external parallel electrodes, most of the potential drop rests across the highly resistive *stratum corneum* while the electric field in the skin layers beneath remains low. Then how is a successful permeabilization and consequently gene transfection of the lower-lying epidermis and dermis possible? The experiments show a drastic decrease in skin resistivity when subjected to electric pulses of a high enough amplitude. Due to this decrease, the skin layers underneath *stratum corneum* are subjected to an electric field high enough to permeabilize the cells thus achieving an efficient gene transfection. The permeabilization of any tissue occurs when critical electric field strength is reached which is, in general, different for different tissues. When measuring the current and the voltage through a tissue sample subjected to electric pulses, a change in the slope of the current/voltage (I/U) dependence is observed at voltages where the electroporation occurs.

To approximately set the voltages needed for a successful permeabilization of the rat skin fold where pulses are delivered through parallel plate electrodes of four millimeter distance, the I/U dependences were measured. Also, the dependence on the quantity of the intradermally injected PBS (phosphate buffered saline) was tested (no intradermal injection, 25  $\mu$ l of PBS, 50  $\mu$ l of PBS). The results showed that the quantity of the injected PBS has an effect on the I/U curves, namely the I/U dependence became more linear when we increased the quantity of the injected PBS. The reason for that is probably twofold: first, the electric field distribution is deformed due to the changed geometry because of the bubble of injected PBS; and second, the electric conductivity of PBS is comparable to the conductivities of the permeabilized skin layers and therefore gets a share of the voltage drop applied on the skin fold, thus changing its I/U dependence. Taking into account the tested I/U dependences, we decided to use an intradermal injection of 25  $\mu$ l of plasmid in our experiments dealing with gene transfer to the skin cells, instead of 50  $\mu$ l. However, the amount of the injected plasmid might have had a lesser influence on the I/U curves because of its low conductivity (lower than the PBS').

The intersections of consecutive linear regressions of current to voltage measurements corresponding to slope changes in the I/U dependence of the skin fold, give us an estimation of the points where the slope changes from the non-permeabilized to the permeabilized state. From our measurements we estimated the reversible threshold for skin to be approximately 180 V, which is in good agreement with the measurements done on rat skin so far [Pavšelj *et al.*, 2005]. Taking into account 4 mm distance between electrodes, if we normalize the voltage between the electrodes with the distance between them, we get an approximation of the electric field between the plate electrodes. In the case of the homogeneous electric field, this would also denote the homogeneous electric field magnitude. But in our case the homogeneity of the electric field is deformed near the edge of the electrode, furthermore, because of the chemical reactions additional voltage drop occurs at the skin-electrode contact. Nevertheless, almost in the entire region between the electrodes where the tissue is, the electric field is almost homogeneous and almost equals the ratio between the voltage and the distance between the electrodes (the true electric field is somewhat lower than

the E/d ratio). Thus the error we make using those electric field values to approximately determine the thresholds of electropermeabilization, is small enough.

### **6.1.1. The effect of the use of the HV+LV protocols on the GFP and luciferase expression in skin**

The localization of the gene expression in skin after electroporation was assessed by pCMVGFP (Green Fluorescent Protein) reporter gene. A plasmid coding for GFP was injected intradermally before the application of the electric pulses. Different pulsing protocols were used: only one high voltage pulse, only one low voltage pulse, and combinations of both (where different amplitudes of the low voltage pulse were tested). The expression after intradermal injection only, without pulsing, and the basal skin fluorescence was also observed. Two days after the experiment, the rats were sacrificed and skin samples were taken and observed under a confocal microscope without fixation or freezing. Dermal and epidermal sides, as well as the anode and the cathode sides of the electroporation site were observed separately. An enhanced expression of GFP in the skin was obtained with a combination of a high and a low voltage pulse. A single high voltage or a single low voltage pulse resulted in a very low transfection, comparable to that of the control group, where no pulse was applied, whereas GFP expression in the epidermis and dermis was enhanced by the combination of high and low voltage pulses. That confirms the hypothesis that deeper skin layers can be electropermeabilized with pulse amplitudes seemingly too low to reach layers beneath *stratum corneum*, due to the changes in the electric conductivities of tissues undergoing electropermeabilization. Comparing the anodal and the cathodal side of each sample, the expression is consistently higher on the anodal side. The reason for that is probably the net negative charge of the phosphate backbone of the DNA chain. Namely, DNA molecules tend to migrate from negative (cathode) to positive electrode (anode), where higher expression was observed.

The quantification of luciferase activity further supports the hypothesis that a combination of a high voltage, followed by a low voltage pulse is more efficient than several high voltage or low voltage pulses alone. Namely, luciferase activity was enhanced by two orders of magnitude when combinations of a high and a low voltage pulse were applied whereas low expression was detected after the application of six high voltage or six low voltage pulses only. These data confirm the hypothesis that both the permeabilizing, short high voltage pulse and the electrophoretic, long low voltage pulses are required for an enhanced electrogene transfer in skin. No or very low statistical difference was found between the groups where different amplitudes of the high voltage or the low voltage were tested, as well as in the experimental groups where the splitting of the low voltage pulse (8x50 ms) was tested against one long low voltage pulse (1x400 ms), or the groups where the delay between the high voltage and the low voltage pulse was used as opposed to groups without the delay. When similar electroporation protocols were used for electrogene transfer in muscle tissue [Šatkauskas *et al.*, 2002; Šatkauskas *et al.*, 2005], little or no variation was found when using HV-LV delays from 300 ms to 100 seconds, although some studies show a decrease in DNA expression for delays shorter than 300 ms [Sukharev *et al.*, 1992]. The decrease for longer delays is supposed to be due to the resealing of the membrane that starts as soon as the HV pulse is turned off. Also, it was demonstrated for the muscle that the expression depends on total LV duration (the product "*number x duration*" of pulses), while the splitting of the LV pulse in muscle showed a much lesser effect,

although one 400 ms LV pulse was somewhat better than 8x50 ms LV pulses [Šatkauskas *et al.*, 2005]. These data coincide well with our results, however, less statistical difference was found for the skin. A factor attributing to the lack of the statistical difference is probably the high scatter of the luciferase results. Namely, the luciferase expression in the skin varied over a factor of 100 inside the same group. This could partly be attributed to variable electrical properties and thickness of the skin depending on the location on the back of the rat, or variable biological responses. However, after the analysis, no correlation was found between the luciferase expression and the location of the electroporation site on the back of the rat. Alternatively, the variation could be caused by experimental conditions, especially DNA injection. Namely, the exact experimental conditions can rarely be repeated even by an experienced operator.

### 6.1.2. Other *in vivo* studies

Kinetic study of the luciferase expression showed the highest expression on the first days after the experiment (24-48 hours after treatment), then it dropped rapidly towards the control values. In the control group of intradermal injection alone, without electroporation, a rather high expression was observed the first day after the injection, then the expression dropped close to zero already on the second day. These data indicate that pulsing increases both the amount and the duration of gene expression in the skin. However, our results show transient gene expression in skin, which can be attributed to the skin's ability to rapidly renew itself. In general, gene expression was shown to be longer when using vectors of viral origins [Thierry *et al.*, 1995; Trainer and Alexander, 1997]. Hence, skin DNA electrotransfer would be more adapted to a short-term gene expression in the skin for immunization or local skin treatment and not for a sustained secretion of a therapeutic protein in the blood.

The combination of a high voltage, followed by a low voltage pulse was also tested for efficiency in skin immunization, using a plasmid coding for a model antigen ovalbumin. These protocols were again compared to electroporation protocols described in the literature [Drabick *et al.*, 2001]. The immune response was enhanced when electroporation was used after intradermal injection of a DNA plasmid coding for the antigen ovalbumin, and the proposed protocols combining a high voltage pulse followed by a low voltage pulse were more efficient than a train of six high voltage pulses. However, the immune response in groups where DNA electrotransfer of a combination of a high voltage and a low voltage pulse was used, were somewhat lower than in mice immunized with ovalbumin and the standard adjuvant alum.

The proposed protocols of a combination of a high voltage pulse, followed by a low voltage pulse have proven to be efficient for gene transfection in skin, so the safety aspect of such electric pulses was also studied. Possible side effects were investigated by standard methods used to assess the effect of skin treatments [Vanbever *et al.*, 1998; Vanbever and Pr at, 1999; Dujardin *et al.*, 2002]. Noninvasive bioengineering methods were used to evaluate *in vivo* if Cliniporator induces an erythema (chromametry) or impairment of barrier function (transepidermal water loss). The anode and the cathode sides of each electroporation site were observed separately. Histology was used to investigate the effect on the skin structure. A small and transient disruption of the skin barrier function due to electroporation was observed from the increase in TEWL values, but the rise in the TEWL values was mostly due to the evaporation of gel water from the skin surface, as proven from comparison with appropriate controls. A slight and transient erythema a few minutes after pulse delivery was observed visually but not by

chromametry. The reason why we did not record that with the chromameter right after pulsing might be the vascular lock in the minutes following the electroporation [Serša *et al.*, 1999; Gehl *et al.*, 2002]. There was a consistent difference between the anode and the cathode side of the electroporation sites. The reasons for the difference are unknown but could be attributed to local changes in ion concentration or pH imbalance. Also, no damage in the histological structure of the skin was observed. These data confirm that the application of a combination of a high voltage and a low voltage pulse delivered through plate electrodes on rat skin fold is well tolerated.

## 6.2. Numerical models

### 6.2.1. The numerical model of a skin fold

The location of GFP expression shows that we successfully permeabilized deeper layers of skin (dermis and epidermis) even though the ratios of the conductivities of the skin layers suggest that the highest voltage drop rests across the *stratum corneum*. That would cause a very high electric field in that layer while its strength would stay below the permeabilization threshold in the layers beneath *stratum corneum*. However, the electric conductivities of tissues subject to electric pulses increase. As a result, the electric field “penetrates” deeper into the skin and permeabilizes skin layers below *stratum corneum*. We constructed a numerical model describing this nonlinear process, using the finite elements method. Using voltage and current measurements recorded during pulse delivery, we aimed at making the response of the model as close as possible to the experimental data. The output of the model was compared with the current and the voltage that were measured during experiments and a good agreement was obtained. However, we focused on the process of electropermeabilization, which takes place inside the first, high-voltage pulse. The electrophoretic low voltage pulse was not modeled. Also, some other processes, such as the resealing of the cell membranes after pulsing, or the polarization effects at the tissue-electrode interface, were not modeled. Therefore, the numerical model of the skin fold presented here is merely an approximation of the real biological processes involved in the tissue permeabilization.

The results from the numerical model of a skin fold suggest that, using the plate electrodes of 4 mm distance and approximately 1x1 cm<sup>2</sup> in contact with skin, voltages above 160 V are required for successful electropermeabilization of the dermis and the epidermis. This is in good agreement with the electropermeabilization thresholds set at the beginning of our *in vivo* studies (subchapter 4.1), where the change in the slope of the I/U curve could be observed for voltages around 180 V. Comparing the voltages needed for a successful electropermeabilization of the skin fold as suggested by the model, with voltages achieving efficient *in vivo* gene transfection, good agreement can be observed. However, due to the high scatter of the *in vivo* results, we can not assert with certainty that 160 V is too low for a successful electrogene transfer. Still, even in the absence of a statistical difference between the groups of different amplitudes of the high voltage pulse, transfection after a 160 V high voltage pulse seems somewhat lower than transfection rates in the rest of the groups where different high voltage pulses were compared. When looking at the electric field distributions given by the model for different voltages, we need to be aware that the region of our interest is the topmost part of the skinfold, where the plasmid is injected intradermally. Therefore, we could conclude that 160 V is too low for a successful permeabilization of the target tissue, while an amplitude of 520 V or more is already too high.

Also, comparing our results with previously published findings on skin electropermeabilization, the voltage amplitudes suggested by the model are also well in the range of the voltage amplitudes believed to cause skin permeabilization and the opening of new aqueous pathways, which should occur for voltages above 50 V applied on a single skin thickness (skin fold is twice as thick) [Weaver *et al.*, 1999]. Further, if we approximate the electric field the skin fold is subjected to, by dividing the applied voltage with the electrode distance, we get irreversible and the irreversible electric field threshold values well in the range of the values from previous experiments on skin folds [Pavšelj *et al.*, 2005]. However, we have to be aware of the error made when comparing results from different studies, as different tissue-electrode setups were used. Namely, dividing the voltage with the distance between the electrodes only gives us an approximation of the electric field between the plates.

The model could be improved by modeling the conductivity changes as an irreversible phase transition problem, thus, once increasing the conductivity in the finite elements where the electric field has exceeded the critical value, the conductivity should not be changed back to a lower value, even if the new electric field distribution should suggest so. In other words, the tissue would not get de-permeabilized during the process. The process could be modeled in discrete steps and would reach its steady state when two conditions were met: (i) there would be no new finite elements in the current step with the magnitude of the electric field exceeding the reversible threshold value; and (ii) the conductivity of the elements with the electric field exceeding the threshold has already been changed in one of the previous steps.

Also, some simplifications of the geometry of the numerical model were necessary due to its complexity. First, the thickness of the *stratum corneum* in the model was set larger than in real skin (6 times thicker). Although its conductivity was also set 6 times higher, an error was introduced. Also, not enough skin fold volume was modeled at the base of the skin fold, thus the natural electrical current flow was somewhat restrained. The reason for this simplification was the large number of the finite elements and the degrees of freedom of the model which made the computation difficult and long.

Further, parameters such as the conductivities of the tissues before and after electropermeabilization and the reversible and the irreversible electric field thresholds were taken from the literature and experiments. However, data on everything, except the conductivities before the electropermeabilization, is very scarce, sometimes non-existent. Namely, the subject of tissue conductivity changes due to electroporation is still a rather unexplored area. Also, due to different measuring conditions, measuring techniques and species used by different researchers, large discrepancies are found in the reported data on tissue conductivities. However, with the model presented we used the available data to try to explain the mechanism of the tissue electropermeabilization propagation beyond the initial conditions dictated by the tissue initial conductivities.

### 6.2.2. The numerical model of skin with local transport regions

The experiments of other researchers revealed, by means of fluorescence microscopy, highly localized molecular transport in skin after electroporation [Pliquett *et al.*, 1998; Pliquett, 1999; Vanbever *et al.*, 1999; Weaver *et al.*, 1999; Pliquett and Gusbeth, 2004]. The circularly shaped regions of increased molecular transport had a diameter between 100 and 600  $\mu\text{m}$  (depending on pulse parameters) and were termed local transport regions (LTRs). We made no attempt to visualize local transport regions during our *in vivo* experiments. However, we constructed a model of skin with local transport regions embedded in the *stratum corneum* (as opposed to the skin fold model

where the *stratum corneum* was a homogeneous structure), based on the data on the size, density and electrical properties of LTRs found in the literature. The geometry of the skin fold model was used as the basis for the LTR model. Namely, all the layer thicknesses, the conductivities and the  $\sigma(E)$  dependences were the same for both models. However, as the inclusion of the local transport regions complicates the geometry of the finite elements model, only a slice the size of one tenth of the skin fold volume between the electrodes was modeled in the LTR model and periodic boundary conditions were set.

The results from the numerical model skin with local transport regions suggest that voltages above 280 V between the electrodes (of 4 mm distance and approximately  $1 \times 1 \text{ cm}^2$  in contact with skin) are required for the electric field strength in the epidermis and dermis to be between the reversible and the irreversible electric field thresholds given by literature and experiments. Comparing this with the results of the skin fold model and the *in vivo* experiments, the voltages suggested for successful electropermeabilization by the LTR model are somewhat higher. Also, in some parts of the skin, the irreversible permeabilization occurs for higher voltages than in the skin fold model. Comparing electric currents at the end of the electropermeabilization process, the currents given by the LTR model are also shifted towards lower values. The reason for all of the above stated discrepancies can be attributed partially to different average conductivities of the permeabilized *stratum corneum* of both models. Namely, in the skin fold model, the permeabilized part of the *stratum corneum* (mainly underneath the electrodes and the conductive gel) has the value of 0.0375 S/m. As opposed to that, the average conductivity of the permeabilized part of the *stratum corneum* in the LTR model (with embedded highly conductive LTRs in the highly resistive *stratum corneum*) amounts to 0.013 S/m. This discrepancy, together with the nonhomogeneous structure of the *stratum corneum* with LTRs, leads to the lower permeabilization of the underlying epidermis and dermis.

Also, the current-voltage dependence of the LTR model is more linear than that of the skin fold model. The reason may lay in the fact that the conductivity of the *stratum corneum* with local transport regions does not follow a nonlinear relation  $\sigma(E)$  but is assumed that tissue permeabilization already occurred in parts of the *stratum corneum*. In relation to this, it might be reasonable to construct different models for each applied voltage, with different number of local transport regions. Namely, as reported in the literature, the number of the LTRs increases with increasing voltage. In this way, the nonlinearity of the model with local transport regions embedded in the *stratum corneum* would be increased.

As the size, density and the conductivity of local transport regions were taken from the literature, where different electroporation protocols were used than in our *in vivo* experiments, the parameters of the local transport regions formed because of electroporation in our experiments might have been different. Namely, trains of exponentially decaying pulses were used by the researchers reporting the visualization of the local transport regions, while only one square electroporative pulse was used in our experiments. Also, the tissue-electrode geometry was different and, more importantly, heat-separated human cadaver epidermis was used in their experiments. None the less, the electric field distributions and the electric currents of the LTR model are well in the range of those of the whole skin fold model and the *in vivo* experiments. As the electroporation protocols and circumstances of our *in vivo* experiments are not directly comparable to the experiments of the researchers using fluorescence microscopy to localize LTRs, we can accept this as a good agreement of the results. Therefore, we can

conclude that the numerical model of skin with local transport regions in the *stratum corneum* is a good representation of the electropermeabilization process in skin.

Just like in the case of the whole skin fold model, the model could be improved if the conductivity changes were modeled as an irreversible phase transition problem. Also, due to the complexity of the numerical model, some simplifications of the geometry were made. First, like in the whole skin fold model, the *stratum corneum* was modeled 6 times thicker than in real skin and second, with the periodic boundary conditions set on the boundaries of the skin fold slice with LTRs, an infinite array of slices was modeled. An error was thus made, as the electric field distribution around the borders of the electrodes differs from the distribution in the tissue situated well in the middle of the electrode. However, the error was small enough.

### **6.2.3. The numerical models of microneedle arrays**

Using external electrodes on skin is problematic, due to the high resistivity of its outermost layer, the *stratum corneum*. Therefore, a new electrode design, arrays of microneedle electrodes, was proposed [Henry *et al.*, 1998; Davis *et al.*, 2004; Mukerjee *et al.*, 2004; Prausnitz, 2004; Davis *et al.*, 2005]. Modeling different settings of the microneedle arrays, only small differences were observed between them. The portions of the volume between the reversible and the irreversible electric field thresholds were comparable, as well as the electric currents through the arrays. However, the electric field distributions seem more favorable in the "crossed" and the "hexagonal" setting, where the electropermeabilized regions are more symmetrically distributed around the electrodes.

Since the electrical barrier of the *stratum corneum* when using the microneedles is breached by piercing it, no layers were modeled in the microelectrode array models. Namely, the error made when using average skin conductivity instead of modeling different skin layers is lower in this electrode-tissue setting. Also, as we had no current-voltage experimental data, nor any data on transfection rates, the model of the electropermeabilization process in the skin using microelectrode arrays could not be validated. Therefore, the currents through the models and the percentages of the volume exposed to electric field magnitude above the permeabilization threshold were used only to compare the different microelectrode array settings modeled.

When comparing the electric field distributions in the models of the microneedle arrays with the model of the skin fold, we suggest that a more uniform tissue permeabilization can be reached when using the former. Also, the volume of the tissue exposed to electric fields exceeding the irreversible threshold seems to be smaller. Despite the lack of experimental data on microneedle arrays, the microneedle array models made are good first approximation and useful for comparison with the skin fold model. As the first prototype of microneedle arrays has been made, the presented models will in the future be validated and improved with the help of experimental data.

## CHAPTER 7

# Conclusions

### 7.1. In vivo experiments

An enhanced expression of GFP in the skin was obtained with a combination of a high and a low voltage pulse. Single high voltage or single low voltage pulse resulted in a low transfection, comparable to the one of the control group where no pulse was applied whereas GFP expression in the epidermis and dermis was enhanced by the combination of high and low voltage pulses. The results obtained confirm the hypothesis that deeper skin layers can be electropermeabilized with pulse amplitudes seemingly too low to reach layers beneath *stratum corneum*. This is explained by the changes in the electric conductivities of tissues undergoing electropermeabilization.

The quantification of luciferase activity further supports the hypothesis that a combination of a high voltage, followed by a low voltage pulse is more efficient than either several high voltage or low voltage pulses. These data confirm the hypothesis that both, the permeabilizing, short high voltage pulse and the electrophoretic, long low voltage pulses are required for an enhanced electrogene transfer in skin. No or very low statistical difference was found between the groups where different amplitudes of the high voltage or the low voltage were tested, as well as in the experimental groups where the splitting of the low voltage pulse was tested against one long low voltage pulse, or a delay between the high voltage and the low voltage pulse was introduced.

Kinetic study of the luciferase expression showed that DNA electrotransfer in skin is better suited for a short-term gene expression in the skin for immunization or local skin treatment. Hence, the combination of a high voltage, followed by a low voltage pulse was also tested for efficiency in skin immunization, using a plasmid coding for a model antigen ovalbumin. The immune response was enhanced when electroporation was used after intradermal injection of the DNA plasmid, and the proposed protocols were more efficient than a train of six high voltage pulses.

As the proposed protocols have proven to be efficient for gene transfection in skin, the safety aspect of such electric pulses was also studied. A small and transient disruption of the skin barrier function due to electroporation was observed from the rise in transepidermal water loss (TEWL) values, but this rise was mostly due to the evaporation of gel water from the skin surface, as proven from comparison with the

controls. A slight and transient erythema a few minutes after pulse delivery was observed visually but not by chromametry. Also, no damage in the histological structure of the skin was observed. The application of a combination of a high voltage and a low voltage pulse delivered through plate electrodes was well tolerated on rat skin.

## 7.2. Numerical models

The location of GFP expression shows that we successfully permeabilized deeper layers of skin (dermis and epidermis); even though the ratios of the conductivities of the skin layers suggest that the highest voltage drop rests across the *stratum corneum*. We constructed a numerical model describing the nonlinear process of tissue conductivity changes during electroporation due to tissue permeabilization, using finite elements method. The output of the model was compared with the current and the voltage measured during *in vivo* experiments and a good agreement was obtained. Also, comparing the voltages needed for a successful electropermeabilization of the skin fold as suggested by the model, with voltages achieving good *in vivo* gene transfection, good agreement can be observed. Finally, a comparison of our results with already published findings on skin electropermeabilization showed that the voltage amplitudes suggested by the model are also well in the range of the voltage amplitudes reported by other authors to cause skin permeabilization.

The experiments of other researchers revealed highly localized molecular transport in skin after electroporation. We thus made a model of skin with local transport regions embedded in the *stratum corneum*, based on the data on the size, density and electrical properties of LTRs found in the literature. The voltages suggested for successful electropermeabilization by the LTR model are somewhat higher when compared to the results of the skin fold model and the *in vivo* experiments. Comparing electric currents at the end of the electropermeabilization process, the currents given by the LTR model are shifted towards lower values. None the less, the electric field distributions and the electric currents of the LTR model are well in the range of those of the whole skin fold model and the *in vivo* experiments. As the electroporation protocols and circumstances of our *in vivo* experiments are not directly comparable to the experiments we took the data on local transport regions from, we can accept this as good agreement of the results.

Using external electrodes on skin is problematic, due to the high resistivity of its outermost layer, the *stratum corneum*. Therefore, new electrode design, the arrays of microneedle electrodes, was proposed. Modeling different settings of the microneedle arrays, only small differences were observed between them. The portions of the volume between the reversible and the irreversible electric field thresholds were comparable, as well as the electric currents through the arrays. When comparing the electric field distributions in the models of the microneedle arrays with the model of the skin fold, we can conclude that a more uniform tissue permeabilization can be reached when using the former. Also, the volume of the tissue exposed to electric fields exceeding the irreversible threshold, seems to be smaller. Despite the lack of experimental data on microneedle arrays, the microneedle array models made are good first approximation and useful for comparison with the skin fold model.

## Original scientific contributions

Based on the presented results in this work, the author claims for recognition of the following original scientific contributions to the research area:

- **The use of the combination of a high- and a low-voltage pulse for successful electrogene transfection in skin**

It has been shown for the skeletal muscle tissue that using a combination of one short high voltage electroporative pulse, followed by a long, low voltage electrophoretic pulse, a very successful *in vivo* gene transfection can be achieved. Gene expression in skin by means of two reporter genes after different electroporation protocols was assessed. We compared protocols consisting of solely high voltage pulses, solely low voltage pulses protocols, and the proposed combination of a high voltage pulse, followed by a low voltage one, and showed that the combination of a high voltage and a low voltage pulse substantially enhances gene expression in skin.

- **Assessment of the kinetics of the gene expression in skin, use of the proposed protocols for skin immunization, and safety aspects of skin electroporation**

Usefulness of a gene transfection method for different applications depends on the level and duration of the gene expression in the tissue. The kinetics of the luciferase expression showed that DNA electrotransfer in skin is adapted to applications such as immunization or local skin treatment, where a short-term gene expression in the skin is needed. We also successfully used the combination of a high voltage, followed by a low voltage pulse for skin immunization. Our experiments also suggest that the application of such electroporative protocols delivered through plate electrodes on rat skin fold is well tolerated.

- **Numerical model of skin electroporation**

We described the process of tissue electropermeabilization in skin, taking into account tissue conductivity changes, with a numerical model based on finite elements method. We used tissue and electrode set-ups and pulse parameters from our *in vivo* experiments. Our numerical model, when compared to the results of our *in vivo* experiments and published findings of other authors, successfully described the process of electropermeabilization in skin. Another numerical model, where local transport regions were modeled in the *stratum corneum*, also showed good results.

- **Study of the effect of different electrode geometries on the electrogene transfection**

Most widely used electrodes in gene transfection in the skin are external plate electrodes of different geometries where the pulse amplitude has to be sufficiently high in order to cause the electrical breakdown of the *stratum corneum*. Therefore, painless microneedle electrodes are under development. Their depth of penetration is small enough not to cause any pain for the patient. A preliminary comparison, by means of numerical models, between different settings of microelectrode arrays was made. Comparison with external plate electrodes showed that more uniform tissue permeabilization while applying pulses of lower amplitudes can be reached when using microelectrodes.

## References

- Banga A.K., Bose S., Ghosh T.K.; Iontophoresis and electroporation: comparisons and contrasts; *International Journal of Pharmaceutics* 179:1-19, 1999.
- Barnett A., Weaver J.C.; Electroporation: a unified, quantitative theory of reversible electrical breakdown and mechanical rupture in artificial planar bilayer membranes; *Bioelectrochemistry and Bioenergetics* 25:163-182, 1991.
- Barry B.W.; Novel mechanisms and devices to enable successful transdermal drug delivery; *European Journal of Pharmaceutical Sciences* 14:101-114, 2001.
- Belehradek J., Orłowski S., Poddevin B., Paoletti C., Mir L.M.; Electrochemotherapy of spontaneous mammary tumors in mice; *European Journal of Cancer* 27 (1):73-76, 1991.
- Bettan M., Ivanov M.-A., Mir L.M., Boissiere F., Delaere P., Scherman D.; Efficient DNA electrotransfer into tumors; *Bioelectrochemistry* 52:83-90, 2000.
- Brandisky K., Daskalov I.; Electrical field and current distributions in electrochemotherapy; *Bioelectrochemistry and Bioenergetics* 48:201-208, 1999.
- Bureau M.F., Gehl J., Deleuze V., Mir L.M., Scherman D.; Importance of association between permeabilization and electrophoretic forces for intramuscular DNA electrotransfer; *Biochimica et Biophysica Acta* 1474:353-359, 2000.
- Canatella P.J., Karr J.F., Petros J.A., Prausnitz M.R.; Quantitative study of electroporation-mediated molecular uptake and cell viability; *Biophysical Journal* 80:755-764, 2001.
- Chizmadzhev Y.A., Cohen F.S., Shcherbakov A., Zimmerberg J.; Membrane mechanics can account for fusion pore dilation in stages; *Biophysical Journal* 69:2489-2500, 1995.
- Chizmadzhev Y.A., Indenbom A.V., Kuzmin P.I., Galichenko S.V., Weaver J.C., Potts R.O.; Electrical properties of skin at moderate voltages: contribution of appendageal macropores; *Biophysical Journal* 74:843-856, 1998.
- COMSOL User's Guide, COMSOL, USA, 2005.
- Cui F.D., Asada H., Kishida T., Itokawa Y., Nakaya T., Ueda Y., Yamagishi H., Gojo S., Kita M., Imanishi J., Mazda O.; Intravascular naked DNA vaccine encoding

- glycoprotein B induces protective humoral and cellular immunity against herpes simplex virus type 1 infection in mice; *Gene Therapy* 10(25):2059-66, 2003.
- Čemažar M., Miklavčič D., Mir L.M., Belehradek J., Bonnay M., Fourcault D., Serša G.; Electrochemotherapy of tumours resistant to cisplatin: a study in a murine tumour model; *European Journal of Cancer* 37:1166-1172, 2001.
- Davalos R.V., Rubinsky B., Otten D.M.; A feasibility study for electrical impedance tomography as a means to monitor tissue electroporation for molecular medicine; *IEEE Transactions on Biomedical Engineering* 49(4):400-403, 2002.
- Davalos R., Rubinsky B.; Electrical impedance tomography of cell viability in tissue with application to cryosurgery; *Journal of Biomechanical Engineering* 126:305-309, 2004.
- Davalos R.V., Otten D.M., Mir L.M., Rubinsky B.; Electrical impedance tomography for imaging tissue electroporation; *IEEE Transactions on Biomedical Engineering* 51:761-767, 2004.
- Davis S.P., Landis B.J., Adams Z.H., Allen M.G., Prausnitz M.R.; Insertion of microneedles into skin: measurement and prediction of insertion force and needle fracture force; *Journal of Biomechanics* 37:1155-1163, 2004.
- Davis S.P., Martanto W., Allen M.G., Prausnitz M.R.; Hollow metal microneedles for insulin delivery to diabetic rats; *IEEE Transactions on Biomedical Engineering* 52:909-915, 2005.
- Debruin K.A., Krassowska W.; Modeling electroporation in a single cell. I. effects of field strength and rest potential; *Biophysical Journal* 77:1213-1224, 1999.
- Debruin K.A., Krassowska W.; Modeling electroporation in a single cell. II. effects of ionic concentrations; *Biophysical Journal* 77:1225-1233, 1999a.
- Denet A.-R., Prétat V.; Transdermal delivery of timolol by electroporation through human skin; *Journal of Controlled Release* 88:253-262, 2003.
- Denet A.-R., Vanbever R., Prétat V.; Skin electroporation for transdermal and topical delivery; *Advanced Drug Delivery Reviews* 56 (5):659-674, 2004.
- Dev S.B., Dhar D., Krassowska W.; Electric Field of a Six-Needle Array Electrode Used in Drug and DNA Delivery In Vivo: Analytical Versus Numerical Solution; *IEEE Transactions on Biomedical Engineering* 50(11):1296-1300, 2003.
- Drabick J.J., Glasspool-Malone J, King A., Malone R.W.; Cutaneous transfection and immune responses to intradermal nucleic acid vaccination are significantly enhanced by in vivo electropermeabilization; *Molecular Therapy* 3(2):249-255, 2001.
- Dujardin N., Van Der Smissen P., Prétat V.; Topical Gene Transfer into Rat Skin Using Electroporation; *Pharmaceutical Research* 18(1):61-66, 2001.
- Dujardin N., Staes E., Kalia Y., Clarys P., Guy R., Prétat V.; In vivo assessment of skin electroporation using square wave pulses; *Journal of Controlled Release* 79:219-227, 2002.
- EMAS Version 4 User's Manual, Brauer J.R., Brown B.S. editors, Ansoft Corporation, USA, 1997.

- Fear E.C., Stuchly M.A.; Modeling assemblies of biological cells exposed to electric fields; *IEEE Transactions on Biomedical Engineering* 45(10):1259-1271, 1998.
- Ferber D.; Gene therapy: safer and virus-free?; *Science* 294:1638-1642, 2001.
- Gabriel C., Gabriel S., Corthout E.; The dielectric properties of biological tissues: I. literature survey; *Physics in Medicine and Biology* 41:2231-2249, 1996.
- Gabriel S., Lau R.W., Gabriel C.; The dielectric properties of biological tissues: II. Measurements in the frequency range 10 Hz to 20 GHz; *Physics in Medicine and Biology* 41:2251-2269, 1996.
- Gallo S.A., Oseroff A.R., Johnson P.G., Hui S.W.; Characterization of electric-pulse-induced permeabilization of porcine skin using surface electrodes; *Biophysical Journal* 72:2805-2811, 1997.
- Gehl J., Mir L.M.; Determination of optimal parameters for in vivo gene transfer by electroporation, using a rapid in vivo test for cell permeabilization; *Biochemical and Biophysical Research Communications* 261:377-380, 1999.
- Gehl J., Sorensen T.H., Nielsen K., Raskmark P., Nielsen S.L., Skovsgaard T., Mir L.M.; In vivo electroporation of skeletal muscle: threshold, efficacy and relation to electric field distribution; *Biochimica et Biophysica Acta* 1428:233-240, 1999.
- Gehl J., Mir L.M.; Electroporation of Muscle Tissue in vivo. In: *Methods in Molecular Medicine*, edited by M.J. Jaroszeski, R. Heller, R. Gilbert, Humana Press, 271-276, 2000.
- Gehl J., Skovsgaard T., Mir L.M.; Vascular reactions to in vivo electroporation: characterization and consequences for drug and gene delivery; *Biochimica et Biophysica Acta* 1569:51-58, 2002.
- Gehl J., Electroporation: theory and methods, perspectives for drug delivery, gene therapy and research; *Acta Physiologica Scandinavica* 177:437-447, 2003.
- Glasspool-Malone J., Somiari S., Drabick J.J., Malone R.W.; Efficient nonviral cutaneous transfection; *Molecular Therapy* 2(2):140-146, 2000.
- Heller R., Jaroszeski M., Leo-Messina J., Perrot R., Van Voorhis N., Reintgen D., Gilbert R.; Treatment of B16 mouse melanoma with the combination of electroporation and chemotherapy; *Bioelectrochemistry and Bioenergetics* 36: 83-87, 1995.
- Heller R., Jaroszeski M., Atkin A., Moradpour D., Gilbert R., Wands J., Nicolau C.; In vivo gene electroinjection and expression in rat liver; *FEBS Letters* 389:225-228, 1996.
- Heller R., Jaroszeski M.J., Reintgen D.S., Puleo C.A., DeConti R.C., Gilbert R., Glass L.F.; Treatment of cutaneous and subcutaneous tumors with electrochemotherapy using intralesional bleomycin; *Cancer* 83:148-157, 1998.
- Heller R., Gilbert R., Jaroszeski M.J.; Clinical application of electrochemotherapy; *Advanced Drug Delivery Reviews* 35:119-129, 1999.
- Henry S., McAllister D.V., Allen M.G., Prausnitz M.R.; Microfabricated microneedles: a novel approach to transdermal drug delivery; *Journal of Pharmaceutical Sciences* 87(8):922-925, 1998.

- Hui S.W.; Low voltage electroporation of the skin, or is it iontophoresis?; *Biophysical Journal* 74:679-680, 1998.
- Jadoul A., Bouwstra J., Pr at V.; Effects of iontophoresis and electroporation on the stratum corneum, Review of the biophysical studies; *Advanced Drug Delivery Reviews* 35:89-105, 1999.
- Jarozeski M., Gilbert R., Nicolau C., Heller R.; In vivo gene delivery by electroporation; *Advanced Drug Delivery Reviews* 35:131-137, 1999.
- Kesmodel S.B., Spitz F.R.; Gene therapy for cancer and metastatic disease; *Expert Reviews in Molecular Medicine* 5:1-18, 2003.
- Khan A.S., Pope M.A., Draghia-Akli R.; Highly efficient constant-current electroporation increases in vivo plasmid expression; *DNA and Cell Biology* 24(12):810-818, 2005.
- Kinosita K., Tsong T.Y.; Voltage-induced pore formation and hemolysis of human erythrocytes; *Biochimica et Biophysica Acta*, 471:227-242, 1977.
- Kong H.-L., Crystal R.G.; Gene Therapy Strategies for Tumor Antiangiogenesis; *Journal of the National Cancer Institute* 90(4):273-285, 1998.
- Kotnik T., Miklav i  D.; Analytical description of transmembrane voltage induced by electric field on spheroidal cells; *Biophysical Journal*, 79:670-679, 2000.
- Kotnik T.; Influence de la dynamique du champ electrique sur l'efficacite de l'electropermeabilisation de la membrane cellulaire, Ph.D. thesis, Facult  de m decine Paris-Sud, Universit  Paris XI, 2000.
- Lane J.F.; Electrical impedances of superficial limb tissues: epidermis, dermis, and muscle sheath; *Annals New York Academy of Science* 1974:812-825, 1974.
- Lawler J.C., Davis M.J., Griffith E.C.; Electrical characteristics of the skin; *The Journal of Investigative Dermatology* 34:301-308, 1960.
- Lee Lucas M., Heller L., Coppola D., Heller R.; IL-12 plasmid delivery by in vivo electroporation for the successful treatment of established subcutaneous B16.F10 melanoma; *Molecular Therapy* 5(6):668-675, 2002.
- Lombry C., Marteleur A., Arras M., Lison D., Louahed J., Renauld J.-C., Pr at V., Vanbever R.; Local and Systemic Immune Responses to Intratracheal Instillation of Antigen and DNA Vaccines in Mice; *Pharmaceutical Research* 21(1):127-135, 2004.
- Loste F., Eynard N., Teissie J.; Direct monitoring of the field strength during electropulsation; *Bioelectrochemistry and Bioenergetics* 47:119-127, 1998.
- Ma ek-Lebar A., Ser a G.,  ema ar M., Miklav i  D.; Elektroporacija; *Medicinski Razgledi* 37:339-354, 1998.
- Ma ek-Lebar A., Miklav i  D.; Cell electropermeabilization to small molecules in vitro: control by pulse parameters; *Radiology and Oncology* 35 (3):193-202, 2001.
- Mathy F.-X., Denet A.-R., Vroman B., Clarys P., Barel A., Verbeeck R.K., Pr at V.; In vivo tolerance assessment of skin after insertion of subcutaneous and cutaneous microdialysis probes in the rat; *Skin Pharmacology and Applied Skin Physiology* 16:18-27, 2003.

- Mehier-Humbert S., Guy R.S.; Physical methods for gene transfer: improving the kinetics of gene delivery into cells; *Advanced Drug Delivery Reviews* 57(5):733-753, 2005.
- Menon G.K.; New insights into skin structure: scratching the surface; *Advanced Drug Delivery Reviews* 54 (Suppl. 1): S3-S17, 2002.
- Miklavčič D., Beravs K., Šemrov D., Čemažar M., Demšar F., Serša G.; The importance of electric field distribution for effective in vivo electroporation of tissues; *Biophysical Journal* 74:2152-2158, 1998.
- Miklavčič D., Šemrov D., Mekid H., Mir L.M.; A validated model of in vivo electric field distribution in tissues for electrochemotherapy and for DNA electrotransfer for gene therapy; *Biochimica et Biophysica Acta* 1523:73-83, 2000.
- Mir L.M., Banoun H., Paoletti C.; Introduction of definite amounts of nonpermeant molecules into living cells after electroporation: Direct access to the cytosol; *Experimental Cell Research* 175:15-25, 1988.
- Mir L.M., Orłowski S., Belehradek J., Paoletti C.; Electrochemotherapy potentiation of antitumor effect of bleomycin by local electric pulses; *European Journal of Cancer* 27(1):68-72, 1991.
- Mir L.M., Bureau M.F., Rangara R., Schwartz B., Scherman D.; Long - term, high level in vivo gene expression after electric pulse - mediated gene transfer into skeletal muscle; *Medical sciences* 321:893-899, 1998.
- Mir L.M., Orłowski S.; Mechanisms of electrochemotherapy; *Advanced Drug Delivery Reviews* 35:107-118, 1999.
- Mir L.M., Bureau M.F., Gehl J., Rangara R., Rouy D., Caillaud J.-M., Delaere P., Branellec D., Schwartz B., Scherman D.; High-efficiency gene transfer into skeletal muscle mediated by electric pulses; *Proceedings of National Academy of Science* 96:4262-4267, 1999.
- Mukerjee E.V., Collins S.D., Isseroff R.R., Smith R.L.; Microneedle array for transdermal biological fluid extraction and in situ analysis; *Sensors and Actuators* 114(1-2):267-275, 2004.
- Neumann E., Schaafer-Ridder M., Wang Y., Hofschneider P.H.; Gene transfer into mouse lymphoma cells by electroporation in high electric fields; *The EMBO Journal* 1(7):841-845, 1982.
- Neumann E., Kakorin S., Toensing K.; Fundamentals of electroporative delivery of drugs and genes; *Biochimica et Biophysica Acta* 48:3-16, 1999.
- Nishi T., Yoshizato K., Yamashiro S., Takeshima H., Sato K., Hamada K., Kitamura I., Yoshimura T., Saya H., Kuratsu J.-I., Ushio Y.; High - efficiency in vivo gene transfer using intraarterial plasmid DNA injection following in vivo electroporation; *Cancer Research* 56:1050-1055, 1996.
- Okino M., Mohri H.; Effects of high-voltage electrical impulse and an anticancer drug on in vivo growing tumors; *Japanese Journal of Cancer Research* 78:1319-1321, 1987.
- Parker A.L., Newman C., Briggs S., Seymour L., Sheridan P.J.; Nonviral gene delivery: techniques and implications for molecular medicine; *Expert Reviews in Molecular Medicine* 5:1-15, 2003.

- Pavlin M., Pavšelj N., Miklavčič D.; Dependence of induced transmembrane potential on cell density, arrangement, and cell position inside a cell system; *IEEE Transactions on Biomedical Engineering* 49(6):605-612, 2002.
- Pavlin M., Kandušer M., Reberšek M., Pucihar G., Hart F.X., Magjarevič R., Miklavčič D.; Effect of cell electroporation on the conductivity of a cell suspension; *Biophysical Journal* 88:4378-4390, 2005.
- Pavšelj N., Bregar Z., Cukjati D., Batiuskaite D., Mir L.M., Miklavčič D.; The course of tissue permeabilization studied on a mathematical model of a subcutaneous tumor in small animals; *IEEE Transactions on Biomedical Engineering* 52:1373-1381, 2005.
- Pawlowski P., Gallo S.A., Johnson P.G. and Hui S.W. Electrorheological modeling of the permeabilization of the stratum corneum: theory and experiment. *Biophysical Journal* 75:2721-2731, 1998.
- Payen E., Bettan M., Rouyer-Fessard P., Ves Beuzard Y., Scherman D.; Improvement of mouse  $\beta$ -thalassemia by electrotransfer of erythropoietin cDNA; *Experimental Hematology* 29:295-300, 2001.
- Pliquett U., Langer R., Weaver J.C.; Changes in the passive electrical properties of human stratum corneum due to electroporation; *Biochimica et Biophysica Acta* 1239:111-121, 1995.
- Pliquett U., Weaver J.C.; Electroporation of human skin: simultaneous measurement of changes in the transport of two fluorescent molecules and in the passive electrical properties; *Bioelectrochemistry and Bioenergetics* 39:1-12, 1996.
- Pliquett U.F., Vanbever R., Pr at V., Weaver J.C.; Local transport regions (LTRs) in human stratum corneum due to long and short 'high voltage' pulses; *Bioelectrochemistry and Bioenergetics* 47:151-161, 1998.
- Pliquett U.; Mechanistic studies of molecular transdermal transport due to skin electroporation; *Advanced Drug Delivery Reviews* 35:41-60, 1999.
- Pliquett U., Prausnitz M.R.; Electrical Impedance Spectroscopy for Rapid and Non-Invasive Analysis of Skin Electroporation. In: *Electrically Mediated Delivery of Molecules to Cells, Electrochemotherapy, Electrogenetherapy and Transdermal Delivery by Electroporation*, edited by M. J. Jaroszeski, R. Gilbert, and R. Heller, Totowa, NJ, USA:Humana Press, 1999.
- Pliquett U., Gusbeth C.; Surface area involved in transdermal transport of charged species due to skin electroporation; *Bioelectrochemistry* 65:27-32, 2004.
- Pliquett U., Elez R., Piiper A., Neumann E.; Electroporation of subcutaneous mouse tumors by rectangular and trapezium high voltage pulses; *Bioelectrochemistry* 62:83-93, 2004.
- Poddevin B., Orłowski S., Belehradek J., Mir. L.M.; Very high cytotoxicity of bleomycin introduced into the cytosol of cells in culture; *Biochemical Pharmacology* 42:67-75, 1991.
- Powell K.T., Morgenthaler A.W., Weaver J.C.; Tissue electroporation: Observation of reversible electrical breakdown in viable frog skin; *Biophysical Journal* 56:1163-1171, 1989.

- Prausnitz M.R., Bose V.G., Langer R., Weaver J.C.; Electroporation of mammalian skin: A mechanism to enhance transdermal drug delivery; *Proceedings of the National Academy of Sciences of the United States of America* 90:10504-10508, 1993.
- Prausnitz M.R., Lau B.S., Milano C.D., Conner S., Langer R., Weaver J.C.; A Quantitative Study of Electroporation Showing a Plateau in Net Molecular Transport; *Biophysical Journal* 65:414-422, 1993.
- Prausnitz M.R., Corbett J.D., Gimm J.A., Golan D.E., Langer R., Weaver J.C.; Millisecond Measurement of Transport During and After an Electroporation Pulse; *Biophysical Journal* 68:1864-1870, 1995.
- Prausnitz M. R.; The effects of electric current applied to skin: A review for transdermal drug delivery; *Advanced Drug Delivery Reviews* 18:395-425, 1996.
- Prausnitz M.R.; Reversible skin permeabilization for transdermal delivery of macromolecules; *Critical Reviews in Therapeutic Drug Carrier Systems* 14(4):455-483, 1997.
- Prausnitz M.R.; A practical assessment of transdermal drug delivery by skin electroporation; *Advanced Drug Delivery Reviews* 35:61-76, 1999.
- Prausnitz M.R.; Microneedles for transdermal drug delivery; *Advanced Drug Delivery Reviews* 56:581-587, 2004.
- Prausnitz M.R., Mitragotri S., Langer R.; Current status and future potential of transdermal drug delivery; *Nature Reviews. Drug Discovery* 3(2):115-124, 2004.
- Rols M.P., Teissié J.; Electroporabilization of mammalian cells: quantitative analysis of the phenomenon; *Biophysical Journal* 58:1089-1098, 1990.
- Rols M.P., Teissié J.; Electroporabilization of mammalian cells to macromolecules: control by pulse duration; *Biophysical Journal* 75:1415-1423, 1998.
- Rols M.P., Delteil C., Golzio M., Dumond P., Cros S., Teissié J.; In vivo electrically mediated protein and gene transfer in murine melanoma; *Nature Biotechnology* 16:168-171, 1998.
- Rosch P.J., Markov M.S. (editors); Bioelectromagnetic medicine, Marcel Dekker Inc., NY, USA, 2004.
- Rubanyi G.M.; The future of human gene therapy; *Molecular Aspects of Medicine* 22:113-142, 2001.
- Serša G., Čemazar M., Miklavčič D.; Antitumor effectiveness of electrochemotherapy with cis-diamminedichloroplatinium (II) in mice; *Cancer Research* 55:3450-3455, 1995.
- Serša G., Čemazar M., Parkins C.S., Chaplin D.J.; Tumour blood flow changes induced by application of electric pulses; *European Journal of Cancer* 35(4):672-677, 1999.
- Serša G., Čemazar M., Rudolf Z.; Electrochemotherapy: advantages and drawbacks in treatment of cancer patients; *Cancer Therapy* 1:133-142, 2003.
- Sinigoj A.R., ELMG polje, Založba FE, Ljubljana, Slovenia, 1996.

- Somiari S., Glasspool-Malone J., Drabick J.J., Gilbert R., Heller R., Jaroszeski M., Malone R.W.; Theory and in vivo application of electroporative gene delivery; *Molecular Therapy* 2(3):178-187, 2000.
- Suchi T.; Experiments on electrical resistance of the human epidermis; *The Japanese Journal of Physiology* 5(1):75-80, 1955.
- Sukharev S.I., Klenchin V.A., Serov S.M., Chernomordik L.V., Chizmadzhev Yu.A.; Electroporation and electrophoretic DNA transfer into cells: The effect of DNA interaction with electropores; *Biophysical Journal* 63:1320-1327, 1992.
- Susil R., Šemrov D., Miklavčič D.; Electric field induced transmembrane potential depends on cell density and organization; *Electro and Magnetobiology* 17(3):391-399, 1998.
- Šatkauskas S., Bureau M., Puc M., Mahfoudi A., Scherman D., Miklavčič D., Mir L.M.; Mechanisms of in vitro DNA electrotransfer: Respective contributions of cell electropermeabilization and DNA electrophoresis; *Molecular Therapy* 5(2):133-140, 2002.
- Šatkauskas S., Andre F., Bureau M.F., Scherman D., Miklavčič D., Mir L.M.; Electrophoretic component of electric pulses determines the efficacy of in vivo DNA electrotransfer; *Human Gene Therapy* 16:1194-1201, 2005.
- Šel D., Cukjati D., Batiuskaite D., Slivnik T., Mir L.M., Miklavčič D.; Sequential finite element model of tissue electropermeabilization; *IEEE Transactions on Biomedical Engineering* 52:816-827, 2005.
- Šemrov D., Miklavčič D.; Vsiljeni transmembranski potencial zaradi zunanjega električnega polja v odvisnosti od oblike in orientacije ter gostote celic; *Elektrotehniški vestnik* 62 (1):35-42, 1995.
- Šemrov D., Miklavčič D.; Calculation of the electrical parameters in electrochemotherapy of solid tumors in mice; *Computers in Biology and Medicine* 28:439-448, 1998.
- Teissié J., Rols M.P.; An experimental evaluation of the critical potential difference including cell membrane electropermeabilization; *Biophysical Journal* 65:409-413, 1993.
- Teissié J., Eynard B., Gabriel B., Rols M.P.; Electropermeabilization of cell membranes; *Advanced Drug Delivery Reviews* 35:3-19, 1999.
- Tekle E., Astumian R.D., Chock P.B.; Electro - permeabilization of cell membranes: Effect of the resting membrane potential; *Biochemical and Biophysical Research Communications* 172(1):282-287, 1990.
- Thierry A.R., Lunardi-Iskandar Y., Bryant J.L., Rabinovich P., Gallo R.C., Mahan L.C.; *Proceedings of the National Academy of Sciences of the United States of America* 92:9742-9746, 1995.
- Tieleman D.P., Leontiadou H., Mark A.E., Marrink S.-J.; Simulation of pore formation in lipid bilayers by mechanical stress and electric fields; *Journal of American Chemical Society* 125:6382-6383, 2003.
- Trainer A.H., Alexander M.Y.; Gene delivery to the epidermis; *Human Molecular Genetics* 6(10):1761-1767, 1997.
- Tsong T.Y.; Electroporation of cell membranes; *Biophysical Journal* 60:297-306, 1991.

- Tungjitkusolmun S., Woo E.J., Cao H., Tsai J.-Z., Vorperian V.R., Webster J.G.; Thermal-electrical finite element modelling for radio frequency cardiac ablation: effects of changes in myocardial properties; *Medical & Biological Engineering & Computing* 38:562-568, 2000.
- Valič B., Golzio M., Pavlin M., Schatz A., Faurie C., Gabriel B., Teissié J., Rols M.P., Miklavčič D.; Effect of electric field induced transmembrane potential on spheroidal cells: theory and experiment; *European Biophysics Journal* 32:519–528, 2003.
- Valič B., Pavlin M., Miklavčič D.; The effect of resting transmembrane voltage on cell electropermeabilization: a numerical analysis; *Bioelectrochemistry* 63:311–315, 2004.
- Vanbever R., Prétat V.; Factors affecting transdermal delivery of metoprolol by electroporation; *Bioelectrochemistry and Bioenergetics* 38:223-228, 1995.
- Vanbever R., Fouchard D., Jadoul A., De Morre N., Prétat V., Marty J.P.; In vivo non-invasive evaluation of hairless rat skin after high-voltage pulse exposure; *Skin Pharmacology and Applied Skin Physiology* 11:23-34, 1998.
- Vanbever R., Pliquett U. F., Prétat V., Weaver J.C.; Comparison of the effects of short, high-voltage and long, medium-voltage pulses on skin electrical and transport properties; *Journal of Controlled Release* 69:35-47, 1999.
- Vanbever R., Prétat V.; In vivo efficacy and safety of skin electroporation; *Advanced Drug Delivery Reviews* 35:77-88, 1999.
- Weaver J.C., Chizmadzhev Y.A.; Theory of electroporation: A review; *Bioelectrochemistry and Bioenergetics* 41:135-160, 1996.
- Weaver J.C., Vaughan T.E., Chizmadzhev Y.A.; Theory of electrical creation of aqueous pathways across skin transport barriers; *Advanced Drug Delivery Reviews* 35:21-39, 1999.
- Wolf H., Rols M.P., Boldt E., Neumann E., Teissié J.; Control by pulse parameters of electric field—mediated gene transfer in mammalian cells; *Biophysical Journal* 66:524-531, 1994.
- Wong T.-K., Neumann E.; Electric field mediated gene transfer; *Biochemical and Biophysical Research Communications* 107(2):584-587, 1982.
- Yamamoto T., Yamamoto Y.; Electrical properties of the epidermal stratum corneum; *Medical and Biological Engineering* 14(2):151-158, 1976.
- Yamamoto T., Yamamoto Y.; Dielectric constant and resistivity of epidermal stratum corenum; *Medical and Biological Engineering* 14(5):494-499, 1976a.
- Yang N.-S., Sun W.H.; Gene gun and other non - viral approaches for cancer gene therapy; *Nature Medicine* 1(5):481-483, 1995.
- Zampaglione I., Arcuri M., Cappelletti M., Ciliberto G., Perretta G., Nicosia A., La Monica N., Fattori E.; In vivo DNA gene electro-transfer: a systematic analysis of different electrical parameters; *The Journal of Gene Medicine* 7:1475-1481, 2005.
- Zhang L., Nolan E., Kreitschitz S., Rabussay D.P.; Enhanced delivery of naked DNA to the skin by non-invasive in vivo electroporation; *Biochimica et Biophysica Acta* 1572:1-9, 2002.

Zhang L., Rabussay D.P.; Clinical evaluation of safety and human tolerance of electrical sensation induced by electric fields with non-invasive electrodes; *Bioelectrochemistry* 56:233-236, 2002.

Zhang L., Widera G., Rabussay D.; Enhancement of the effectiveness of electroporation-augmented cutaneous DNA vaccination by a particulate adjuvant; *Bioelectrochemistry* 63:369-373, 2004.

## **Appendix**

Three published papers relevant to this work and a chapter in press with the author of this doctoral thesis as the first author or a co-author are given in continuation.



## PAPER 1

### **Dependence of Induced Transmembrane Potential on Cell Density, Arrangement, and Cell Position Inside a Cell System**

**Mojca Pavlin, Nataša Pavšelj and Damijan Miklavčič**

**Published in:** IEEE Transactions on Biomedical Engineering: 49(6): 605-612, 2002

**Abstract:** A nonuniform transmembrane potential (TMP) is induced on a cell membrane exposed to external electric field. If the induced TMP is above the threshold value, cell membrane becomes permeabilized in a reversible process called electropermeabilization. Studying electric potential distribution on the cell membrane gives us an insight into the effects of the electric field on cells and tissues. Since cells are always surrounded by other cells, we studied how their interactions influence the induced TMP. In the first part of our study, we studied dependence of potential distribution on cell arrangement and density in infinite cell suspensions where cells were organized into simple-cubic, body-centered cubic, and facecentered cubic lattice. In the second part of the study, we examined how induced TMP on a cell membrane is dependent on its position inside a three-dimensional cell cluster. Finally, the results for cells inside the cluster were compared to those in infinite lattice. We used numerical analysis for the study, specifically the finite-element method (FEM). The results for infinite cell suspensions show that the induced TMP depends on both: cell volume fraction and cell arrangement. We established from the results for finite volume cell clusters and layers, that there is no radial dependence of induced TMP for cells inside the cluster.



# Dependence of Induced Transmembrane Potential on Cell Density, Arrangement, and Cell Position Inside a Cell System

Mojca Pavlin, Nataša Pavšelj, and Damijan Miklavčič\*

**Abstract**—A nonuniform transmembrane potential (TMP) is induced on a cell membrane exposed to external electric field. If the induced TMP is above the threshold value, cell membrane becomes permeabilized in a reversible process called electropermeabilization. Studying electric potential distribution on the cell membrane gives us an insight into the effects of the electric field on cells and tissues. Since cells are always surrounded by other cells, we studied how their interactions influence the induced TMP. In the first part of our study, we studied dependence of potential distribution on cell arrangement and density in infinite cell suspensions where cells were organized into simple-cubic, body-centered cubic, and face-centered cubic lattice. In the second part of the study, we examined how induced TMP on a cell membrane is dependent on its position inside a three-dimensional cell cluster. Finally, the results for cells inside the cluster were compared to those in infinite lattice. We used numerical analysis for the study, specifically the finite-element method (FEM). The results for infinite cell suspensions show that the induced TMP depends on both: cell volume fraction and cell arrangement. We established from the results for finite volume cell clusters and layers, that there is no radial dependence of induced TMP for cells inside the cluster.

**Index Terms**—Cell cluster, cell suspension, electropermeabilization, finite-element modeling, transmembrane potential.

## I. INTRODUCTION

EXTERNAL electric field causes biochemical and physiological changes in biological cells and tissues. When an electric field is applied to a cell or cell system, a nonuniform transmembrane potential (TMP) is induced on exposed cells. If the induced TMP is large enough, i.e., above the threshold value ( $TMP_c$ ), the cell membrane becomes permeabilized in a reversible process called electropermeabilization, thus allowing entrance of molecules that otherwise cannot easily cross the cell membrane [1]–[3]. Further increase of the electric field causes irreversible membrane permeabilization and cell death. Induced TMP in biological cells exposed to electromagnetic fields is of interest in a variety of applications, such as gene transfection [4], electrochemotherapy [5], the study of forces on cells un-

Manuscript received July 20, 2001; revised February 3, 2002. This work was supported in part by the Ministry of Education Science and Sports of the Republic of Slovenia and European Commission under the 5th framework under the Grant Cliniporator QLK-1999-00484. Asterisk indicates corresponding author.

M. Pavlin and N. Pavšelj are with the University of Ljubljana, Faculty of Electrical Engineering, SI-1000 Ljubljana, Slovenia.

\*D. Miklavčič is with the University of Ljubljana, Faculty of Electrical Engineering, Tržaška 25, SI-1000 Ljubljana, Slovenia (e-mail: damijan@svarun.fe.uni-lj.si).

Publisher Item Identifier S 0018-9294(02)04850-4.

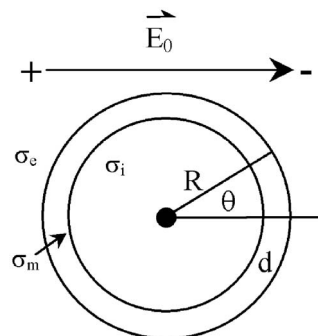


Fig. 1. Model of a cell, where  $\sigma_e$ ,  $\sigma_i$  and  $\sigma_m$  represent specific conductivities of external medium, internal medium and cell membrane, respectively,  $\theta$  is an angle measured with respect to the electric field direction ( $E_0$ ),  $R$  denotes cell radius and  $d$  membrane thickness.

dergoing fusion, models of cardiac tissue response to defibrillating currents, and the study of potential health effects of electric and magnetic fields [6], [7]. Therefore, investigation of induced potential distribution on the cell membrane is important in studying the effects of the electric field on biological cells.

Potential distribution on the surface of a cell placed in an electric field can be calculated analytically or numerically. Even though analytical solutions are possible only for some analytically defined shapes, such as spheroids [8], they give us a rough picture of the dependence of the induced TMP on electric and geometric parameters.

In the spherical coordinate system, a cell can be represented by a sphere surrounded with a shell. In Fig. 1, we see a cross section of such a sphere.

A cell membrane is shown as a shell, where  $d$  denotes membrane thickness and  $R$  the cell radius. Membrane thickness is exaggerated for easier representation.  $\sigma_e$  and  $\sigma_i$  represent specific conductivity of the external and the internal medium, respectively, and  $\sigma_m$  represents specific conductivity of the membrane.  $\theta$  is an angle measured with respect to the electric field direction. Analytical solution for static case for induced TMP is given by Schwan's equation [9]

$$\Delta\Psi = \text{TMP} = g(\lambda)E_0R \cos\theta \quad (1)$$

where  $\Delta\Psi$  represents potential drop across the cell membrane. Factor  $g(\lambda)$  is a function of cell parameters and  $E_0$  is the applied electric field. For physiological conditions where  $d \ll R$  and  $\sigma_m \ll \sigma_e, \sigma_i$ , [10], (1) simplifies to

$$\text{TMP} = 1.5RE_0 \cos\theta \quad (2)$$

which is an exact solution for potential on a surface of a nonconducting sphere. However, for low conducting media the exact equation (1) has to be applied [11].

In majority of experiments, cells are surrounded by other cells, so the aim of this study was to get an insight into cell interactions in monolayers, suspensions, aggregates, clusters and tissues and how this influences the induced TMP. Each cell in electric field behaves as a dipole, which modifies external electric field. Mutual interactions between dipoles lead to problem of many-body system for which analytical solutions are too complex to obtain [12]–[14]. Therefore, numerical methods have to be applied to obtain the solution for field distribution and induced TMP in cell suspensions and cell clusters. In this paper, we shall limit ourselves only to the analysis for the static direct current, which holds also for the frequencies under the relaxation frequency (approximately 1 MHz). To obtain the solution for higher frequencies one has to consider also the dielectric properties of the cell, however in the low frequency range the conductive properties of the cells are dominant.

In the first part of our study, we modeled infinite cell suspensions where cells were arranged into simple-cubic (sc), body-centered cubic (bcc), and face-centered cubic (fcc) lattice. We studied the influence of cell arrangement and density on induced TMP distribution in a cell membrane. We also calculated fraction of a cell surface where the induced TMP is above the threshold value ( $TMP_c$ ) for different cell densities and arrangements.

In the second part of our study, we studied three-dimensional cell clusters as models of multicellular tumor spheroids [15]. A multicellular tumor spheroid is an *in vitro* model of a real tumor, used for studying molecular transport, cell viability and electroporation protocols in tumors. We examined how induced TMP in a cell depends on its position inside a cluster. Finally, we compared the results for cells inside the cluster to those in infinite lattice, i.e., cell suspensions.

## II. METHODS

### A. Finite-Element Modeling

Since the analytical equations are too complex for problem of many interacting cells, we used numerical analysis for the study. Numerical calculations were performed by finite-element modeling software EMAS (Ansoft, Pittsburgh, PA), using finite-element method (FEM). Details of this program and FEM method are described elsewhere [16]. Briefly, FEM solves partial differential equation by dividing the volume into smaller elements and solving differential equation on elements. These elements have various shapes and sizes so that complex geometries can be modeled. Resolution of the model is increased by increasing number of elements. The maximum number of elements, however, is limited by the computer memory capacity.

### B. Models

Biological cells were modeled as nonconductive spheres, since under normal conditions membrane conductivity is many orders smaller than that of the external medium and, therefore, can be neglected [10]. Cells were organized either into sc, bcc, or fcc lattice shown in Fig. 2. Using the symmetry of cubic

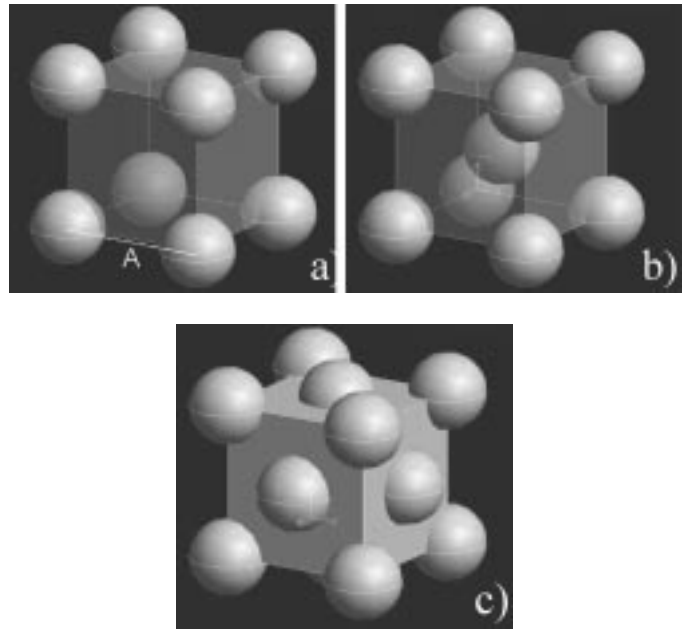


Fig. 2. Unit cells for (a) sc, (b) bcc, and (c) fcc lattices.  $A$  is length of unit cell side shown in (a).

lattices and applying appropriate boundary conditions, we were able to model infinite cubic lattices with a model of a primitive cell.

We studied the difference in the induced TMP distribution between infinite lattice arrangements for two cases. To compare our results with our previous work [17], we first calculated the induced TMP for different packing ratios (PRs). The PR was defined as a ratio of cell distance to cell diameter. Second, we analyzed differences in induced TMP for different volume fractions. Volume fraction is defined as a percentage of volume occupied by cells [see (9) in the Appendix]. The relation between volume fraction and PR for the simple cubic lattice is given by

$$f_{sc} = \frac{4\pi}{3} \cdot \left( \frac{R}{2(1 + PR_{sc})} \right)^3 \quad (3)$$

and can be easily calculated from geometry of the unit cells (Fig. 2). To get a better idea of the relation between the two parameters, we calculated PRs for given volume fraction for the sc lattice. The conversion is in Table I.

For the bcc and fcc arrangement, however, the PR cannot be uniquely defined, therefore, PR is not adequate parameter for this study. On the other hand, volume fraction is usually the parameter that gives us information about the cell density and is also the only factor contributing to equivalent conductivity of an array of cells [12], [18], [19]. Therefore, we compared the induced TMP for different lattices for the same volume fraction— $f$ . Varying sphere radius calculations were performed for different cell volume fraction  $f$ , where  $f = 4\pi/3N(R/A)^3$ , where  $A$  is the length of the unit cell side shown in Fig. 2(a) and  $N$  number of the spheres in the unit cell. Maximum volume fractions for hard spheres are 0.52 for sc, 0.64 for bcc, and 0.74 for fcc lattice.

It was suggested in the literature [20] that permeabilization is linearly proportional to the area above the  $TMP_c$ . We, therefore,

TABLE I  
CONVERSION BETWEEN VOLUME FRACTION AND PR FOR SC LATTICE

volume fraction $f^*$	PR sc
0.01	2.741
0.05	1.188
0.1	0.736
0.3	0.204
0.5	0.015

\* from (3)

calculated fraction of the cell surface having the induced TMP above the threshold value  $\text{TMP}_c$ , which was chosen within the range reported in the literature (200–1000 mV) [2], [21]–[25].

Dependency of induced TMP on angle  $\theta$  was fitted with a polynomial of third order  $p(\theta)$  with least square method. Critical angle  $\theta_c$  can be defined as the angle where threshold value for permeabilization is reached

$$\text{TMP}_c/E_0R = p(\theta_c). \quad (4)$$

From the critical angle the permeabilized area was calculated with

$$S_c/S_0 = (1 - \cos \theta_c) \quad (\text{where } S_0 = 4\pi R^2). \quad (5)$$

In the second part of the study, we analyzed cell clusters as models of multicellular tumor spheroids [15]. Potential and electric field distribution around a densely packed cell cluster is similar to the distribution around a single isolated cell. When defining the boundary conditions of the model, we must ensure that the boundary placement does not influence the electric field in the cluster. Again, cubic symmetry enabled us to model the whole cluster by calculating only its one-fourth. In Fig. 3, we see the whole cluster, where 675 cells (seven cells or approximately  $140 \mu\text{m}$  in diameter) were arranged in fcc lattice as close to spherical shape as possible. In multicellular tumor spheroids, cells are tightly packed ( $f = 0.46$ – $0.65$ ) [26]–[28] so we chose fcc lattice, because it is the arrangement where the highest volume fraction of cells is possible (up to 0.74).

Unless otherwise specified, all results for the induced TMP are normalized to the applied electric field magnitude and cell radius.

### III. RESULTS AND DISCUSSION

#### A. Cell Suspensions

In this first part of the study, we analyzed how induced TMP depends on cell arrangement and volume fraction. We first calculated the induced TMP for the simple cubic lattice for different PRs. For the  $\text{PR} = 0$ , we obtained the decrease of factor 1.5 to 1.0 which was already shown previously [17]. However, for further analysis we analyzed the induced TMP for different volume fractions [for correlation between PR and volume fraction see (3) and Table I]. In Fig. 4, we show the results for sc, bcc,

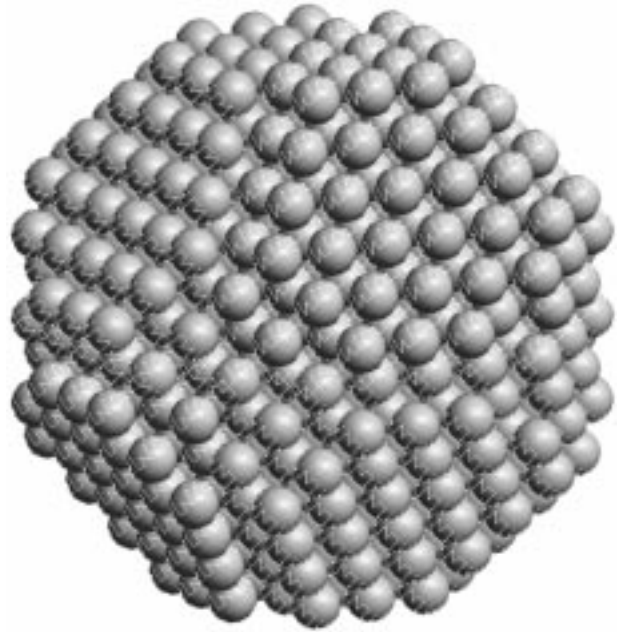


Fig. 3. Model of a cell cluster representing multicellular tumor spheroid, composed of 675 cells arranged in fcc lattice.

and fcc lattices having the same volume fraction. Since maximum volume fraction for hard spheres arranged in sc lattice is 0.52, we were able to compare three different arrangements studied up to  $f = 0.52$ .

As reported previously [17], a change in induced TMP distribution on cell membrane and a decrease of its maximum value was observed in cell suspensions. These changes are due to interaction with neighboring cells.

We can see from Fig. 4 that induced TMP depends not only on the volume fraction, but also on cell arrangement inside the lattice (sc, bcc, or fcc) which can be explained with different number of nearest neighbors and different cell arrangement in different lattices. Therefore, the induced TMP depends on both; on cell volume fraction and cell arrangement.

In real suspensions, cells arrange randomly or under the gravitational force. For volume fractions above 0.52, cells can order only in bcc and fcc lattices, and above 0.62 only the latter is possible. Hexagonal packing is also possible but since this arrangement is similar to fcc we presumed that fcc lattice is the most representative.

We then calculated fraction of the cell surface having the induced TMP above the threshold value  $\text{TMP}_c$  for the hexagonal packing. The fraction of permeabilized area was obtained with (5) derived in the Methods section. The results for the fraction of permeabilized area are represented in Fig. 5.

The fraction of permeabilized area decreases with increasing volume and depends on the critical TMP. Therefore, efficiency of electroporation depends also on cell density.

In all our calculations, we neglected the resting potential of the cell. In literature, there is a general agreement that induced TMP is superimposed on the resting potential [21]. The critical voltage for membrane permeabilization was reported to be in the range from 200 up to 1000 mV while the resting potential is between 50 and 100 mV for excitable cells and even lower for

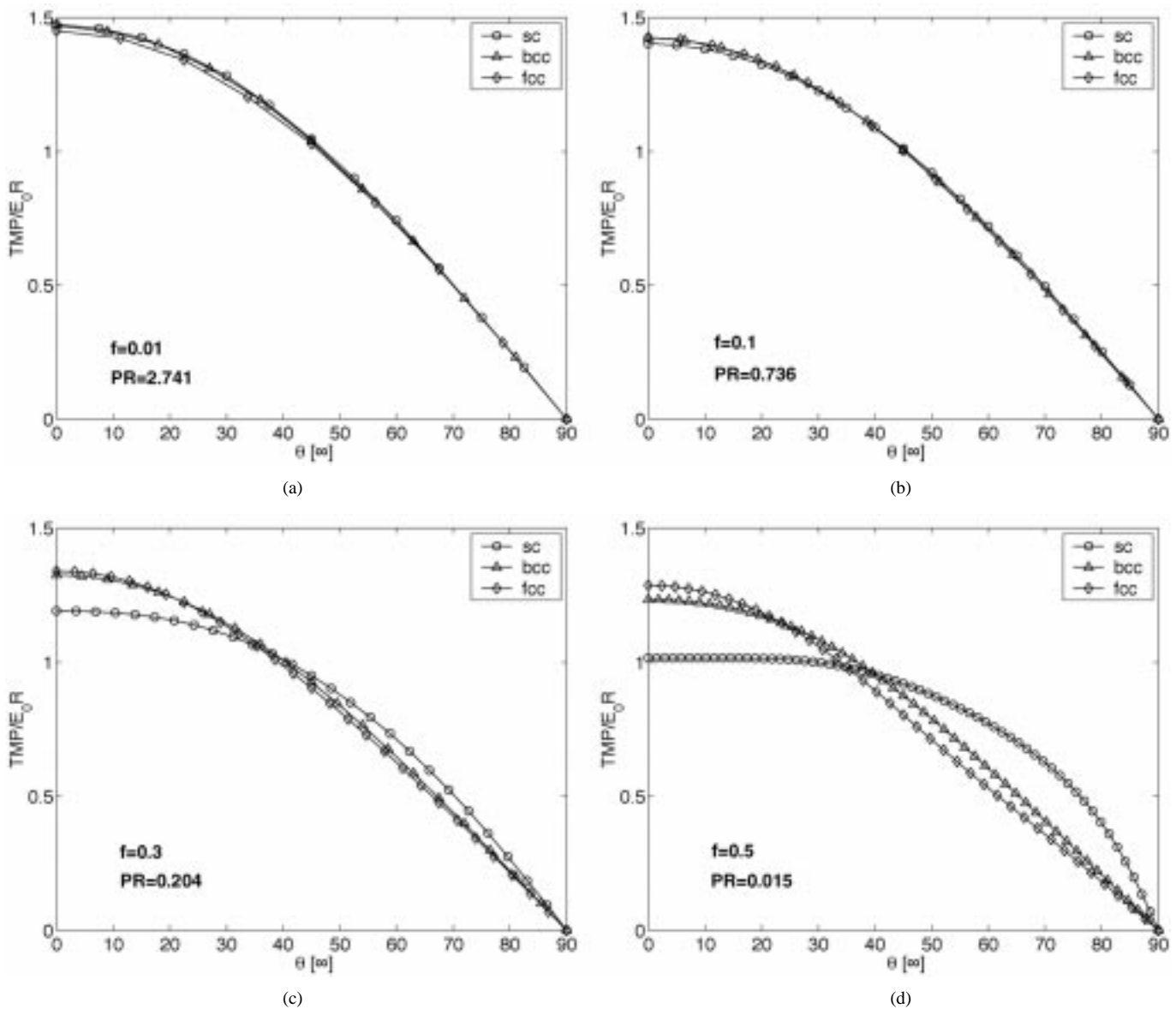


Fig. 4. Comparison of induced TMP, normalized to electric field magnitude and cell radius, on cells in suspensions arranged in sc, bcc, fcc lattice for volume fractions  $f = 0.01, 0.1, 0.3,$  and  $0.5$ .

non excitable cells as chinese hamster lung cells (20–29 mV) [22]. Therefore, TMP is increased on one side of the cell and decreased on the other in the range of 5% to 50%. If the induced TMP is under critical value on larger part of the cell the change due to resting potential has no significant effect on the fraction of permeabilized area since the smaller fraction on one side of the cell is compensated with larger area on the other side. However, if the maximum induced TMP is just above the critical value, the effect of increased TMP on one side of the cell is significant and should be taken into account.

### B. Cell Clusters

In the second part of our study, we observed induced TMP on cells in the mid section plane of the cluster, parallel to the field direction. As mentioned before, we only modeled one-fourth of the cluster, due to the symmetry of the model. We chose electric field magnitude outside the cluster to be 1 MV/m, which is

quite large in terms of cell permeabilization, but since the model is linear, the results can easily be scaled to the electric field magnitude of interest. We analyzed induced TMP values on the cells in a cross section of the cluster. The average maximum induced TMP inside the cluster for cell diameter  $16 \mu\text{m}$  was 11.24 V (induced TMP scaled to 500 mV corresponds to 44.5 kV/m of applied field). We noticed some small differences between the cells inside the cluster. But these differences are in the range of 1% and are most probably due to numerical calculations. However, we noticed larger deviations in the induced TMP for the cells on the edge of the cluster. We established that there is no radial dependence of induced TMP except for those small differences in the outer cells. This can be attributed to the fact that the cluster deviates from spherical shape. In order to confirm this, we amplified this effect by building an FEM model of a layer of cells, with large irregularities in circular shape. We removed some cells from the circular layer. Deviations of induced TMP

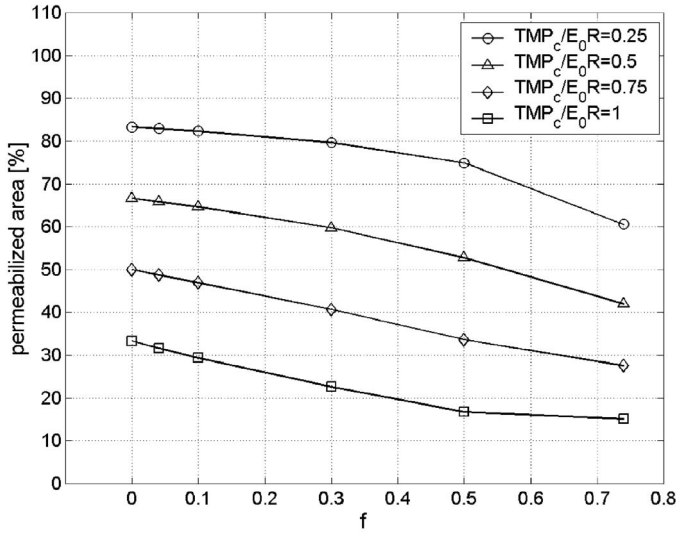


Fig. 5. Percentage of permeabilized area for fcc lattice for different normalized critical TMPs. For  $\text{TMP}_c/E_0R$  given in range reported in literature (0.25–1 V) and for a typical cell size ( $R \sim 10 \mu\text{m}$ ) is  $E_0 \sim 100 \text{ kV/m}$ . For  $f = 0$ , we have the case of an isolated cell.

are shown in Fig. 6, where for easier presentation only the deviations above 2% are shown. We can see that deviations in induced TMP are much amplified for the cells near the irregularities.

To better understand why the position of a cell inside the cluster does not play any role in the cell's induced TMP, we built a model where a cluster of cells was represented with a sphere having an equivalent conductivity. To calculate equivalent conductivity of the cluster— $\sigma$  we used Maxwell equation [19], [29], [30] (see the Appendix) and by inserting  $\sigma_p = 0$  for conductivity of a cell into (8), we obtain

$$\sigma/\sigma_e = \frac{1-f}{1+0.5f} \quad (6)$$

where parameter  $f$  is volume fraction of cells in cluster and  $\sigma_e$  is extracellular conductivity.

Electric field inside the cluster depends only on the ratio between equivalent and external conductivity [10], [9]

$$E = \frac{3\sigma_e}{2\sigma_e + \sigma}. \quad (7)$$

According to (6) and (7), average electric field inside the cluster increases, due to the decrease of equivalent conductivity.

In Fig. 7(a), we see equipotential planes of this model. Equipotentials inside the sphere are equidistant, the electric field is homogeneous and, therefore, all the cells inside the sphere have the same induced TMP. However, in reality a cluster of cells is never a perfect sphere, so we can observe irregularities for the cells on the edge. To illustrate this, we built a model that has four irregularities: two hollows and two knobs, one on the side that is parallel and the other on the side of the cluster that is perpendicular to the electric field. In Fig. 7(b), we can see how the homogeneity of the electric field is deformed near the irregularities. In a cluster of cells, such irregularities lead to the deviation of induced TMP for the cells in these areas from centrally located cells.

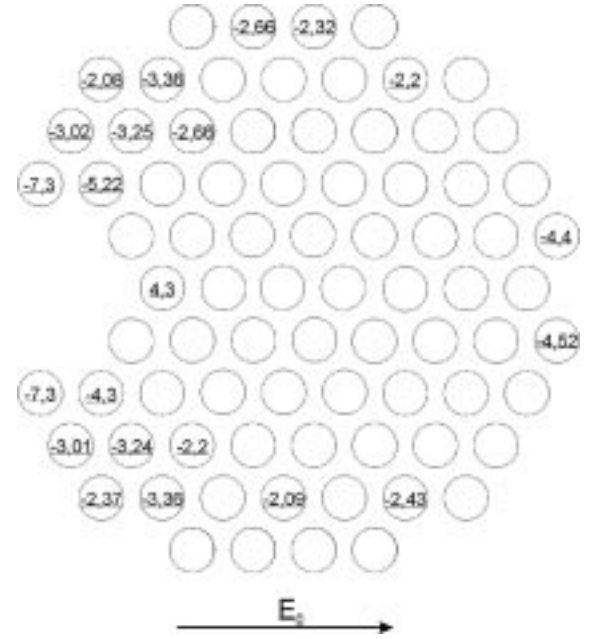


Fig. 6. A model of a layer of cells with large irregularities. Layer is arranged into hexagonal lattice (not fcc), which enables us to even better approximate circular shape. The deviations from the average middle cell are shown in percentage.

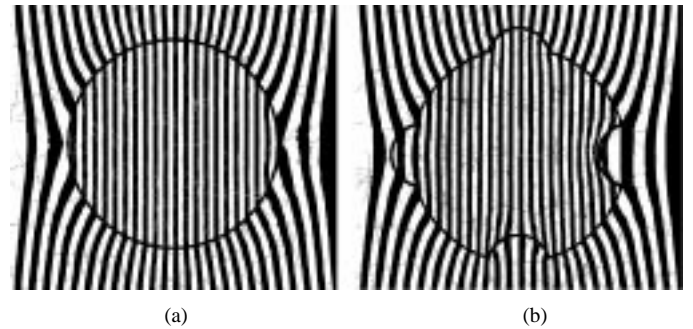


Fig. 7. Equipotentials of models, where a cluster of cells is represented with equivalent conductivity (a) a cluster is represented with a perfect sphere, (b) a cluster with irregularities in spherical shape.

Volume fraction of our cell cluster was 0.38, which is a little lower than the volume fraction of real multicellular spheroids (0.45–0.65), but unfortunately we were limited with computer memory capacity. We analyzed induced TMP inside the cluster and its radial dependency. If we compare values of normalized induced TMP in the strand of cells in the middle of the cluster, parallel to the electric field direction, we can see there is no radial dependency, except for small differences for the outer two cells. We can also notice a drop of factor 1.5 in (1) (for an isolated cell) to approximately 1.4, which can be explained by two contributing effects acting in opposite directions. First, an increase of average electric field inside the cluster due to lower equivalent conductivity of the cluster [(6) and (7)]. And second, a decrease of induced TMP is observed and described for infinite lattices of cells (Fig. 4) because of a decrease of local electric field inside the cluster, due to interactions between cells.

We compared the results of the cluster with those for infinite lattice having the same density and cell arrangement. The comparison is shown in Fig. 8(a). It should be stressed that in

order to normalize the calculated TMP inside the cluster, we used the average field  $E$  inside the cluster, which is higher than the applied field  $E_0$  ( $E_{\text{numerical}} = 1.13 E_0$ ). The calculation of the average field  $E$  inside the cluster is shown in Fig. 8(b). We can see that equipotential surfaces follow the symmetry of the fcc lattice. By determining the potential difference between two symmetric points, the average field inside the cluster was calculated. We also calculated field  $E$  inside the cluster theoretically, according to (7) for equivalent sphere. However, we obtained a slightly different result ( $E_{\text{theoretical}} = 1.2 E_0$ ) due to the fact that one cannot assign a discrete border to a cluster. Therefore, equipotentials bend slightly on the border of a real cluster and are not straight as they are in equivalent sphere [see Fig. 7(a)].

In Fig. 8(a), we compared the results for cells arranged in infinite fcc lattice with the results for cells in cluster normalized to local electric field— $E$  for both cases—the field obtained numerically and theoretically [Fig. 8(b)]. We can see that there is no observable difference between the numerically obtained results for the cluster and the infinite lattice. In this way, we also demonstrated that induced TMP of a cell inside the cluster depends on local field and not on its position inside the cluster. The only change is observed on the border of the cluster where local electric field is changed. Therefore, we can conclude that cluster size does not have any impact on induced TMP for cells inside the cluster, provided that cell density and size throughout the cluster are uniform.

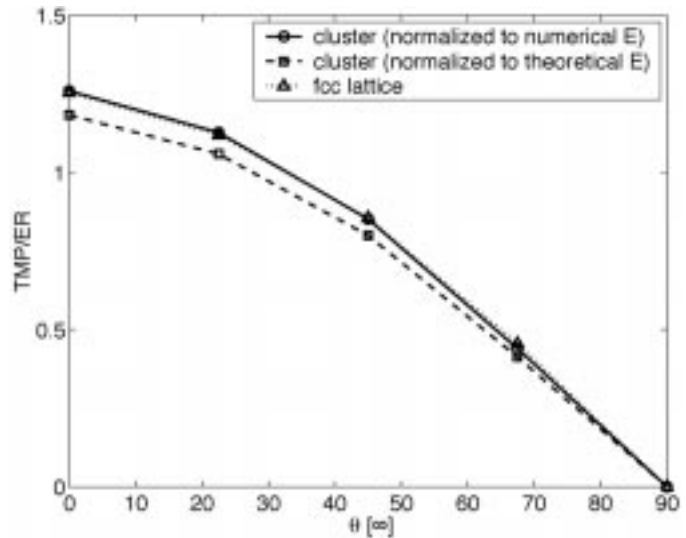
#### IV. CONCLUSION

In our study, we used finite-elements modeling to study induced TMP dependence on cell arrangement, volume fraction and PR. As models of cell suspensions in the first part of the study, we used infinite array of cells arranged into sc, bcc, and fcc lattices. In the second part of the study, we used cell clusters as models of multicellular tumor spheroids. From the theory of dispersed systems we know that bulk conductivity depends on volume fraction—density of cells in suspension [19]. So one might expect that volume fraction has a direct proportional effect on induced TMP as well. However, we showed that volume fraction and cell arrangement both influence the induced TMP. It should be stressed that our calculations are valid for cells that are not electrically connected which is true for cell suspensions and multicellular tumor spheroids as *in vitro* models of tumors [15]. For the tissue cells and cells that are electrically connected with gap junctions (epithelial tissues, nerve, and cardiac cells), other approaches have to be used [6], [7].

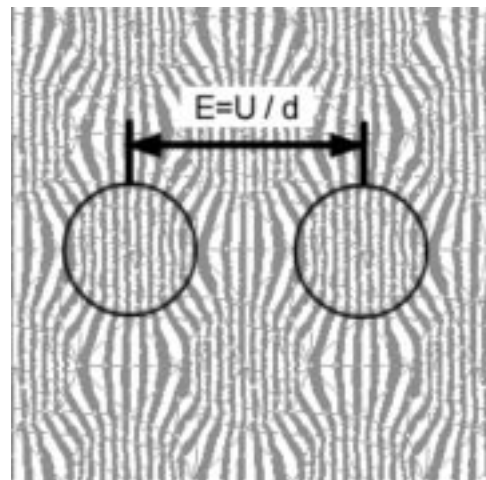
In all our calculations, we neglected resting TMP. We limited our calculations to a dc case, which holds also for the frequencies under the relaxation frequency—about 1 MHz.

In real suspensions, cells order randomly so that cells are as far as possible from each other, therefore, fcc lattice is probably the closest approximation to real suspensions. We showed that for fcc lattice we get considerable decrease in induced TMP compared to Schwan equation for isolated cell (up to 15%) and fraction of permeabilized area (up to 50%). For other arrangements of cells, even larger decrease is obtained.

As we see from the results for cell clusters and layers, there is no radial dependence inside the finite arrangements of cells.



(a)



(b)

Fig. 8. (a) Comparison of finite-volume fcc cell cluster and infinite fcc lattice,  $E$  is the average field inside the cell cluster for both cases—obtained numerically and theoretically,  $R$  is the cell radius. For infinite lattice,  $E = E_0$ . (b) Calculation of the average field  $E$  inside the cluster.

But it has to be emphasized that this is only true for the homogeneous arrangements of cells that can be represented with a sphere having equivalent homogeneous conductivity. We observed small differences in induced TMP on the border of a cluster are due to the fact that clusters deviate from spherical shape, which alters electric field on the border of a cluster.

Finally, we analyzed values of induced TMP inside the cluster. We showed that the drop of factor  $g$  from 1.5 for isolated cell [(1) and (2)] to approximately 1.4 for the case of fcc lattice with volume fraction 0.38, can be explained by two contributing factors having the opposite effects. First, an increase of the electric field inside the cluster due to the decrease in equivalent conductivity, and second, a decrease of induced TMP due to interaction between the cells. We verified this by comparing induced TMP between the cells that are arranged in infinite lattice and those inside a finite cluster of cells. Taking into account both contributing factors for cells in clusters we obtained the same result as for cells arranged in infinite lattice.

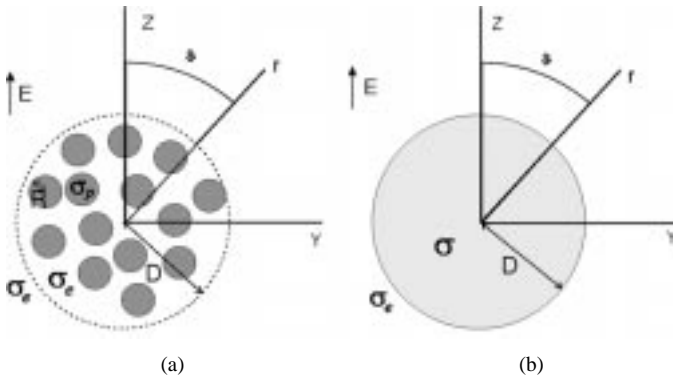


Fig. 9. Maxwell's derivation of conductivity for dilute suspension of particles. (a)  $N$  spheres dispersed in medium that induces the same potential under external field  $E$  as (b) one sphere of radius  $D$  having effective conductivity  $\sigma$ .

Drawback of our approach is that using FEM method we were not able to model a suspension or a multicellular spheroid of randomly dispersed cells such as in realistic suspensions and spheroids. Also, the size of cells can vary, so the reality is somewhat different from the ideal case of our study. Size and density of our cell clusters though was in the range of the size and the density of real multicellular tumor spheroids. The models we used in our study are in fact very idealized, but as such give us an answer to our question: Does a cell position inside the cluster itself, not taking into account the distribution of cells and their size, have any effect on induced TMP in a cell?

From literature we know [12]–[14] that random or ordered arrangement does not significantly change effective conductivity, but for calculations of TMP this could be of some importance. Also, for more accurate result of fraction of permeabilized area, membrane resting potential should be taken into account.

In summary, we showed that for evaluation of experimental results one should consider deviation of induced TMP due to cell arrangement, especially for dense cell suspensions and multicellular spheroids. For experiments on multicellular tumor spheroids, it is also necessary to evaluate changes around nonhomogenates (deviations from round shape) which alter induced TMP on the border of a tumor.

## APPENDIX

### A. Maxwell Equation

Maxwell was first to derive the equation for effective conductivity  $\sigma$  of dilute suspension [29], [30]. He realized that potential due to  $N$  spheres lying in external field having conductivity  $\sigma_p$  and dispersed in medium  $\sigma_e$  [Fig. 9(a)] is equal to the potential of equivalent sphere having effective conductivity  $\sigma$  [Fig. 9(b)]. With this he derived his equation

$$\frac{\sigma_e - \sigma}{2\sigma_e + \sigma} = f \frac{\sigma_e - \sigma_p}{2\sigma_e + \sigma_p}. \quad (8)$$

Parameter  $f$  is volume fraction of particles dispersed in medium and is defined as

$$f = \frac{NR^3}{D^3} \quad (9)$$

where  $D$  denotes radius of equivalent sphere. The parameter  $f$  indicates how tightly the cells are packed together and can range from nearly zero (dilute suspensions) up to 0.74 (maximum for spherical cells).

It was shown experimentally [10] and numerically [19] that for suspensions of nonconductive particles Maxwell equation is valid also for volume fractions up to 0.74.

## ACKNOWLEDGMENT

The authors would like to thank J. Švajger for valuable suggestions. D. Miklavčič would like to thank M. Prausnitz for stimulating discussion on multicellular tumor spheroids.

## REFERENCES

- [1] L. M. Mir, "Therapeutic perspectives of *in vivo* cell electroporation," *Bioelectrochemistry*, vol. 53, pp. 1–10, 2000.
- [2] E. Neumann, A. E. Sowers, and C. A. Jorda, *Electroporation and Electrofusion in Cell Biology*. New York: Plenum, 1989.
- [3] S. Orłowski and L. M. Mir, "Cell electroporation: A new tool for biochemical and pharmacological studies," *Biochim. Biophys. Acta*, vol. 1154, pp. 51–62, 1993.
- [4] L. M. Mir, M. F. Bureau, J. Gehl, R. Rangara, D. Rouy, J. M. Caillaud, P. Delaere, D. Branellec, B. Schwartz, and D. Scherman, "High-efficiency gene transfer into skeletal muscle mediated by electric pulses," in *Proc. Nat. Acad. Sci. USA*, vol. 96, 1999, pp. 4262–4267.
- [5] G. Sersa, T. Cufer, M. Cemazar, M. Rebersek, and Z. Rudolf, "Electrochemotherapy with bleomycin in the treatment of hypernephroma metastasis," *Case Report and Literature Review, Tumori*, vol. 86, pp. 163–165, 2000.
- [6] C. E. Fear and M. A. Stuchly, "Biological cells with gap junctions in low-frequency electric fields," *IEEE Trans. Biomed. Eng.*, vol. 45, pp. 856–866, July 1998.
- [7] —, "Modeling assemblies of biological cells exposed to electric fields," *IEEE Trans. Biomed. Eng.*, vol. 45, pp. 1259–1271, Oct. 1998.
- [8] T. Kotnik and D. Miklavčič, "Analytical description of transmembrane voltage induced by electric fields on spheroidal cells," *Biophys. J.*, vol. 79, pp. 670–679, 2000.
- [9] H. P. Schwan, "Electrical properties of tissue and cell suspensions," *Adv. Biol. Med. Phys.*, vol. 5, pp. 147–209, 1957.
- [10] C. Polk and E. Postow, "Dielectric properties of tissues," in *Handbook of Biological Effects of Electromagnetic Fields*, 2nd ed, C. Polk and E. Postow, Eds. Boca Raton, FL: CRC, 2000, pp. 28–92.
- [11] T. Kotnik, F. Bobanović, and D. Miklavčič, "Sensitivity of transmembrane voltage induced by applied electric fields—A theoretical analysis," *Bioelectrochem. Bioen.*, vol. 43, 1997.
- [12] S. S. Dukhin, "Dielectric properties of disperse systems," in *Surface and Colloid Science*, E. Matijević, Ed. New York: Wiley-Interscience, 1971, vol. 3, pp. 83–165.
- [13] S. Takhasima, *Electrical Properties of Biopolymers and Membranes*. Bristol, U.K.: Adam Hilger, 1989.
- [14] T. Hanai, "Electrical properties of emulsions," in *Emulsion Science*, P. Sherman, Ed. London, U.K.: Academic Press, 1968, pp. 353–478.
- [15] R. M. Sutherland, "Cell and environment interactions in tumor microregions: The multicell spheroid model," *Science*, vol. 240, pp. 177–184, 1988.
- [16] D. Šemrov and D. Miklavčič, "Numerical modeling for *in vivo* electroporation," in *Electrochemotherapy, Electrotherapy and Transdermal Drug Delivery: Electrically Mediated Delivery of Molecules to Cells*, M. J. Jaroszeski, R. Heller, and R. Gilbert, Eds. Totowa, NJ: Humana, 1999, pp. 63–81.
- [17] R. Susil, D. Šemrov, and D. Miklavčič, "Electric field—Induced transmembrane potential depends on cell density and organization," *Electro. Magnetobiol.*, vol. 17, no. 3, pp. 391–399, 1998.
- [18] L. Rayleigh, "On the influence of obstacle arranged in rectangular order upon the properties of a medium," *Phil. Mag.*, vol. 34, pp. 481–502, 1892.
- [19] M. Pavlin, T. Slivnik, and D. Miklavčič, "Effective conductivity of cell suspensions," *IEEE Trans. Biomed. Eng.*, vol. 49, pp. 77–80, Jan. 2002.

- [20] B. Gabriel and J. Teissie, "Fluorescence imaging in the millisecond time range of membrane electroporation of single cells using a rapid ultra-low-light intensifying detection system," *Eur. Biophys. J.*, vol. 27, pp. 291–298, 1998.
- [21] U. Zimmermann, "Electric field-mediated fusion and related electrical phenomena," *Biochimica et Biophysica Acta*, vol. 694, pp. 227–277, 1982.
- [22] H. G. Sachs, P. J. Stambrook, and J. D. Ebert, "Changes in membrane potential during the cell cycle," *Exp. Cell Res.*, vol. 83, pp. 2362–2666, 1974.
- [23] D. Miklavčič, D. Šemrov, H. Mekid, and L. M. Mir, "A validated model of *in vivo* electric field distribution in tissues for electrochemotherapy and for DNA electrotransfer for gene therapy," *Biochim. Biophys. Acta*, vol. 1519, pp. 73–83, 2000.
- [24] M. Hibino, M. Shigemori, H. Itoh, K. Nagayama, and K. Kinoshita, Jr., "Membrane conductance of an electroporated cell analyzed by submicrosecond imaging of transmembrane potential," *Biophys. J.*, vol. 59, pp. 209–220, 1991.
- [25] J. Tessie and M. Rols, "An experimental evaluation of the critical potential difference inducing cell membrane electroporation," *Biophys. J.*, vol. 65, pp. 409–413, 1993.
- [26] R. K. Jain, "Barriers to drug delivery in solid tumors," *Scientif. Amer.*, pp. 42–49, July 1994.
- [27] A. C. Guyton and J. E. Hall, *Textbook of Medical Physiology—Ninth Edition. Unit IV—The Circulation & Unit V—The Kidneys and Body Fluids*. Philadelphia, PA: Saunders, 1996.
- [28] I. F. Tannock and R. P. Hill, *The Basic Science of Oncology—Third Edition*. New York: McGraw-Hill, 1998.
- [29] J. C. Maxwell, *Treatise on Electricity and Magnetism*. London, U.K.: Oxford Univ. Press, 1873.
- [30] V. H. Pauly and H. P. Schwan, "Über die Impedanz einer Suspension von kugelförmigen teilchen mit einer Schale," *Z. Naturforschg.*, vol. 14b, pp. 125–131, 1959.



**Mojca Pavlin** was born in 1973 in Ljubljana, Slovenia. She received the B.Sc. degree in physics from the University of Ljubljana, Faculty of Mathematics and Physics in 1998 and the M.Sc. degree from the Faculty of Electrical Engineering in 2001. She is working towards the Ph.D. degree in electrical engineering at the University of Ljubljana.

Her main research interests lie in the field of biophysics, especially in the analysis of the interactions of the electric fields and many cells systems including numerical modeling and experimental work on cells.



**Nataša Pavšelj** was born in 1974 in Ljubljana, Slovenia. She received the B.Sc. degree in electrical engineering from the University of Ljubljana, Faculty of Electrical Engineering in 1999 and is currently a researcher working towards the M.Sc. degree at the Faculty of Electrical Engineering.

Her main research interests lie in the field of electroporation, including numerical modeling of electric field distribution in different biological tissue setups and cell systems, and comparison of the theoretical results with the experimental work.



**Damijan Miklavčič** was born in 1963 in Ljubljana, Slovenia. He received the M.Sc. and Ph.D. degrees in electrical engineering from University of Ljubljana.

Since 1997, he is an Associate Professor at Faculty of Electrical Engineering, University of Ljubljana, and the Head of Laboratory of Biocybernetics. He works in the field of biomedical engineering. His interest in the last years focuses on electroporation assisted drug delivery, including cancer treatment by means of electrochemotherapy, tissue oxygenation, and modeling.

## PAPER 2

### Electric Properties of Tissues

**Damijan Miklavčič, Nataša Pavšelj and Francis X. Hart**

**Chapter in press:** The Encyclopedia of Biomedical Engineering, John Wiley & Sons, Inc., 2006

**Introduction:** The electrical properties of biological tissues and cell suspensions have been of interest for over a century for many reasons. They determine the pathways of current flow through the body and, thus, are very important in the analysis of a wide range of biomedical applications such as functional electrical stimulation and the diagnosis and treatment of various physiological conditions with weak electric currents, radio-frequency hyperthermia, electrocardiography, and body composition. On a more fundamental level, knowledge of these electrical properties can lead to an understanding of the underlying basic biological processes. Indeed, biological impedance studies have long been important in electrophysiology and biophysics; one of the first demonstrations of the existence of the cell membrane was based on dielectric studies on cell suspensions. To analyze the response of a tissue to electric stimulation, we need data on the specific conductivities and relative permittivities of the tissues or organs. A microscopic description of the response is complicated by the variety of cell shapes and their distribution inside the tissue as well as the different properties of the extracellular media. Therefore, a macroscopic approach is most often used to characterize field distributions in biological systems. Moreover, even on a macroscopic level, the electrical properties are complicated. They can depend on the tissue orientation relative to the applied field (directional anisotropy), the frequency of the applied field (the tissue is neither a perfect dielectric nor a perfect conductor), or they can be time- and space-dependent (e.g., changes in tissue conductivity during electropermeabilization).



## ELECTRIC PROPERTIES OF TISSUES

DAMIJAN MIKLAVČIČ  
 NATAŠA PAVŠELJ  
 FRANCIS X. HART  
 University of Ljubljana  
 Ljubljana, Slovenia

### 1. INTRODUCTION

The electrical properties of biological tissues and cell suspensions have been of interest for over a century for many reasons. They determine the pathways of current flow through the body and, thus, are very important in the analysis of a wide range of biomedical applications such as functional electrical stimulation and the diagnosis and treatment of various physiological conditions with weak electric currents, radio-frequency hyperthermia, electrocardiography, and body composition. On a more fundamental level, knowledge of these electrical properties can lead to an understanding of the underlying basic biological processes. Indeed, biological impedance studies have long been important in electrophysiology and biophysics; one of the first demonstrations of the existence of the cell membrane was based on dielectric studies on cell suspensions (1).

To analyze the response of a tissue to electric stimulation, we need data on the specific conductivities and relative permittivities of the tissues or organs. A microscopic description of the response is complicated by the variety of cell shapes and their distribution inside the tissue as well as the different properties of the extracellular media. Therefore, a macroscopic approach is most often used to characterize field distributions in biological systems. Moreover, even on a macroscopic level, the electrical properties are complicated. They can depend on the tissue orientation relative to the applied field (directional anisotropy), the frequency of the applied field (the tissue is neither a perfect dielectric nor a perfect conductor), or they can be time- and space-dependent (e.g., changes in tissue conductivity during electropermeabilization).

### 2. BIOLOGICAL MATERIALS IN AN ELECTRIC FIELD

The electrical properties of any material, including biological tissue, can be broadly separated into two categories: conducting and insulating. In a conductor, the electric charges move freely in response to the application of an electric field, whereas in an insulator (dielectric), the charges are fixed and not free to move. A more detailed discussion of the fundamental processes underlying the electrical properties of tissue can be found in Foster and Schwan (2).

If a conductor is placed in an electric field, charges will move within the conductor until the interior field is zero. In the case of an insulator, no free charges exist, so net migration of charge does not occur. In polar materials, however, the positive and negative charge centers in the molecules do not coincide. An electric dipole moment,  $p$ , is

said to exist. An applied field,  $E_0$ , tends to orient the dipoles and produces a field inside the dielectric,  $E_p$ , which opposes the applied field. This process is called polarization. Most materials contain a combination of orientable dipoles and relatively free charges so that the electric field is reduced in any material relative to its free-space value. The net field inside the material,  $E$ , is then

$$E = E_0 - E_p. \quad (1)$$

The net field is lowered by a significant amount relative to the applied field if the material is an insulator and is essentially zero for a good conductor. This reduction is characterized by a factor  $\epsilon_r$ , which is called the relative permittivity or dielectric constant, according to

$$E = \frac{E_0}{\epsilon_r}. \quad (2)$$

In practice, most materials, including biological tissue, actually display some characteristics of both insulators and conductors because they contain dipoles as well as charges that can move, but in a restricted manner. For materials that are heterogeneous in structure, charges may become trapped at interfaces. As positive and negative ions move in opposite directions under the applied field, internal charge separations can then result within the material, producing an effective internal polarization that acts like a very large dipole.

On a macroscopic level, we describe the material as having a permittivity,  $\epsilon$ , and a conductivity,  $\sigma$ . The permittivity characterizes the material's ability to trap or store charge or to rotate molecular dipoles, whereas the conductivity describes its ability to transport charge (3). The permittivity also helps to determine the speed of light in a material so that free space has a permittivity  $\epsilon_0 = 8.85 \times 10^{-12}$  F/m. For other media,

$$\epsilon = \epsilon_r \epsilon_0. \quad (3)$$

The energy stored per unit volume in a material,  $u$ , is

$$u = \frac{\epsilon E^2}{2}, \quad (4)$$

and the power dissipated per unit volume,  $p$ , is

$$p = \frac{\sigma E^2}{2}. \quad (5)$$

We can represent these tendencies by using a circuit model to describe the tissue (1,4). Consider a sample of material that has a thickness,  $d$ , and cross-sectional area,  $A$ . If the material is an insulator, then we treat the sample as a capacitor with capacitance

$$C = \epsilon \cdot A/d. \quad (6)$$

If it is a conductor, then we treat it as a conductor with

## 2 ELECTRIC PROPERTIES OF TISSUES

conductance

$$G = \sigma \cdot A/d. \quad (7)$$

A simple model for a real material, such as tissue, would be a parallel combination of the capacitor and conductor. Such a model is referred to as “Debye-type.” Other, more complicated models are sometimes used, as will be described later. If a constant (dc) voltage  $V$  is applied across this parallel combination, then a conduction current  $I_C = GV$  will flow and an amount of charge  $Q = CV$  will be stored.

Suppose, instead, that an alternating (ac) voltage were applied to the combination:

$$V(t) = V_0 \cos(\omega t). \quad (8)$$

Here,  $V_0$  is the amplitude of the voltage and  $\omega = 2\pi f$ , where  $f$  is the frequency of the applied signal. The charge on the capacitor plates now is changing with frequency  $f$ . This change is associated with a flow of charge or current in the circuit. We characterize this flow as a displacement current:

$$I_d = dQ/dt = -\omega CV_0 \sin(\omega t). \quad (9)$$

The total current flowing through the material is the sum of the conduction and displacement currents, which are 90 degrees apart in phase because of the difference in the trigonometric functions. This phase difference can be expressed conveniently by writing

$$V(t) = V_0 e^{i\omega t}, \quad \text{where } i = \sqrt{-1} \quad (10)$$

and taking its real part for physical significance. The total current is  $I = I_c + I_d$ , hence

$$I = GV + C \cdot dV/dt = (\sigma + i\omega\epsilon)A \cdot V/d. \quad (11)$$

The actual material, then, can be characterized as having an admittance,  $Y^*$ , given by

$$Y^* = G + i\omega C = (A/d)(\sigma + i\omega\epsilon), \quad (12)$$

where  $*$  indicates a complex-valued quantity. In terms of material properties, we define a corresponding, complex-valued conductivity

$$\sigma^* = (\sigma + i\omega\epsilon). \quad (13)$$

Describing a material in terms of its admittance emphasizes its ability to transport current. Alternatively, we could emphasize its ability to restrict the flow of current by considering its impedance,  $Z^* = 1/Y^*$ , or, for a pure conductance, its resistance,  $R = 1/G$ .

Factoring  $i\omega\epsilon_0$  in Equation 11 yields

$$I = (\epsilon_r - i\sigma/\omega\epsilon_0)i\omega\epsilon_0 A/d = C \frac{dV}{dt}. \quad (14)$$

We can define a complex-valued, relative permittivity

$$\epsilon^* = \epsilon_r - \frac{i\sigma}{\omega\epsilon_0} = \epsilon'_r - i\epsilon''_r, \quad (15)$$

with  $\epsilon'_r = \epsilon_r$  and  $\epsilon''_r = \sigma/(\omega\epsilon_0)$ . The complex conductivity and complex permittivity are related by

$$\sigma^* = i\omega\epsilon^* = i\omega\epsilon_0\epsilon_r^*. \quad (16)$$

In physical terms, we can regard the conductivity of a material as a measure of the ability of its charge to be transported throughout its volume by an applied electric field. Similarly, its permittivity is a measure of the ability of its dipoles to rotate or its charge to be stored by an applied external field. Note that if the permittivity and conductivity of the material are constant, the displacement current will increase with frequency whereas the conduction current does not change. At low frequencies, the material will behave like a conductor, but capacitive effects will become more important at higher frequencies. For most materials, however, these material properties are not constant, but vary with the frequency of the applied signal.  $\sigma^*$  and  $\epsilon^*$  are frequency-dependent. Such a variation is called dispersion. Biological tissues exhibit several different dispersions over a wide range of frequencies.

Dispersions can be understood in terms of the orientation of the dipoles and the motion of the charge carriers. At relatively low frequencies, it is relatively easy for the dipoles to orient in response to the change in the applied field, whereas the charge carriers travel larger distances over which a greater opportunity exists for trapping at a defect or interface. The permittivity is relatively high and the conductivity is relatively low. As the frequency increases, the dipoles are less able to follow the changes in the applied field, and the corresponding polarization disappears. In contrast, the charge carriers sample shorter distances during each half-cycle and are less likely to be trapped. As frequency increases, the permittivity decreases and, because trapping becomes less important, the conductivity increases (4,5). The dispersion can be characterized by an angular relaxation frequency  $\omega_r = 2\pi f_r$  or, equivalently, by a relaxation time  $T_r = 1/f_r$ .

In a heterogeneous material, such as biological tissue, several dispersions are observed as illustrated in Fig. 1 (4), which shows the variation with frequency of the complex permittivity of Equation 15. For frequencies below about 10 kHz, the  $\alpha$  dispersion is caused by counterion polarization along cell membranes. The extremely high values of permittivity reflect the trapping of charges at internal interfaces and are not related to dipole orientation. Note that even at the lowest frequencies a residual or dc conductivity  $\sigma_0$  exists. The dispersion in the MHz frequency range originates in interfacial polarization of cell membranes, which act as a barrier for passive ion transport between the inner and the outer cell media. Basically, the membrane can be modeled as a parallel combination of a capacitor and a resistor. This so-called beta dispersion occurs in the frequency range where the reactance of the membrane capacitance short-circuits the membrane re-

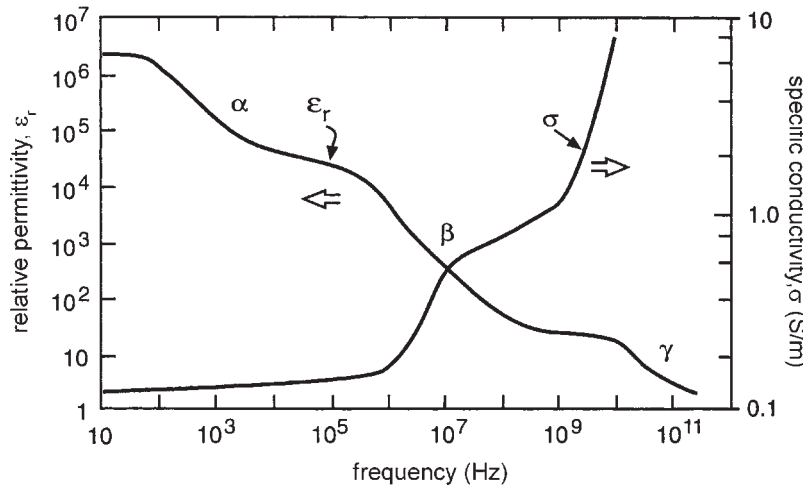


**Figure 1.** Typical frequency dependence of the complex permittivity of a heterogeneous material such as biological tissues (4).

sistance, so that the external electric field begins to penetrate into the cell interior. Additional contributions to this  $\beta$  dispersion can develop because of the polarization of proteins and other organic macromolecules. In the GHz range ( $10^9$  Hz),  $\gamma$  dispersion is caused by the polarization of water molecules.

The relative importance of the permittivity and conductivity in determining the electrical properties of the tissue can be compared by taking the ratio of the displacement and conduction currents;  $I_d/I_c = \omega\epsilon/\sigma$ . For frequencies below the MHz range, this ratio is very low, even with the large increase in permittivity of  $\alpha$  dispersion. Hence, at low frequencies, biological tissue is essentially conductive in nature.

For a Debye-type response, which corresponds to parallel RC elements, dispersion can be represented as

$$\epsilon_r^* = \epsilon_\infty + \frac{(\epsilon_S - \epsilon_\infty)}{(1 - i\omega\tau)} - i\sigma_0/\omega\epsilon_0 \quad (17)$$

and

$$\sigma^* = \sigma_\infty + \frac{(\sigma_0 - \sigma_\infty)}{(1 - i\omega\tau)}, \quad (18)$$

where the time constant,  $\tau = 1/RC$ .  $\epsilon_\infty$  and  $\epsilon_S$  refer, respectively, to the relative permittivities at frequencies well above and well below the dispersion.  $\sigma_\infty$  and  $\sigma_0$  refer, respectively, to the conductivities at frequencies well above and well below the dispersion.

The complexity of the dispersions illustrated in Fig. 1, however, cannot be readily described by three successive, simple Debye relaxations. The widths of the dispersions, in particular, are greater than predicted for simple RC parallel elements. A similar situation occurs for most materials. Therefore, in place of a simple RC element, a more general, empirical relation, the Cole–Cole response, is used in which

$$\epsilon_r^* = \epsilon_\infty + \frac{(\epsilon_S - \epsilon_\infty)}{(1 - (i\omega\tau)^\alpha)} - i\sigma_0/\omega\epsilon_0 \quad (19)$$

and

$$\sigma^* = \sigma_\infty + \frac{(\sigma_0 - \sigma_\infty)}{(1 - (i\omega\tau)^\alpha)}, \quad (20)$$

where  $\alpha$  is a parameter that depends on the nature of the material.  $\alpha$  is equal to 1 for a Debye-type dispersion and becomes smaller as the width of the dispersion increases.

Two physical interpretations exist for  $\alpha$ . Some researchers regard a wide dispersion as an indication of numerous Debye-type dispersions with a distribution of simple relaxation times. Other researchers regard the spread as an indication that the fundamental charge-transport and dipole-reorientation processes are essentially cooperative in nature and that, as the degree of cooperation increases,  $\alpha$  becomes smaller than 1.

The representation of the dispersion in a circuit model can then be achieved in two ways. First, several Debye-type RC elements connected in series could be used to represent the single, broad dispersion. This process is unwieldy. Second, and more commonly, the circuit model is generalized by the introduction of a “Constant Phase Element” (CPE) with a complex-valued impedance given by

$$Z_{CPE}^* = A(i\omega)^{-n}, \quad (21)$$

where  $A$  is a parameter and  $n = \alpha$ . This CPE impedance reduces to a simple resistance for  $n = 0$  and to a capacitive reactance for  $n = 1$ . For a diffusive process,  $n = 0.5$ . The Cole–Cole dispersion can be represented in circuit terms as the parallel combination of a resistor and a CPE. Other dispersions, such as Cole–Davidson and Havriliak–Negami, differ somewhat from Equations 19 and 20 and are used for many materials. However, the Cole–Cole model is generally used for biological materials.

### 3. COMPLICATIONS IN DIELECTRIC MEASUREMENTS OF TISSUES

The measurement of tissue dielectric properties can be complicated because of several factors, such as tissue inhomogeneity, anisotropy, the physiological state of the tis-

#### 4 ELECTRIC PROPERTIES OF TISSUES

sue, and electrode polarization. Therefore, caution must be used in the design of the measurement procedure.

##### 3.1. Inhomogeneity of Tissues

Tissue is a very inhomogeneous material. The cell itself is comprised of an insulating membrane enclosing a conductive cytosol. A suspension of cells can be regarded at low frequencies simply as insulating inclusions in a conducting fluid. The insulation is provided by the cell membrane. At frequencies in the MHz range, capacitive coupling across this membrane becomes more important. Beginning in this range, the dispersive properties of the membrane and ultimately the cytosol must also be considered. For a thorough discussion of how the dielectric properties of cell suspensions vary with frequency, see Kotnik and Miklavcic (6,7) and Pavlin et al. (8).

In tissue, the cells are surrounded by an extracellular matrix, which can be extensive, as in the case of bone, or minimal, as in the case of epithelial tissue. Tissue does not contain cells of a single size and function. For example, bone contains osteoblasts, osteocytes, and osteoclasts embedded in a collagen/hydroxyapatite matrix as well as bone marrow with stroma cells (9). The tissue is perfused with blood and linked to the central nervous system by neurons. It is thus difficult to extrapolate from the dielectric properties of a cell suspension to those of an intact tissue.

A large discrepancy exists between various data on electrical properties of biological materials found in the literature. Why is there such a wide range of values obtained by different researchers? Excised samples carry along with them various amounts of body fluids, and the lack of standardization of measurement techniques presents its own difficulties and probably widens the range of resistivity values. Moreover, there are seasonal, age, and disease-linked changes as well as those that accompany the physiological function of various biologic materials (10).

##### 3.2. Anisotropy of Tissues

Some biological materials, such as bone and skeletal muscle, are distinctly anisotropic. Therefore, when referring to published conductivity and permittivity values, we need to check the orientation of the electrodes relative to the major axis of the tissue (e.g., longitudinal, transversal, or a combination of both).

Electrical anisotropy is often related to the physiological demands made on the tissue. Major bones and muscles of limbs are designed to produce and support significant longitudinal forces. For example, muscles are composed of fibers that are very large individual cells and are aligned in the direction of muscle contraction. Electrical conduction along the length of the fiber is thus significantly easier than conduction between the fibers in the extracellular matrix because the extracellular matrix is less conductive than the cell. Therefore, muscle tissue manifests typical anisotropic electric properties (4). The longitudinal conductivity is significantly higher than the transverse conductivity even when path differences in the charge transport are taken into account, especially in the low-

frequency range (11). A similar anisotropy exists in the long bones of the body where charge transport is easier along the longitudinal axis than transverse to it.

Moreover, tissue anisotropy is frequency-dependent. Namely, if the frequency of the current is high enough, the anisotropic properties disappear (specifically for muscle tissue, that happens in the MHz frequency range). At higher frequencies, charge movement takes place over shorter distances so large-scale structures become less important and capacitive coupling across membranes becomes more important.

A practical problem occurs when measuring the electrical properties of anisotropic materials: how to accurately align the applied electric field and tissue fibers (12). Namely, it has been shown that perfect alignment is crucial for obtaining accurate longitudinal and transverse values. A study on skeletal muscle tissue shows (13) that a 5 degree misalignment from true perpendicular or parallel orientations would result in an 18% overestimate in the perpendicular direction and a 0.4% underestimate in the parallel direction when measuring specific conductivity.

##### 3.3. Physiological Factors and Changes of Tissue

Any changes in tissue physiology should produce changes in the tissue electrical properties (14). This principle has been used to identify or monitor the presence of various illnesses or conditions such as body fluid shift, blood flow, cardiac output, and muscular dystrophy (15) by various impedance diagnostic techniques, such as impedance plethysmography, rheoencephalography, and thoracic impedance cardiograph. For a detailed discussion of the applications of bioimpedance methods in medicine and biotechnology, see (16,17).

Tumors generally have higher water content than normal cells because of cellular necrosis but also irregular and fenestrated vascularization. In addition, differences may exist in the membrane structure. Although an increased conductivity may be used to identify the presence of tumors (18), parameters associated with the fitting of the overall dielectric spectrum to a circuit model may be more reliable (19). In clinical practice, the presence of skin may complicate the interpretation of impedance changes in tissue, such as the breast (20). The higher conductivity of tumors in the MHz frequency range could lead to their selective targeting by radio-frequency hyperthermia treatment (21).

Fat is a poorer conductor of electricity than water. Changes in the percentage of body fat or water are reflected in tissue impedance changes. For example, Biggs et al. (22) estimated the whole-body fat percentage by measurement of the resistivity of the upper arm and leg at 50 kHz. Van Kreel et al. (23) determined the total body water content by measurement of body impedance at several frequencies. This method can even be applied to individual organs. For example, Schaefer et al. (24) correlated the complex permittivity of heart tissue with the level of ischemia.

In an extreme case, one can imagine that tissue death or excision would result in significant changes in electrical properties. Tissue metabolism decreases after the tissue

has been excised and, often, the temperature falls. If the tissue is supported by temperature maintenance and perfusion systems, the tissue may be stabilized for a limited period of time in a living state *in vitro* (*ex vivo*). If the tissue is not supported, however, irreversible changes will occur, followed by cell and tissue death (3). If the blood flow is interrupted, metabolism continues, but in an anaerobic way. Osmosis will cause cell swelling and tissue damage. As a consequence, the extracellular pathways narrow, which typically leads to an increase in the low-frequency impedance ( $< 10$  kHz). The time of occurrence of these phenomena is different for different tissues. Decreased blood flow also accounts for changes in tissue resistivity, because blood is a good conductor (12).

Conductivity changes caused by cell and tissue death have been studied by different researchers (10,12,25). The results show that in the first hour after the tissue sample has been excised, the specific conductivity is almost constant, although the change depends on the tissue type. Liver tissue shows changes after only 30 minutes from excision, brain tissue after one hour, and the muscle tissue two hours after excision. In all cases, the conductivity increases with time (10). Changes in the frequency range above 100 Hz are lower and take a longer time to occur. However, because tissue impedance at low frequencies is almost entirely ohmic, permittivity errors do not play any major role. For these reasons, considerable caution must be taken in the interpretation of electrical measurements that were performed on excised tissues.

The electrical properties of tissue also depend on its temperature. The mobility of the ions that transport the current increases with the temperature as the viscosity of the extracellular fluid decreases. A general increase of about  $2\%/^{\circ}\text{C}$  occurs in the conductivity of tissue (2) in the frequency range below 1 GHz, up to a temperature of about  $40^{\circ}\text{C}$ . Above that point, the cell membrane begins to deteriorate and allows the cytosol to leak into the extracellular space. The rapid increase of conductivity with temperature was suggested to be used to monitor the progress of hyperthermia treatment (26).

### 3.4. Electrode Polarization

The measurement of tissue electrical properties, *in vivo*, is complicated (12). Two main sources of systematic error exist, electrode polarization and lead inductance, which become apparent at the lower and higher ends of the frequency range, respectively (27). Electrode polarization is a manifestation of molecular charge organization that occurs at the sample-electrode interface in the presence of water molecules and hydrated ions. In its simplest form, the phenomenon can be modeled as a frequency-dependent capacitor in series with a resistor. The effect increases with increasing sample conductivity, and its consequences are more pronounced on the capacitance than the conductance of ionic solutions as well as biological samples.

In a cell suspension, a counterion layer can form at each electrode. The potential drop in this layer reduces the electric field available to drive charge transport in the bulk suspension, resulting in apparently low suspension

conductivity. As the frequency increases, the counterion layer is less able to follow the changes in the applied signal, the potential drop at the suspension/electrode interface decreases, and the apparent conductivity of the suspension increases. The nature of the ions in the layer is determined by both the suspension and the material of the electrode. Hence, changing either the electrode material or the nature of the suspension will modify the magnitude and frequency response of this electrode polarization.

The process is more complicated in tissue. Insertion of electrodes can first cause the release of electrolytes from the surrounding tissue and, later, the development of a poorly conductive wound region may occur. This region can shield part of the electrode from the ionic current and thus reduce the polarization effects compared with an ionic solution equivalent in conductivity to the intracellular fluid. As with a cell suspension, the material of the electrode plays an important part in determining its polarization impedance, the relative importance of which decreases with increasing frequency. It is good practice to measure tissue impedance *in vivo* after waiting a sufficient time for the electrode polarization processes to stabilize. The waiting time will depend, in general, on the nature of the electrodes and the type of tissue. If possible, one should perform a preliminary experiment in which impedance spectra are taken every few minutes until no further changes occur in order to determine the waiting time. A typical time might be on the order of 30 minutes.

Two different electrode setups are used to measure the electric properties of biological materials; the two-electrode method and the four-electrode method (28).

**3.4.1. Two-electrode Method.** This method is suitable for alternating current measurements. We can not use it as such for direct current measurements because of the electrode polarization that consequently gives incorrect results for the conductivity of the sample between the electrodes. For alternating current measurements, the frequency range over which electrode polarization is important depends to some extent on the system being measured and the electrode material. For cell suspensions, it is important up to nearly 100 kHz, whereas for tissue measured *in vivo*, it is significant only up to about 1 kHz. By varying the separation of the electrodes (29), the contribution of the electrode polarization can be determined and eliminated.

**3.4.2. Four-electrode Method.** This method can be used for direct and alternating current measurements. Two pairs of electrodes are used: the outer current electrodes and the inner voltage electrodes. The current from the source passes through the sample. Voltage electrodes of known separation are placed in the sample between the current electrodes. By measuring the current as the voltage drop across a resistor in series with the sample and the voltage drop across the inner electrodes, one can determine the specific conductance of the sample between the inner electrodes. The advantage of this method is that the polarization on the current electrodes has no influence on the voltage difference between the voltage electrodes.

## 6 ELECTRIC PROPERTIES OF TISSUES

Polarization at the voltage electrodes is negligible for direct and alternating currents because of the high input impedance of the measurement system. Some authors recommend the two-electrode system with a polarization error correction (12). They believe the four-electrode method does not completely eliminate the polarization on voltage electrodes. Some authors report 20% higher results when measuring muscle resistance with the two-electrode technique without error correction (30).

With direct current measurements, care must be taken to use small currents to avoid electrochemical injection of ions at the electrodes and nerve stimulation if the measurements are conducted *in vivo*.

In the MHz frequency range and higher, lead inductance becomes an important factor as the inductive couplings between the leads to each other, to the measuring instruments, and to nearby metal surfaces produce extraneous voltage drops that increase with frequency. It is good practice to identify and then reduce the effects of electrode polarization at low frequencies and lead inductance at high frequencies by replacing the sample to be measured by a saline solution for which the electrical properties should not vary with frequency until the GHz frequency range.

#### 4. DIELECTRIC PROPERTIES OF SOME TISSUES

Large differences exist in electric properties of biological materials. These differences are determined, to a large extent, by the fluid content of the material. For example, blood and brain conduct electric current relatively well. Lungs, skin, fat, and bone are relatively poor conductors. Liver, spleen, and muscle are intermediate in their conductivities. An excellent, detailed review of the electrical properties of various tissues over a wide range of frequencies can be found in the series of three articles by Gabriel et al. (27,31,32). Of particular interest is their use of Cole-Cole response function, given by Equations 19 and 20, to parameterize the dielectric properties of tissue. Such parameterization allows one to calculate a reasonable estimate for the conductivity and permittivity at any frequency for different tissue types.

In the literature, we usually find data on specific conductivity and relative permittivity only at frequencies above 100 Hz. For most tissues, data below that frequency are very scarce or do not exist at all. The reason is not lack of interest, but because electrode effects can produce significant experimental errors for that frequency range. The results that have been published indicate that the impedance at frequencies under 100 Hz is almost entirely resistive and that the capacitive component accounts for only around 10% in most tissues. Between 100 Hz and 100 kHz, most tissues, with the exception of the anisotropic tissues, show almost no frequency-dependence.

We will now briefly present the electric properties of skeletal muscle, tumor, and skin and give the permittivity and specific conductivity ranges of some other tissues. The basic principles described earlier can be used to understand the differences in the electrical properties of various tissues.

##### 4.1. Skeletal Muscle

Data on skeletal muscle are the most abundant in the literature. As a result of the anisotropy of this tissue, the data are usually presented separately for the transverse and longitudinal directions, although some results with random orientation have been reported. In Figs. 2–5 we have compiled some data from the literature (13,27,28,30–34). The tissue samples were taken from different species and the measurements were made at different times after excision and with two different measurement methods (two and four-electrode technique). Therefore, the scatter of the data is rather high, especially in the low-frequency range. The anisotropy is also more pronounced in the low-frequency range. However, these differences are greater in the conductivity data than in the permittivity data, where fewer measurements are available.

##### 4.2. Tumor

A tumor is an abnormal mass of tissue surrounded by one or more normal body tissues. It has no useful function and grows at the expense of healthy tissues. As noted previously, many tumors have a significantly different electrical conductivity and permittivity from normal, surrounding tissues. This fact was attempted to be used in diagnosing tumors. For this reason, electrical impedance measuring and imaging systems are being designed and tested to screen for tumors. A study by Smith et al. (35) on tumors in liver tissue showed a significant difference in electrical properties between healthy liver tissue and tumors. Results show that tumor conductivity is 6–7.5-fold higher than liver conductivity; the difference in permittivity values is 2–5 fold. However, the dielectric properties of tumors cannot be generalized as large differences exist between different tumor types and even between tumors of the same type. Electrical properties also depend a great deal on the size or the development stage of the tumor. Namely, the tumor core can already exert tissue necrosis (35,36).

##### 4.3. Skin

Skin is a very interesting tissue because of its highly inhomogeneous structure, which thus leads to inhomogeneous dielectric properties. Generally, skin has three different layers: the epidermis, dermis, and subcutaneous tissue. The epidermis is the outer layer of skin. The thickness of the epidermis varies in different types of skin. It is the thinnest on the eyelids at 0.05 mm and the thickest on the palms and soles at 1.5 mm (3). The epidermis contains different layers, but the one that defines its dielectric properties the most is the outermost layer, the stratum corneum. That layer is composed of dead, flat skin cells that shed about every two weeks. Although it is very thin (typically around 20  $\mu\text{m}$ ), it contributes a great deal to the dielectric properties of the skin. Its high resistivity makes skin one of the most resistive tissues in the human body. Its main function is protection of the body from the external environmental factors. The lower-lying layers, hence the rest of the epidermis (important in the immune response), the dermis (which gives firmness and elasticity),

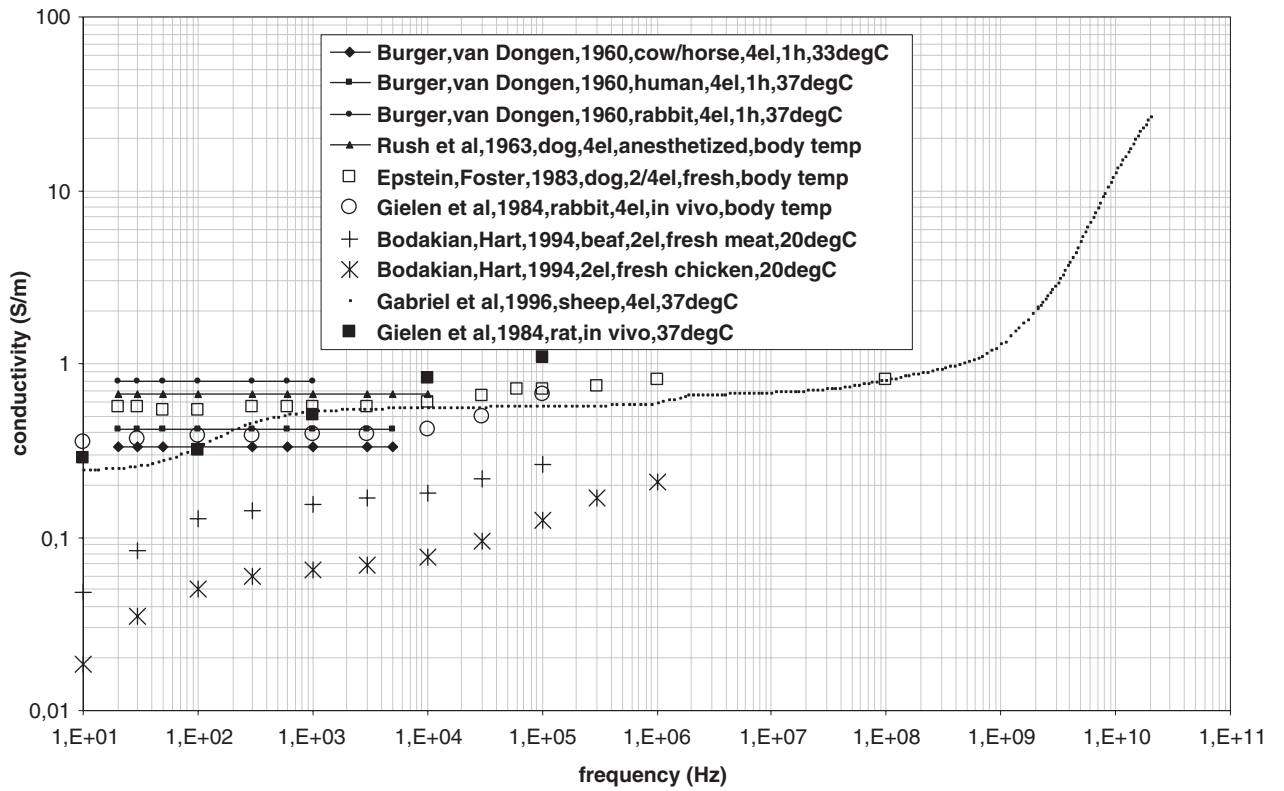


Figure 2. Specific conductivity for skeletal muscle, longitudinal direction.

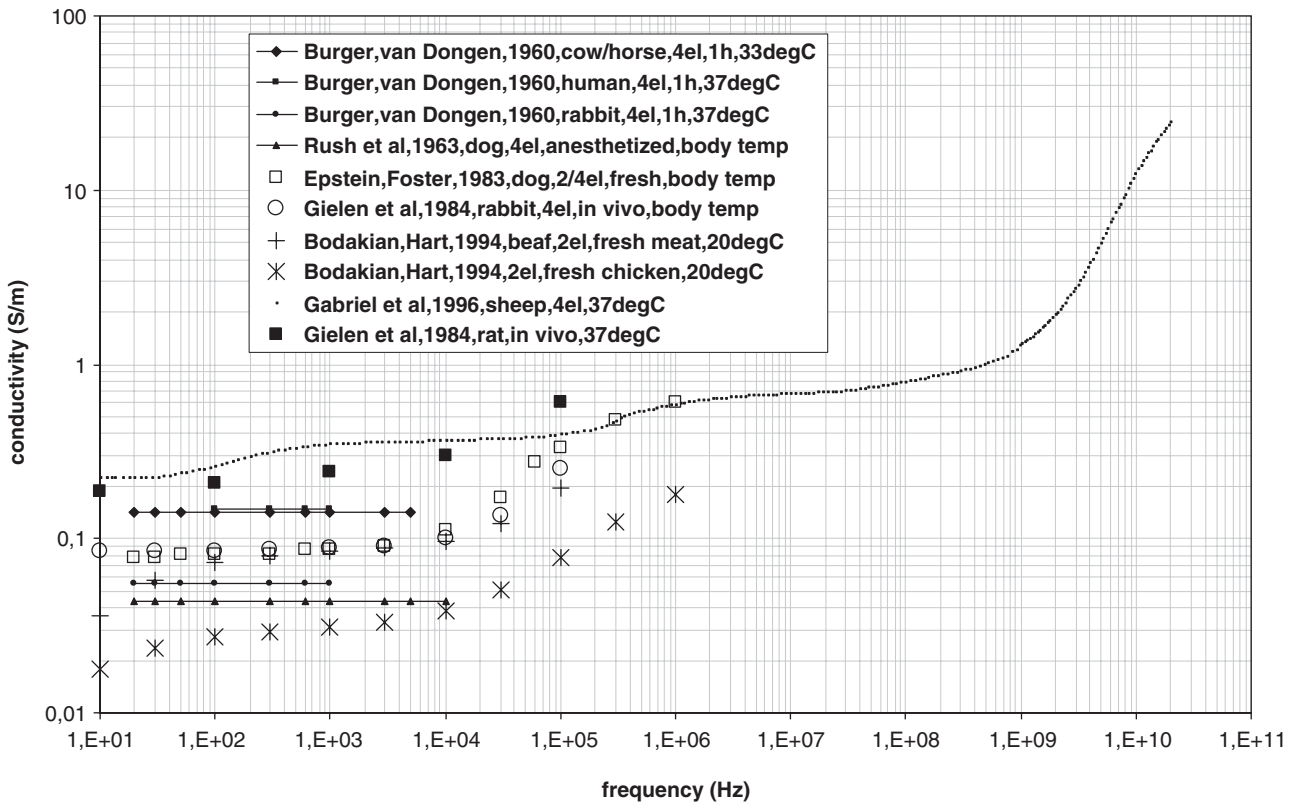


Figure 3. Specific conductivity for skeletal muscle, transverse direction.

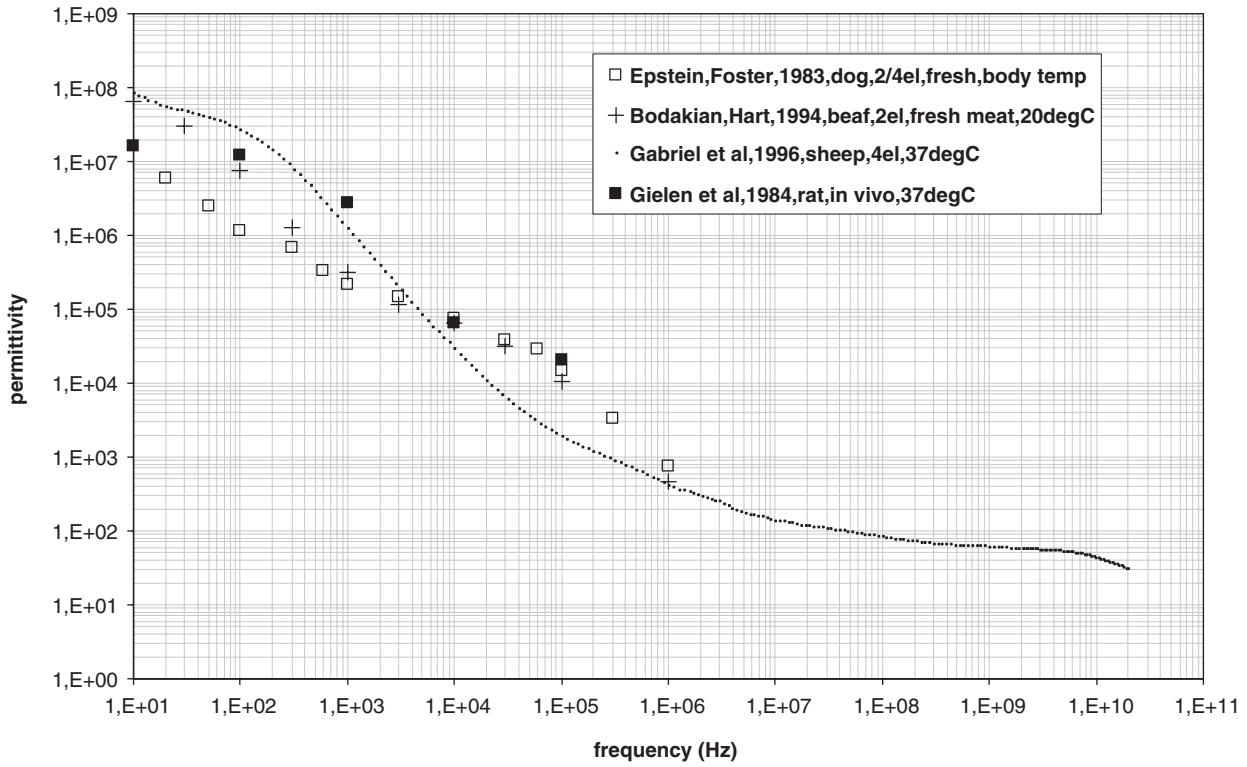


Figure 4. Relative permittivity for skeletal muscle, longitudinal direction.

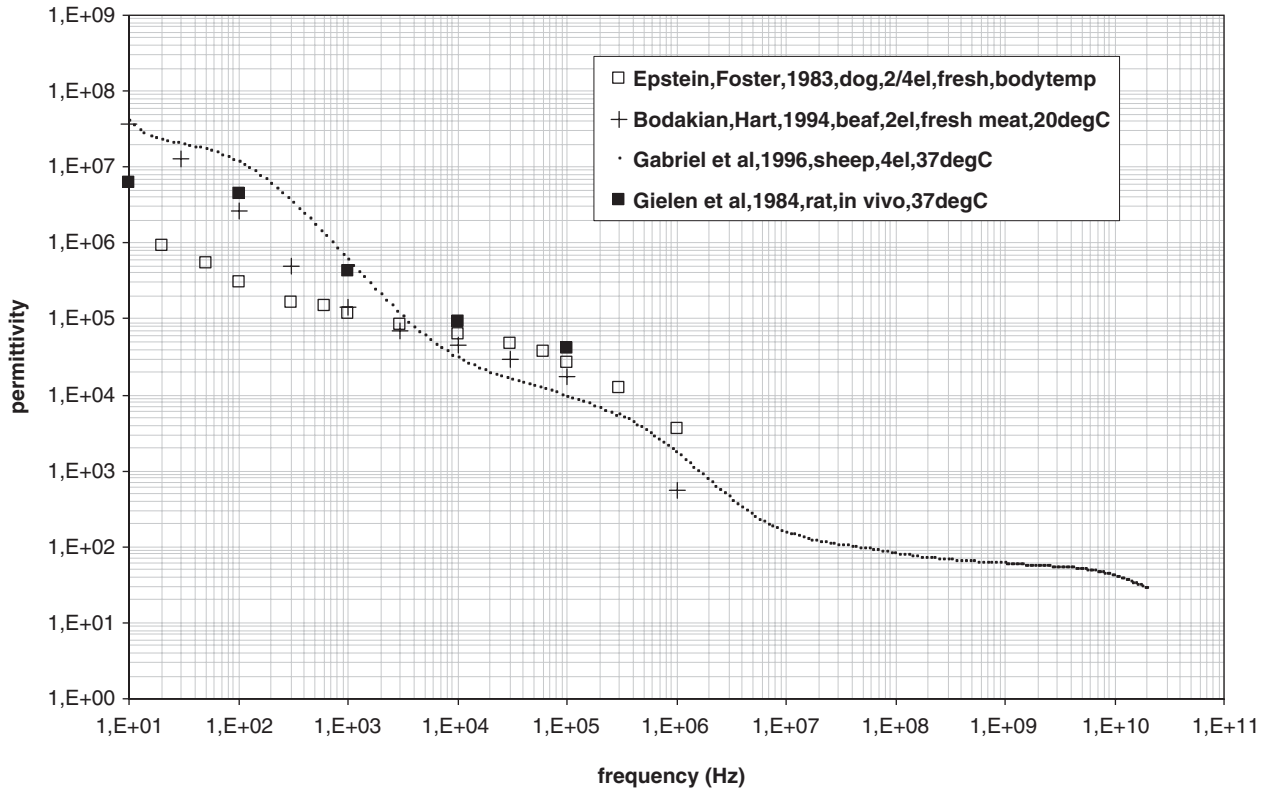


Figure 5. Relative permittivity for skeletal muscle, transverse direction.

and the subcutaneous tissue (fat, connective tissue, larger blood vessels, and nerves), all have much lower resistivities.

Especially in the low-frequency range (under 10 kHz), the impedance of skin is dominated by the stratum corneum even though this layer is very thin. Studies show that, for frequencies under 10 kHz, the share of stratum corneum in the total impedance of skin is around 50% (37), but at 100 kHz drops to around 10% (38).

In Figs. 6 and 7, we can see the specific conductivity and relative permittivity, respectively, of intact skin whose dielectric properties are dominated by stratum corneum (diamonds) and lower-lying layers of skin (boxes) (39,40). The measurements were made first on intact skin. The stratum corneum was then removed by cellulose adhesive tape stripping, and the measurements were repeated.

#### 4.4. Dielectric Properties Data Ranges of Some Body Tissues

See Table 1 for data ranges of some body tissues.

### 5. USES OF BIOIMPEDANCE MEASUREMENTS

Today, bioimpedance measurements provide an important method for the noninvasive investigation of tissue structure and properties or for monitoring physiological change (i.e., “static” or “dynamic” human organism properties). One of the main problems one encounters using bioimpedance measurements is still the reliability of the results. The scatter of the data for the electrical parameters of tissue in Figs. 2–7 illustrates the problem of measurement reproducibility. Some of the scatter may result from

problems in measuring technique, such as electrode polarization, but some may simply be caused by the individual variability among samples. At present, the relative importance of these two factors in determining the overall scatter is not clear. This scatter makes it difficult to establish criteria of normality or reference value for particular measurement results. However, in spite of the large differences between reported data on dielectric properties of different tissues, we can still find some very useful applications based on the measurements of the differences or changes in the specific conductivity or relative permittivity.

As noted previously, tumor diagnosis is one of the important applications of the measurements of bulk electrical properties of tumors and the surrounding tissues (35). Comparing dielectric properties of tumor and healthy surrounding tissues, one notices that a tumor has a much higher specific conductivity. The tumor tissue is more conductive at low frequencies because of its smaller volume fraction of intact cells, and at high frequencies because of its higher water content and its irregular and fenestrated vascularization. As stated above, the dielectric properties of the tumor and normal tissue appear to be distinctly different, by factors of 6–7.5 in the conductivity and 2–5 in the permittivity. Pronounced differences in the bulk electrical properties of a tumor and the surrounding normal tissue, if consistently present, could lead to a variety of clinical applications. Moreover, because we only need to measure the dielectric properties of tumors relative to normal surrounding tissue, the exact values for both are not critical.

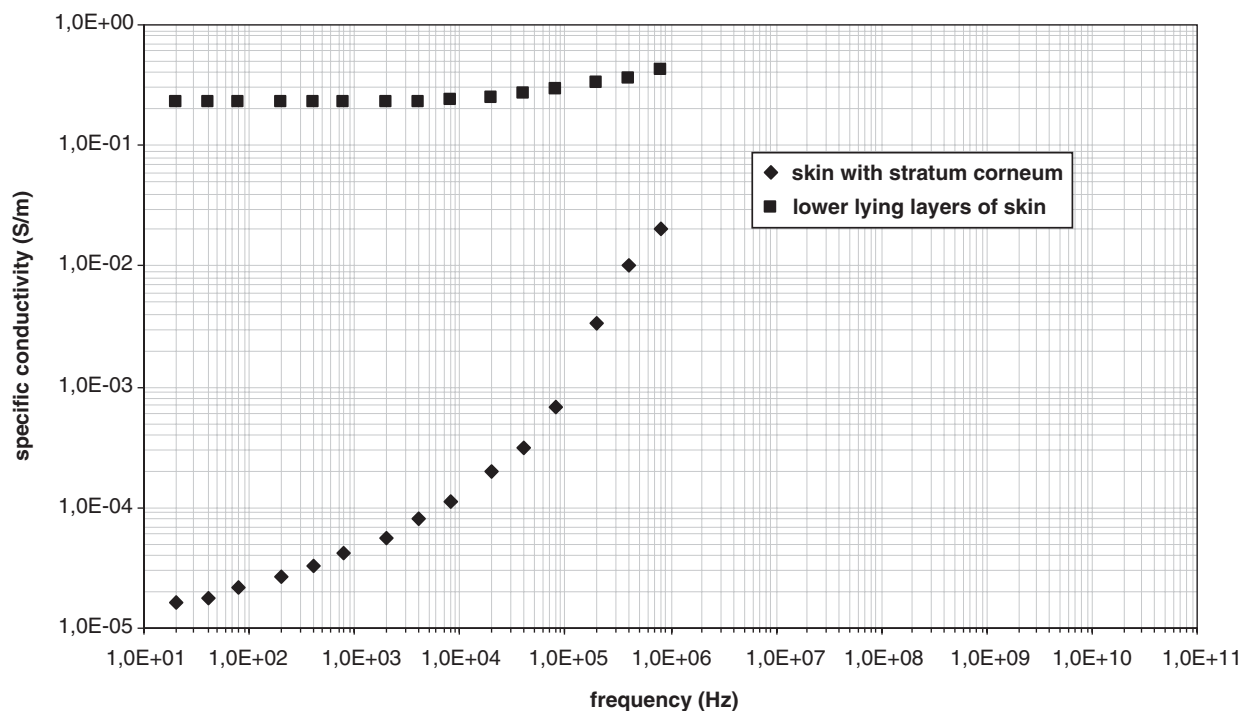


**Figure 6.** Specific conductivity of intact skin with dominating stratum corneum (diamonds) and lower-lying layers of skin alone (boxes).

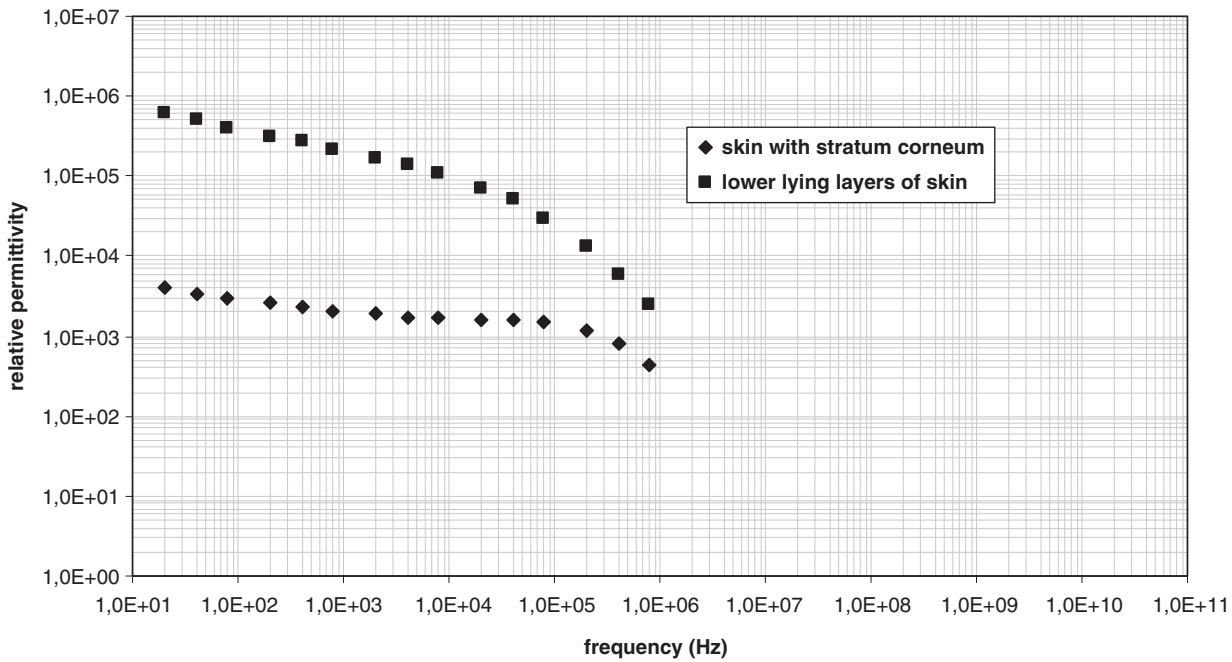


**Figure 7.** Relative permittivity of intact skin with dominating stratum corneum (diamonds) and lower-lying layers of skin alone (boxes).

**Table 1. Data Ranges of Specific Conductivities and Relative Permittivities of Some Other Tissues in the Low-Frequency Range 10,12,13,27,28,30,32–36,39–44**

	Spec. Conductivity (S/m)	Rel. Permittivity
Tumor	0.22–0.4	60 000 (at 1 kHz)
Fat	0.02–0.04	10 000 000 (at 10 Hz)
Muscle		
Transversal	0.04–0.14	1 500 000–40 000 000 (at 10 Hz)
Longitudinal	0.3–0.8	10 000 000–66 000 000 (at 10 Hz)
Skin (dry)	0.00002–0.0002	1400–6600 (at 10 Hz)
Stratum corneum	0.0000125	10 000 (at 2 Hz)
Lower-lying layers	0.227	1 200 000 (at 2 Hz)
Bone	0.01–0.06	40000–1 000 000 (d.c.)
Blood	0.43–0.7	3000 (at 1 kHz)
Heart	0.06–0.4	7 000 000–20 000 000 (d.c.)
Kidney	0.6	30 000 000 (d.c.)
Liver	0.023–0.2	15 000 000–50 000 000 (d.c.)
Lung (inflated)	0.024–0.09	10 000 000 (d.c.)
Spleen	0.043	45 000 000 (d.c.)
Gray matter	0.033	50 000 000 (d.c.)
White matter	0.023	30 000 000 (d.c.)

Specific conductivities are given for direct current measurements (0 Hz); measuring frequencies for relative permittivities are stated in brackets.

Another application is monitoring of the changes in conductivity of the tissue during the process of the electroporation (45–48). To effectively use electroporation in clinical applications, we need to detect whether the target tissue area has been permeabilized. This feedback could then be used to adjust the electroporation parameters during the treatment to make it more efficient. As the specific conductivity of tissue increases when permeabilized, its measurement can be used as an indicator of the level of the electroporation in the tissue. Again,

we are only dealing with relative changes in tissue dielectric properties before and after tissue electroporation and not the exact absolute values. A feasibility study for electrical impedance tomography as a means to monitor tissue electroporation has been made (49). In this preliminary demonstration, the electroporated regions in liver were clearly distinguishable. However, more work needs to be done to bring this technique to clinical practice.

Electrical impedance tomography may also be used for other *in vivo* applications such as cryosurgery (50). Cryosurgery is a surgical procedure that destroys tissue by freezing it with a cryogen-cooled surgical probe that is in contact with the targeted tissue. However, although the extent of freezing can be monitored with an array of imaging techniques, the effective application of cryosurgery is still hampered by the fact that the extent of freezing does not necessarily correspond to the extent of tissue destruction. Substantial changes in tissue electrical properties caused by tissue destruction can be monitored by means of electrical impedance tomography in order to evaluate the effectiveness of the procedure.

A more commercially orientated application is measurement of the dielectric properties of meat products that could serve as a monitoring tool of their storage and preparation history (34). Dielectric properties of beef and chicken were measured on commercially purchased fresh meat, as well as thawed and cooked meat. The results show that the anisotropy of skeletal muscle is lower in the commercially purchased samples. In addition, the conductivity values are much higher for the commercial samples, particularly at low frequencies. Further changes are produced by freezing and cooking, which indicates that dielectric spectroscopy can be used to determine the storage/preparation history of meat products.

With bioimpedance measurements, it is also possible to estimate the ratio of muscle to fat mass because fat has lower conductivity than muscle tissue (3). The intention is often to determine total body water, extracellular/intracellular fluid balance, muscle mass, and fat mass. Application areas are as diverse as sports medicine, nutritional assessment, and fluid balance in renal dialysis and transplantation. Other applications of the theories of measuring electric properties of biomaterials, ranging from diagnostic to therapeutic applications or laboratory procedures, can be found in the literature (3,16,17).

## BIBLIOGRAPHY

1. K. R. Foster and H. P. Schwan, Dielectric properties of tissues. In: C. Polk and E. Postow, eds., *Handbook of Biological Effects of Electromagnetic Fields*. New York: CRC Press, 1996.
2. K. R. Foster and H. P. Schwan, Dielectric properties of tissues and biological materials: a critical review. *Crit. Rev. Biomed. Eng.* 1989; **17**:25-104.
3. S. Grimnes and O. G. Martinsen, *Bioimpedance & Bioelectricity Basics*. San Diego, CA: Academic Press, 2000.
4. J. P. Reilly, Applied Bioelectricity, *From Electrical Stimulation to Electropathology*. New York: Springer-Verlag, 1998.
5. R. Pethig, *Dielectric and Electronic Properties of Biological Material*. New York: Wiley, 1979.
6. T. Kotnik and D. Miklavcic, Second-order model of membrane electric field induced by alternating external electric fields. *IEEE Trans. Biomed. Eng.* 2000; **47**:1074-1081.
7. T. Kotnik and D. Miklavcic, Theoretical evaluation of the distributed power dissipation in biological cells exposed to electric fields. *Bioelectromagnetics* 2000; **21**:385-394.
8. M. Pavlin, T. Slivnik, and D. Miklavcic, Effective conductivity of cell suspensions. *IEEE Trans. Biomed. Eng.* 2002; **49**:77-80.
9. R. S. Chiu and M. A. Stuchly, Electric fields in bone marrow sub-structures at power-line frequencies. *IEEE Trans. Biomed. Eng.*, in press.
10. L. A. Geddes and L. E. Baker, The specific resistance of biological material - a compendium of data for the biomedical engineer and physiologist. *Med. Biolog. Eng.* 1967; **5**:271-293.
11. F. X. Hart, N. J. Berner, and R. L. McMillen, Modelling the anisotropic electrical properties of skeletal muscle. *Phys. Med. Biol.* 1999; **44**:413-421.
12. H. P. Schwan and C. F. Kay, Specific resistance of body tissues. *Circ. Res.* 1956; **4**:664-670.
13. B. R. Epstein and K. R. Foster, Anisotropy in the dielectric properties of skeletal muscle. *Med. Biol. Eng. Comput.* 1983; **21**:51-55.
14. E. Pacelat, R. Magjarevic, and V. Išgum, Measurement of electrode-tissue interface characteristics during high current transcranial pulse electrical stimulation. *Measurement* 2000; **27**:133-143.
15. M. Noshiro, T. Morimoto, H. Nagao, and H. Matsuda, Electrical impedance in the lower limbs of patients with Duchenne muscular dystrophy: a preliminary study. *Med. Biol. Eng. Comput.* 1993; **31**:97-102.
16. Bioelectrical impedance techniques in medicine. *Crit. Rev. Biomed. Eng.* 1996; **24**(4-6).
17. P. J. Riu, J. Rosell, R. Bragos, and O. Casas, *Electrical Bioimpedance Methods: applications to Medicine and Biotechnology*. New York: The New York Academy of Sciences, 1999.
18. D. Haemmerich, S. T. Staelin, J. Z. Tsai, S. Tungjitkusolmun, D. M. Mahvi, and J. G. Webster, In vivo electrical conductivity of hepatic tumours. *Physiol. Meas.* 2003; **24**:251-260.
19. B. Blad, P. Wendel, M. Jonsson, and K. Lindstrom, An electrical impedance index to distinguish between normal and cancerous tissues. *J. Med. Eng. Tech.* 1999; **22**:1-5.
20. Y. Ultsch, U. Nachaliel, and A. Ori, Indirect calculation of breast tissue impedance values. *Physiol. Meas.* 2002; **23**:177-182.
21. W. T. Joines, Y. Zhang, C. Li, and R. L. Jirtle, The measured electrical properties of normal and malignant human tissues from 50 to 900 MHz. *Med. Phys.* 1994; **21**:547-550.
22. J. Biggs, K. Cha, and K. Horch, Electrical resistivity of the upper arm and leg yields good estimates of whole body fat. *Physiol. Meas.* 2001; **22**:365-376.
23. B. K. van Kreel, N. Cox-Reyven, and P. Soeters, Determination of total body water by multifrequency bio-electric impedance: development of several models. *Med. Biol. Eng. Comput.* 1998; **36**:337-345.
24. M. Schaefer, W. Gross, J. Ackemann, and M. M. Gebhard, The complex dielectric spectrum of heart tissue during ischemia. *Bioelectrochemistry* 2002; **58**:171-180.
25. D. Haemmerich, O. R. Ozkan, J.-Z. Tsai, S. T. Staelin, S. Tungjitkusolmun, D. M. Mahvi, and J. G. Webster, Changes in electrical resistivity of swine liver after occlusion and post-mortem. *Med. Biol. Eng. Comput.* 2002; **40**:29-33.
26. D. A. McRae and M. A. Esrick, Changes in electrical impedance of skeletal muscle measured during hyperthermia. *Int. J. Hypertherm.* 1993; **9**:247-261.
27. S. Gabriel, R. W. Lau, and C. Gabriel, The dielectric properties of biological tissues: II. Measurements in the frequency range 10 Hz to 20 GHz. *Phys. Med. Biol.* 1996; **41**:2251-2269.
28. H. C. Burger and R. van Dongen, Specific electric resistance of body tissues. *Phys. Med. Biol.* 1960; **5**:431-447.

29. F. X. Hart and W. R. Dunfee, In vivo measurement of the low-frequency dielectric spectra of frog skeletal muscle. *Phys. Med. Biol.* 1993; **38**:1099–1112.
30. S. Rush, J. A. Abildskov, and R. McFee, Resistivity of body tissues at low frequencies. *Circ. Res.* 1963; **12**:40–50.
31. S. Gabriel, R. W. Lau, and C. Gabriel, The dielectric properties of biological tissues: III. Parametric models for the dielectric spectrum of tissues. *Phys. Med. Biol.* 1996; **41**:2271–2293.
32. C. Gabriel, S. Gabriel, and E. Corthout, The dielectric properties of biological tissues: I. Literature survey. *Phys. Med. Biol.* 1996; **41**:2231–2249.
33. F. L. H. Gielen, W. Wallinga-de Jonge, and K. L. Boon, Electrical conductivity of skeletal muscle tissue: Experimental results from different muscles in vivo. *Med. Biol. Eng. Comput.* 1984; **22**: 569–577.
34. B. Bodakian and F. X. Hart, The dielectric properties of meat. *IEEE Trans. Dielect. Elect. Insul.* 1994; **1**:181–187.
35. S. R. Smith, K. R. Foster, and G. L. Wolf, Dielectric properties of VX-2 carcinoma versus normal liver tissue. *IEEE Trans. Biomed. Eng.* 1986; **33**:522–524.
36. A. J. Surowiec, S. S. Stuchly, J. R. Barr, and A. Swarup, Dielectric properties of breast carcinoma and the surrounding tissues. *IEEE Trans. Biomed. Eng.* 1998; **35**:257–263.
37. Y. Yamamoto, T. Yamamoto, and T. Ozawa, Characteristics of skin admittance for dry electrodes and the measurement of skin moisturisation. *Med. Biol. Eng. Comput.* 1986; **24**:71–77.
38. O. G. Martinsen, S. Grimnes, and E. Haug, Measuring depth depends on frequency in electrical skin impedance measurements. *Skin Res. Technol.* 1999; **5**:179–181.
39. T. Yamamoto and Y. Yamamoto, Electrical properties of the epidermal stratum corneum. *Med. Biol. Eng.* 1976; **14**(2):151–158.
40. T. Yamamoto and Y. Yamamoto, Dielectric constant and resistivity of epidermal stratum corneum. *Med. Biol. Eng.* 1976; **14**(5):494–499.
41. H. P. Schwan, Electric characteristics of tissues. *Biophysik.* 1963; **1**:198–208.
42. F. X. Hart, The impedance spectroscopy of skeletal muscle. *Proc. Tenth Electrotechnical and Computer Science Conference ERK 2001*, Invited lecture, Slovenia, 2001.
43. H. P. Schwan and C. F. Kay, The conductivity of living tissues. *Ann. NY Acad. Sci.* 1957; **65**:1007–1013.
44. T. J. C. Faes, H. A. van der Meij, J. C. De Munck, and R. M. Heethaar, The electric resistivity of human tissues (100 Hz–10 MHz): a meta-analysis of review studies. *Physiol. Meas.* 1999; **20**:R1–R10.
45. M. Pavlin, M. Kanduđer, M. Reberšek, G. Pucihar, F. X. Hart, R. Magjarević, and D. Miklavčič, Effect of cell electroporation on the conductivity of a cell suspension. *Biophys. J.*, in press.
46. U. Pliquet and M. R. Prausnitz, Electrical impedance spectroscopy for rapid and non-invasive analysis of skin electroporation. In: M. J. Jaroszeski, R. Gilbert, and R. Heller, *Electrically Mediated Delivery of Molecules to Cells, Electrochemotherapy, Electrogenotherapy and Transdermal Delivery by Electroporation*. Totowa, NJ: Humana Press, 2000.
47. U. Pliquet, R. Langer, and J. C. Weaver, Changes in the passive electrical properties of human stratum corneum due to electroporation. *BBA.* 1995; **1239**:111–121.
48. U. Pliquet and J. C. Weaver, Electroporation of human skin: simultaneous measurement of changes in the transport of two fluorescent molecules and in the passive electrical properties. *Bioelectrochem. Bioenerget.* 1996; **39**:1–12.
49. R. V. Davalos, B. Rubinsky, and D. M. Otten, A feasibility study for electrical impedance tomography as a means to monitor tissue electroporation for molecular medicine. *IEEE Trans. Biomed. Eng.* 2002; **49**:400–403.
50. R. V. Davalos and B. Rubinsky, Electrical impedance tomography of cell viability in tissue with application to cryosurgery. *J. Biomechan. Eng.* 2004; **126**:305–309.

**KEYWORDS**

permittivity, specific conductivity, dielectric dispersion, tissue inhomogeneity, electrical anisotropy, electrode polarization

**ABSTRACT**

Passive electric properties of biological tissues such as permittivity and conductivity are important in applied problems of electrical stimulation in studying of human electromagnetic fields interactions and development of diagnostic and therapeutic procedures. The current densities and pathways resulting from an applied electrical stimulus are dictated to a large extent by the relative permittivity and specific conductivity of biological tissues; energy absorption also depends on tissue properties. We briefly present some theoretical basis for the current conduction in biologic materials and factors affecting the measurement of tissue dielectric properties that need to be taken into account when designing the measurement procedure. Large discrepancies between the data reported by different researchers are found in the literature, which are caused by factors such as different measuring techniques used, the fact that tissue samples were taken from different species, circumstances under which the measurements were performed, and many others. Electric properties of some biological tissues are summarized and data ranges of values found for relative permittivity and specific conductivity in the literature are given. Finally, we present some applications of bioimpedance measurements.

## Author Query Form



**Title:** Encyclopedia of Biomedical Engineering

**Article/Number:** Electric Properties of Tissues/jwus\_Ebs\_403

Dear Author,

During the preparation of your manuscript for typesetting some questions have arisen. These are listed below. Please check your typeset proof carefully and mark any corrections in the margin of the proof or compile them as a separate list. This form should then be returned with your marked proof/list of corrections to John Wiley.

**This form should then be returned with your marked proof/list of corrections to N.S. Pandian, Deputy Manager, Macmillan India Ltd., Book Division-IPD, Midford Crescent, New No. 159/1 (Old No. 53/1), Richmond Road, Bangalore-560025, India, Tel: +91-80-51237312; +91-80-51237313, Fax: +91-80-51237310, E-mail: ns.pandian@macmillan-india.co.in**

### Queries and/or remarks

AU:1	Please provide citation for references 41, 42, 43, 44 in the text part.
------	---

## PAPER 3

### **DNA electrotransfer into the skin using a combination of one high- and one low-voltage pulse**

**Nataša Pavšelj and Véronique Prétat**

**Published in:** Journal of Controlled Release: 106: 407–415, 2005

**Abstract:** Electroporation is an effective alternative to viral methods to significantly improve DNA transfection after intradermal and topical delivery. The aim of the study was to check whether a combination of a short high-voltage pulse (HV) to permeabilize the skin cells and a long low-voltage pulse (LV) to transfer DNA by electrophoresis was more efficient to enhance DNA expression than conventional repeated HV or LV pulses alone after intradermal injection of DNA plasmid. GFP and luciferase expressions in the skin were enhanced by HV+LV protocol as compared to HV or LV pulses alone. The expression lasted for up to 10 days. Consistently, HV+LV protocol induced a higher Th2 immune response against ovalbumin than HV or LV pulses. Standard methods were used to assess the effect of electric pulses on skin: the application of a combination of HV and LV pulses on rat skin fold delivered by plate electrodes was well tolerated. These data demonstrate that a combination of one HV (700 to 1000 V/cm; 100 As) followed by one LV (140 to 200 V/cm; 400 ms) is an efficient electroporation protocol to enhance DNA expression in the skin.





## DNA electrotransfer into the skin using a combination of one high- and one low-voltage pulse

N. Pavšelj<sup>1</sup>, V. Prémat\*

*Université Catholique de Louvain, Department of Pharmaceutical Technology, Unité de Pharmacie Galénique, Avenue Emmanuel Mounier, 73 UCL, 7320 B-1200 Brussels, Belgium*

Received 16 November 2004; accepted 11 May 2005

Available online 27 June 2005

### Abstract

Electroporation is an effective alternative to viral methods to significantly improve DNA transfection after intradermal and topical delivery. The aim of the study was to check whether a combination of a short high-voltage pulse (HV) to permeabilize the skin cells and a long low-voltage pulse (LV) to transfer DNA by electrophoresis was more efficient to enhance DNA expression than conventional repeated HV or LV pulses alone after intradermal injection of DNA plasmid. GFP and luciferase expressions in the skin were enhanced by HV+LV protocol as compared to HV or LV pulses alone. The expression lasted for up to 10 days. Consistently, HV+LV protocol induced a higher Th2 immune response against ovalbumin than HV or LV pulses. Standard methods were used to assess the effect of electric pulses on skin: the application of a combination of HV and LV pulses on rat skin fold delivered by plate electrodes was well tolerated. These data demonstrate that a combination of one HV (700 to 1000 V/cm; 100  $\mu$ s) followed by one LV (140 to 200 V/cm; 400 ms) is an efficient electroporation protocol to enhance DNA expression in the skin.

© 2005 Elsevier B.V. All rights reserved.

*Keywords:* Electroporation; Electrotransfer; Skin; Non-viral gene therapy; DNA vaccination; DNA plasmid

### 1. Introduction

When an electric field is applied to a cell or cell system, a non-uniform transmembrane potential is

induced in the exposed cells. If the induced transmembrane potential is above the threshold value, cell membrane becomes permeabilized and thus more conductive. That increases the uptake of some molecules into the cells, such as drugs or DNA. Reversible increase of the cell membrane permeability caused by the electric field is called electroporation or electropermeabilization [1]. Electroporation has been used for different applications, such as electrochemotherapy, transdermal drug delivery and gene transfection. Electrochemotherapy is a treatment of solid tumors

\* Corresponding author. Tel.: +32 2 764 73 09; fax: +32 2 764 73 98.

*E-mail addresses:* [natasa@lbk.fe.uni-lj.si](mailto:natasa@lbk.fe.uni-lj.si) (N. Pavšelj), [preat@farg.ucl.ac.be](mailto:preat@farg.ucl.ac.be) (V. Prémat).

<sup>1</sup> Present address: Faculty of Electrical Engineering, University of Ljubljana, Trzaska 25, SI-1000 Ljubljana, Slovenia. Tel.: +38 6 1 476 82 69; fax: +38 6 1 426 46 58.

which combines a cytotoxic non-permeant drug with locally delivered permeabilizing electric pulses. It is very successful in eliminating local tumors, e.g. subcutaneous tumors and is more efficient than the chemotherapy alone [2,3]. Transdermal drug delivery has many advantages over conventional routes of drug administration. However, the barrier properties of the skin limit transdermal drug transport. One of the methods to enhance it is electroporation which causes reversible permeabilization of the outer layer of the skin — the stratum corneum [4,5]. Since the first report of Neumann [6], electroporation has been widely used to introduce small molecules and macromolecules, including DNA, into prokaryotic and eukaryotic cells *in vitro*. Electroporation is currently one of the most efficient and simple non-viral method of gene transfer *in vivo* [7].

Skin is an attractive target tissue for gene therapy for a variety of reasons. Its accessibility facilitates *in vivo* gene delivery. Skin is also a very good target organ for DNA vaccination because of the large number of potent antigen presenting cells, critical to an effective immune response. If necessary, large areas of skin can be treated and can easily be monitored [8]. Beside viral methods that are controversial because of their safety issues, chemical and physical methods have been developed to enhance gene expression in the skin [9]. Electroporation seems particularly effective to improve DNA transfection after intradermal [9–14] and topical [15] delivery without any significant alteration of skin structure.

However, the effect of electrical parameters and electrode design on the efficacy of transfection in the skin and the mechanism of enhancement have not been studied systematically so far. It has been shown for muscle tissue that efficient cell electrotransfection can be achieved using combinations of high-voltage (HV) and low-voltage (LV) pulses. Luciferase-encoding DNA was injected in skeletal muscle and luciferase expression was studied after various pulse combinations. HV pulses alone resulted in a high level of muscle permeabilization (permeabilizing pulse), but very low DNA transfer. However, in combination with one or more LV pulses (electrophoretic pulse), a large increase in DNA transfer occurred [16–19].

We hypothesized that DNA electrotransfer into the skin is also a two-step process consisting in

membrane permeabilization and DNA electrophoresis and that a combination of a high-voltage pulse to permeabilize the target cells, followed by a low-voltage pulse to electrophoretically transport the DNA would improve gene transfection in the skin too. Hence, the efficacy of the delivery of DNA in the skin was investigated using a combination of HV+LV pulses in comparison to protocols reported in literature [10–20]. The qualitative and quantitative measure of the expression of two reporter genes in the skin, the kinetics of this expression, intradermal DNA vaccination and skin tolerance using HV+LV pulses were investigated.

## 2. Materials and methods

### 2.1. Reporter genes and plasmid injection

The electrotransfer of gene into the skin was evaluated and optimized with two reporter genes, pCMVluc and pCMVGFP. We prepared the plasmids using a Qiagen kit for plasmid purification. The plasmids were injected intradermally (50 µg/25 µl PBS) 30 s before the application of the electric pulses, using a Hamilton syringe with a 27-gauge needle.

### 2.2. Animals

The animals used in all studies except the vaccination study, were male Wistar rats from Laboratoires Janvier, France, 8–10 weeks old. They were anaesthetized with 700 µl of a mixture of ketamine (100 mg/kg, Ketalar, Panpharma) and xylazine (40 mg/kg, Rompun, Bayer). The skin on the back was shaved 1–2 days prior to the experiments, first with an electric razor, then with a depilatory cream (Veet for sensitive skin) to thoroughly remove all the hair. Shaving allowed a better visualization of DNA injection and electroporated area. We placed 5 to 8 electroporation sites on the back of each rat.

For the vaccination study we used 6-week-old female Balbc mice (Janvier, France). They were anaesthetized with 15 µl of a mixture of ketamine and xylazine. The skin on the back was shaved with depilatory cream (Veet for sensitive skin) 1 day prior to immunization.

### 2.3. DNA electrotransfer

For the delivery of HV and/or LV pulses, we used a square-wave electropulsator Cliniporator (IGEA, Carpi, Italy). Different protocols, all consisting of one HV pulse (700 or 1000 V/cm 100  $\mu$ s), followed by one LV pulse (80, 140 or 200 V/cm 400 ms), using no lag between them were tested. We compared these protocols with protocols reported in literature [10–20]. The electric pulses were delivered about 30 s after the intradermal injection of plasmid (50  $\mu$ g/25  $\mu$ l PBS), using two parallel, stainless-steel plate electrodes of 0.5 mm thickness and 4 mm distance between them (IGEA, Carpi, Italy). The area of the electrodes in contact with skin was about 1 cm  $\times$  1 cm. To assure good contact between the skin fold and the electrodes, a conductive gel (EKO-GEL, ultrasound transmission gel, Egna, Italy) was applied. The electrodes used for the vaccination study were 2.5 mm apart, due to the lower thickness of mouse skin.

### 2.4. GFP localization

Two days after the electroporation, the rats ( $n=3$  per group) were sacrificed and skin samples were taken. Both the epidermal and dermal sides of the skin were observed without fixation or freezing with a confocal microscope [15]. Two blinded observers evaluated the fluorescence intensity (2 skin samples per rat).

### 2.5. Luciferase assay

Two days after the electroporation (1, 2, 3, 4, 7, 10, 14, 21, 25 days for the kinetic study), the rats were sacrificed and the electroporated areas of the skin were taken. The skin samples were weighed to 200 mg, cut into pieces and homogenized in 1 ml cell culture lysis reagent solution (10 ml cell culture lysis reagent (Promega) diluted with 40 ml distilled water and supplemented with one tablet of protease inhibitor cocktail (Boehringer Mannheim)). After centrifugation at 12000 rpm for 10 min at 4  $^{\circ}$ C, we assessed the luciferase activity on 10  $\mu$ l of the supernatant, using a luminometer, with delay time 3 s and integration time 15 s, starting after the addition of 50  $\mu$ l of Luciferase Assay Substrate (Promega) to the skin lysate. The results from the luminometer were collected in relative light units (RLU). The final results were

expressed as pg of luciferase per mg of tissue by calibration with purified firefly luciferase protein (Sigma).

### 2.6. Vaccination study

The immune response after delivery of a plasmid coding for an immunogenic model protein ovalbumin (pcDNA 3.1-OVA) was assessed. Mice were injected intradermally with  $2 \times 15$   $\mu$ l of this plasmid coding for ovalbumin at 2 mg/ml (groups 1–4), ovalbumin at 1 mg/ml (group 5), ovalbumin 1 mg/ml+adjuvant Alum (group 6) and PBS (negative control, group 7). Electric pulses (1 HV+1 LV pulses in the first two groups and 6 HV pulses [11] in the third group) were applied 30 s after DNA injection. Two and four weeks after the priming, 2 boosts were applied. Blood samples were collected by retroorbital bleeding 2, 4 and 6 weeks after priming.

The humoral immune response i.e. titers of antibodies (IgG) to ovalbumin in the serum was measured by ELISA. Isotypes (IgG1, IgG2a or IgG2b) were determined using appropriate secondary antibodies as described previously [21]. The antibodies were first measured in the pools coming from individual mice in equivalent part. Individual mice responses were measured when a positive response was detected in the pooled sera.

### 2.7. Tolerance study

Side effects on the skin of one HV and one LV pulses (1000 V/cm 100  $\mu$ s+200 V/cm 400 ms) generated by the Cliniporator were investigated by standard methods [22–24]. Skin folds with or without gel with the electrodes applied for as long as needed to deliver pulses (30 s) were used as controls.

As Cliniporator measures the voltage and the current during pulsing, conductivity changes were estimated. Non-invasive bioengineering methods were used to evaluate in vivo if electroporation induced a trauma in the skin (transepidermal water loss TEWL, chromametry). Histology was used to investigate the effect on the skin structure. TEWL measurement is a non-invasive method for assessing the skin barrier function. The probe of the Tewameter TW 210 (Germany) was placed on the electroporation site and the measurements were taken

Table 1  
The results of the immunization study

Group	Injection	Electroporation	Week 4		Week 6	
			IgG <sup>a</sup>	Responder <sup>b</sup>	IgG <sup>a</sup>	Responder <sup>b</sup>
1	DNA	700 V/cm 100 $\mu$ s+200 V/cm 400 ms	3.41 $\pm$ 0.44	8/8	3.49 $\pm$ 0.40	5/5
2	DNA	700 V/cm 100 $\mu$ s+200 V/cm 400 ms 4.2 s lag	3.24 $\pm$ 0.35	5/5	4.14 $\pm$ 0.13	5/5
3	DNA	6 $\times$ 1750 V/cm 100 $\mu$ s (8 Hz)	2.61 $\pm$ 0.16	3/7	3.03 $\pm$ 0.29	7/7
4	DNA	/	2.80 $\pm$ 0.42	2/7	2.86 $\pm$ 0.45	8/8
5	OVA	/	3.39 $\pm$ 0.64	8/8	3.49 $\pm$ 0.38	8/8
6	OVA+Alum	/	4.0 $\pm$ 0.14	6/6	4.45 $\pm$ 0.2	5/5
7	PBS	/	/	/	/	/

The results are expressed in: a) Mean IgG titer ( $\pm$  S.D.) in responding mice determined by ELISA in individual mice, and b) number of mice showing IgG titers higher than the background values.

when TEWL values stabilized. TEWL values are expressed in  $\text{g/m}^2 \text{ h}$ . Skin color and erythema were measured by Minolta Chromameter CR-200 (Minolta, Japan) calibrated using a white calibration tile. During measurements the apparatus was perpendicularly kept to the skin surface. The measurements were taken right before, right after the delivery of pulses, 30, 60, 120 min and 24 h after pulsing. We separately measured the anode and the cathode side of each electroporation site. For the histology study, the tissue was fixed in a 4% formalin solution for at least a week and embedded in paraffin wax. Sections 3  $\mu$ m thick were cut perpendicularly to the surface of the skin and stained with hematoxylin–eosin.

### 2.8. Statistical analysis

For the statistical analysis of the results, we used Sigma Stat for Windows, version 2.0, Jandel Corporation. When normality test over the experimental groups failed, the data was represented with a median (horizontal line), 25th and 75th percentile (grey box) and 10th and 90th percentile (error bars). Black dots represent all the outliers. The ANOVA on ranks and Dunnett's test were used to compare different protocols.

## 3. Results

### 3.1. GFP expression in the skin

To localize the expression of a gene in the skin after intradermal injection of a plasmid followed by electroporation and to compare the efficacy of different pulsing protocols to enhance this gene expression,

a plasmid coding for GFP was used as a reporter gene [15].

The control epidermis showed some autofluorescence of the hair follicles (see Fig. 1a, d, f) but no fluorescence in the dermis (data not shown). After intradermal injection of the plasmid without electroporation, a very slight and diffuse fluorescence was observed in some area of the dermis (Fig. 1b).

When only one HV pulse (1000 V/cm 100  $\mu$ s) (Fig. 1c) or only one LV pulse (200 V/cm 400 ms) (Fig. 1d–e) was applied, the expression of GFP remained very low both in the epidermis (Fig. 1d) and to a lesser extent in the dermis (Fig. 1c, e).

The expression of GFP was enhanced by a combination of one HV pulse (1000 V/cm 100  $\mu$ s) and one LV pulse (80, 140 or 200 V/cm 400 ms). The fluorescence was elevated in some part of the dermis (Fig. 1g, h). Expression in the epidermis was also observed (Fig. 1f). A semi-quantitative analysis indicates that 140 or 200 V/cm pulses were more efficient than 80 V/cm LV pulses and that the expression at the anodal side was slightly higher than expression at the cathodal side.

### 3.2. Luciferase expression in the skin

To confirm that the combination of one HV and one LV pulse is more efficient than HV or LV pulses alone, a quantitative study with another reporter gene coding for luciferase, was conducted. The efficiency of the HV and LV pulses to enhance gene transfer in rat skin was investigated in order to find the most efficient combination of the high- and low-voltage pulses delivered by the Cliniporator. As shown in Fig. 2, two HV+LV protocols (1: 1000 V/cm 100

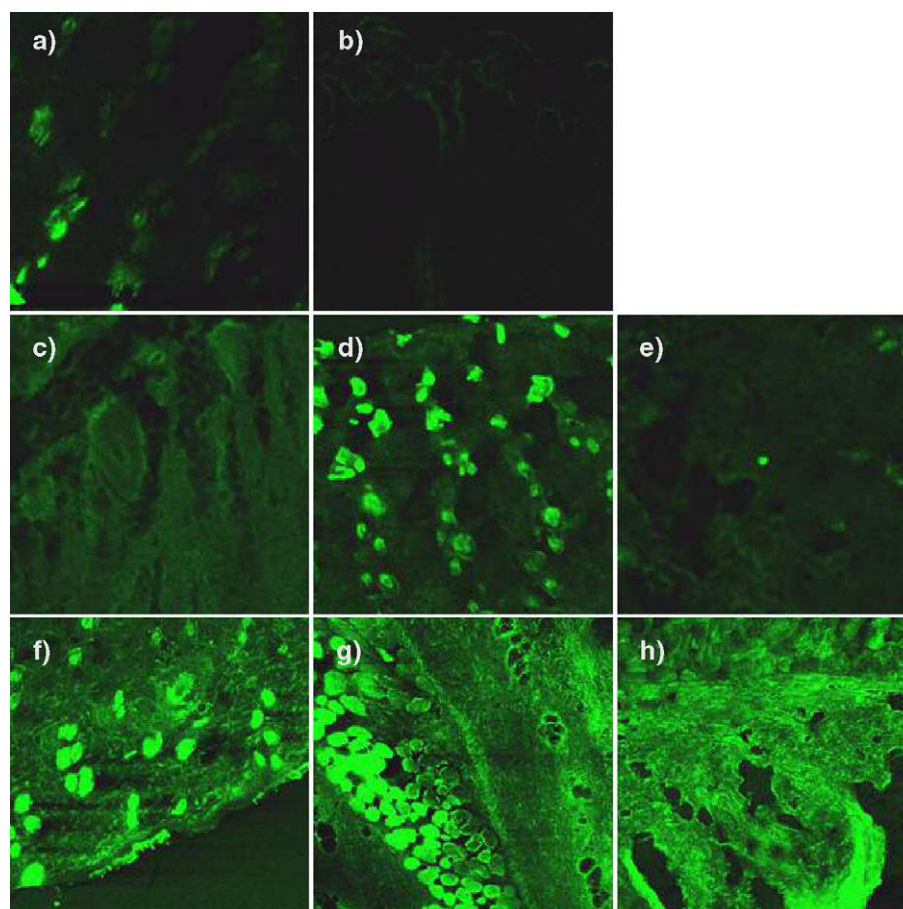


Fig. 1. Expression of GFP in the epidermis (a, d, f) or in the dermis (b, c, e, g, h) after intradermal injection of 50  $\mu\text{g}$  of a plasmid coding for GFP; (a–b) no electroporation; (c) 1000 V/cm 100  $\mu\text{s}$  pulse; (d, e) 200 V/cm 400 ms; (f, g) 1000 V/cm 100  $\mu\text{s}$ +140 V/cm 400 ms; (h) 1000 V/cm 100  $\mu\text{s}$ +200 V/cm 400 ms.

$\mu\text{s}$ +140 V/cm 400 ms, or 2: 700 V/cm 100  $\mu\text{s}$ +200 V/cm 400 ms) were compared with those reported in literature so far [10–20], consisting of 6 HV pulses ( $6 \times 1750$  V/cm 100  $\mu\text{s}$ ) (3) or 6 LV pulses ( $6 \times 250$  V/cm 20 ms) (4). Four control groups were included in the study. In the first control group the rats were only administered plasmid DNA intradermally without electroporation (5). In the second and third control groups the intradermal injection was followed by a single HV pulse (6) or by a single LV pulse (7). Basal luciferase activity of skin samples was also measured (8).

The application of electrical pulses increased luciferase expression: higher expressions were detected in protocols 1 to 4 as compared to the protocols 5–8 ( $p < 0.05$ ). HV+LV pulses (protocols 1 and 2)

induced a statistically significant higher luciferase expression than repeated HV pulses or LV pulses (protocols 3 and 4).

### 3.3. Kinetics of the luciferase expression

To follow the kinetics of gene expression in the skin, the expression of the gene coding for luciferase was measured between day 1 and day 25 after application of HV+LV pulses (700 V/cm 100  $\mu\text{s}$ +200 V/cm 400 ms). The control group was injected with plasmid DNA intradermally, without electroporation.

The kinetic study shows the highest expression on the first day after the electroporation and a rapid drop towards the 4th day. A low expression can be seen for up to about 10 days after. In the control group of

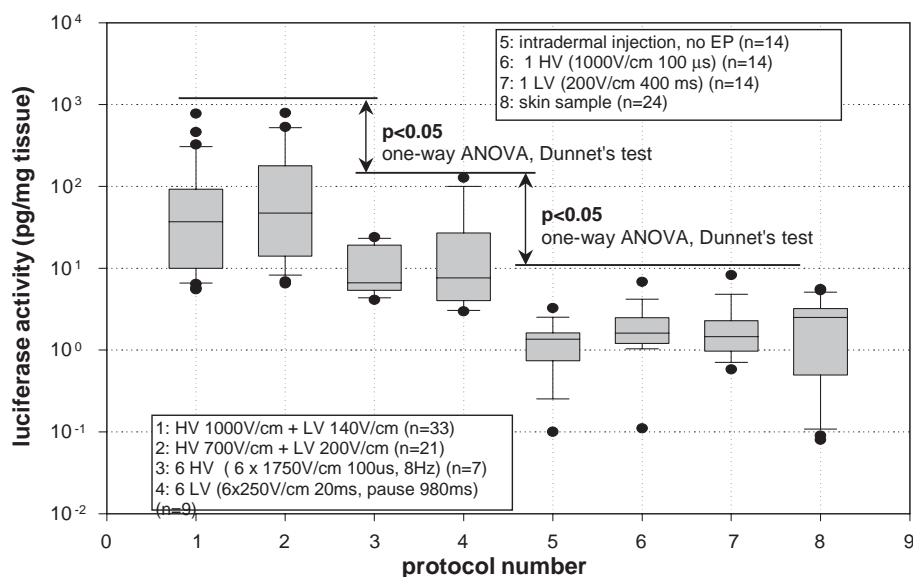


Fig. 2. Luciferase expression after different electroporation protocols: Group 1: HV+LV (1000 V/cm 100  $\mu$ s+140 V/cm 400 ms); Group 2: HV+LV (700 V/cm 100  $\mu$ s+200 V/cm 400 ms); Group 3: 6 HV (6  $\times$  1750 V/cm 100  $\mu$ s, 8 Hz); Group 4: 6 LV (6  $\times$  250 V/cm 20 ms, pause 980 ms); Group 5: DNA injection, no electroporation; Group 6: 1 HV (1000 V/cm 100  $\mu$ s); Group 7: 1 LV (200 V/cm 400 ms); Group 8: skin sample. All groups except group 8 were injected intradermally with 50  $\mu$ g of pCMVluc. Results are represented on a log scale with pg of luciferase per mg of tissue. Normality test over the experimental groups failed, so the data is represented with a median (horizontal line), 25th and 75th percentile (grey box) and 10th and 90th percentile (error bars). Black dots represent all the outliers.

intradermal injection alone, without electroporation, some expression can be seen the first day after the injection, then the expression dropped close to zero already the second day (Fig. 3). A statistical difference ( $p < 0.05$ ) between electroporated rats and control rats was observed at days 2, 3, 4 and 7.

These data suggest that skin DNA electrotransfer would be more appropriate for short term treatment of the skin or for immunization.

### 3.4. Immunization study

As skin is also a very attractive target tissue for DNA vaccination and as gene expression in the skin is rather pulsed, an immunization study using a plasmid coding for a model antigen ovalbumin was performed [21]. HV+LV protocols were compared to electroporation protocols described in the literature [10–20]. Two and four weeks after the priming, two boosts were applied.

IgG responses were detected in the mice immunized with ovalbumin or the plasmid coding for ovalbumin whereas no response was observed in the

control group 7. Application of electric pulses increased the immune response (groups 1, 2, 3 versus group 4,  $p < 0.05$ ). The groups receiving HV+LV protocols had a higher immune response (groups 1, 2) than the group treated with 6 HV pulses (group 3) ( $p < 0.05$ ). The IgG levels after DNA electrotransfer with HV+LV were equivalent to the IgG level in mice immunized with ovalbumin but lower than in mice immunized with ovalbumin and the standard adjuvant alum (Table 1).

No IgG2a and IgG2b response was detected (except for 2 mice in group 1), suggesting that only a Th2 response was induced.

### 3.5. Tolerance of the skin to HV+LV pulses

The trauma on the skin induced by HV+LV electroporation (1000 V/cm 100  $\mu$ s+200 V/cm 400 ms) was investigated by non-invasive bioengineering methods to check if the pulses induce an erythema (chromametry) or impairment of barrier function (transepidermal water loss) and by histology to investigate the effect on the skin structure [22–24].

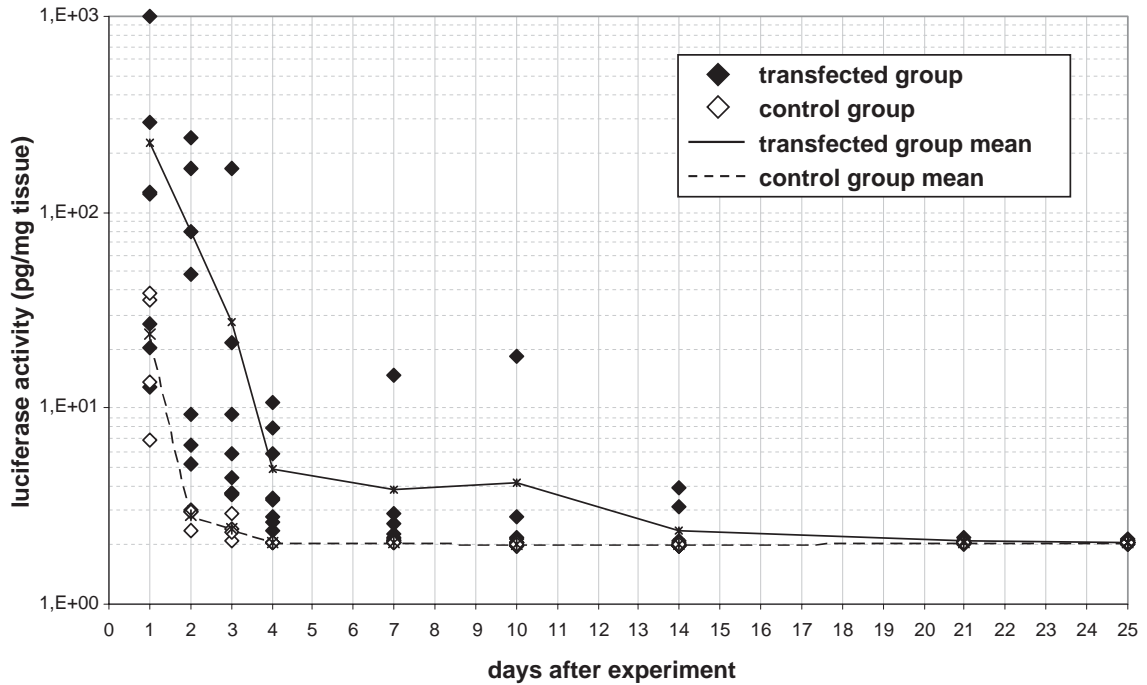


Fig. 3. Kinetics of luciferase expression in the skin after intradermal injection of 50 µg pCMVluc. (◆) Electroporation, 700 V/cm 100 µs + 200 V/cm 400 ms ( $n=8$ ); (◇) No electroporation ( $n=4$ ). The data is represented with mean values.

A slight muscle contraction was observed after the HV pulse. Changes in conductivity were measured during pulsing. They varied from one animal to an-

other and depended on the voltage amplitude used. The higher the voltage, the higher the conductivity change (or the lower the skin resistance). For exam-

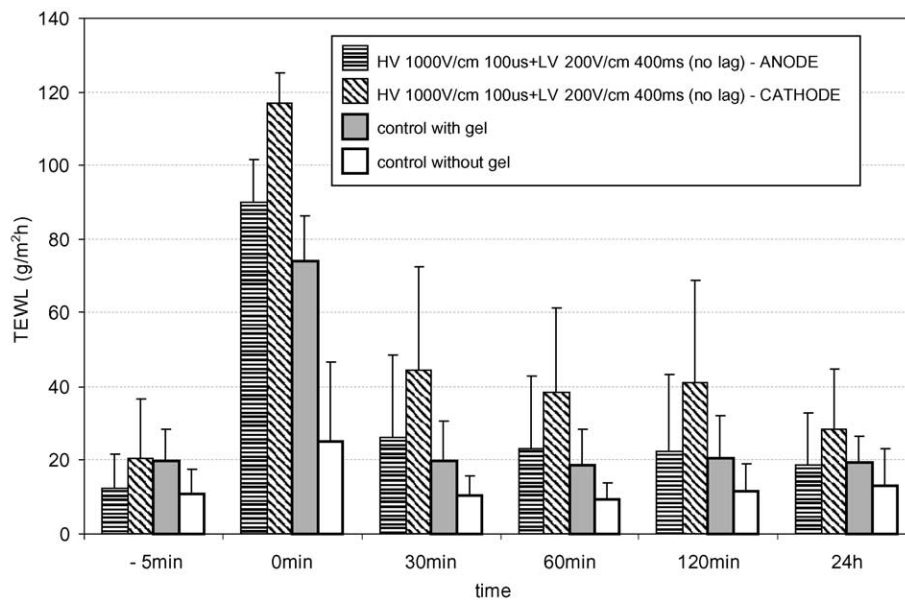


Fig. 4. Transdermal water loss (TEWL) values in rat skin as a function of time after electroporation.

ple, the conductivity during a 100  $\mu$ s pulse at 1000 V/cm increased up to 50%.

An increase in the TEWL values right after the delivery of the pulses can be observed (Fig. 4) but the controls where we applied conductive gel also had high TEWL values, suggesting that the high TEWL values resulted from evaporation of gel water from the skin surface. Although electroporation does disrupt the skin barrier as evidenced by the low skin resistance, the change in TEWL was small and short. TEWL values were down to normal within 30 min. TEWL values on the anode side of the electroporation side were consistently lower than the ones on the cathode side.

Values of parameter *a* (redness of skin) indicate that no erythema was induced by HV+LV pulses (data not shown). During the experiments we noticed some redness with the naked eye. The electroporation site turned red a few minutes after pulsing but it was a short-term change. There was a consistent difference between the anode and the cathode side of the electroporation sites. The reason why we did not record that with the chromameter right after pulsing might be the vascular lock in the minutes following the electroporation [25].

No damage in the histological structure of the skin was observed. Neither inflammation nor necrosis was detected 24 h after application of HV+LV pulses.

#### 4. Discussion

The efficiency of combination of HV+LV pulse on DNA electrotransfer in skin was investigated. As already proposed for gene transfection in skeletal muscle [16–19], the rationale for this electroporation protocol was that the first, high-voltage pulse results in a high level of cell permeabilization (permeabilizing pulse), while the second, low-voltage pulse provides a driving force for transport of DNA into cells (electrophoretic pulse). So far the protocols reported in literature for DNA electrotransfer into the skin consisted of 6 to 8 HV pulses or of 6 to 16 LV pulses [10–15]. To check if the combination of 1 HV+1 LV pulses enhances gene expression in skin, both a localization of GFP expression and a quantitative measure of luciferase activity were evaluated. An enhanced expression of GFP in the skin was observed when a combination of HV+LV was used. One HV or

one LV alone resulted in a very low transfection, comparable to the one of the control group where no pulse was applied whereas GFP expression in the epidermis and dermis was enhanced by the combination of HV+LV pulses. The quantification of luciferase activity further supports the hypothesis that HV+LV pulses are more efficient than several HV or LV pulses. Indeed, luciferase activity was enhanced by 2 orders of magnitude when a combination of HV+LV pulse was applied whereas a low expression was detected after application of 6 HV or 6 LV pulse only. These data confirm the hypothesis that as reported for the muscle [16–19], the association of a HV+LV is more efficient for DNA electrotransfer in the skin than repeated HV or LV. This also demonstrates that both the permeabilizing HV pulse and the electrophoretic LV pulses are required.

Luciferase expression in the skin varied over a factor of 100 after electrotransfer. This could partly be attributed to variable electrical properties of the skin or variable biological responses to DNA injection. Alternatively, the variation could be caused by experimental conditions e.g. DNA injection.

Kinetic study of the luciferase expression showed the highest expression on the first days after the experiment, then it dropped rapidly as reported previously for other delivery methods [8]. Hence, skin DNA electrotransfer would be more adapted to a short-term gene expression in the skin for immunization or skin treatment than for the secretion of a therapeutic protein in the blood.

The combination of HV+LV pulse was also tested for efficiency in skin immunization. This immunization experiment demonstrated that i) electroporation enhances the immune response induced after intradermal injection of a DNA plasmid coding for an antigen [11,14] ii) our protocols (1 HV+1 LV pulse) are more efficient than protocols (6 to 8 HV pulses) previously described.

The proposed protocols have proven to be efficient, so the safety aspect of such electric pulses was also studied. Side effects were investigated by standard methods. Some disruption of the skin barrier function due to electroporation was observed as evidenced by the low skin resistance, but the change in TEWL values was small and transient. A slight and transient erythema was observed visually but not by chromametry. The erythema and TEWL values on the anode

site of the electroporation site were consistently lower than the ones on the cathode side. The reasons for the difference are unknown but could be attributed to local changes in ion concentration or pH imbalance. These data confirm that the application of HV and/or LV pulses on rat skin forming a fold between two plate electrodes is well tolerated [22–24].

In conclusion, the combination of one high-voltage pulse to permeabilize the skin cells followed by one low-voltage pulse to transfer DNA enhances DNA transfection in the skin, compared to the protocols used so far. Such HV+LV pulses also have no major effects on skin for the voltage amplitudes used.

### Acknowledgments

This research was supported by the European Commission under the 5th framework under the grant Cliniporator QLK-1999-00484.

### References

- [1] J.C. Weaver, Y.A. Chizmadzhev, Theory of electroporation: a review, *Bioelectrochem. Bioenerg.* 41 (1996) 135–160.
- [2] L.M. Mir, S. Orlowski, Mechanisms of electrochemotherapy, *Adv. Drug Deliv. Rev.* 35 (1999) 107–118.
- [3] R. Heller, R. Gilbert, M.J. Jaroszeski, Clinical applications of electrochemotherapy, *Adv. Drug Deliv. Rev.* 35 (1999) 119–129.
- [4] A.-R. Denet, R. Vanbever, V. Pr at, Skin electroporation for transdermal and topical delivery, *Adv. Drug Deliv. Rev.* 56 (2004) 659–674.
- [5] M.R. Prausnitz, A practical assessment of transdermal drug delivery by skin electroporation, *Adv. Drug Deliv. Rev.* 35 (1999) 61–76.
- [6] E. Neumann, M. Schaefer-Ridder, Y. Wang, P.H. Hofschneider, Gene transfer into mouse lymphoma cells by electroporation in high electric fields, *EMBO J.* 1 (7) (1982) 841–845.
- [7] S. Somiari, J. Glasspool-Malone, J.J. Drabick, R.A. Gilbert, R. Heller, M. Jaroszeski, R.W. Malone, Theory and in vivo application of electroporative gene delivery, *Mol. Ther.* 2 (3) (2000) 178–187.
- [8] V. Pr at, N. Dujardin, Topical delivery of nucleic acids in the skin, *STP Pharma Sci.* 11 (2001) 57–68.
- [9] S. Mehier-Humbert, R.H. Guy, Physical methods for gene transfer: improving the kinetics of gene delivery into cells, *Adv. Drug Deliv. Rev.* 57 (5) (2005) 733–753.
- [10] J. Glasspool-Malone, S. Somiari, J. Drabick, R.W. Malone, Efficient nonviral cutaneous transfection, *Mol. Ther.* 2 (2) (2000) 140–146.
- [11] J.J. Drabick, J. Glasspool-Malone, A. King, R.W. Malone, Cutaneous transfection and immune responses to intradermal nucleic acid vaccination are significantly enhanced by in vivo electroporation, *Mol. Ther.* 3 (2) (2001) 249–255.
- [12] L. Zhang, E. Nolan, S. Kreitschitz, D.P. Rabussay, Enhanced delivery of naked DNA to the skin by non-invasive in vivo electroporation, *Biochim. Biophys. Acta* 1572 (2002) 1–9.
- [13] M. Lee Lucas, L. Heller, D. Coppola, R. Heller, IL-12 plasmid delivery by in vivo electroporation for the successful treatment of established subcutaneous B16.F10 melanoma, *Mol. Ther.* 5 (6) (2002) 668–675.
- [14] L. Zhang, G. Widera, D. Rabussay, Enhancement of the effectiveness of electroporation-augmented cutaneous DNA vaccination by a particulate adjuvant, *Bioelectrochemistry* 63 (1–2) (2004) 369–373.
- [15] N. Dujardin, P. Van Der Smissen, V. Pr at, Topical gene transfer into rat skin using electroporation, *Pharm. Res.* 18 (1) (2000) 61–66.
- [16] L.M. Mir, M.F. Bureau, R. Rangara, B. Schwartz, D. Scherman, Long-term, high level in vivo gene expression after electric pulse-mediated gene transfer into skeletal muscle, *Med. Sci.* 321 (1998) 893–899.
- [17] L.M. Mir, M.F. Bureau, J. Gehl, R. Rangara, D. Rouy, J.-M. Caillaud, P. Delaere, D. Branellec, B. Schwartz, D. Scherman, High-efficiency gene transfer into skeletal muscle mediated by electric pulses, *Proc. Natl. Acad. Sci. U. S. A.* 96 (8) (1999) 4262–4267.
- [18] M.F. Bureau, J. Gehl, V. Deleuze, L.M. Mir, D. Scherman, Importance of association between permeabilization and electrophoretic forces for intramuscular DNA electrotransfer, *Biochim. Biophys. Acta* 1474 (2000) 353–359.
- [19] S. Satkauskas, M.F. Bureau, M. Puc, A. Mahfoudi, D. Scherman, D. Miklavcic, L.M. Mir, Mechanisms of in vivo DNA electrotransfer: respective contributions of cell electroporation and DNA electrophoresis, *Mol. Ther.* 5 (2) (2002) 133–140.
- [20] R. Heller, M. Jaroszeski, A. Atkin, D. Moradpour, R. Gilbert, J. Wands, C. Nicolau, In vivo gene electroinjection and expression in rat liver, *FEBS Lett.* 389 (3) (1996) 225–228.
- [21] C. Lombry, A. Marteleur, M. Arras, D. Lison, J. Louhahed, J.C. Renaud, V. Pr at, Local and systemic immune responses to intratracheal instillation of antigen and DNA vaccines in mice, *Pharm. Res.* 21 (1) (2004) 127–135.
- [22] R. Vanbever, D. Fouchard, A. Jadoul, N. De Morre, V. Pr at, J.P. Marty, In vivo non-invasive evaluation of hairless rat skin after high-voltage pulse exposure, *Skin Pharmacol. Appl.* 11 (1998) 23–34.
- [23] N. Dujardin, E. Staes, Y. Kalia, P. Clarys, R. Guy, V. Pr at, In vivo assessment of skin electroporation using square wave pulses, *J. Control. Release* 79 (1–3) (2002) 219–227.
- [24] R. Vanbever, V. Pr at, In vivo efficacy and safety of skin electroporation, *Adv. Drug Deliv. Rev.* 35 (1999) 77–88.
- [25] J. Gehl, T. Skovsgaard, L.M. Mir, Vascular reactions to in vivo electroporation: characterization and consequences for drug and gene delivery, *Biochim. Biophys. Acta* 1569 (2002) 51–58.



## **PAPER 4**

### **The Course of Tissue Permeabilization Studied on a Mathematical Model of a Subcutaneous Tumor in Small Animals**

**Nataša Pavšelj, Zvonko Bregar, David Cukjati, Danute Batiuskaite, Lluís M. Mir and Damijan Miklavčič**

**Published in:** IEEE Transactions on Biomedical Engineering: 52(8): 1373-1381, 2005

**Abstract:** One of the ways to potentiate antitumor effectiveness of chemotherapeutic drugs is by local application of short intense electric pulses. This causes an increase of the cell membrane permeability and is called electropermeabilization. In order to study the course of tissue permeabilization of a subcutaneous tumor in small animals, a mathematical model was built with the commercial program EMAS, which uses the finite element method. The model is based on the tissue specific conductivity values found in literature, experimentally determined electric field threshold values of reversible and irreversible tissue permeabilization, and conductivity changes in the tissues. The results obtained with the model were then compared to experimental results from the treatment of subcutaneous tumors in mice and a good agreement was obtained. Our results and the reversible and irreversible thresholds used coincide well with the effectiveness of the electrochemotherapy in real tumors where experiments show antitumor effectiveness for amplitudes higher than 900 V/cm ratio and pronounced antitumor effects at 1300 V/cm ratio.



# The Course of Tissue Permeabilization Studied on a Mathematical Model of a Subcutaneous Tumor in Small Animals

Nataša Pavšelj, Zvonko Bregar, David Cukjati, Danute Batiuskaite, Lluís M. Mir, and Damijan Miklavčič\*

**Abstract**—One of the ways to potentiate antitumor effectiveness of chemotherapeutic drugs is by local application of short intense electric pulses. This causes an increase of the cell membrane permeability and is called electropermeabilization. In order to study the course of tissue permeabilization of a subcutaneous tumor in small animals, a mathematical model was built with the commercial program EMAS, which uses the finite element method. The model is based on the tissue specific conductivity values found in literature, experimentally determined electric field threshold values of reversible and irreversible tissue permeabilization, and conductivity changes in the tissues. The results obtained with the model were then compared to experimental results from the treatment of subcutaneous tumors in mice and a good agreement was obtained. Our results and the reversible and irreversible thresholds used coincide well with the effectiveness of the electrochemotherapy in real tumors where experiments show antitumor effectiveness for amplitudes higher than 900 V/cm ratio and pronounced antitumor effects at 1300 V/cm ratio.

**Index Terms**—Electropermeabilization, electroporation, finite element modeling, subcutaneous tumor model, tissue conductivity change.

## I. INTRODUCTION

THE application of electric pulses to cells, either in suspension or in tissue, causes structural changes in the cell membrane, which becomes more permeable [1]–[4]. If pulse amplitude, duration and number of pulses are correctly set, the change in the membrane permeability facilitates the cell uptake of ions, molecules such as DNA or drugs, which otherwise can not cross the membrane. Electropermeabilization is used in gene transfection, electrochemotherapy and transdermal drug delivery. The cell membrane is permeabilized when a threshold

transmembrane voltage is reached, i.e., when the external electric field is above the reversible threshold value. Unfortunately the portion of the cells that suffers permanent damage is increased by increasing the electric field, so when the electric field reaches an irreversible threshold value, the electropermeabilization becomes irreversible and causes cell death. In the case of electrochemotherapy, exceeding the irreversible threshold in tumor is less problematic, since killing tumor cells is the aim of the treatment, while in electrogenetransfer the electroporation should not damage the electroporated cells. Therefore, the goal is to apply an electric field that will be between the reversible and irreversible permeabilization thresholds [5].

Electropermeabilization of cells depends on the cell and tissue parameters (tissue specific conductivity, cell size, shape, and distribution [6]–[8]), pulse parameters (pulse duration, amplitude, and number of pulses [9]), and the most important parameter, the electric field strength, which causes a transmembrane voltage change on the cell membrane [10]. The specific conductivity of the tissue increases when permeabilized, which could be used as an indicator of the level of the electropermeabilization in the tissue in question [11], [12].

To use electroporation in clinical applications effectively, we have to detect if the target tissue area is permeabilized or not. This feedback could then be used to adjust the electroporation parameters during the treatment to make it more efficient. A theoretical study was performed to monitor the process by means of electrical impedance tomography imaging [12]. Studying the electric field distribution in the biological systems is a relatively simple and useful method to get an insight into some biological processes [13]–[15]. Experimenting on mathematical models is easier and more ethical than performing *in vivo* experiments. We can easily change the excitation of the model by simply applying different boundary conditions. A good mathematical model, verified by experimental data gives us a good insight into the process, but we have to be aware of its limitations. A mathematical model is only an approximation of a very complicated real system and it can not be a substitute for all *in vivo* experimental work. However, it helps us as a source of extra information and helps us to plan future *in vivo* experiments.

Monitoring cell or tissue permeabilization in real time has been of interest for many researchers [12], [16], [17]. In our study, we built a mathematical model of a subcutaneous tumor in small animals and with the help of the model studied the electroporation process during the electrochemotherapy taking into account the increase in tissue conductivity due to cell membrane electroporation. Namely, when the electric field exceeds

Manuscript received September 22, 2004; revised January 9, 2005. This work was supported in part by the European Commission under the 5th framework under Grant Cliniporator QLK-1999-00484 and in part by the Ministry of Science, Education and Sports of the Republic of Slovenia. *Asterisk indicates corresponding author.*

N. Pavšelj and D. Cukjati are with the Faculty of Electrical Engineering, University of Ljubljana, Ljubljana 1000, Slovenia (e-mail: natasa@lbk.fe.uni-lj.si; david@lbk.fe.uni-lj.si).

Z. Bregar was with the Faculty of Electrical Engineering, University of Ljubljana, 1000 Ljubljana, Slovenia. He is now with Milan Vidmar Electroinstitute, 1000 Ljubljana, Slovenia (e-mail: zvonko.bregar@eimv.si).

D. Batiuskaite was with the UMR 8121 CNRS, Institute Gustave-Roussy, Villejuif, France. She is now with the Department of Biology, Vytautas Magnus University, 44248 Kaunas, Lithuania (e-mail: a8daba@vaidila.vdu.lt).

L. M. Mir is with the UMR 8121 CNRS, Institute Gustave-Roussy, 94805 Villejuif, France (e-mail: luismir@igr.fr).

\*D. Miklavčič is with the Faculty of Electrical Engineering, University of Ljubljana, 1000 Ljubljana, Slovenia (e-mail: damijan@lbk.fe.uni-lj.si).

Digital Object Identifier 10.1109/TBME.2005.851524

the reversible threshold, the tissue conductivity increases. This change subsequently causes the change of the electric field distribution and of the corresponding current. This process continues until the magnitude of the electric field nowhere in the model exceeds the reversible threshold value or the specific conductivity was already changed in that part of the tissue. We modeled the dynamics of the electroporation process with a sequence of static models that describe electric field distribution at discrete time steps during the process. This is another attempt to describe change of specific conductivity ( $\sigma$ ) during electroporation *in vivo* as a process and to determine the ratio ( $\sigma_1/\sigma_0$ ) between the specific conductivity of the electroporated tissue ( $\sigma_1$ ) and the specific conductivity of the same tissue before the pulses are applied ( $\sigma_0$ ) [18]–[21]. We tuned the model to the experimental data that are also reported, on different separate tissues and compared it with the experimental data on subcutaneous tumors with plate electrodes pressed against the skin.

## II. MATERIALS AND METHODS

### A. Finite-Element Method

Electric field and reaction current calculations were made by means of the commercial program EMAS [22] (Ansoft, Pittsburgh, PA) based on finite element method [23]. This method solves partial differential equations by dividing the model into small elements where the quantity to be determined is approximated with a function or is assumed to be constant throughout the element. Finite elements can be of different shapes and sizes, which allows modeling of intricate geometries. Nonhomogeneities and anisotropies can also be modeled and different excitations and boundary conditions can be easily applied. Building a mesh is an important part of the modeling process. One has to be aware where in the model to expect higher gradients of the quantities to be determined. The mesh has to be denser there for the calculation to be exact. Therefore, the mesh has to be denser around the electrodes and on the border between the regions of very different specific conductivities. One of the basic verifications of the model is making a denser mesh to see if it has any effect on the results. If not, the mesh density is adequate. Using the symmetry of the geometry [24], models can also be simplified by applying appropriate boundary conditions.

### B. In Vivo Experiments and Measurements

The study is based on the data collected during an extensive study of the response of different tissues to high voltage pulses. The pulses were delivered through plate electrodes to rat skeletal muscle, skinfold, and mouse tumors. Plate electrodes consisted of two parallel metal plates, separated by 5.7 mm for rat's skeletal muscles (the triceps brachii muscle of the hind limb and the gastrocnemius medialis muscle of the forelimb), 5.2 mm for mouse tumors and by 2.8 mm for skinfold. Good contact between the electrodes and tissue was assured by the use of a conductive gel (EKO-GEL, Camina, ultrasound transmission gel, Egna, Italy). The plate electrodes were placed directly to the skeletal muscle and tumor as presented in Fig. 1(a) and Fig. 3(a), respectively. For the electroporation protocol a train of 8 square-wave pulses of 100  $\mu$ s duration, delivered at a repetition frequency of 1 Hz and generated by a PS 15 electropulsator

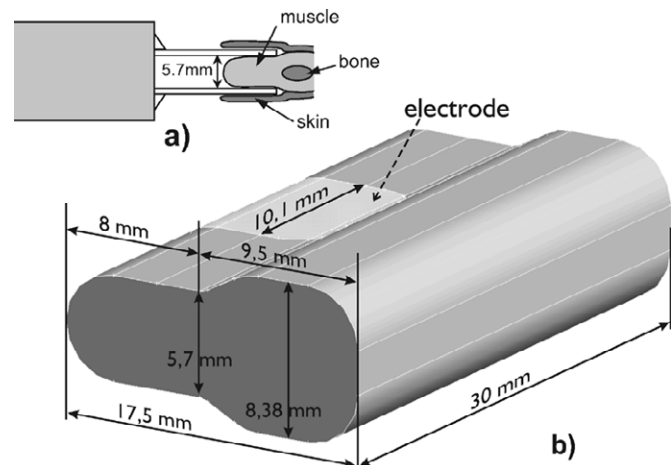


Fig. 1. (a) Geometry of the measurement setup. (b) Model made in EMAS for rat muscle without skin.

(Jouan, St. Herblain, France) was used in all experiments. One experiment per rat extremity (38 muscles) and one per tumor (45 melanomas B16, 46 LPB sarcomas) was performed. Female C57Bl/6 mice purchased from Janvier (France) were used for experiments. They were maintained at 22 °C with a natural day/night light cycle in a conventional animal colony, fed, and watered ad libitum. Subcutaneous tumors were implanted by injecting viable syngeneic LPB sarcoma cells under the skin on the mice flanks of 8–12 wk old mice. The animals were used after 10 to 12 d, when tumors reached at least 5.2 mm in diameter. In addition 12 experiments were performed on rat skinfold.

During the electric pulse the actual current delivered and the applied voltage were acquired by digital oscilloscope. Furthermore, we determined tissue cell permeabilization level by means of the quantitative  $^{51}\text{Cr}$  – EDTA uptake method [25]. Briefly, animals were anesthetized by means of the intraperitoneal administration of the anesthetics Ketamine (100 mg/kg; Ketalar, Panpharma, France) and Xylazine (10 mg/kg; Rompun, Bayer, France). Then rats were given 200  $\mu$ l and mice 100  $\mu$ l of  $^{51}\text{Cr}$  – EDTA (Amersham, U.K.) with a specific activity of 3.7 MBq/ml, by an intravenous injection, 5 min before the delivery of the electric pulses. The injected  $^{51}\text{Cr}$  – EDTA distributes freely in the vascular and extracellular compartments, but does not enter the intracellular compartments unless access is provided, e.g., by electroporation. Animals were sacrificed 24 hours after  $^{51}\text{Cr}$  – EDTA injection and tissues exposed to electric pulses were taken out, weighed and counted in a Cobra 5002 gammacounter (Packard Instrument, Meridien, CT). The net  $^{51}\text{Cr}$  – EDTA uptake as a result of electroporation was calculated as the measured activity per gram of the tissue exposed to the electric pulses. The measured activity could then be converted to the corresponding nanomoles of  $^{51}\text{Cr}$  – EDTA internalized per gram of tissue as a result of tissue cell electroporation.

## III. NUMERICAL MODELS

### A. Single Tissue Models

First we modeled the *in vivo* experimental tissue-electrode setups of each tissue separately: muscle, skinfold, and tumor. We modeled the electroporation process in each tissue separately and compared the results of the model with the measured

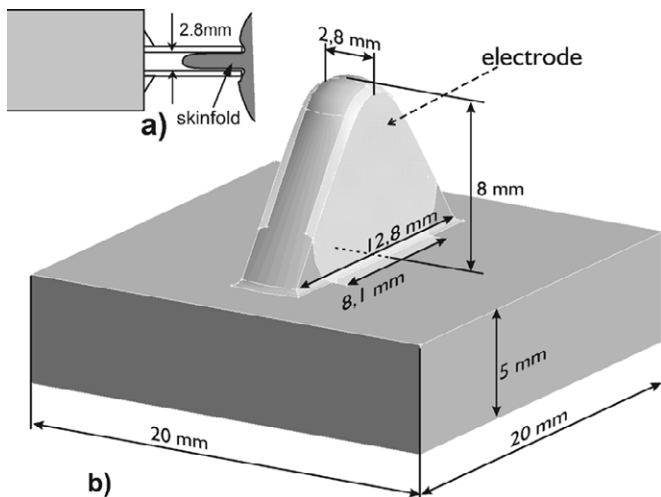


Fig. 2. (a) Geometry of the measurement setup. (b) Model made in EMAS for rat skinfold.

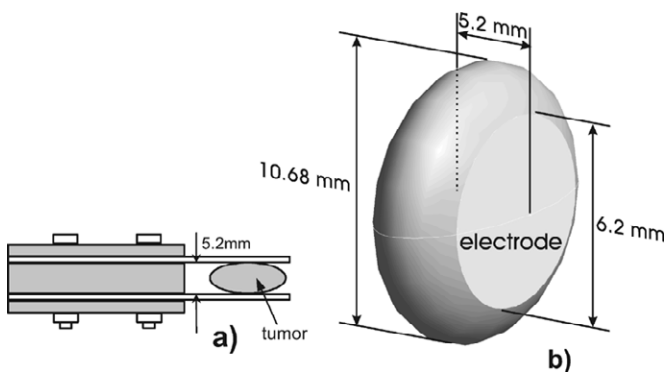


Fig. 3. (a) Geometry of the measurement setup. (b) Model made in EMAS for mouse tumor without skin.

data. We fine tuned the electroporation parameters of the single tissue models, such as initial specific conductivities, electroporation thresholds, changes in specific conductivity and the function describing the specific conductivity dependence ( $\sigma(E)$ ) between the reversible and the irreversible thresholds, until we established good agreement between the output of the model and the experimental data.

The geometries of measurement setups for the muscle, skin and tumor are presented in Fig. 1(a), Fig. 2(a), and Fig. 3(a) and the corresponding models in EMAS are described in Fig. 1(b), Fig. 2(b), and Fig. 3(b).

In the EMAS models the electrodes were not modeled as a physical element but as boundary conditions. In this way the number of elements in the model was reduced without affecting the results. The presence of the conductive gel between the electrodes and the tissue was also modeled in similar manner, i.e., the area of contact between the tissue and the electrodes is larger, thus the boundary condition is applied to the area beyond the boundaries of the electrode dimensions, typically 0.5 mm on each side. In the muscle model the bone was not considered since its conductivity is low and the bone in the experiments was rather distant from the electrodes. Nor were in the skinfold model modeled different layers of skin. Instead the tissue was considered as homogeneous throughout the model. Namely, large differences in thickness between different layers would unnecessarily complicate the model to the extent where numerical

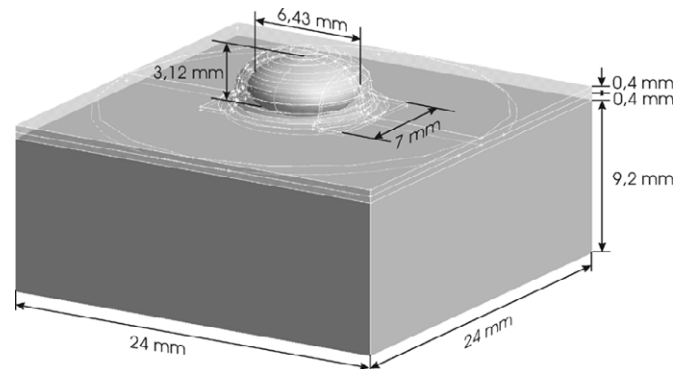


Fig. 4. Model made in EMAS for subcutaneous tumor.

problems could make the calculation impossible. The skin itself was not the primary target of investigation; therefore, an average specific conductivity was assigned to the skin tissue.

### B. Intricate Subcutaneous Tumor Model

After setting the threshold values, conductivity changes and the conductivity dependence function between the thresholds for each tissue separately in single tissue models, we built an intricate subcutaneous tumor model. The electric pulses were applied on the skin with plate electrodes pressed against the skin. The model is composed of four different tissues: skin, connective tissue, tumor, and muscle. Underlying tissues such as the bone were not modeled since the field is limited to the tissues lying closer to skin. In Fig. 4, the geometry of the tumor model is presented. The electrodes were again modeled as a boundary condition, not as a physical element, and the boundary condition was extended for 0.5 mm to each side of the electrode to account for the presence of the conductive gel. The distance between electrodes is 8 mm. We later compared the results with measurements done on subcutaneous tumors where the same electrode distance was used.

### C. The Electroporation Process

To model the electric field distribution in the tissue-electrode setups, the numerical values of tissue dielectric properties, such as specific conductivity and permittivity were needed. A literature survey of dielectric properties of the biological tissues used here was carried out [26]–[45].

In the model, only the specific conductivity data were used. Namely, direct current analysis was performed, so different permittivity values of the tissues do not play any role in the electric field distribution. When voltage is applied to the electrodes, the electric field is distributed in the tissue according to geometry and specific conductivity ratios of the tissues in the model.

During the analysis, tissue specific conductivities had to be changed according to the level of the tissue electroporation. However, in EMAS we cannot dynamically change material properties, such as specific conductivity. Therefore, we developed a subprogram that uses input and output files of the program EMAS to simulate the electroporation process in discrete steps. Time intervals between steps are, in general, not uniform. Different steps represent stages of specific conductivity changes in tissue and do not have a time value associated with them. They do, however, follow a chronological order starting at step

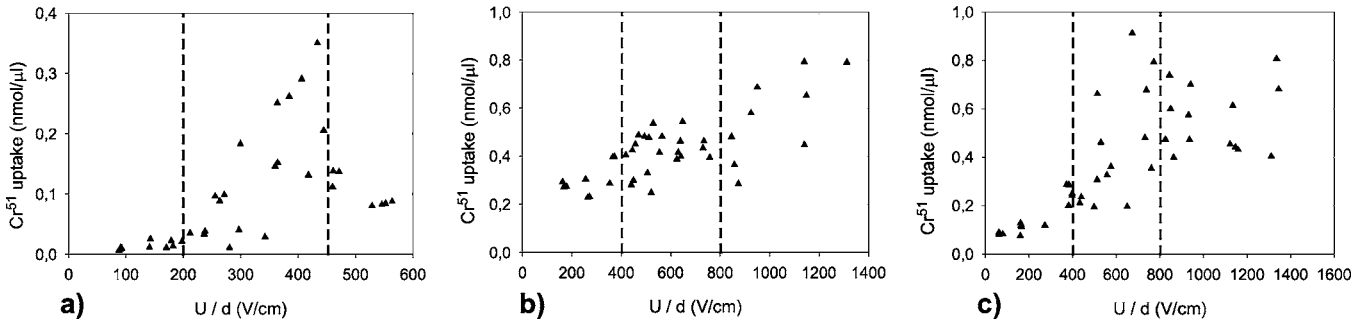


Fig. 5.  $^{51}\text{Cr}$  – EDTA uptake values with respect to the applied voltage for (a) muscle (electrode distance: 5.7 cm). (b) Tumor melanoma B16 (electrode distance: 5.2 cm). (c) Tumor LPB sarcoma (electrode distance: 5.2 cm).

0 and ending at step 5 when the process of electroporation is considered to be completed. Also, it needs to be emphasized that the number of iterations is not equivalent to the number of pulses. The whole process is considered to be completed during the first pulse and well inside the first 100  $\mu\text{s}$ . At the beginning of the process, the electric field distribution in the model is computed using EMAS, then after the analysis the subprogram searches in the output file the elements where the electric field exceeds the reversible electropermeabilization threshold. In the second step, the specific conductivities of those elements are changed according to the preset parameters of the electroporation process. Thus the quasi-dynamic model consists of a sequence of static models where according to electric field intensities from the preceding time discrete step, tissue conductivity is changed in the next step. The process is repeated until the electric field distribution reaches its steady state. The steady state occurs when two conditions are met: 1) there are no more elements in the model where the magnitude of the electric field exceeds the reversible threshold value and 2) the specific conductivity was already changed in the elements in which the threshold was reached and exceeded. The process of electroporation is then considered to be completed.

The sequential analysis is performed automatically; the user needs to provide an input file with all the data of the model and a file with all the electroporation parameters, such as the electric field threshold values for reversible and irreversible electropermeabilization, the change in conductivity and the function describing the specific conductivity dependence on the electric field between the reversible and irreversible thresholds. The subprogram that was developed gives us a choice of five different conductivity dependence Step 1) ( $\sigma(E)$ ) functions; 2) linear function; 3) and 4) two exponential function-based dependences; and 5) a sigmoid

$$\sigma(E) = \begin{cases} \sigma_0 & E < E_0 \\ \sigma_1 & E \geq E_0 \end{cases} \quad (1)$$

$$\sigma(E) = \frac{\sigma_1 - \sigma_0}{E_1 - E_0} \cdot E + \sigma_0 \quad (2)$$

$$\sigma(E) = A \left( 1 - e^{-\frac{E-E_0}{B}} \right) + \sigma_0$$

where

$$A = \frac{(\sigma_1 - \sigma_0)}{\left( 1 - e^{-\frac{E_0 - E_1}{B}} \right)} \quad (3)$$

$$\sigma(E) = A \left( e^{-\frac{E-E_1}{B}} - 1 \right) + \sigma_1$$

where

$$A = \frac{(\sigma_0 - \sigma_1)}{\left( e^{-\frac{E_0 - E_1}{B}} - 1 \right)} \quad (4)$$

$$\sigma(E) = \sigma_0 + \frac{(\sigma_1 - \sigma_0)}{\left( 1 + e^{-\frac{A-E}{B}} \right)}$$

where

$$A = \frac{E_0 + E_1}{2}. \quad (5)$$

Symbols  $\sigma_0$  and  $\sigma_1$  in (1) to (5) are the specific conductivity values before and after the permeabilization, respectively, and  $E_0$  and  $E_1$  are the reversible and the irreversible electric field thresholds, respectively. Parameter B defines the shape of the exponential and sigmoid functions.

## IV. RESULTS

### A. The Threshold Values and the Specific Conductivity Changes in Single Tissues

To build a sequential model of electroporation of subcutaneous tumor, we have to know the electropermeabilization threshold values and conductivity changes for all tissues involved. To estimate these values we used data from literature (for skin [18] and [19]) and experimentally collected data (for muscle, skinfold, and tumor), such as current-voltage dependencies and  $^{51}\text{Cr}$  – EDTA uptake.

The electric field threshold values of the reversible and the irreversible electropermeabilization of the skeletal muscle and tumor melanoma and sarcoma were estimated based on  $^{51}\text{Cr}$  – EDTA uptake method and are graphically presented in Fig. 5. We obtained data for all the tissues of our model, except for the connective tissue.

Current-voltage dependences measured at the end of the pulse for all tissues were used to fine tune the sequential model parameters. Current-voltage curves for the tissues included in the study are presented in Fig. 6. On the abscissa the voltage between the electrodes is normalized with the distance between them. In the case of the homogeneous electric field that would also denote the homogeneous electric field magnitude. But in our case the homogeneity of the electric field is deformed near the edge of the electrode, furthermore because of the chemical reactions additional voltage drop occurs at the skin-electrode

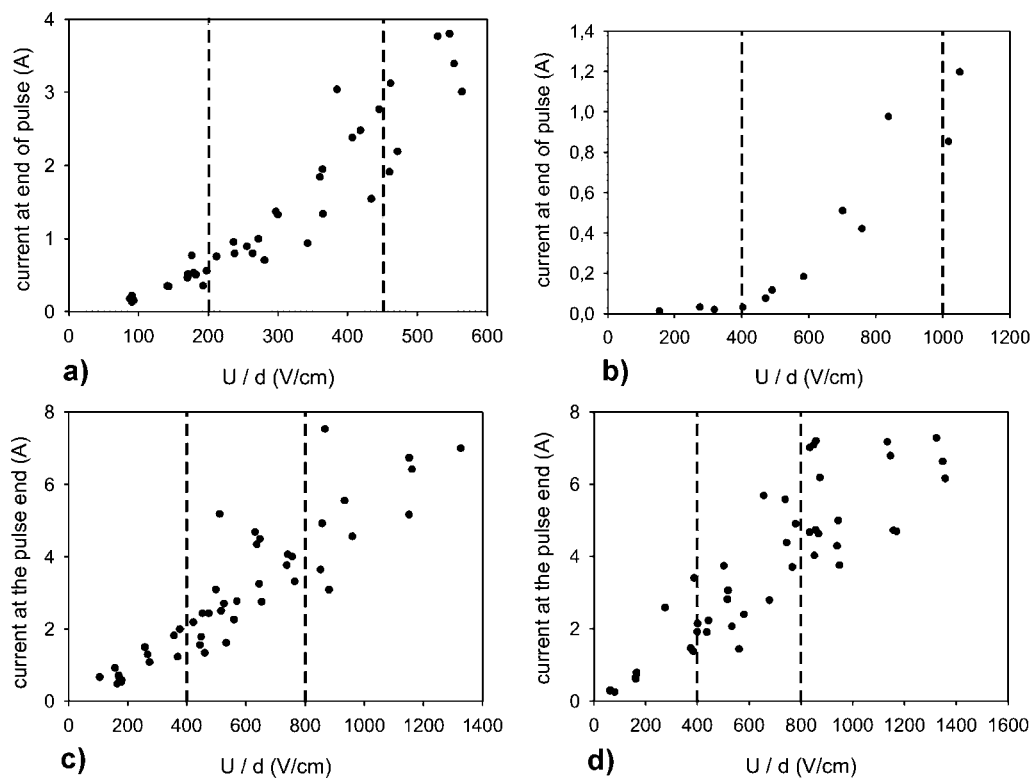


Fig. 6. Current at the end of the pulse with respect to the applied voltage for (a) muscle (electrode distance: 5.7 cm, pulse length: 100  $\mu$ s). (b) Skinfold (electrode distance: 2.8 cm, pulse length: 100  $\mu$ s). (c) Tumor melanoma B16 (electrode distance: 5.2 cm, pulse length: 100  $\mu$ s). and (d) Tumor LPB sarcoma (electrode distance: 5.2 cm, pulse length: 100  $\mu$ s).

contact. Nevertheless, almost in the entire region between the electrodes where the tissue is, the electric field is almost homogeneous and equals the ratio between the voltage and the distance between the electrodes. Thus the error we make using those electric field values to approximately determine the thresholds of electropermeabilization for the sequential analysis, is small enough. To approximately determine the electropermeabilization thresholds and the specific conductivity changes of the tissues, we used the  $^{51}\text{Cr}$  – EDTA uptake measurements at different pulse voltage amplitudes between the electrodes (Fig. 5). We can also use the current at the end of the pulse at a range of pulse voltage amplitudes (Fig. 6).

The threshold values of the electric field intensity were determined empirically using data on  $^{51}\text{Cr}$  – EDTA uptake and current at the end of the pulse. Thresholds present linear regressions to field intensities corresponding to low uptake values, increasing uptake values, and decreasing uptake values (Fig. 5); as well as linear regressions to field intensities corresponding to slope changes in the current at the end of the pulse measurements (Fig. 6). Threshold values of reversible and irreversible electropermeabilization were determined as the field intensities corresponding to intersections of consecutive linear regressions. They are plotted on Figs. 5 and 6 using dashed vertical lines. We determined the approximate threshold values to be: for the muscle: 200 V/cm (reversible) and 450 V/cm (irreversible), for the skin: 400 V/cm (reversible) and 1000 V/cm (irreversible) and for the tumor: 400 V/cm (reversible) and 800 V/cm (irreversible).

With the sequential analysis we calculated the electric field distribution and the reaction current through the single tissue

model at the end of the electropermeabilization process. The reaction currents for different voltages were then compared with the experimental data on graphs in Fig. 6. The electropermeabilization process data [initial specific conductivities, electropermeabilization thresholds, change in specific conductivity and the specific conductivity dependence between the thresholds ( $\sigma(E)$ )] was then fine tuned so that we found a good agreement between the current measured in experiments and that given by the model.

No experimental data on electropermeabilization of the connective tissue existed. Therefore the electric field thresholds and specific conductivity changes could not be established for that layer. Those parameters were therefore set without any experimental confirmation of the model. Fig. 7 shows the reaction currents of single tissue models compared to the experimental data shown above.

In Table I the electropermeabilization parameters for all the tissues used in the subcutaneous tumor model are presented. We chose the functions describing the specific conductivity dependence on electric field intensity between the reversible and the irreversible thresholds based on criteria that the output of the models should best fit the experimental data. Since we did not have any experimental data on connective tissue, we used the simplest of the functions—the step function. Theoretically, a sigmoid model of the electropermeabilization process seems the most logical one. Namely, due to the nonuniformity of the cell size and shape in the tissue, not all the cells are permeabilized at the same time once  $E_0$  is reached. Furthermore, when the electric field is reaching the irreversible threshold  $E_1$ , cell nonuniformity would also lead to a gradual saturation of the

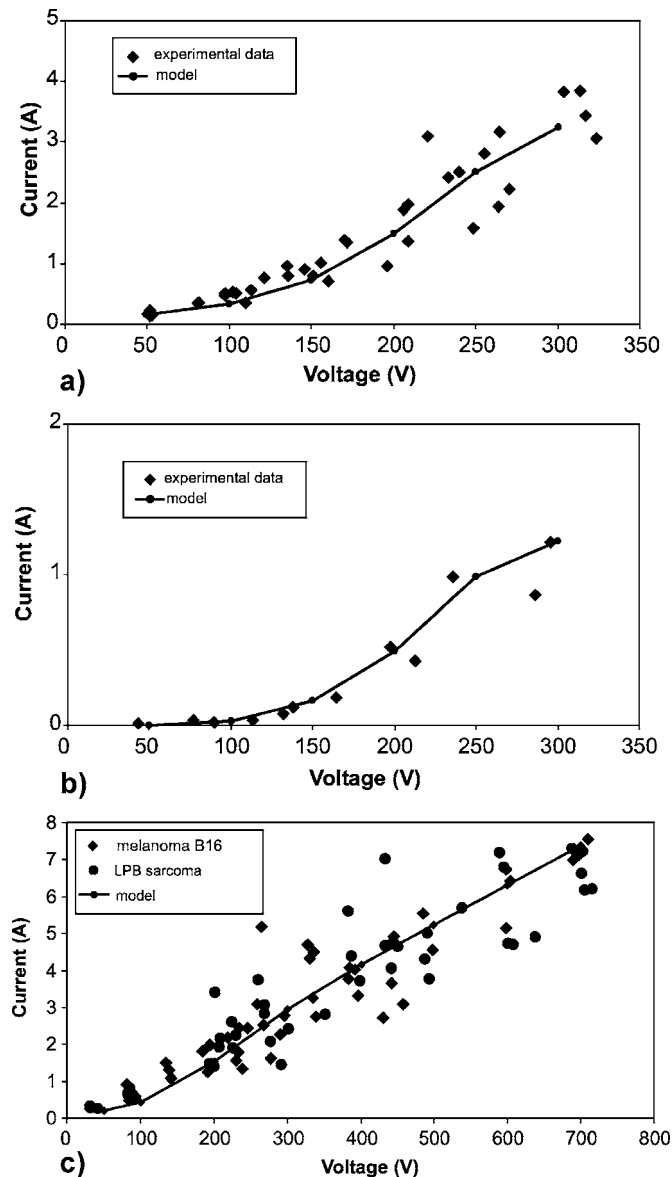


Fig. 7. The comparison of the reaction current vs. applied voltage between the experimental data and the EMAS models of (a) muscle (electrode distance: 5.7 cm, pulse length: 100  $\mu$ s), (b) skinfold (electrode distance: 2.8 cm, pulse length: 100  $\mu$ s), and (c) tumor—melanoma B16 and LPB sarcoma together, (electrode distance: 5.2 cm, pulse length: 100  $\mu$ s).

$\sigma(E)$  curve. We tried all the functions available to describe the  $\sigma(E)$  dependences on all the tissues. We noticed that the  $\sigma(E)$  behavior of all tissues can be described with practically each of the functions tested, with proper adjustments of other parameters such as the reversible and irreversible thresholds and the increase in the specific conductivity of the tissue. However, the adjustments may be too far from the biologically justifiable values determined from the experiments. So we always chose the function that best presented the  $\sigma(E)$  dependence without the need for significant adjustments of other parameters. This empirical approach resulted in choosing electroporation models other than the sigmoid.

The irreversible threshold of skin used in the numerical model was slightly different to the one proposed in Fig. 6 (1000 V/cm), to better fit the *in vivo* measurements. The reversible threshold and the conductivity change of connective tissue were set sim-

ilar to those of the muscle and the tumor since it seemed that that is the order of magnitude of the conductivity changes in tissues except skin.

### B. Intricate Subcutaneous Tumor Model

The electric field threshold values, changes in specific conductivity and the functions describing the conductivity changes due to electroporation for each tissue separately determined in the previous section were used in the subcutaneous tumor model. The electric field distribution was modeled before, during and after the electroporation process.

Sequential analysis was initiated three times with three different voltages between the electrodes: 500, 1000, and 1500 V. In Fig. 8 six steps of the electroporation process in the subcutaneous tumor model for the voltage of 1000 V between the electrodes are shown. The electric field distribution is shown in V/cm. Step 0 denotes the electric field distribution as it was before the electroporation process started, thus when all the tissues had their initial specific conductivities.

When the voltage is applied to the electrodes, the electric field is distributed in the tissue according to specific conductivity ratios of the tissues in the model. The field strength is the highest in the tissues with the lowest specific conductivity, where the voltage drop is the largest and the voltage gradient the highest. In our case, almost the entire voltage drop occurs in the skin layer which has a specific conductivity of about 10–100 times lower than the tissues lying underneath [18], [19], [40]–[49].

If we look at the last step of the sequential analysis, step 5, at 1000 V (Fig. 8) the tumor is entirely permeabilized, in some areas the electric field is also above the irreversible threshold (800 V/cm). Looking at the sequential analysis at 500 and 1500 V (data shown in Fig. 9, only the last step of the sequential analysis), we can establish that the tumor is partially permeabilized already at 500 V (reversible threshold in the tumor is at 400 V/cm). At 1500 V, a large part of the tumor is above the irreversible electric field threshold. Observing all the steps of the electroporation process, we can see that at the beginning the electric field is the highest in the skin layer. Therefore, the first tissue permeabilized is the skin, and only then the electric field “penetrates” to the deeper layers of the model and causes the rest of the tissues being permeabilized as well. We can see that already in the third step almost the final electric field distribution is reached.

## V. DISCUSSION

We built a finite element model of a subcutaneous tumor on small animals to study electroporation of tissues involved. The model was composed of skin, connective tissue, tumor and muscle. We studied the electric field distribution and the reaction currents through the model before, during and after the electroporation process in discrete time steps. The tissue specific conductivity increases when permeabilized, so the electric field distribution changes. Therefore, to study the electroporation process, we need data on the initial, prepulse specific conductivities of the tissues in the model, changes of the specific conductivities of the tissues when permeabilized, and the electric field threshold values for reversible and irreversible electroporation for each tissue separately. We collected nu-

TABLE I  
PARAMETERS OF THE ELECTROPORATION PROCESS FOR TISSUES IN THE SUBCUTANEOUS TUMOR MODEL AS OBTAINED FROM MEASUREMENTS AND SINGLE TISSUE MODELING

tissue	$\sigma(E)$	initial specific cond. (S/m)	spec. cond. increase	electric field thresholds (V/cm)
muscle	$e^x-1$ (B=15.000)	0,735 / 0,11	4 x	rev.: 200; irrev.: 450
skin	$e^x-1$ (B=30.000)	0,002	80 x	rev.: 400; irrev.: 900
tumor	$1-e^x$ (B=15.000)	0,3	2,5 x	rev.: 400; irrev.: 800
connective tiss.	step	0,03	3 x	rev.: 300

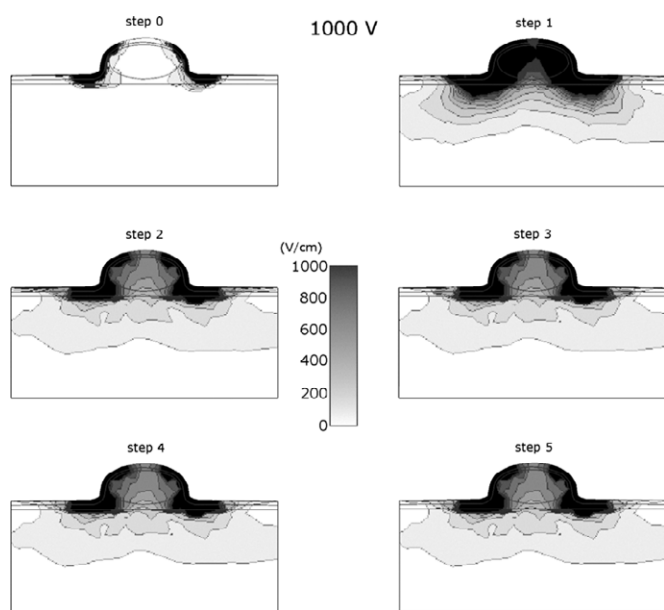


Fig. 8. Six steps of the sequential analysis of the electroporation process in the subcutaneous tumor model at 1000 V between two plate electrodes with distance of 8 mm. Time intervals between steps are in general not uniform. Different steps follow a chronological order but do not have an exact time value associated with them. The electric field distribution is shown in V/cm.

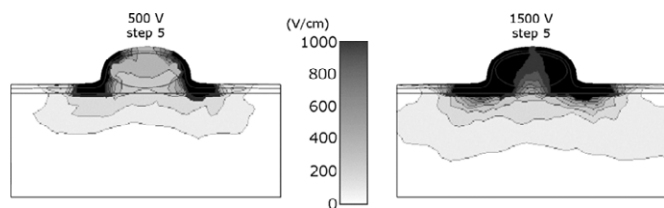


Fig. 9. The last step of the sequential analysis of the electroporation process in the subcutaneous tumor model at 500 and 1500 V, respectively, between two plate electrodes with distance of 8 mm. Time intervals between steps are in general not uniform. Different steps follow a chronological order but do not have an exact time value associated with them. The electric field distribution is shown in V/cm.

merical values of the initial specific conductivity from [18], [19], [26]–[45].

We noticed large discrepancies between the data reported by different researchers. These are due to many factors, such as different measuring techniques used, the fact that tissue samples were taken from different species, circumstances under which the measurements were performed (*in vivo*, *ex vivo*, time elapsed after the death of the animal, tissue temperature. . .), and others

TABLE II  
RANGES OF VALUES FOR SPECIFIC CONDUCTIVITIES FOUND IN THE LITERATURE [18], [19], AND [26]–[45]

	specific conductivity (S/m)
tumor	0.22 0.4
connective tissue	0.02 0.04
muscle transversal	0.04 0.14
muscle longitudinal	0.3 0.8
skin (dry)	0.00002 0.0002
skin (wet)	0.0003 0.2
stratum corneum	0.0000125
skin lower layers	0.227

(tissue seasonal changes, the age of the object, possible pathological condition of the object, . . .). In Table II we present the low-frequency (all below 100 Hz) value ranges of the tissues in question.

We set the reversible and irreversible electric field threshold values and the conductivity changes of the tissues with the help from  $^{51}\text{Cr}$  – EDTA uptake data and current vs. voltage dependences, comparing the model with experimental data we collected for each tissue separately. Finite element models of the experimental tissue-electrode setups were built for each tissue. In the models, we had to change the specific conductivities during the electroporation process. We developed a computer application which in combination with the commercial software package EMAS, computes the electroporation process in discrete steps.

Not the same function could be used to describe the specific conductivity dependence on the electric field ( $\sigma(E)$ ) for all the tissues. This is probably due to the biological differences between the tissues (such as cell size and distribution, different electrical properties of the intracellular media, differences in the structural inhomogeneity of the tissues (necrosis in tumors), ion concentration. . .). We believe those differences are the reason for different propagation of permeabilization in tissues.

We compared our results for skin tissue with data from [18] and [19]. Good agreement was established in both, threshold values and conductivity changes. Namely, in the abovementioned papers a big change in tissue resistivity was observed for voltages above 50 V. It has to be emphasized that in this case the experiments were made through a single skin thickness, while

in our case we have a skinfold which corresponds to a double thickness, thus, 100 V of applied voltage. We indeed observed changes in skin conductivity above 100 V. Also the changes in specific conductivity are in good agreement, namely the values found in the literature state the range of approximately 40 to 2000 times increase of specific conductivity, depending on the applied voltage.

After tuning the current vs. voltage dependences of the single tissue models with the experimental data, we used the electric field threshold values, changes in specific conductivity and the specific conductivity dependences ( $\sigma(E)$ ) between the reversible and the irreversible electric field in the subcutaneous tumor model. We initiated the sequential analysis three times, with three different voltages between the electrodes: 500, 1000, and 1500 V. Studying the last step for each sequential analysis, we can see that the tumor is partially permeabilized already at 500 V, at 1000 V the tumor is entirely permeabilized and in some areas, the electric field is already above the irreversible threshold, and at 1500 V, almost the entire tumor is above the irreversible threshold.

The model was validated by comparison of the computed electric field distributions with some experimental results of electrochemotherapy [50], [51]. Experimental results for treatments with 8 mm distance between electrodes show antitumor effectiveness of electrochemotherapy with cis-diamminedichloroplatinum(II) (CDDP) for amplitudes exceeding 720 V. Antitumor effect increased at 1200 V, however this or higher amplitudes can result in severe side effects as a result of tumor lysis syndrome, due to massive tumor destruction. Nevertheless, antitumor effects (increased tumor growth delay) can be achieved also at 1040 V, where minimal antitumor effect of electroporation itself is observed and most of the tumor cells are permeabilized. Our model distributions together with the reversible and irreversible electric field thresholds obtained from *in vivo* measurements coincide well with the effectiveness of the electrochemotherapy and the necrosis stage of tumors, depending on the electroporation amplitude.

Thus a preliminary numerical model of subcutaneous tumor in small animals has been made available. Its extension to other geometries would allow forecasting the outcome of pulse delivery before the treatment. Such an approach could optimize the choice of electrodes and their placement in both electrochemotherapy and gene transfer.

#### REFERENCES

- [1] E. Neumann, A. E. Sowers, and C. A. Jordan, *Electroporation and Electrofusion in Cell Biology*. New York: Plenum, 1989.
- [2] J. C. Weaver and Y. A. Chizmadzhev, "Theory of electroporation: a review," *Bioelectrochem. Bioenerg.*, vol. 41, pp. 135–160, 1996.
- [3] T. Y. Tsong, "Electroporation of cell membranes," *Biophys. J.*, vol. 60, pp. 297–306, 1991.
- [4] L. M. Mir, "Therapeutic perspectives of *in vivo* cell electroporation (Review Article)," *Bioelectrochem.*, vol. 53, pp. 1–10, 2000.
- [5] D. Miklavčič, D. Šemrov, H. Mekid, and L. M. Mir, "A validated model of *in vivo* electric field distribution in tissues for electrochemotherapy and for DNA electrotransfer for gene therapy," *Biochim. Biophys. Acta*, vol. 1519, pp. 73–83, 2000.
- [6] M. Pavlin, N. Pavšelj, and D. Miklavčič, "Dependence of induced transmembrane potential on cell density, arrangement and cell position inside a cell system," *IEEE Trans. Biomed. Eng.*, vol. 49, no. 6, pp. 605–612, Jun. 2002.
- [7] B. Valič, M. Golzio, M. Pavlin, A. Schatz, C. Faurie, B. Gabriel, J. Teissié, M. P. Rols, and D. Miklavčič, "Effect of electric field induced transmembrane potential on spheroidal cells: theory and experiment," *Eur. Biophys. J.*, vol. 32, pp. 519–528, 2003.
- [8] B. Valič, M. Pavlin, and D. Miklavčič, "The effect of resting transmembrane voltage on cell electroporation: a numerical analysis," *Bioelectrochemistry*, vol. 63, pp. 311–315, 2004.
- [9] H. Wolf, M. P. Rols, E. Boldt, E. Neumann, and J. Teissié, "Control by pulse parameters of electric field-mediated gene transfer in mammalian cells," *Biophys. J.*, vol. 66, pp. 524–531, 1994.
- [10] D. Miklavčič, K. Beravs, D. Šemrov, M. Čemažar, F. Demšar, and G. Serša, "The importance of electric field distribution for effective *in vivo* electroporation of tissues," *Biophys. J.*, vol. 74, pp. 2152–2158, 1998.
- [11] M. Pavlin and D. Miklavčič, "Effective conductivity of a suspension of permeabilized cells: a theoretical analysis," *Biophys. J.*, vol. 85, pp. 719–729, 2003.
- [12] R. V. Davalos, B. Rubinsky, and D. M. Otten, "A feasibility study for electrical impedance tomography as a means to monitor tissue electroporation for molecular medicine," *IEEE Trans. Biomed. Eng.*, vol. 49, no. 4, pp. 400–403, Apr. 2002.
- [13] D. Šemrov and D. Miklavčič, "Numerical modeling for *in vivo* electroporation," in *Methods in Molecular Medicine*. Totowa, NJ: Humana, 2000, vol. 37, Electrically mediated delivery of molecules to cells.
- [14] —, "Calculation of the electrical parameters in electrochemotherapy of solid tumours in mice," *Comput. Biol. Med.*, vol. 28, pp. 439–448, 1998.
- [15] S. Tungjitkusolmun, E. J. Woo, H. Cao, J.-Z. Tsai, V. R. Vorperian, and J. G. Webster, "Thermal-electrical finite element modeling for radio frequency cardiac ablation: effects of changes in myocardial properties," *Med. Biol. Eng. Comput.*, vol. 38, pp. 562–568, 2000.
- [16] P. M. Ghosh, C. R. Keese, and I. Giaever, "Monitoring electroporation in the plasma membrane of adherent mammalian cells," *Biophys. J.*, vol. 64, pp. 1602–1609, 1993.
- [17] R. V. Davalos, D. M. Otten, L. M. Mir, and B. Rubinsky, "Electrical impedance tomography for imaging tissue electroporation," *IEEE Trans. Biomed. Eng.*, vol. 51, pp. 761–767, 2004.
- [18] U. Pliquet, R. Langer, and J. C. Weaver, "Changes in the passive electrical properties of human stratum corneum due to electroporation," *BBA*, vol. 1239, no. 5, pp. 111–121, May 1995.
- [19] U. Pliquet and J. C. Weaver, "Electroporation of human skin: simultaneous measurement of changes in the transport of two fluorescent molecules and in the passive electrical properties," *Bioelectrochem. Bioenerg.*, vol. 39, pp. 1–12, 1996.
- [20] U. Pliquet, R. Elez, A. Piiper, and E. Neumann, "Electroporation of subcutaneous mouse tumors by rectangular and trapezium high voltage pulses," *Bioelectrochemistry*, vol. 62, pp. 83–93, 2004.
- [21] M. Schmeer, T. Seipp, U. Pliquet, S. Kakorin, and E. Neumann, "Mechanism for the conductivity changes caused by membrane electroporation of CHO cell-pellets," *Phys. Chem. Chem. Phys.*, vol. 6, no. 24, pp. 5564–5574, 2004.
- [22] *EMAS User's Manual*, Ansoft Corp., Jul. 1997.
- [23] B. Irons and S. Ahmad, *Techniques of Finite Elements*. New York: Wiley, 1986.
- [24] R. Susil, D. Šemrov, and D. Miklavčič, "Electric field-induced transmembrane potential depends on cell density and organization," *Electro. Magnetobiol.*, vol. 17, no. 3, pp. 391–399, 1998.
- [25] J. Gehl and L. M. Mir, "Determination of optimal parameters for *in vivo* gene transfer by electroporation, using a rapid *in vivo* test for cell permeabilization," *Biochem. Biophys. Res. Commun.*, vol. 261, pp. 377–380, 1999.
- [26] L. A. Geddes and L. E. Baker, "The specific resistance of biological material—a compendium of data for the biomedical engineer and physiologist," *Med. Biol. Eng.*, vol. 5, pp. 271–293, 1967.
- [27] H. P. Schwan and C. F. Kay, "Specific resistance of body tissues," *Circ. Res.*, vol. 4, pp. 664–670, 1956.
- [28] B. R. Epstein and K. R. Foster, "Anisotropy in the dielectric properties of skeletal muscle," *Med. Biol. Eng. Comput.*, vol. 21, no. 1, pp. 51–55, 1983.
- [29] H. C. Burger and R. Van Dongen, "Specific resistance of body tissues," *Phys. Med. Biol.*, vol. 5, pp. 431–447, 1960.
- [30] S. Rush, J. A. Abildskov, and R. McFee, "Resistivity of body tissues at low frequencies," *Circ. Res.*, vol. 12, pp. 40–50, 1963.
- [31] F. X. Hart, "The impedance spectroscopy of skeletal muscle," in *10th Electrotech. Comput. Science Conf. ERK 2001*, vol. A, 2001, pp. 13–16.
- [32] C. Gabriel, S. Gabriel, and E. Corthout, "The dielectric properties of biological tissue: i. literature survey," *Phys. Med. Biol.*, vol. 41, pp. 2231–2249, 1996.

- [33] S. Gabriel, R. W. Lau, and C. Gabriel, "The dielectric properties of biological tissue: ii. measurements in the frequency range 10 Hz to 20 GHz," *Phys. Med. Biol.*, vol. 41, pp. 2251–2269, 1996.
- [34] —, "The dielectric properties of biological tissue: iii. parametric models for the dielectric spectrum of tissues," *Phys. Med. Biol.*, vol. 41, pp. 2271–2293, 1996.
- [35] S. R. Smith, K. R. Foster, and J. L. Wolf, "Dielectric properties of VX-2 carcinoma vs. normal liver tissues," *IEEE Trans. Biomed. Eng.*, vol. BME-33, no. 5, pp. 522–524, May 1986.
- [36] A. J. Surowiec, S. S. Stuchly, J. R. Barr, and A. Swarup, "Dielectric properties of breast carcinoma and the surrounding tissues," *IEEE Trans. Biomed. Eng.*, vol. 35, no. 4, pp. 257–263, Apr. 1988.
- [37] H. P. Schwan and C. F. Kay, "The conductivity of living tissues," *Ann. NY Acad. Sci.*, vol. 65, pp. 1007–1013, 1957.
- [38] F. L. H. Gielen, W. Wallinga-de Jonge, and K. L. Boon, "Electrical conductivity of skeletal muscle tissue: experimental results from different muscles *in vivo*," *Med. Biolog. Eng.*, vol. 22, pp. 569–577, 1984.
- [39] B. Bodakian and F. X. Hart, "The dielectric properties of meat," *IEEE Trans. Dielect. Elect. Insul.*, vol. 1, no. 2, pp. 181–187, Apr. 1994.
- [40] W. Kaufman and F. D. Johnston, "The electrical conductivity of the tissues near the heart and its bearing on the distribution of cardiac action currents," *Am. Heart J.*, vol. 26, pp. 42–54, 1943.
- [41] A. Hemingway and J. F. McLendon, "The high frequency resistance of human tissue," *Am. J. Physiol.*, vol. 102, pp. 56–59, 1932.
- [42] H. P. Schwan and K. Li, "Capacity and conductivity of body tissues at ultrahigh frequencies," in *Proc. IRE*, vol. 41, 1953, pp. 1735–1740.
- [43] E. Kinnen, W. Kubicek, P. Hill, and G. Turton, "Thoracic Cage Impedance Measurements. (Tissue Resistivity *in vivo* and Transthoracic Impedance at 100 kc/s)," School of Aerospace Medicine, Brooks AFB, TX, Tech. Doc. Rep. SAM-TDR 64-5, 1964.
- [44] T. Yamamoto and Y. Yamamoto, "Electrical properties of the epidermal stratum corneum," *Med. Biol. Eng.*, vol. 14, no. 2, pp. 151–158, 1976.
- [45] —, "Dielectric constant and resistivity of epidermal stratum corneum," *Med. Biol. Eng.*, vol. 14, no. 5, pp. 494–500, 1976.
- [46] U. Pliquett, "Mechanistic studies of molecular transdermal transport due to skin electroporation," *Adv. Drug Deliv. Rev.*, vol. 35, pp. 41–60, 1999.
- [47] M. R. Prausnitz, V. G. Bose, R. Langer, and J. C. Weaver, "Electroporation of mammalian skin: a mechanism to enhance transdermal drug delivery," *Proc. Nat. Acad. Sci. USA*, vol. 90, pp. 10 504–10 508, 1993.
- [48] Y. A. Chizmadzhev, A. V. Indenbom, P. I. Kuzmin, S. V. Galichenko, J. C. Weaver, and R. O. Potts, "Electrical properties of skin at moderate voltages: contribution of appendageal macropores," *Biophys. J.*, vol. 74, pp. 843–856, 1998.
- [49] S. A. Gallo, A. R. Oseroff, P. G. Johnson, and S. W. Hui, "Characterization of electric-pulse-induced permeabilization of porcine skin using surface electrodes," *Biophys. J.*, vol. 72, pp. 2805–2811, 1997.
- [50] G. Serša, M. Čemažar, and D. Miklavčič, "Anti-tumor effectiveness of electrochemotherapy with cis-Diamminedichloroplatinum(II) in mice," *Cancer Res.*, vol. 55, pp. 3450–3455, 1995.
- [51] G. Serša, M. Čemažar, D. Miklavčič, and D. J. Chaplin, "Tumor blood flow modifying effect of electrochemotherapy with bleomycin," *Anti-cancer Res.*, vol. 19, pp. 4017–4022, 1999.



**Nataša Pavšelj** was born in 1974 in Ljubljana, Slovenia. She received the B.Sc. and M.Sc. degree in electrical engineering from the Faculty of Electrical Engineering, University of Ljubljana. She is currently working toward the Ph.D. degree at the University of Ljubljana.

Her main research interests lie in the field of electroporation, including numerical modeling of electric field distribution in different biological tissue setups and cell systems and comparison of the theoretical results with the experimental work.



**Zvonko Bregar** was born in 1964 in Kamanje, Croatia. In 1988, he received the B.Sc. degree in application mathematics and the M.Sc. degree in 2000 in computer science from the University of Ljubljana, Ljubljana, Slovenia.

He is with Milan Vidmar Electrotechnical Institute, Ljubljana. His interests lie in various forms of computer modeling and simulations of electric systems.



**David Cukjati** was born in 1970 in Ljubljana, Slovenia. He received the M.Sc. and Ph.D. degrees in electrical engineering from the University of Ljubljana.

He is currently a Teaching Assistant with the Faculty of Electrical Engineering, University of Ljubljana. He works in the field of biomedical engineering. His current research interests are electrical soft tissue healing and electroporation-assisted drug delivery involving modeling, expert systems, biomedical database, and web applications design.



**Danute Batiuskaite** was born in 1971. She received the Ph.D. degree in biophysics from the Vytautas Magnus University of Kaunas, Kaunas, Lithuania.

Currently she is a lecturer with the Vytautas Magnus University of Kaunas. Her main research interest is in the field of electroporation of cells and tissues, the search for the optimal electrochemotherapy conditions.



**Lluís M. Mir** was born in 1954 in Barcelona, Spain. He received the B.Sc. degree from the University of Paris VI, Paris, France, in 1976, and the Ph.D. degree from the University of Toulouse, Toulouse, France, in 1983.

He is a Fellow with the Ecole Normale Supérieure de Paris, France. He is currently Director of Research of the CNRS at the UMR 8121 CNRS-Institute Gustave-Roussy, Villejuif, France. His main interests lie in the fields of membrane electroporation *in vitro* and *in vivo*, especially with regard to the transfer of antitumor drugs after tumor cells electroporation (electrochemotherapy) and to the electrotransfer of genes (electrogenotherapy) to healthy and malignant tissues. He is also Professor Adjunct, and since December 2004, Honorary Senator, of the University of Ljubljana, Slovenia.



**Damijan Miklavčič** was born in 1963 in Ljubljana, Slovenia. He received the Ph.D. degree in electrical engineering from the University of Ljubljana.

He is a Professor with the Faculty of Electrical Engineering, University of Ljubljana, and the Head of Laboratory of Biocybernetics. He is active in the field of biomedical engineering. His current interest focuses on electroporation-assisted drug delivery, including cancer treatment by means of electrochemotherapy, tissue oxygenation, and modeling.

